UNIVERSIDAD DE JAÉN

ESCUELA POLITÉCNICA SUPERIOR DE JAÉN

DEPARTAMENTO DE INGENIERÍA MECÁNICA Y MINERA

TESIS DOCTORAL

INTEGRACIÓN DE PROYECCIÓN DE FRANJAS Y CORRELACIÓN DIGITAL DE IMÁGENES 2D PARA LA MEDIDA DE DEFORMACIONES Y DESPLAZAMIENTOS 3D

PRESENTADA POR:

LUIS ANTONIO FELIPE SESÉ

DIRIGIDA POR:

DR. D. FRANCISCO ALBERTO DÍAZ GARRIDO

DR. D. PHILIP SIEGMANN

JAÉN, 25 DE MARZO DE 2014

ISBN 978-84-8439-869-1

Resumen

Diversas aplicaciones de ingeniería requieren la medida de desplazamientos las tres direcciones espaciales de un objeto sometido a cargas mecánicas, por ejemplo, en pruebas estructurales o en controles de calidad de fabricación. En la actualidad, se emplea comúnmente la técnica Correlación Digital de Imágenes (3D-DIC) (Sutton, et al., 2009). Esta técnica utiliza dos cámaras que adquieren imágenes del objeto que está siendo deformado desde diferentes ángulos de visión. Las cámaras deben estar perfectamente sincronizadas y calibradas para poder llevar a cabo la reconstrucción de formas en 3D y el seguimiento de la posición de cada elemento de la superficie del objeto mientras se produce la deformación. El proceso de calibración de esta técnica requiere de la adquisición de una secuencia de imágenes de un objeto de calibración y de una alta cantidad de recursos computacionales.

Recientemente se han propuesto una técnica alternativa para la medida de campos de desplazamiento 3D mediante la combinación de proyección de franjas (FP) con DIC bidimensional (2D-DIC) (Tay, et al., 2004) (Barrientos, et al., 2008) (Siegmann, et al., 2011) (Mares, et al., 2011) (Felipe-Sesé, et al., 2014). Esta técnica híbrida tan sólo precisa de una cámara y un proyector de franjas. En esta tesis se presenta un novedoso sistema que permite medir los desplazamientos en las direcciones *X*-, *Y*- y Z ocurridos en la superficie de un objeto sometido a deformación. El método empleado se basa en combinar las técnicas 2D-DIC y FP para obtener los mapas de desplazamiento medidos en el plano y fuera de éste (3D). Éste sistema propuesto obtiene dichos resultados a partir de la adquisición de tan sólo una imagen por cada etapa de la deformación del objeto, lo que permite la adquisición de datos en tiempo real. Uno de los intereses de esta investigación reside en que el sistema permite una alineación perpendicular precisa de la cámara con respecto a un superficie plana de referencia, y también permite la auto-calibración (no se emplea ningún objeto de calibración). Además, permite el determinación de una constante de calibración de proyección de franjas para cada píxel, así como todos los parámetros necesarios para la corrección de los desplazamiento medidos en el plano (Felipe-Sesé, et al., 2014). Para ilustrar el potencial del sistema propuesto, se ha realizado una serie de experimentos estáticos y dinámicos sobre materiales hiperelásticos. El mayor

desplazamiento medido fuera de plano ha sido de 20 mm con una incertidumbre de 0,023 mm y de 0,0083 mm para la medida de desplazamientos en el plano. Los resultados se han comparado con los obtenidos empleando un sistema Correlación Digital de Imágenes 3D comercial, manifestando un nivel de concordancia muy alto.

Abstract

In many engineering applications, the measurement of displacements maps in all three spatial directions over the surface of a loaded object is often required, such an example is, structural testing or manufacturing quality control. At present, for this proposes, typically 3-dimensional digital image correlation (3D-DIC) (Sutton, et al., 2009) is often used. This technique employs two cameras acquiring images from different viewing angles of the object while it is deformed. The cameras have to be perfectly synchronized and calibrated for both: 3D reconstruction and for tracking each surface element while the deformation occurs. The calibration process of the technique requires acquiring a sequence of several images of a calibration object and a high amount of computational resources.

Alternative techniques have been proposed to obtain 3D displacement maps by combining Fringe Projection (FP) with two-dimensional DIC (2D-DIC) (Tay, et al., 2004) (Barrientos, et al., 2008) (Siegmann, et al., 2011) (Mares, et al., 2011) (Felipe-Sesé, et al., 2014). The hybrid technique only requires one camera and a fringe projector. In this thesis it is presented a novel device that allows obtaining the maps of displacements in *X*-, *Y*- and *Z*- direction at the surface of an object during deformation. The system is based on a method that combines 2D-DIC and FP to obtain the in- and out-of-plane components of displacement during deformation. The device operates by acquiring only one image at each deformation stage of the object, thereby allowing real time data acquisition. The goal of the presented work is that the device allows both: a precise perpendicular alignment respect to a flat reference surface, and a self-calibration (i.e. no calibration object is employed). Thus, a fringe calibration constant is estimated for each pixel as well as all the required parameters for the in-plane displacement correction (Felipe-Sesé, et al., 2014). To illustrate the potential of the proposed device, a set of static and dynamic experiments have been conducted using hyperelastic materials. The maximum out-of-plane displacement achieved was 20 mm with an uncertainty of 0,023 mm and an in-plane displacement uncertainty of 0,0083 mm. Results have been compared with those obtained using a commercial three dimensional digital image correlation system showing a very high level of agreement

Acknowledgements

I would like to start my acknowledgements by thanking my supervisors, Francisco Diaz Garrido and Philip Siegmann, for all their time, dedication, patience, and of course their great support, orientation and ideas. Of course, thanks to Ruben Dorado Vicente for his orientation, and sympathy along those first years. And especially thanks to Eann Patterson from whom I learned a lot, for all his time teaching me new ideas, support and patience with my English. It was a pleasure to be supervised by them all.

Thanks to my colleagues José Vasco Olmo, Elías López Alba, Alberto García Collado, for their friendly contribution to the development of this research and from bringing forward their knowledge and advice. And in general to all the member of the Department of Ingenieria Mecáncia y Minera in special the area of Ingenieria Mecánica for their daily support in my research and teaching work. Definitely thanks to the technicians team for their friendly advice and willingness to help. In addition thanks for the financial support of Junta de Andalucía through the program “Programa para la formación de PDI pre-doctoral en Universidades Públicas Andaluzas en áreas de conocimiento consideradas deficitarias por necesidades docentes”.

Many thanks to all those who made so lovely my five months working at University of Liverpool: Christopher Sebastian, Nick Underwood, Jacobo Angulo, John Sellars and all Patterson´s team.

Of course thanks to all my good friends: Alvaro, Angel, Antonio, Jacinto, Paco, Romu, David, and especially to Macarena who had a very important role in understanding and helping in my worst moments and encouraged me to enjoy the good ones.

Finally, really, really thanks a lot to my family, my parents Manuel and Maria del Carmen, my brothers Maite, Elvira and Manolo. They gave me the opportunity and all the possible facilities to reach here. Their encouragement, support and advice was always crucial.

Nomenclature

ϕ	Modulated phase (rad)
K_f	Fringe constant (mm/rad)
α	Angle between camera and projector optical axis (rad)
x,y	Image coordinates
r	Background illumination
i	Image intensity
p	Pitch of projected fringe pattern(mm)
b	Fringe amplitude
f	Frequency of projected fringe pattern (mm^{-1})
A_n	Weighting factor of Fourier
z_0	Distance reference plane to optical centre of lens (mm)
d	Distance between projector and camera optical centre (mm)
[illegible]	Relative retardation
h	Thickness of photoelastic material
f_{σ}	Material fringe value for stress
f_{ε}	Material fringe value for Strain
S	Thermoelastic constant
T	Temperature
x_{CCD}, y_{CCD}	Camera sensor physical coordinates (pixel)
x_1, y_1	Spatial coordinates (mm)
z_{CCD}	Distance optical centre of lens to camera sensor (mm)
$\Delta x, \Delta y, \Delta z$	Displacements in *X*-,*Y*- and *Z*- directions
u,v,w	Displacements in *X*-,*Y*- and *Z*- directions
L	Camera magnification, ($mm.pixel^{-1}$)

m	Slope of the cone of radial displacements(adimensional)
Δr	In-plane displacement modulus
$\varepsilon_x, \varepsilon_y, \gamma$	Strain in *x*- and *y*- direction a shear strain
$\varepsilon_{1,}\varepsilon_2$	Principal strains
$\sigma_{x,}\sigma_y$	Stresses in x and y direction
$\sigma_{1,}\sigma_2$	Principal stresses (MPa)
C_{ZNCC}	Zero Normalized Cross Correlation
cr	Correlation coefficient
Or	Original image
Re	Reconstructed image from shape descriptors

Contenidos

Contents

Chapter 1. Introducción

1.1. Introducción

Diversas aplicaciones de ingeniería requieren la medida de desplazamientos las tres direcciones espaciales de un objeto sometido a cargas mecánicas, por ejemplo en pruebas estructurales o en controles de calidad de fabricación.

En la actualidad, con éste propósito se emplea comúnmente la técnica Correlación Digital de Imágenes (3D-DIC) (Sutton, et al., 2009). Esta técnica utiliza dos cámaras que adquieren imágenes del objeto que está siendo deformado desde diferentes ángulos de visión. Las cámaras deben estar perfectamente sincronizadas y calibradas para poder llevar a cabo la reconstrucción de formas en 3D y para el seguimiento de la posición de cada elemento de la superficie del objeto mientras se produce la deformación. El proceso de calibración de ésta técnica requiere de la adquisición de una secuencia de imágenes de un objeto de calibración y de una alta cantidad de recursos computacionales.

Recientemente se han propuesto una técnica alternativa para la medida de campos de desplazamiento 3D mediante la combinación de proyección de franjas (FP) con DIC bidimensional (2D-DIC) (Tay, et al., 2004) (Barrientos, et al., 2008) (Siegmann, et al., 2011) (Mares, et al., 2011) (Felipe-Sesé, et al., 2014). Esta técnica híbrida tan sólo precisa de una cámara y un proyector de franjas.

El objetivo principal de esta tesis es la integración de las técnicas 2D-DIC y FP para la medición de desplazamientos 3D empleando una sola cámara. Para la definición de este objetivo, se desarrolló un estudio preliminar sobre los fundamentos, campos de aplicación, ventajas e inconvenientes de algunas de las técnicas ópticas más

comúnmente empleadas en el ámbito de la mecánica experimental. Como resultado de esta investigación, se observó que 3D-DIC es la única técnica que permite la medida de desplazamientos en el plano y fuera de éste (3D), además, presenta la ventaja adicional de que puede ser empleada en un amplio rango de aplicaciones, ya sean en condiciones estáticas o dinámicas. No obstante, una de las principales desventajas de 3D-DIC es que precisa de un sistema estereoscópico (con un mínimo de dos cámaras) y de un complejo procedimiento de calibración. Ésto implica un sensible aumento del coste del equipo, especialmente notable en el estudio de problemas dinámicos. Por otra parte, 2D-DIC y FP son dos técnicas ampliamente conocidas caracterizadas por una gran aplicabilidad y sensibilidad, pero se encuentran limitadas a la medida de desplazamientos en el plano y fuera de éste respectivamente. No obstante, ambas poseen un montaje experimental muy parecido (una cámara dispuesta perpendicularmente a un plano de referencia). Por lo tanto, la integración de ambas técnicas de manera simultánea para la medida de desplazamientos en el plano y fuera de éste disminuiría el coste y la complejidad del montaje experimental y del procesado en comparación con 3D - DIC.

La integración de 2D-DIC y FP permitiría solventar las restricciones que ambas técnicas presentan individualmente. Sin embargo, no se ha encontrado ningún método específico para la integración de la FP y 2D-DIC que pueda emplearse como posible alternativa a 3D-DIC para la medición de desplazamiento 3D. No obstante, sí existen estudios sobre esta integración de éstas técnicas, pero ninguno de ellos desarrolla una forma explícita de medir el desplazamiento en 3D.

Adicionalmente se ha estudiado el montaje experimental necesario para la integración ambas técnicas. Básicamente consta en una cámara RGB, dispuesta perpendicularmente respecto a la superficie de referencia, y de un proyector LCD colocado oblicuamente respecto al eje óptico de la cámara. El proyector proyecta un patrón de franjas verticales sobre el elemento analizado, el cual ha sido previamente pintado con un patrón de pequeñas manchas aleatorias (speckle). Para diferenciar las franjas y el speckle, se ha adoptado un sistema de codificación de color RGB. Además, el desplazamiento medido en el plano por 2D-DIC requiere una corrección especial si no se han empleado lentes telecéntricas en la cámara. Por esto motivo, se ha realizado

un análisis óptico basado en un modelo de lente pin-hole. El resultado es una relación matemática que permite la corrección de la distorsión de esos desplazamientos medidos por 2D-DIC.

Todo el sistema descrito debe ser calibrado y alineado perpendicularmente con respecto al plano de referencia. Debido a ello se ha desarrollado una metodología de calibración/alineación mediante el uso de un puntero de láser y de una plataforma de movimiento lineal micrométrico.

Finalmente, la integración de ambas técnicas ha sido validada experimentalmente. En todos los casos los resultados se compararon con los obtenidos con 3D-DIC mostrando un alto nivel de concordancia, destacando el potencial de FP+2D-DIC como una alternativa de bajo coste a la técnica 3D-DIC.

1.2. Motivaciones y objetivos del trabajo de investigación

La motivación de este trabajo de investigación surge a raíz de la hipótesis destacada por la investigación anteriormente llevada a cabo por Siegmann, et al. (Siegmann,et al. , 2011), quienes demostraron que es posible llevar a cabo simultáneamente FP y 2D-DIC mediante una sola cámara a color . Por lo tanto, la principal motivación se resume en facilitar el análisis experimental de deformaciones 3D a la industria mediante el desarrollo de una técnica de bajo coste alternativa a 3D-DIC que permitiera dicho análisis en ambientes industriales.

Previamente a esta tesis se han realizado algunos estudios sobre la unión de 2D-DIC y FP (Weber, et al., 2002), (Tay, et al., 2004), (Quan, et al., 2004), (Barrientos, et al., 2008), (Nguyen , et al., 2011), (Nguyen, et al., 2011), (Siegmann, et al., 2011), (Mares, et al., 2011), (Shi, et al., 2013). Sin embargo no se ha obtenido una alternativa real de bajo coste a 3D-DIC para la medida en tiempo real (de forma dinámica) de desplazamientos dentro y fuera de plano o no tuvieron en cuenta la distorsión de los desplazamientos medidos en el plano debido a los desplazamientos fuera de plano necesaria cuando no se emplean lentes telecéntricas como en el caso de Mares, et al. (Mares, et al. 2011). La existencia de esta distorsión se puede entender fácilmente

mediante un ejemplo sencillo usando una de nuestras manos: Si se extiende totalmente el brazo la palma está dispuesta perpendicularmente a nuestros ojos, la palma se observa de un tamaño específico. Si la mano se aproximara a uno de los ojos, la mano parece ser más grande. Este efecto es percibido también por 2D-DIC midiendo desplazamientos radiales en 2D, cuando en realidad no se están produciendo.

Por lo tanto, el objetivo de esta tesis es el desarrollo de una alternativa a 3D-DIC de bajo coste para la medida de desplazamientos dentro y fuera del plano mediante la combinación FP y 2D-DIC y que sea adecuada para el uso en un entorno industrial. Además, la metodología debería permitir el estudio de eventos estáticos y dinámicos, incluso a alta velocidad, y llegar a un nivel de precisión comparable a 3D-DIC.

Para llevar a cabo la presente investigación, el trabajo se ha dividido en cuatro áreas principales. La primera de estas áreas es el análisis crítico exhaustivo de anteriores investigaciones con el fin de averiguar las metodologías más apropiadas para alcanzar el objetivo propuesto y estudiar las posibles fuentes de error en la integración de la FP y 2D-DIC. Un segundo paso es desarrollar una completa y novedosa metodología para unir ambas técnicas y resolver los errores observados en estudios anteriores incluyendo una sencilla pero robusta metodología de calibración del montaje experimental. El siguiente paso es validar la integración de técnicas mediante experimentos controlados y seguidamente evaluar los resultados obtenidos. Por último, el cuarto paso es emplear la técnica propuesta en experimentos en los que se producen grandes desplazamientos en 3D, donde la técnica mostrará su versatilidad, robustez y precisión.

1.3. Organización de la tesis

Para conseguir la integración de FP+DIC, ésta tesis se ha organizado en 8 capítulos.

Inicialmente, en el capítulo 2 se describen los conceptos básicos acerca de algunas de las técnicas ópticas más ampliamente empleadas en mecánica experimental. Estos conceptos se agrupan en tres áreas principales. La primera de las áreas tiene que ver con los fundamentos en los que se basan esas técnicas experimentales, describir sus

objetivos, su clasificación y sus principales características físicas. Posteriormente, se presentan algunos conceptos teóricos generales, su alcance y sus ventajas e inconvenientes. Finalmente se realiza una profunda descripción de los fundamentos de la Proyección de Franjas y Correlación Digital de Imágenes, ya que son la base de la técnica propuesta en esta tesis.

En el capítulo 3 se realiza una revisión del estado del arte de las técnicas de Correlación Digital de Imágenes y Proyección de Franjas. También se realiza un profundo análisis los anteriores trabajos realizados sobre la combinación de ambas técnicas. El objetivo es comprobar la viabilidad y las posibles fuentes de error del método FP+2D-DIC.

El Capítulo 4 describe los equipos y la metodología experimental utilizados a lo largo de esta investigación con una descripción detallada de las metodologías y los componentes del set-up requeridos para integrar Correlación Digital de Imágenes 2D y Proyección de Franjas.

En el capítulo 5 se presenta una metodología para la corrección de los desplazamientos distorsionados medidos por DIC 2D. Como resultado, se establece un método basado en el modelo de lente pin-hole que permite la corrección de dichos desplazamientos distorsionados por los desplazamientos fuera de plano. Se observa que es indispensable una calibración precisa del set-up, por lo que se propone y analiza un completo procedimiento de calibración.

En el capítulo 6 se valida la metodología propuesta en el capítulo 5 mediante cuatro experimentos controlados. Los resultados se compararan con los obtenidos empleando 3D-DIC.

En el capítulo 7, se emplea la técnica propuesta, ya validada, para estudiar eventos en los que ocurren grandes desplazamientos. El estudio consta de la realización de tres experimentos de interés científico e industrial diferentes.

Finalmente, el capítulo 8 realiza una discusión general del trabajo descrito en esta tesis. Por último, también se abordan las principales conclusiones y recomendaciones de trabajo futuro.

Chapter 1. Introduction

1.1. Introduction

In many engineering applications, the measurement of displacements maps in all three spatial directions over the surface of a loaded object is often required, such an example is, structural testing or manufacturing quality control. At present, for this proposes, typically 3-dimensional digital image correlation (3D-DIC) is often used (Sutton, et al., 2009). This technique employs two cameras acquiring images from different viewing angles of the objects while is deformed. The cameras have to be perfectly synchronized and calibrated for both: 3D reconstruction and for tracking each surface element while the deformation occurs. The calibration process of this technique requires acquiring a sequence of several images of a calibration object and a high amount of computational resources.

Alternative technique have been proposed to obtain 3D displacement maps by combining fringe projection (FP) with 2-dimensional DIC (2D-DIC)) (Tay, et al., 2004) (Barrientos, et al., 2008) (Siegmann, et al., 2011) (Mares, et al., 2011) (Felipe-Sesé, et al., 2014). This hybrid technique only requires one camera and a fringe projector.

The main purpose of this thesis is the integration of 2D Digital Image Correlation (2D-DIC) and Fringe Projection (FP) techniques for 3D displacements measurement employing a single camera. To set to this goal, a preliminary study of the basis, field of application, advantages and disadvantages of some of the most common optical techniques employed in experimental mechanics has been developed. As a result of this investigation, it was observed that 3D-DIC is the only technique that measures in- and out-of-plane (3D) displacements and the same time, with the additional advantage that it could be employed for a wide range of applications, in either static or dynamic conditions. However, one of the main disadvantages of the 3D-DIC is that it requires a stereoscopic system (with a minimum of two cameras) and a complex calibration

procedure. All these imply a significant increase of the equipment cost especially notorious for the study of dynamic problems. Moreover, 2D-DIC and FP are two well-known techniques with a wide range of applicability and sensitivity, but they are limited to only in- and out-of-plane displacement measurement respectively. However, both of them have a similar experimental set-up (one camera placed perpendicular to the reference plane). Thus, the simultaneous integration of both techniques for in- and out-of-plane displacement measurement would decrease the cost and the complexity of the set-up and the processing in contrast with 3D-DIC.

The integration of 2D-DIC and FP would be able to solve the restrictions of both techniques individually. Nevertheless it has not been found any specific methodology for the integration of the FP and 2D-DIC that can be employed as a possible alternative to the 3D-DIC for 3D displacement measurement. There exists in the literature studies about this integration of techniques, but in none of the cases an explicit way of measuring 3D displacement has been developed.

The experimental set-up required to integrate both techniques has been also studied. The basic set-up consists on one RGB camera perpendicularly placed over the referenced surface and a LCD projector placed obliquely to the optical axis of the camera. The projector projects a vertical fringe pattern over the tested specimen previously painted with a speckle pattern. To separate fringes and the speckle, a RGB colour encoding system has been adopted. In addition, the measured in-plane displacement require a special correction if telecentric lenses are not employed. For this reason, it has been performed an optical analysis based on a pin-hole model of lens. The result is a mathematical relationship which allows correcting the distortion of those displacement measured by 2D-DIC.

The whole system needs to be calibrated and aligned perpendicular-to-reference plane. Thus, a calibrating/alignment methodology has been developed using a laser pointer and a micrometric lineal movement platform.

The integration of both techniques has been experimentally validated. In all the cases, results were compared with those obtained with 3D-DIC showing a high level of agreement, highlighting the potential of FP+2D-DIC as a low cost alternative to 3D-DIC technique.

1.2. Motivations and aims of the research

The motivation for this research emerged from the hypothesis highlighted from previous research from Siegmann, *et al*. (Siegmann, et al., 2011) who demonstrated that is possible to perform FP and 2D-DIC simultaneously employing a single colour camera. Thus, the main motivation is to bring the experimental study of 3D deformations closer to the industry by developing a low-cost alternative technique to 3D-DIC which should be suitable to be used in a hard environment.

Some approaches joining 2D-DIC and FP have been previously performed (Weber, et al., 2002), (Tay, et al., 2004), (Quan, et al., 2004), (Barrientos, et al., 2008), (Nguyen , et al., 2011), (Nguyen, et al., 2011), (Siegmann, et al., 2011), (Mares, et al., 2011), (Shi, et al., 2013). However they could not obtain an actual low cost alternative to 3D-DIC to measure in-plane and out-of-plane displacements in real time (dynamically) or they did not consider the in-plane displacements distortion due to out-of-plane displacement when telecentric lenses were not employed as in the case of Mares, *et al*. (Mares, et al., 2011). The presence of this distortion can be easily understood with a simple example using one of our hands: If the arm is extended and palm is disposed perpendicular to our eyes, the palm is observed of a specific size. If the hand approximates to one of the eyes, the hand seems to get bigger. This effect is also occurring with 2D-DIC showing radial in-plane displacements, when in fact they are not occurring.

The aim of this thesis is to develop a low cost alternative to 3D-DIC suitable for using in an industrial environment by combining FP and 2D-DIC for the measurement of real in-plane and out of plane displacements. In addition, the methodology should enable the study of static or dynamic events, even at high speed, and reach a comparable level of accuracy to 3D-DIC.

To perform the current investigation, the work has been divided into four main areas. The first of these areas was the exhaustive critical analysis of previous approaches performed in order to find out the more suitable methodologies to reach the proposed objective and study the possible errors in the integrating of FP and 2D-DIC. A second

step is to develop a complete new methodology to join both techniques and solve the errors observed in previous approaches by a proper calibration of the set-up. The next step is to validate the proposed procedure during controlled experiment and evaluate the results. Finally, the fourth step is to apply the proposed technique to experiments where large 3D displacements occur and where the technique could show its versatility, robustness and accuracy.

1.3. Scope of this thesis

To achieve the integration of FP+2D-DIC, this thesis is organized into 8 chapters.

Initially, chapter 2 describes the basics about of some of the most extended optical techniques employed in experimental mechanics. These concepts are grouped into three main areas. The first of the areas is concerned with the fundamentals of the experimental techniques, describing their aims, classification and their main physical features. Subsequently, some general theoretical concepts are presented, their scope and their advantages and disadvantages. Finally a deep description of the fundamentals of Fringe Projection and Digital Image Correlation is presented as they are the basis the technique proposed in the current thesis.

In chapter 3 an analysis of the state of the art in relation to digital image correlation and fringe projection techniques is performed. In addition, previous researches about the combination of both techniques are studied and analysed. The objective is to analyze the viability and possible sources of error of the FP+2D-DIC method

Chapter 4 describes the equipment and methods employed throughout the course of this investigation with a detailed description of the set-up components and methodologies required to integrate both techniques.

In chapter 5 a methodology for the correction of the distorted in-plane displacements measured by 2D-DIC is presented. As result, a method based on the pin-hole model which correct in-plane displacement distorted by out-of plane displacements is

adopted. Moreover, a set-up calibration is compulsory, so a complete calibration procedure is proposed and discussed.

In chapter 6 the methodology proposed in chapter 5 is validated by four different controlled tests. Results are compared with those obtained by 3D-DIC.

In Chapter 7, the validated technique is employed to study large displacements events. Thus, three different test of scientific and industrial interest are performed.

Chapter 8 is concerned with an overall discussion of the work described in this thesis. Finally, major conclusions and recommendations for future work are also addressed.

Chapter 2. Theoretical background

This chapter will provide an overview of the working principles of the most commonly used optical methods for strain and displacement measurement. The purpose is to find out what (i.e. what is measured) and how (i.e. conditions needed to perform the measurements) they are applied. This analysis allows establishing an implementation framework for the new proposed optical techniques developed in the present thesis, i.e. where this new technique can be applied and what the advantages and disadvantages will be in using it in the place of other alternative techniques. Since the technique presented in this thesis is the combination of two existing techniques (i.e. Fringe Projection and Digital Image Correlation), a more detailed description of these two techniques is given in order to provide a better insight into the fundamentals which will be required in the following chapters.

2.1. Introduction

The aim of Experimental Mechanics is to observe, discover, verify and explain the mechanical properties of solids. Experimental mechanics is based on testing materials and specimens. It is used, for instance, to find out their real behaviour when subjected to an external load, as validation procedure in the development of theoretical models and numerical simulations or as a starting point for theoretical and numerical studies of new materials and designs (Cloud, 1998), (Sharpe & al, 2008) , (Asundi, 2002). Over the last few years experimental techniques have being significantly developed due to the electronic and digital revolution. Optical based techniques have become especially successful thanks to digital cameras, among other inventions, that allow whole field

measurements and further computer aided digital image processing. Right now, optical techniques are still improving their performance and capabilities due to the technical advances being made (e.g. high speed cameras) and the continuous improvement of computers and data processing algorithms (Sun, et al., 2013).

Experimental mechanics uses different kind of techniques to perform Experimental Stress Analysis. However, stress and strain are not the only engineering parameters of interest, but other related ones, like displacements, from which the desired information has to be inferred. Moreover, some techniques do not provide full-field detection but rather point-wise, like the strain gauges, and some others they can only be applied to specific materials, such as photoelasticity. Another important variable the size and range of deformation to be measured and the sensitivity required. In addition, the cost of the technique may also be an important factor to take into account. Thus, for each specific stress analysis only a few, one or none of the existing techniques may be suitable.

The technique proposed in this thesis is a full-field optical technique and will therefore be compared to similar existing full-field techniques. For this purpose, these techniques will be presented based on what has been measured, the resolution and other aspects like the capability to measure in real time, the required specimen preparation, the environmental influence and the amount of post-processed data .

In optical techniques the information is extracted from a light beam of visible light that either reflects from the specimen surface or, if the specimen is transparent, is transmitted through it. Most of the specimens are not transparent and therefore the obtained information comes only from the specimen surface. Information from inside the specimen can only be obtained by slicing the stress frozen specimen (3D photoelasticity) or by using techniques based on rays or waves that can propagate through the material like X-ray or sound waves (Sharpe & Krishnaswamy, 2008).

Depending on the kind of observed interaction between the light beam and the specimen, it can distinguish between interferometric and intensity based techniques. Interferometric techniques rely on the wave nature of the light that produces interferences when superposed, it takes the form of fringe patterns and is very

sensitive to small specimen deformation (e.g. photoelasticity, holographic interferometer, electronic speckle interferometry and shearography). Intensity based techniques (or non-interferometric techniques) can be explained using simple geometrical optics and are therefore not as sensitive as interferometric technique one but they can still be quite sensitive to very small deformations (e.g. moiré methods, fringe projection, and electronic speckle photography) as well as for quite large deformation (e.g. digital image correlation) having therefore a very large measurements range. Other techniques are based on non-linear interaction between very intense optical beams and the specimen material, like the Raman spectroscopy for measuring micro residual stress (Ferreiraa, et al., 2003), (Schadler & Galiotis, 1995), but these are still point-wise measurements and will therefore not be considered here.

Another interesting full-field technique is thermoelasticity which measures temperature variation from a cyclically loaded specimen. The temperature variation measured on each pixel is proportional to the local volume variation of the specimen, which is directly related to the sum of the principal stresses. Thermoelasticity is an considered as optical technique, although the wavelengths of the detected infrared rays are quite over the visible light for which special lenses and a detector must be used.

The following paragraphs will provide a brief description of digital photoelasticity, electronic speckle photography and interferometry. Techniques based on Moiré will be presented, paying special attention to Fringe Projection and Digital Image Correlation techniques.

2.2. Optical methods in experimental mechanics.

In this epigraph, the most commonly used optical techniques for strains and displacement measurements will be presented in order to establish their implementation framework.

The theoretical bases of most optical techniques for stress/strain measurement were developed theoretically before 1980´s; however, the delivered data was not easy to interpret, not yet being suitable for industrial applications. There was still a need to further process the acquired data and display quantitative information in a manner that was best suitable for the problems being solved. With the advances in technology and the decrease in costs, the industrial implementation and the general use of these experimental techniques has become more common. Nowadays most optical techniques, even the most sensitive ones, have been constructed in compact, robust, portable and relatively easy to handle equipment that includes quite complex data processing algorithms in order to provide suitable information for engineering applications.

2.2.1. Digital Photoelasticity

Current photoelasticity techniques, (known as digital photoelasticity), provide full-field reliable information about principal stress/strain differences ($\sigma_1-\sigma_2$ or $\varepsilon_1-\varepsilon_2$).

Photoelasticity can be classified as an interferometric technique since it relies on the interference between light waves travelling through a transparent specimen. The specimen is a slice with uniform thickness and it may have certain strain distribution due, for instance, to an external applied load. The flat surface of the specimen is illuminated with a light with a known state of polarization. The stress/strain within the specimen will then produce a change in the state of polarization of the transmitted light. For each surface element, the light beam, when transmitted through the specimen, can be divided into two waves following the same path but one oscillating in the direction of maximum stress/strain (σ_1) and the other one oscillating in the direction of the minimum stress/strain (σ_2, which is perpendicular to the previous one). These two perpendicularly oscillating waves travel at different speed according to the amount of stress/strain suffered by the specimen in the respective perpendicular directions. Thus, when the two waves are combined again into one, they interfere either constructively (when the two waves have no phase difference), destructively (if the phase difference is pi) or somewhere in between. Then

constructive interference produces a maximum intensity value when impinging on a digital camera, while minimum intensity value will be observed for destructive interference. For each phase difference in between a specific grey level is measured. The relation between the phase difference also called relative retardation (δ), and the principal stress/strain differences can be expressed as:

$$\boldsymbol{\sigma_1 - \sigma_2 = \frac{f_\sigma}{2\pi h}\delta} \qquad \text{Eq 2.1}$$

$$\boldsymbol{\varepsilon_1 - \varepsilon_2 = \frac{f_\varepsilon}{2\pi h}\delta}$$

Where the material fringe value (f_σ for stress, f_ε for strain) is a material property material for a given wavelength (typically 546.1 nm) and h is the specimen thickness.

This constructive and destructive interference occurs for each wavelength of the used light beam in different places. When monochromatic light is used a typical fringe pattern consisting of dark and bright fringes where each grey level refers to a specific relative retardation which is obtained between –π and π (i.e. wrapped). When white light is used fringes appear with different colours, In this case each specific colour indicates a specific relative retardation Figure 2.1.

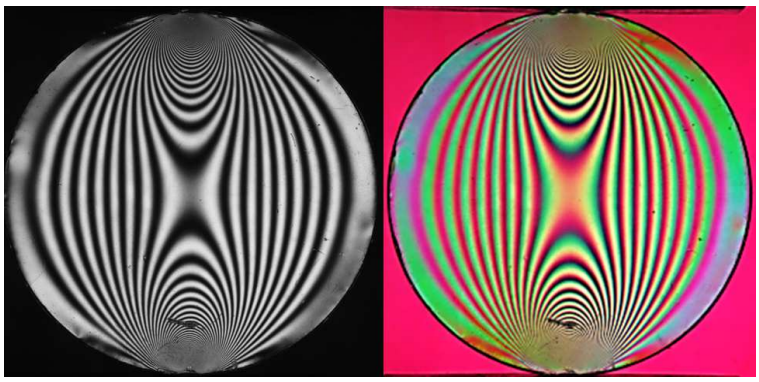

Figure 2.1 Fringe pattern of a polycarbonate compressed disc, illuminating the model: monochromatic light (left), white light (right)

Photoelasticity can be applied either in transmission (the specimen has to be made with a birrefringent material) or in reflexion where measurements are made over a

sheet of photoelastic material (photoelastic witness coating) glued to the specimen surface. Thus, the specimen deformation is transmitted to the photoelastic coating.

The sensitivity of the technique depends on how the induced stress/strain which affects the relative retardation between the two perpendicularly oscillating waves. This phenomenon is known as induced birefringence and special photoelastic material has to be used in order to achieve either high sensitivity or a large range of stress/strain since the material has to be deformed within the elastic zone.

Summarizing, some main advantages of Digital Photoelasticity are the following.

- It can be employed to measure important mechanical features, i.e. the principal stress/strain differences and their direction.
- It is robust and offers very reliable measurements.
- It can be used for real time or dynamic measurements (using a poleidoscope) (Patterson & Wang, 1998).
- If real time or dynamic measurements are not required, the experimental set-up does not require expensive optical components that need to be precisely arranged.

Some main disadvantages of photoelasticity are:

- It requires a complex specimen preparation, i.e. the specimen has to be replicated or coated with a photoelastic material.
- It requires post-processing of the acquired fringe pattern in order to obtain the continuous map of principal stress/strain differences.

2.2.2. Electronic speckle photography and interferometry

If the specimen surface is not ideally specular, it will have a certain roughness level. Therefore, when the surface is illuminated with a coherent laser beam, slight phase differences will appear between illuminated and reflected beams (according to

Huygens-Fresnel's principle (Huygens, 1690)). The result is a randomly grainy pattern of bright and dark dots known as laser speckle. The size of the individual speckle depends on the numerical aperture of the illumination or viewing system. In "electronic" speckle methods the specimen surface is observed by a digital camera using a lens and a matrix sensor (mainly a CCD) with a certain pixel size. The size of the pixel has to be equal to or smaller than the speckle size which is typically in the range of 5 to 50 μm.

The speckle pattern does not change as the surface is displaced; thus it moves with the specimen. If two equal but displaced speckle patterns are acquired with the camera before and after displacing it, the in-plane displacements can then be tracked and measured by following the speckle movement. This is performed in digital or Electronic Speckle Photography (ESP) (Sjödahl, 1994)

Smaller displacements can be measured by using Speckle Pattern Correlation Interferometry (SPCI) (Cloud, 1998). In this case the speckle pattern should not displace more than a fraction of the speckle diameter. Thus the random phase variation from the scattered wave should not vary significantly, and a fringe pattern is obtained due to in-plane displacements.

In Electronic Speckle Pattern Interferometry (ESPI) (Gan, et al., 2008), the speckle pattern generated by the object beam scattered from the undeformed specimen surface is coherently mixed on a photo detector matrix of a digital camera with a reference beam (or a second object beam also scattered from the specimen surface). The superposition makes the speckle brightness very dependent on the phase difference between the two beams. Thus, a fringe pattern is obtained (although it is usually is quite noisy and presents low contrast) by digitally subtracting the acquired speckle patterns resulting from superimposed beams (undeformed state) from the speckle pattern observed at the deformed specimen surface. This resulting fringe pattern must be high-pass filtered, contrast enhanced and displayed to observe real time the fringes. In addition post-processing must be applied to calculate displacements information in the form of a continuous map from the analyses of the phase change caused by displacements. The displacement direction to which the

system is sensitive (in-plane or out-of-plane) depends on the optical configuration of the experimental set-up. (i.e. for in-plane the two coherent beams interfering on the CCD are scattered from the specimen surface). A commonly employed method for phase extraction is phase shifting (Gan, et al., 2008).

Another commonly used Speckle Pattern Correlation Interferometry is Speckle Pattern Shearing Interferometry (SPSI or shearography) (Sharpe & Pryputniewicz, 2008), where the two coherent beams interfering on the CCD are identical except for the specimen surface zones from where they are scattered: they are slightly displaced from each other (by using a shearing element). The phase of the generated fringes is related to the derivate of the out-of-plane displacement. Since no additional reference beam is needed, the set-up for shearography is much simpler than ESPI. Furthermore, compared with ESPI, shearography is somewhat less sensitive to disturbances from the environment and is more suitable for measurement under industrial conditions. In Figure 2.2.A a typical shearography fringe pattern is shown and in B) it is shown a typical wrapped phase map obtained after processing the fringe pattern in A).

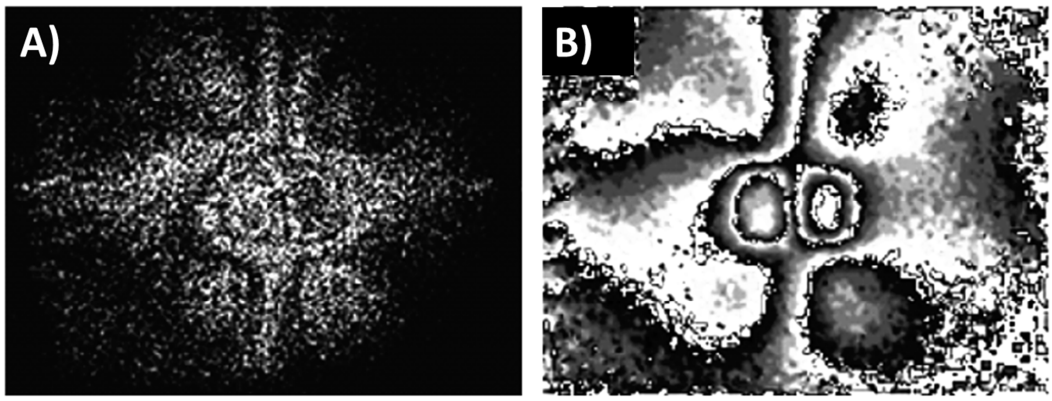

Figure 2.2 Defect revealed using Shearography. Left interference and right phase map

At present, different commercial versions of ESPI and Shearography systems are available in the market. Some of the most relevant features of these systems are:

- They are very sensitive (a fraction of the wavelength of a laser) for small in- and out-of-plane displacements measurements.
- The maximum displacement range is limited by the speckle size.

- They are very sensitive to environmental disturbances.
- These techniques are limited to static measurements due to the necessity of acquiring several images for the same deformation step.
- Minimal specimen preparation.
- Complex and expensive experimental set-up.
- Post-processing required to obtain continuous displacement maps.
- Not suitable for large surface areas.

2.2.3. Thermoelastic Stress Analysis

Thermoelastic Stress Analysis (TSA) is a technique which measures the small changes in temperature at the surface of a specimen and, from them; the first invariant of the stress tensor is obtained.

The theory of thermoelastic stress analysis is based on the laws of thermodynamics. When an element is subjected to tensile stress, its temperature of that element decreases and conversely when it is subjected to compressive stress its temperature increases. Hence, when that element is cyclically loaded, at enough frequency to achieve adiabatic condition, a temperature change can be measured and related to the change in the sum of principal stresses to Eq 2.2.

$$\Delta T = S\,\Delta(\sigma_1 + \sigma_2) \qquad \text{Eq 2.2}$$

Where S is the thermoelastic constant, which depends on the material; ΔT is the temperature change observed at the specimen surface and $\Delta(\sigma_1 + \sigma_2)$ is the change in the sum of principal stresses. The loading frequency must be fast enough to achieve adiabatic conditions, so heat transfer through the element studied can be neglected. The specimen preparation consists on applying a thin layer of matt black paint to ensure uniform surface emissivity.

The temperature change is measured using an infrared detector which computes the thermal emission from the specimen surface. However, the detector also collects the infrared radiation coming from other undesired sources as the background radiation or reflections. This problem is solved by using a reference signal with the same frequency as the applied loading. This signal is employed to extract only the information due to the thermoelastic effect (Diaz-Garrido, 2004).

The minimum temperature sensitivity reported for the photondetectors is 0.001◦C. Thus, with this temperature resolution, the available strain sensitivity will depend on the material properties. For the particular case of steel, the strain sensitivity is 3.5 µstrains (Greene, et al., 2008).

Some of the most significant features of TSA technique are the following:

- High sensitivity and accuracy
- Minimal environmental disturbances.
- Dynamic events can be measured as long as adiabatic conditions are ensured.
- Minimal specimen preparation.
- Simple experimental set-up, but very expensive.

2.2.4. Techniques based on the Moiré effect

Moiré effect is the optic consequence of constructive and destructive interferences of the light that passes through two grids (Cloud, 1998). These techniques are intensity based optical methods since the interference is due to pure geometric light obstruction and not to wave interferometry. Hence, in general it is not as sensitive as interferometric techniques. Nevertheless, the effect is similar as interferometric techniques since a fringe pattern is obtained. From that fringe pattern the relative grid displacement can be inferred.

Examples of Moiré effect are shown in Figure 2.3. In Figure 2.3.A two identical grids are placed one above the other so that their gaps coincide. If one of the grids is slightly rotated with an angle alpha it will produce the intensity pattern of the transmitted light shown in Figure 2.3.B, where oblique fringes are appreciated. These fringes are examples of Moiré's Fringes and their frequency is very sensitive to the rotated angle (if alpha increases the fringe period decreases).

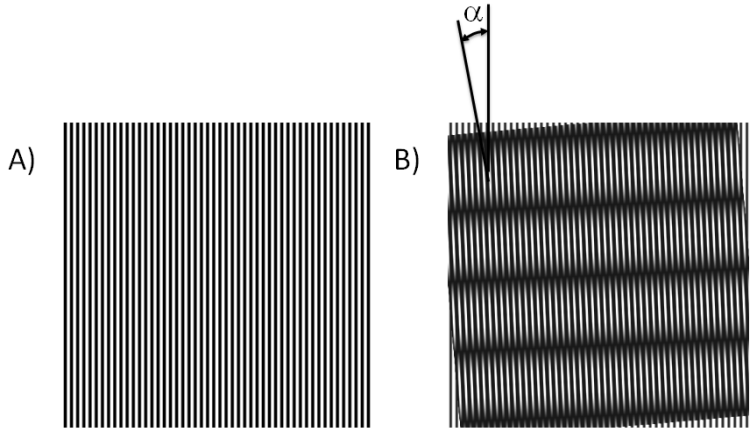

Figure 2.3 Basics of Moiré effect. A) Two superimposed vertical grids B) Upper grid rotated respect the bottom one

The most common Moiré effect based techniques are the Geometric Moiré, Shadow Moiré and Projection Moiré which are presented in next epigraphs.

2.2.4.1 Geometric Moiré

Geometric Moiré is a technique that provides in-plane displacement from Moiré Fringes. Figure 2.4 schematically illustrates the principle behind geometric Moiré technique. From Figure 2.4 it can be concluded that a full cycle of Moiré fringe is created when n grid lines are compressed to fit the space of n-1 pattern grid lines.

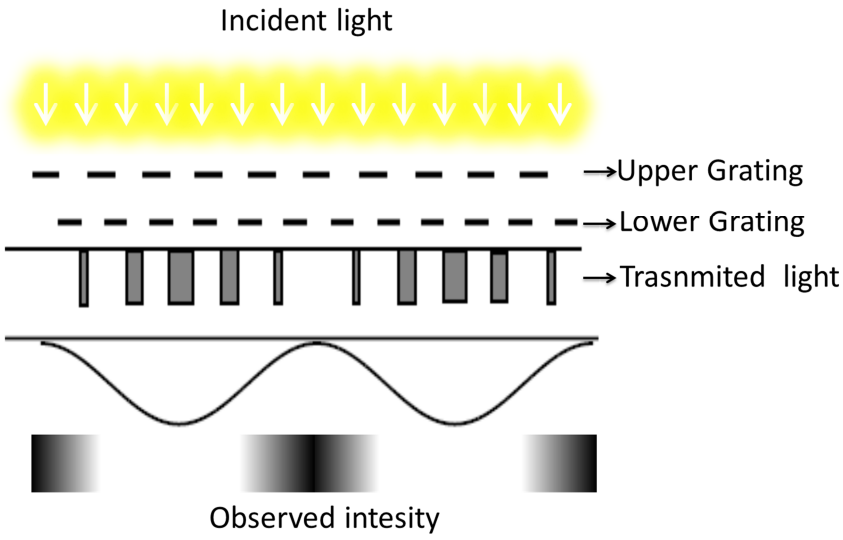

Figure 2.4 Schematic illustration showing the physical principle of geometric Moiré technique

It can also be noted that the same Moiré Fringes are created when *n*-1 grid lines are stretched to fit the space of *n* grid lines. Hence, the fringe pattern is generated due to the interference between a grid attached to the specimen (or impressed on it) and another placed over the specimen. Fringes provide information about the displacement in the direction perpendicular to the grid. In addition, information is provided in the form of steps, thus, to obtain a continuous displacement map the extracted information has to be interpolated.

Historically, the observed fringe pattern was manually operated into displacements maps. Nowadays, numerous automatic methodologies have been proposed such as the Gabor strain Segmentation (Asundi, 2002).

2.2.4.2 Shadow Moiré

Shadow Moiré is a variant of Geometric Moiré and provides out-of-plane distance (Cloud, 1998). This technique is based on the interference of a grid placed over a tested specimen and its own shadow when illuminated at a certain angle α as is illustrated in Figure 2.5. The interference will show a fringe pattern that encodes the distance between the specimen and the grid.

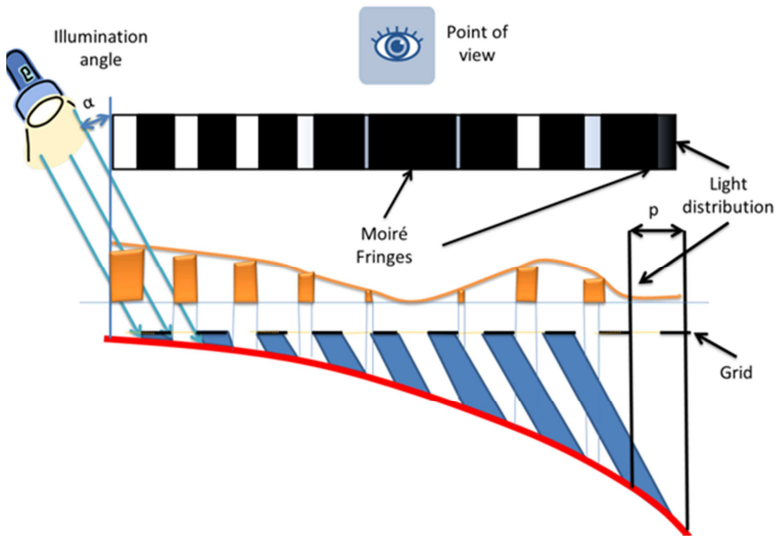

Figure 2.5 Schematic illustration showing the basis of Shadow Moiré Technique

This technique also needs an interpretation to transform the fringe pattern into distance from the specimen to the grid.

2.2.4.3 Projection Moiré

Projection Moiré is an alternative technique to Shadow Moiré based on the Moiré effect which provides out of plane displacements. This technique provides big improvements with respect to the Shadow Moiré, making it more versatile (Cloud, 1998).

The procedure involves projecting a grid onto the studied specimen and capturing an image of it in its reference state (*S* in Figure 2.6). After that, the specimen is deformed (*S* deforms into *S'* Figure 2.6). The shape of the projected grid will be different from the previous state, and another image is captured. If the two captured images are superimposed, Moiré Fringes will appear encoding the out of plane displacements.

In contrast (to Shadow Moiré), Projection Moiré provides a complete fringe map encoding the displacements *Z*- direction (*w* displacement) between two states of deformation. Hence, Projection Moiré is more useful for measuring out of plane displacement or differences in shape.

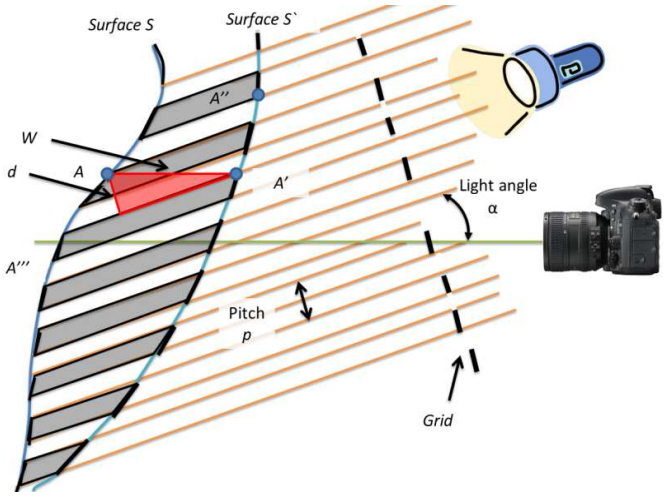

Figure 2.6 Illustration showing the fundamentals of projection Moiré

2.2.4.4 Conclusions about Moiré based techniques

From the previous analysis of techniques based on Moiré effect, the following conclusions can be extracted:

- Geometric Moiré allows measuring in-plane displacements, while Shadow Moiré and Projection Moiré are employed to measure out-of-plane displacements or shapes.
- The field of application and accuracy of Moiré based techniques is very flexible. The technique accuracy strongly depends on the pitch of the grid.
- Geometric Moiré requires one grid attached to the specimen. Thus, the specimen preparation is relatively important.
- In Shadow Moiré it is necessary to have always the grid in contact with the specimen.
- A common drawback for the three techniques is that a map of fringes is achieved; with discrete values depending on the fringe order.

2.3. Fringe Projection

The principle that underlies Fringe Projection (FP) is, in fact, the same as Projection Moiré; Parallel fringes are projected over the specimen surface to infer the out-of-plane displacements due to shape changes or surface deformation. But in FP the fringes before and after surface deformation are not superimposed to generate Moiré Fringes, they are analysed in a different way to extract a continuous map of out-of-plane displacements.

The principle of FP was first proposed by (Takeda & Mutoh, 1983) and (Srinivasan, et al., 1985). As shown in Figure 2.7.A, parallel straight and equidistant fringes are projected over the specimen surface with a non-cero incidence angle (α).Fringes have to be perpendicular to the incidence plane. Projected fringes are viewed by a camera placed perpendicular to the specimen surface. If the surface is completely flat (reference surface) then fringes are straight with a certain pitch value *p* (Figure 2.7.B). Furthermore, the intensity profile across the projected fringes has to be sinusoidal. When the specimen surface is displaced out-of-plane, then the projected fringes viewed by the camera move accordingly to their oblique incidence angle as illustrated in Figure 2.7. B. Since fringes have a sinusoidal profile, their displacement can be measured as a phase shift (ϕ) which is related to the-out-of plane movement (*Z*-) as follows:

$$\boldsymbol{z = K_f \phi = \frac{p}{2\pi\, tan\alpha} \phi} \qquad \text{Eq 2.3}$$

Where the K_f is called *fringe constant* with units (mm/rad).

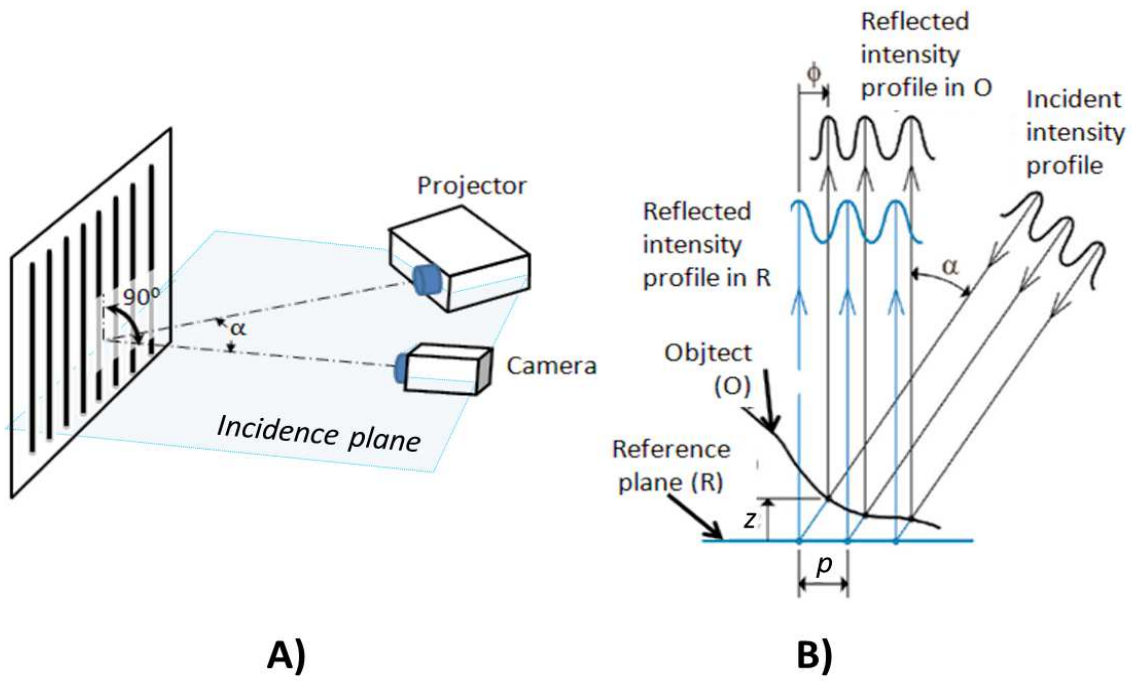

Figure 2.7 A) Fringe Projection schematic set-up. B) Illustration showing the physical principle of Fringe Projection technique

Hence, the idea of projecting sinusoidal fringes is to encode the displacement of the fringes in the phase of the recorded fringe pattern. As an example, Figure 2.8 shows the deformation of the fringe pattern when a cone (Figure 2.8.B) is placed onto a flat surface (Figure 2.8.A).

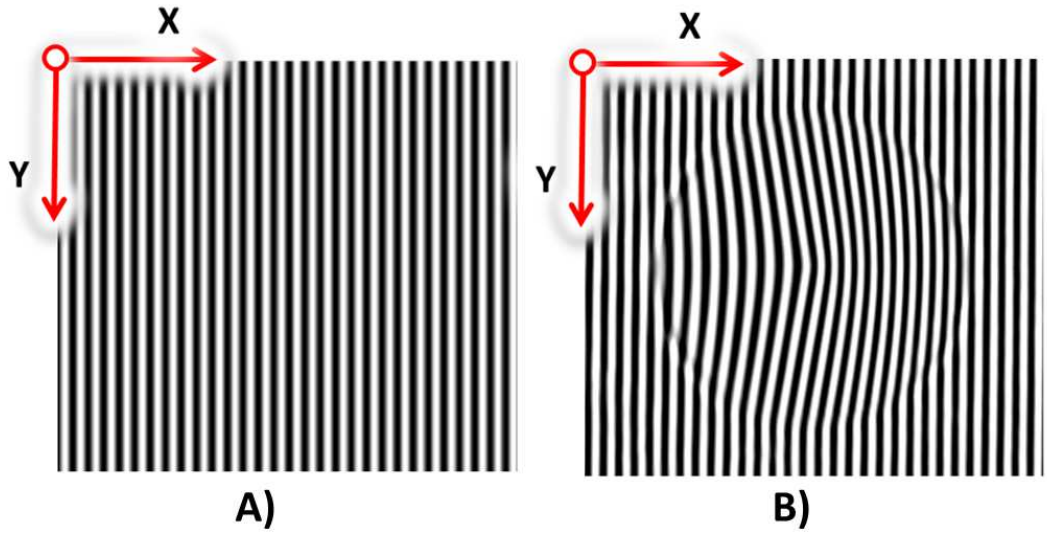

Figure 2.8 Fringe pattern projected onto A) Flat reference plane B) Cone onto reference plane

The intensity profile along the x-direction (perpendicular to the fringes) can then be expressed as Eq 2.4:

$$\boldsymbol{i(x,y) = r(x,y) + b(x,y) \cdot \cos\left(\frac{2\pi}{p}x + \phi(x,y)\right)} \qquad \text{Eq 2.4}$$

Where *r is* the background illumination and *b* is the amplitude. Several methods exist for retrieving the phase from the fringe pattern so that it can be classified into spatial and the temporal (Gorthi & Rastogi, 2010).

Temporal methods (commonly Phase-Shifting methods) perform a controlled variation of the phase of the projected fringes when are captured. Whilst the spatial methods only need two images: the undeformed and the deformed fringe image (Figure 2.9.A)

Since just one image of the deformed fringe pattern is used, the spatial methods will allow extracting the phase during dynamic deformation processes. On the contrary, temporal methods requires several phase-shifted fringe images of the deformed object, therefore, the analysis of dynamic events is not possible. However, the recovery of the phase is more robust and precise, allowing the retrieval of more reliable out-of-plane displacement map than the spatial methods.

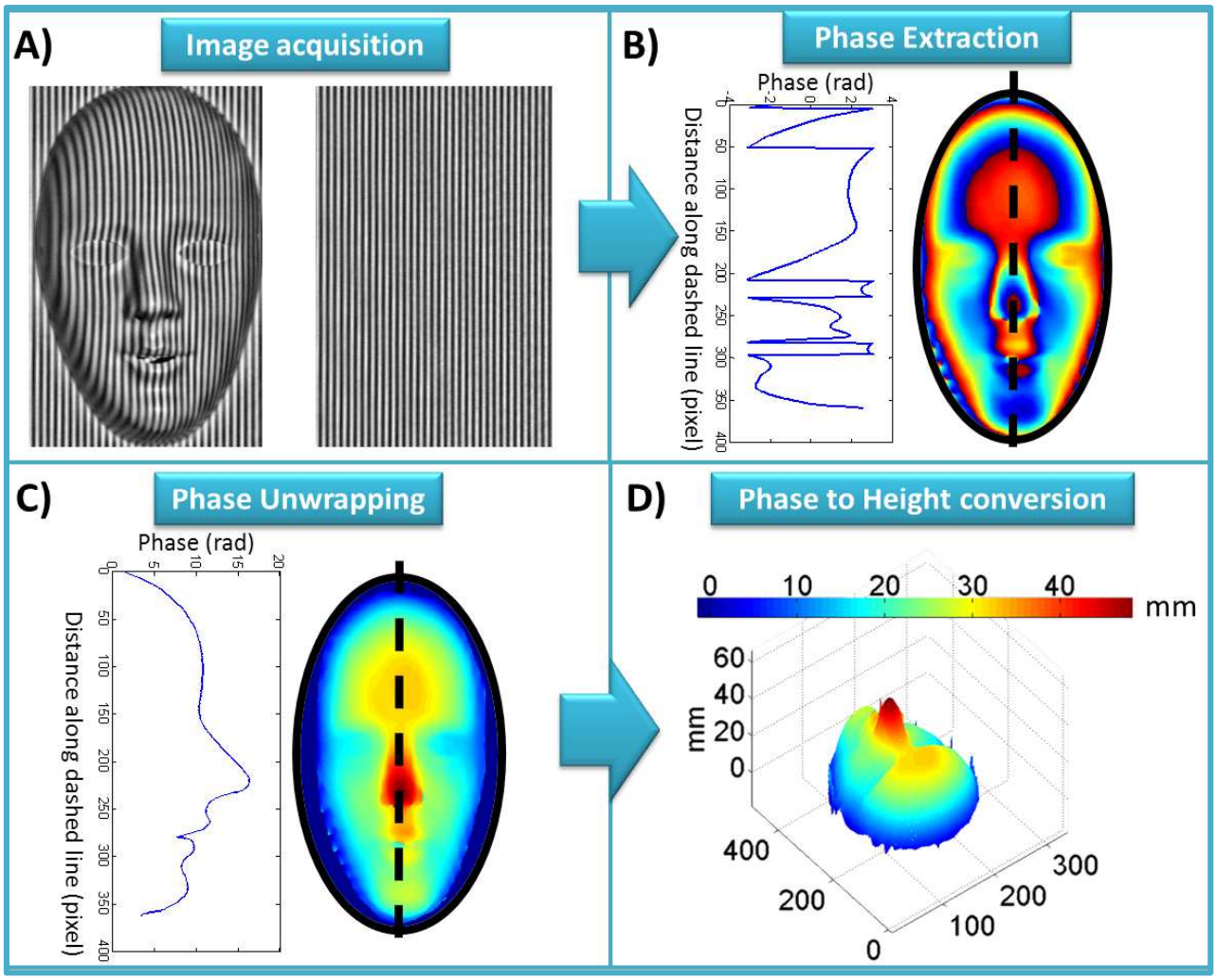

Figure 2.9 Fringe Projection schematic procedure A) Captured images of a mask on a reference flat surface B) Wrapped Phase extraction C) Phase Unwrapping procedure D) Phase to height conversion

Due to the periodic nature of the signal, the retrieved phase using any of the existing methods will be "wrapped". This means that the difference between the maximum and minimum retrieved phase has a value between -π and π. Since the phase difference between the fringes displaced in X- direction is the same as the phase difference between the fringes displaced *x+nP*, with *n*=0,1,2,… It will then produce a discontinuous phase map with phase jumps of 2π called *wrapped phase map* (Figure 2.9.B).

A continuous map of the phase corresponding to a continuous out-of-plane displacement can be obtained using "*unwrapping algorithms*". Again, there are different ways to perform the unwrapping (Ghilia and Pritt, 1998).

As in Moiré techniques, Fringe Projection accuracy depends on the fringe pitch that can still be observed by the camera. From Eq 2.3 it is clear that the sensitivity increases with *p* and the incidence angle (α). These two adjustments allow the FP technique to be very easy to adapt to both sensitivity and required range of displacement, making the technique very versatile. Obviously, factors like the non-sinusoidal intensity profiles of the projected fringes, limited resolution of the digital camera (there is a minimum number of pixels per fringe to represent the senoidal intensity distribution) and non-linear camera response to the incoming light intensity will introduce errors in the fringe displacement retrieval. In addition, using spatial phase retrieval methods, will introduce error will be as high as when using temporal method. Nevertheless an accuracy of 1% of the measured range can been achieved using spatial phase retrieval method (Heredia Ortiz, 2004).

2.3.1. Review of the fundamentals of Spatial Phase Measurement methods

In this epigraph, attention is focused on the spatial procedures developed to obtain out-of-plane displacements maps using a single image, since this will allow performing dynamic studies.

2.3.1.1. Phase Stepping Method

In this epigraph the five-step phase extraction algorithm employed by Heredia, (Heredia Ortiz, 2004) is explained. Based on previous studies on phase measurements (Shough, et al., 1990), Phase Stepping is a multiple-step phase-shift method based on phase shifting methods but in this case the phase shifts is artificially generated on two acquired images: one before the deformation (reference image) and the other after the deformation (test image). It computes two separate maps of phase, one for the reference and the other for the tested image. Figure 2.10 shows an example of these two captured images from a flat reference surface and a cone.

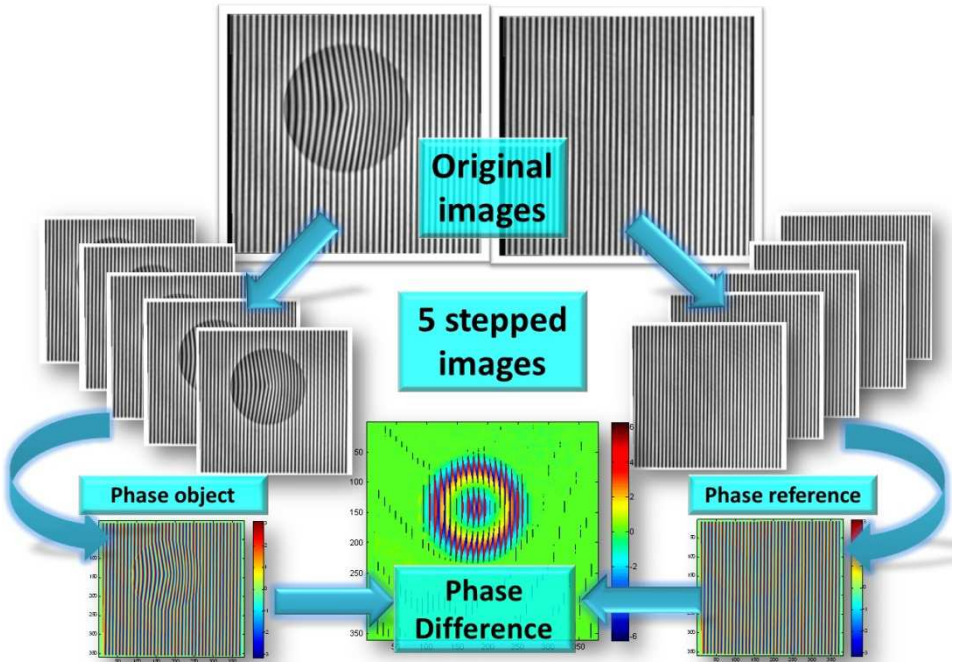

Figure 2.10 Phase Stepping flow chart

The phase estimation is performed from the mathematical description of the intensity distribution of a digitised image collected by the CCD of the camera according to the following equation:

$$\boldsymbol{i(x,y) = r(x,y) + b(x,y) \cdot \cos(2\pi \cdot f_0 x + \phi(x,y))} \qquad \text{Eq 2.5}$$

Where $\boldsymbol{f_0 = \frac{1}{p}}$ **.** The image is virtually shifted along the normal direction to the grid a set of integer fractions values of the pitch (*p*). Thus, intensity distribution obtained will be:

$$\begin{aligned} \boldsymbol{i_1(x,y)} &= \boldsymbol{i\left(x - integer\left(\frac{p}{2}\right), y\right)} \\ \boldsymbol{i_2(x,y)} &= \boldsymbol{i\left(x - integer\left(\frac{p}{4}\right), y\right)} \\ \boldsymbol{i_3(x,y)} &= \boldsymbol{i(x,y)} \\ \boldsymbol{i_4(x,y)} &= \boldsymbol{i\left(x + integer\left(\frac{p}{4}\right), y\right)} \\ \boldsymbol{i_5(x,y)} &= \boldsymbol{i\left(x + integer\left(\frac{p}{2}\right), y\right)} \end{aligned} \qquad \text{Eq 2.6}$$

To estimate the pitch (*p*) of a certain image, a one-pixel row from the reference image is extracted and the 1-D FFT of this vector is performed. Then, the DC component is removed and the main frequency can be extracted, as illustrated in Figure 2.11. To

increase the accuracy of this method it is convenient to repeat the procedure in different rows and to perform the average of the value *p*.

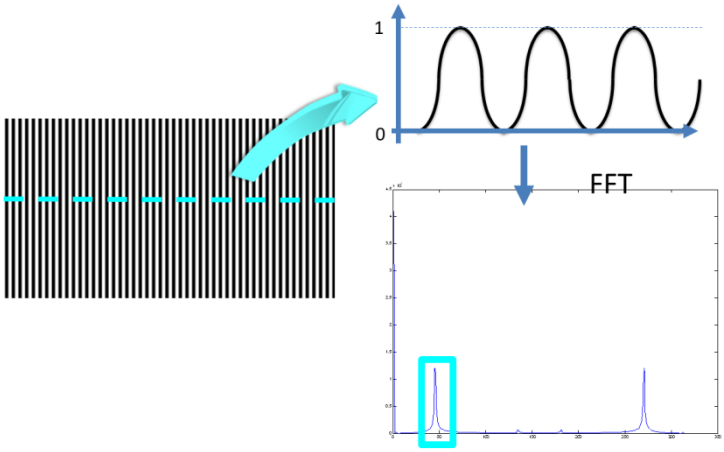

Figure 2.11 Pitch extraction procedure

From the virtually shifted images, the corresponding phase of the processed image is calculated by solving the equation system Eq 2.6 for ϕ as follows:

$$\boldsymbol{\phi(x,y) = arctan\left(\frac{2(I_2(x,y) - I_4(x,y))}{2I_3(x,y) - I_5(x,y) - I_1(x,y)}\right)} \qquad \text{Eq 2.7}$$

The required information is the difference of phase between the reference state and the deformed image, which is obtained by subtracting the estimators calculated from those states:

$$\boldsymbol{\Delta\phi(x,y) = \phi_2(x,y) - \phi_{Ref}(x,y)} \qquad \text{Eq 2.8}$$

This procedure is optimized by taking into account the following assumptions:

The background of the images and the modulated phase slowly vary relative to the carrier frequency.

If the studied element shows changes in the surface that makes the amplitude modulation vary rapidly and the procedure will not work properly.

The accuracy of the method is reduced when very pronounced slopes are present in the surface. This limitation could be solved if the projected pitch is smaller than the size of the discontinuity being measured.

Figure 2.12. A illustrates an example of the wrapped phase for a cone.

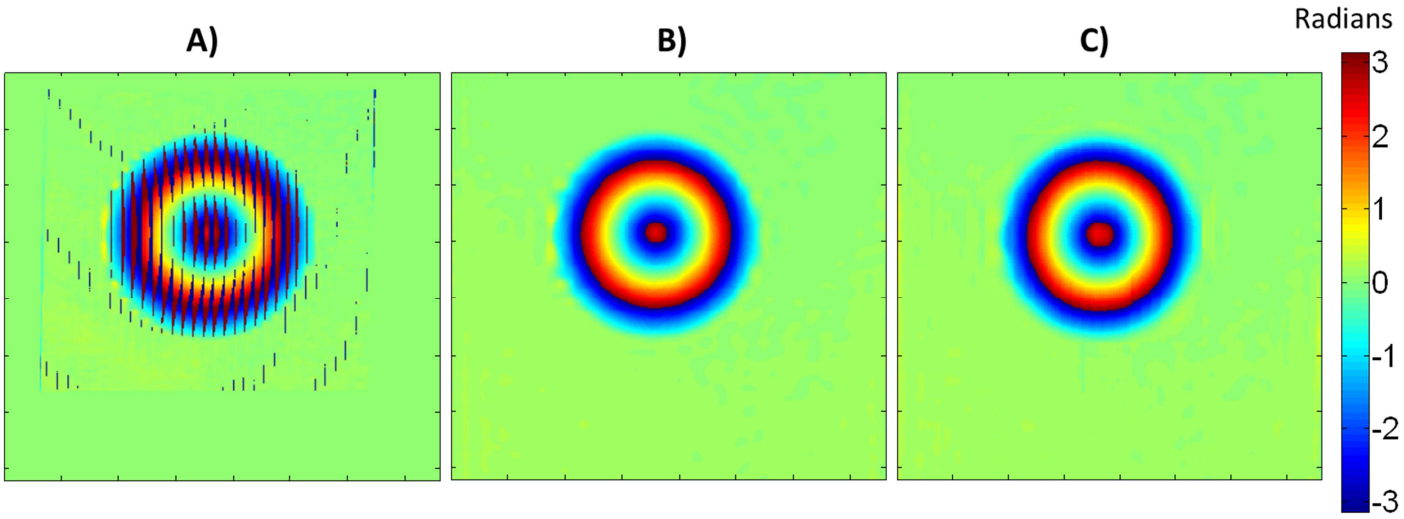

Figure 2.12 Phase calculated using A) Phase stepping B) Fourier Transform Profilometry C) Windowed Fourier Transform

Heredia presented a set of numerical and experimental tests to make an evaluation of the presented method for phase measurements. He concluded three main sources of error (Heredia Ortiz, 2004):

The possibility of random errors due to different uncontrollable elements such as reflections from the surface, noise in the sensor of the camera or dust in the lenses. As the noise increases, the suppression of the calculated phase increases. At a value of noise of 60% the phase is corrupted and introduces errors in the unwrapping procedure. Normally very noise images have a noise below 40%., which could introduce an error of 0,2 radians. This error could be improved using image filtering tools, reducing the error to 0,08 radians.

Some error appears cyclically with the fringe pitch. This source of the error is inherent to the Phase Stepping Algorithm due to aspects like considering constant or rounding the calculated value of pitch (p) or performing rounded virtual phase shifts in the phase extraction. This error increases with the slope of the measured surface up to a

numerically found limit of $2\pi/p$. It was concluded that an error of 0.3 radians could be present cyclically. This error increases drastically if the slope increases the 80%.

Some errors could appear as a result of optic aberration. This effect increases strongly if the specimen is close to the camera. Some correction of perspective could improve this effect.

2.3.1.2. Fourier transformation Profilometry method

Another common spatial method for phase measurement is Fourier Transform Profilometry (FTP) which was introduced by Takeda et al. (Takeda & Mutoh, 1983). As in the Phase Stepping Method, FTP requires only one image of the deformed fringe pattern, which makes real-time and dynamic data processing possible. To study this FTP methodology the intensity of light across the fringe pattern could be represented in exponential mode (Su & Wenjing, 2001) rather than senoidal mode:

For the reference image:

$$\boldsymbol{i_{Ref}(x,y) = r_{Ref}(x,y) \sum_{n=-\infty}^{\infty} A_n \, exp^{i(2\pi n f_0(x) + n\phi_{Ref}(x,y)}}$$

For the studied image:

$$\boldsymbol{i(x,y) = r(x,y) \sum_{n=-\infty}^{\infty} A_n \, exp^{i(2\pi n f_0(x) + n\phi(x,y)}}$$

Eq 2.9

What A_n is a weighting factor in the Fourier Transform.

The first step is to compute the Fourier transform of

Eq 2.9 in order to obtain the Fourier spectra. For illustrative purpose, Figure 2.13 represent the 1-D FFT of a typical senoidal projected fringe pattern. The spectrum is then filtered with a suitable filter function to keep only the fundamental components (blue dashed close section). The inverse Fourier transform is applied to these

fundamental components, and a complex signal is obtained for the reference and the studied image respectively:

$$\hat{\boldsymbol{i}}_{\boldsymbol{Ref}}(\boldsymbol{x},\boldsymbol{y}) = \boldsymbol{A_1 r_{Ref}}(\boldsymbol{x},\boldsymbol{y})\boldsymbol{exp}^{\boldsymbol{i}(2\pi \mathrm{f}_0 \boldsymbol{x}+\boldsymbol{\phi_{Ref}}(\boldsymbol{x},\boldsymbol{y})}$$

Eq 2.10

$$\hat{\boldsymbol{i}}(\boldsymbol{x},\boldsymbol{y}) = \boldsymbol{A_1 r}(\boldsymbol{x},\boldsymbol{y})\boldsymbol{exp}^{\boldsymbol{i}(2\pi \mathrm{f}_0 \boldsymbol{x}+\boldsymbol{\phi}(\boldsymbol{x},\boldsymbol{y})}$$

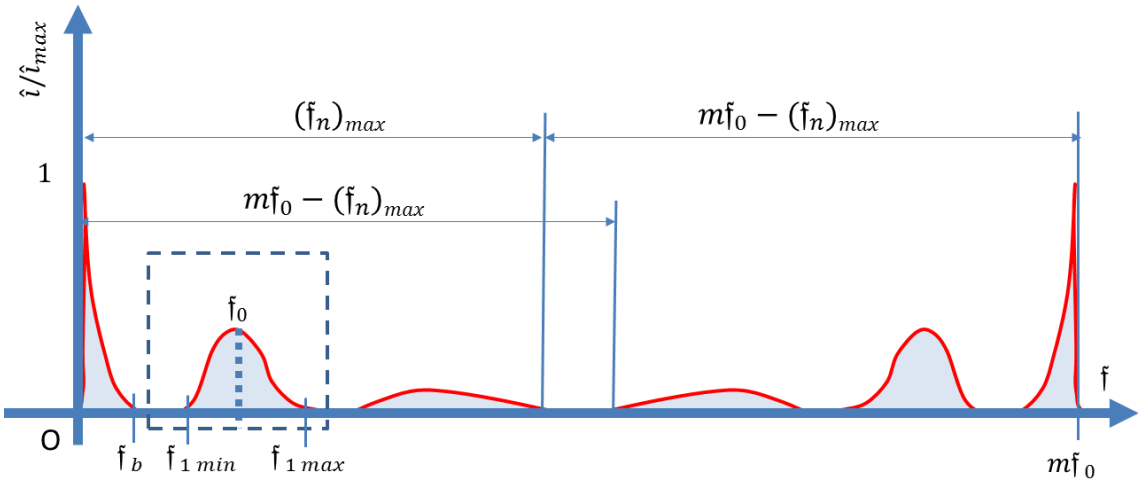

Figure 2.13 Principal component of frequency for phase measurement

The phase difference $\Delta\phi(x,y)$ which varies directly with the height distribution is estimated as follows:

$$\boldsymbol{\Delta\phi}(\boldsymbol{x},\boldsymbol{y}) = \boldsymbol{\phi}(\boldsymbol{x},\boldsymbol{y}) - \boldsymbol{\phi_{Ref}}(\boldsymbol{x},\boldsymbol{y}) = \boldsymbol{Im}(\boldsymbol{log}[\hat{\boldsymbol{i}}(\boldsymbol{x},\boldsymbol{y}) \cdot \hat{\boldsymbol{i}}_{\boldsymbol{Ref}}{}^{*}(\boldsymbol{x},\boldsymbol{y})]) \quad \text{Eq 2.11}$$

The phase of each image could be extracted separately as follows (Huang, et al., 2010):

$$\boldsymbol{\phi}(\boldsymbol{x},\boldsymbol{y}) = \mathbf{tan}^{-1}\left[\frac{\boldsymbol{im}\ \hat{\boldsymbol{i}}(\boldsymbol{x},\boldsymbol{y})}{\boldsymbol{Re}\ \hat{\boldsymbol{i}}(\boldsymbol{x},\boldsymbol{y})}\right] \quad \text{Eq 2.12}$$

However, special care is required in the filtering of fundamental components due to the fact that the Fourier spectra of the deformed fringe pattern usually has multiple components, which can be expressed as

$$f_n = nf_0 + \frac{n}{2\pi}\frac{\partial\phi(x,y)}{\partial x} \qquad \text{Eq 2.13}$$

Consequently, filtering should separate the fundamental components from all other spectra, as represented in Figure 2.13 by dashed square, to reconstruct the image correctly or to avoid some errors due to the frequency sampling (Chen, et al., 1999). The limiting conditions in the filtering process will be:

$$(f_1)_{max} < (f_n)_{m1n}\,, \qquad n > 1$$

$$(f_1)_{min} > f_b\,, \qquad \text{Eq 2.14}$$

$$(f_1)_{max} < mf_0 - (f_n)_{max}\,,$$

Where $m = \left(\Delta f / f_0\right)$

A Gauss distribution filter centred at f_0 with a diameter equal to $2(f_0 - f_b)$ is employed to filter out the rest of the frequencies within the restrictions described in Eq 2.14.

Consequently, the phase variation caused by height modulation must be limited as:

$$\left|\frac{\partial\phi(x,y)}{\partial x}\right|_{max} < \frac{2\pi f_0}{3}\,, \qquad \text{Eq 2.15}$$

Subsequently, designating $Z(x,y)$ the object height measured at a tested point, *d* the distance between projector and camera optical centre, z_0 the distance between reference and optical centre and assuming that $z_0 >> Z(x,y)$, an approximation result is obtained:

$$\phi(x,y) \approx \Delta\phi(x,y) = -\frac{2\pi f_0 d}{z_0} Z(x,y) \qquad \text{Eq 2.16}$$

Combining Eq 2.15 and Eq 2.16 the following expression is obtained:

$$\left|\frac{\partial Z(x,y)}{\partial x}\right|_{max} < \frac{z_0}{3d} \qquad \text{Eq 2.17}$$

That means that FTP can be employed only for surfaces on which the slopes do not exceed the limitation of $\frac{z_0}{3d}$. When the measurable slope of height variation extends this limitation, the fundamental components overlap the zero component and other high components.

Figure 2.12.B illustrates the phase achieved by employing this FTP method for the cone.

2.3.1.3. Windowed Fourier transform method

Windowed Fourier transform is a method for phase retrieval that is based on Fourier Transformation Profilometry. The basis is to perform the phase calculation of an image by studding it block by block independently of the rest of the image. Hence, the phase calculation of an area of the image is not perturbed by the noise present in the rest of it. Therefore, this method is more robust against noise and errors present in the image than FTP. In fact it is based on a fringe map filtering procedure (Kemao, 2007).

The procedure consists of studying the reference and the studied image which is divided into small windows at least twice as big as the minimum pitch of the projected fringes to obtain information related to the frequency of the fringe pattern. Then, Fourier Transformation Profilometry method is performed independently for each area (Figure 2.14).

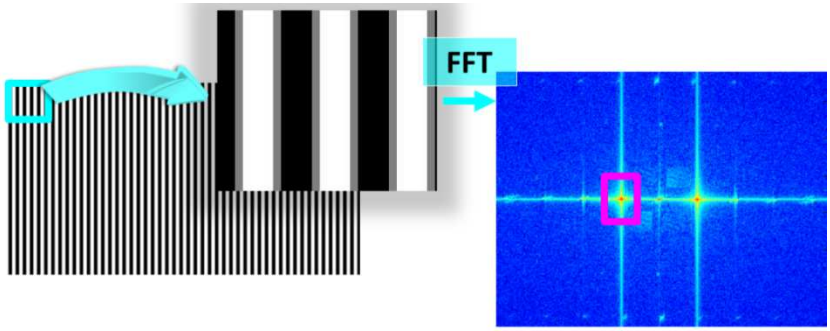

Figure 2.14 Scheme showing the fundamentals of WFT method.

As described by Huang, *et al*. (Huang, et al., 2010), this method improves the results of Fourier Transformation Profilometry. It is easier to achieve the sampling frequency needed in Fourier transformation Profilometry (Figure 2.13) since there is less noise the in Fourier spectrum which may hide the principal frequencies making it more robust and accurate. However, this is a disadvantage, since high computational cost and processing time is required. Thus, this method will be especially useful for noisy images with the limitation of computation time.

For illustrative purposes, Figure 2.12.C shows the phase map obtained by employing the Windowed Fourier Transform method.

2.3.2. Phase Unwrapping

As mentioned before, the phase map provided by spatial methods shows discontinuities due to the impossibility of measuring the phase differences higher than 2π radians in a senoidal signal, as illustrated in Figure 2.15.

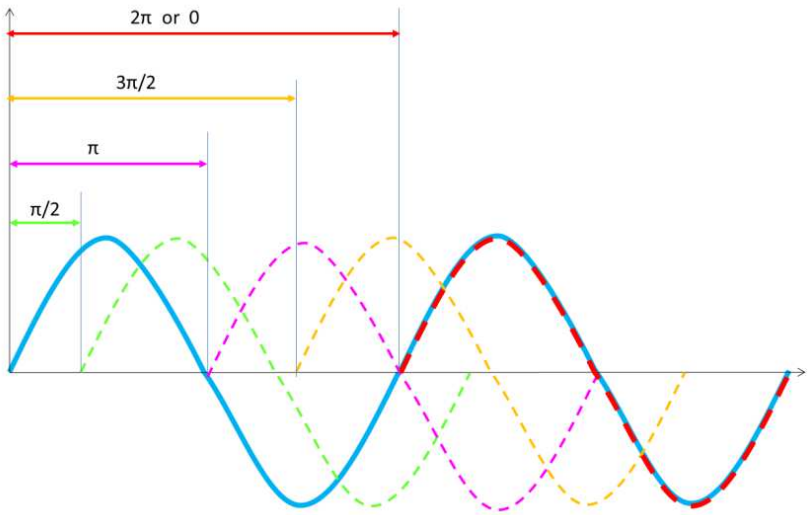

Figure 2.15 Maximum phase difference measured I a senoidal signal

The phase map is therefore wrapped between -π and π and an unwrapping process is needed. This procedure requires the detection of those jumps and the addition of the phase value to reconstruct a continuous phase map as is schematically illustrated in Figure 2.16.

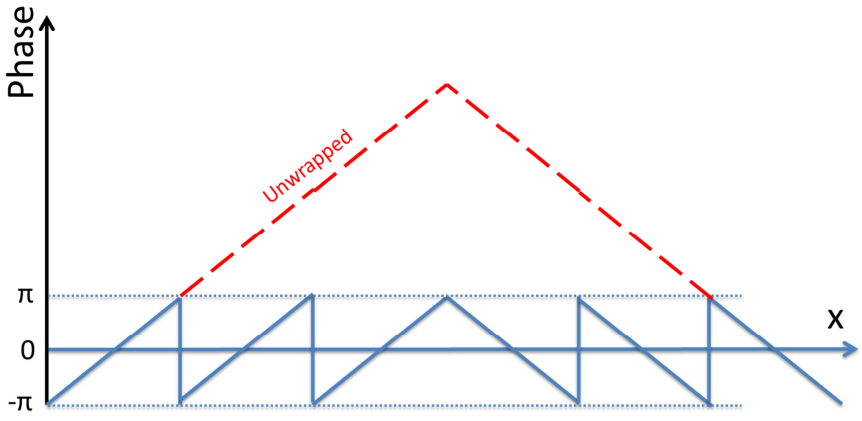

Figure 2.16 Unwrapping scheme

When using real images some noise or aliasing effect is normally present. This may corrupt the phase map, causing the appearance of some errors. When errors exist in the phase, the unwrapping process is a path-dependent process. This means that if the unwrapping process finds an error in the phase map, it will propagate it along the image. Different unwrapping processes have been developed to reduce this effect. A

study was conducted by Ghiglia and Pritt in 1998 (Ghiglia & Pritt, 1998) to review unwrapping methods. It was concluded that two main unwrapping methods exist:

- Path-following algorithms: They determine the best path to follow in the phase map to minimize propagating errors. This is a pixel level operation. They are usually fast but they cannot avoid error propagation.

- Global algorithms: These algorithms make some mathematical operations reducing the differences between the gradients of the wrapped and unwrapped phase maps. It achieves better results but they require greater computational and time cost.

In this Thesis the Quality Guided algorithm (Ghiglia & Pritt, 1998) is employed since it offers a good balance between speed and results (Heredia Ortiz, 2004).

This method requires some measurable characteristic concerning with the quality of the original images or the phase map (known as a quality map). The goal is to process the region where the data is more reliable (where there are no errors) first and then the procedure continues according to the quality of the data. Hence, the errors due to the low quality of the phase map do not affect the high quality areas. Nevertheless, it is important to take into account that if this procedure is performed pixel to pixel along a row of decreasing quality it will be very time consuming. One approach, which makes the process less demanding, is to divide the phase map according to the quality of different stages (Ghiglia & Pritt, 1998). First, pixel groups of a higher quality are processed followed by the unwrapping of groups of pixels of a lower quality, and so on. In this thesis 5 stages of quality were considered (Heredia Ortiz, 2004).

The quality factor used to guide the unwrapping process was the variance of the phase distribution along the phase map. It was presented by Ghiglia (Ghiglia & Pritt, 1998) that the areas of highly varying phase were regions of low quality. Thus a good quality map is that with a small value of variance:

$$\boldsymbol{variance}_{x,y} = \frac{\sqrt{\sum\left(\Delta^{x}_{x,y} - \overline{\Delta^{x}_{x,y}}\right)^{2}} + \sqrt{\sum\left(\Delta^{y}_{x,y} - \overline{\Delta^{y}_{x,y}}\right)^{2}}}{\boldsymbol{k^{2}}} \qquad \text{Eq 2.18}$$

Where the terms $\Delta^{x}_{x,y}$ and $\Delta^{y}_{x,y}$ are the partial derivates of the wrapped phase difference and $\overline{\Delta^{x}_{x,y}}$ and $\overline{\Delta^{y}_{x,y}}$ are the averages values of those derivate in a *k*x*k* window.

After the unwrapping process, Figure 2.17 shows the results of the three different methods reviewed for phase measurement. It can be observed that the results from WFT and Fourier are the best; Phase Stepping also produces similar results but they show a higher level of noise.

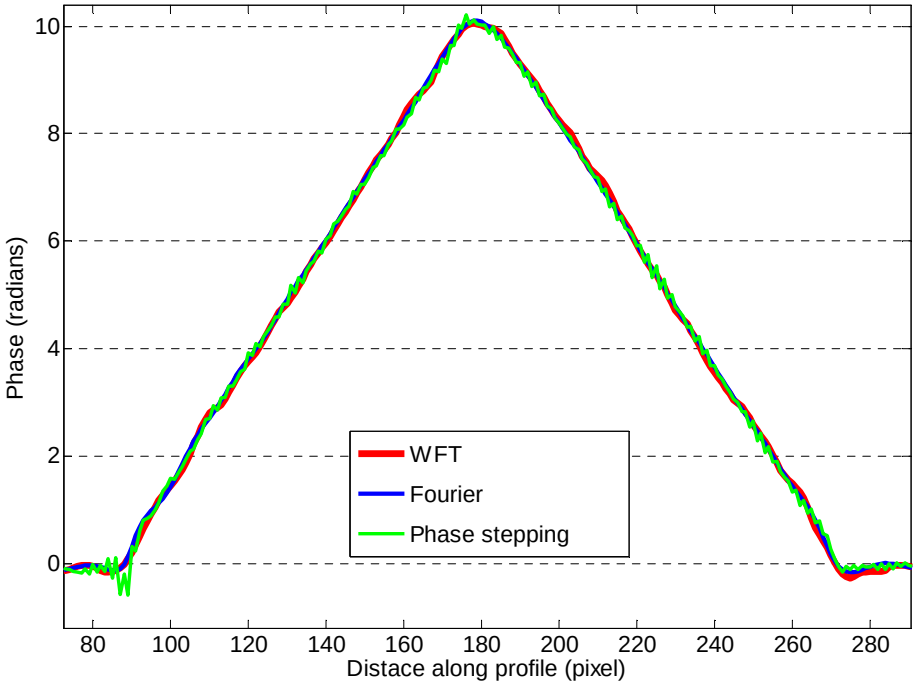

Figure 2.17 Plot showing a comparison of three phase unwrapping methods

2.3.3. Conclusion about Fringe Projection

In this epigraph the most significant features of Fringe Projection technique using a spatial phase retrieval method are summarized.

- It measures out-of-plane displacements with an accuracy of 1% of the measured range.
- The range of displacement is adjustable. Hence, the accuracy varies from a few microns in small specimens to a few mm in large ones.
- It allows real-time measurements (using spatial phase retrieval).
- It is a simple, non-expensive and versatile technique.
- It requires practically no specimen preparation (although white painting for uniform light reflection is advisable)
- WFT spatial phase retrieval achieves good levels of accuracy and low noise; nevertheless, it requires high computational resources.
- Phase-stepping and Fourier Profilometry are well known methods since they offer high level of accuracy, robustness and low computational resources consuming. Nevertheless, especial attention must be paid in frequency sampling since it could affect to shape reconstruction. In addition, Phase-Stepping present more noise in its results.
- Due to PF measures phase difference, an unwrapping procedure is required. Quality guided unwrapping algorithm offers good balance between speed and results.

2.4. Digital Image Correlation

2.4.1. Introduction to DIC

Digital Image Correlation (DIC) is a full-field optical technique for measuring surface displacements. This technique is intensity based and relies on the use of digital cameras and image processing capabilities. In this technique, rectangular groups of pixels of the digital camera represent a single surface element that can be tracked

when displaced. The way each surface element corresponding to each of the cameras pixels is unambiguously identified, is by randomly painting the specimen surface with speckle. Then, each surface element can be identified because the intensity pattern closed around it is unique and will practically not change with surface deformation. This technique, developed in the middle of the 80's ((Sutton, et al., 1983), is quite similar to Electronic Speckle Photography. The only difference is that speckle is bigger since it is generated by physically adding (for example painting) spots onto the specimen surface instead of using laser generated speckle.

When a single camera is used, only in-plane displacements can be measured, this is known as 2D-DIC. A scheme of 2D-DIC is shown in Figure 2.18. Digital images of the undeformed and deformed specimen surface are acquired. Then, each pixel of the image of the undeformed specimen surface is localized on the image of the deformed specimen surface by using an image correlation algorithm. From the difference of the pixel position the in-plane displacement (i.e. on the CCD) is obtained. The real displacement of the corresponding surface element on the specimen surface is obtained by just multiplying the pixel displacement by the lateral magnification of the used lens. By measuring the in-plane displacement, it has to be considered that additional out-of-plane displacement can affect the results (if telecentric lenses are not used) since the lateral magnification will be different depending on the distance between the lens and the specimen surface.

The sensitivity of DIC depends primarily on the lateral magnification of the used lens and the pixel size. It is interesting to point out that digital image correlation algorithms allow the measurement of sub-pixel displacements with a resolution of about 0.1 $\pm$ 0.01 pixel (Sutton, et al., 2009). For the speckle pattern, a good contrast between speckle and background is desirable. The speckle size should be big enough so that the image of the speckle is slightly bigger than the pixel size (if it is smaller a diffuse grey pattern is observed with low contrast).

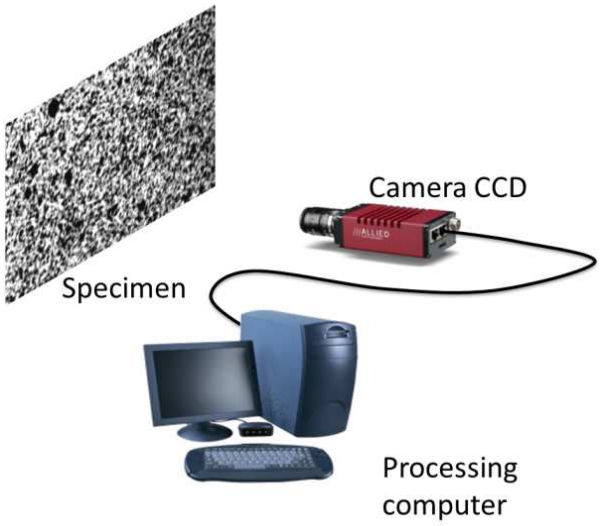

Figure 2.18 Conventional 2D –DIC set-up consisting on a digital camera and a computer.

To measure displacements in the three spatial directions, a second camera is required (Figure 2.19). This is known as 3D-DIC. In this case, for each deformation state of the specimen surface, the pixel corresponding to each of the surface elements has to be identified on the images of both cameras (this implies the application of a first digital image correlation algorithm). These two pixels are called corresponding pixels. Once all the corresponding pixels are localized, a stereo-triangulation is then performed between each pair of them to obtain the three dimensional position of the corresponding element surfaces. The same procedure is performed with the deformed specimen surface (thus, a second DIC algorithm and stereo-triangulation is applied) to obtain the three dimensional positions of the displaced element surfaces. Finally, a third digital image correlation is applied between the images of the undeformed and the deformed specimen surfaces to identify the element surface before and after it has been displaced. Thus, for 3D-DIC two cameras are used and extensive image processing is applied to finally obtain the three dimensional displacement components of each surface element. Furthermore, in order to perform stereo-triangulation, the two cameras need to be calibrated to obtain their relative position and orientation with respect to the specimen surface (up to 6 extrinsic parameters) and up to 5 internal or intrinsic parameters for each camera (focal length, pixel size,…) (Sutton, et al., 2009). The sensitivity and accuracy achieved with 3D-DIC is somewhat lower than 2D-DIC since stereo-triangulation is very sensitive to the calibration parameters that

need to be estimated very precisely and the experimental set-up has to be very stable and carried out very carefully (Sutton, et al., 2009). In addition, the out-of-plane displacement should occur within the depth of field of both used lenses which could be restricted to the depth of field of a single camera.

Figure 2.19 Typical 3D-DIC set-up (Dantec Dynamics)

One big advantage of both 2D-DIC and 3D-DIC is that they can be applied on dynamic processes since only one image for each deformation stage is required. For 3D-DIC when performing dynamic tests it is extremely important to synchronize both cameras so that both images and the same area can be captured at exactly the same instant from two different points of view.

2.4.2. Digital image correlation algorithm

The key point of DIC is the image correlation algorithm that allows the identification and localization of the speckle images and the corresponding pixels.

As shown in Figure 2.20, the DIC algorithm divides the first speckle image (the reference speckle image) into square subsets of size (2*M*+1) x (2*M*+1) with M, an integer number, and a central pixel **P** at position (x_0, y_0), (Pan, et al., 2009). Every subset has a unique intensity pattern within the subset due to the randomness of the speckle pattern. The most similar intensity pattern of this subset in the first speckle image is then searched for in the second speckle image in an area around the same pixel position (x_0, y_0). Once the intensity pattern of the subsets closely coincides

(because of a maximum correlation value *C*) then the displaced pixel **P'** at position (x_1, y_1) is found. The displacement of the pixel is then the difference between the two pixel positions:

$$\Delta x = x_1 - x_0$$
$$\Delta y = y_1 - y_0 \qquad \text{Eq 19}$$

Since two pixel position differences have been subtracted, the displacement has a maximum resolution of a pixel size. Sub-pixel resolution can be achieved by different techniques, for example, by allowing sub-set deformation/rotation or by adjusting a 2D-quadratic surface to the correlation values around the displaced pixel position. Then, the maximum of this surface will give a more accurate displaced sub-pixel position.

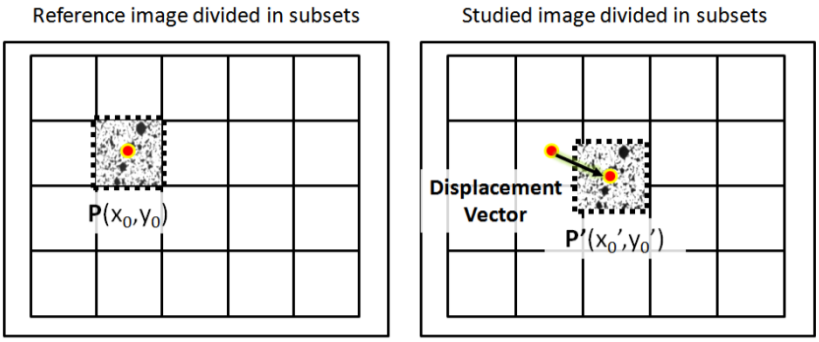

Figure 2.20 Digital image Correlation theory scheme

For 3D-DIC, the basics are similar to the commented procedure; nevertheless, as previously started, it has to be processed by the two cameras and a complex system of 3D coordinates transform matrix will combine the information of the displacement in the three spatial coordinates.

2.4.3. Correlation procedure in 2D-DIC.

Although different definitions of correlation criteria are found in the literature, these correlation criteria can be categorized into two methods, namely cross-correlation

criterion (CC) and sum-squared difference (SSD) correlation criteria (Pan, et al., 2009). At the same time, CC methods are divided into simple Cross-correlation (CC), Normalized cross-correlation (NCC) and Zero-normalized cross-correlation (ZNCC)). Those defined as SSD can be divided into simple Sum of squared differences (SSD), Normalized sum of squared differences (NSSD) or Zero-normalized sum of squared differences (ZNSSD). Pan *et.al* reviewed them and concluded that the ZNCC or ZNSSD correlation criterion offers the most robust noise-proof performance and are insensitive to the offset and linear scale in illumination lighting against simple CC or SSD correlation criterion (which are too sensitive to all lighting fluctuations).

Recently, a universally applicable reliability-guided DIC (RG-DIC) method has been proposed by (Pan, et al., 2010) for the reliable measurement of displacements. In this method, the ZNCC coefficient is employed to identify the reliability of the point computed. This methodology minimized the error propagation as the calculation path is always in the most reliable direction.

This procedure is one of the most robust and consists of firstly defining a region of interest in the reference image. Subsequently, it is necessary to manually or automatically select the first pixel (or subset) to be processed. This is when the algorithm of 2D-DIC starts the automatic quality guide correlation procedure based on performing Zero Normalized Cross Correlation defined as:

$$C_{ZNCC}(p) = \sum_{x \in S} \sum_{y \in S\prime} \left[\frac{[i - i_{ave}] x [i^* - i^*{}_{ave}]}{\Delta i \Delta i^*} \right] \qquad \text{Eq 2.20}$$

Where i and i^* are the grey level intensity at coordinates (*x, y*) in the reference subset (*S*) and the deformed subset (*S'*) respectively, of the reference image and *i** is the grey level intensity at coordinates (x', y') in the target subset of the deformed image. And where $i_m = \frac{1}{(2M+1)^2} \sum_{x \in S} [i]$ and $i^*{}_m = \frac{1}{(2M+1)^2} \sum_{x \in S\prime} [i^*]$ are the mean intensity values of reference and target subsets, respectively. Finally $\Delta i = \sqrt{\sum_{x \in S} [i - i_{ave}]^2}$ and $\Delta i^* = \sqrt{\sum_{x \in S} [i^* - i^*{}_{ave}]^2}$ are normalizing factors of the correlation value to optimize background illumination.

By keeping S still and varying S' in the search window, it calculates the values of ZNCC around the original position of the facet. Finally the maximum value of the ZNCC coefficient is where the centre of the subset S is displaced.

The displacements obtained in x- and y- direction have one pixel resolutions; hence, a sub-pixel resolution procedure should be performed. Several procedures exist for this purpose (Pan, et al., 2009). The one presented by (Hung & Voloshin, 2003) is considered a good balance between speed and accuracy. It consist of a procedure called pick finding though which the nine values of ZNCC obtained around the maximum value are adjusted to a 6 parameter 2D quadratic function. The maximum of the adjusted function correspond to the subpixel displacement and the displacement values are obtained.

After this first operation, this quality guided procedure calculates the displacements with their respective values of ZNCC for the next 4 closest neighbour subsets and continues with that which obtains a higher value of ZNCC. This procedure is repeated until the whole region of interest is processed.

In certain cases, the subset may have heterogeneous deformation. Then, a second-order displacement mapping function, which is capable of approximating more complicated deformation of the deformed subset, should be used and will provide more accurate measurements (Pan, et al., 2007).

Finally, the displacement map achieved by 2D-DIC is offered in pixels units and a conversion to length unit is necessary. Normally this is easily performed by obtaining the Lateral Magnification of the camera-lenses (L) by observing and measuring the distance of two points of the specimen and relating it to the distance in pixels in the image captured for the test.

2.4.4. 3D Digital Image Correlation.

Since 2D-DIC systems are limited to plane elements that experience little or no out-of-plane displacements, 3D-DIC overcomes both limitations by employing two or more cameras observing the surface from different directions. The fundamentals of 3D-DIC to obtain displacement maps are similar to 2D-DIC. The main difference is in the

calibration process (Sutton, et al., 2009). Once the cameras are calibrated, the two flat camera sensors (CCD or CMOS) can determine accurately the three dimensional position by performing respective correlation procedures along the test as is performed in 2D-DIC.

There are two main approaches that are commonly employed to calibrate cameras in a stereo-vision system. One is the independent calibration of the cameras and another is to calibrate all the cameras at the same time (Sharpe & Sutton, 2008). Normally cameras are calibrated by using a calibration grid which presents a certain pattern on it. The procedure consists of the capturing of several images in different positions and the orientation of the grid with one or both cameras, depending on whether the cameras are calibrated independently or at the same time. Then, the shape recognition software can obtain six extrinsic parameters (depending on set-up) and five intrinsic (depending in the set-up properties as are camera, lenses, light). The extrinsic parameters are those which offer the relative position of the cameras and from which the relation of the coordinates in 3 dimensions are obtained. Once the cameras are calibrated, the process for determining three-dimensional positions requires the sensor location at the same point onto the element to be identified in both cameras. After calibration has been completed, the image acquisition process is synchronized so that both cameras acquire images simultaneously during the experiment. This is a very important step if dynamic events are to be studied due to the fact that images captured with both cameras have to represent exactly the same deformation state.

2.4.5. Conclusion about DIC

Some concluding remarks regarding to Digital Image Correlation can be extracted:

- Digital image correlation is an optical technique for in-plane displacement measurement (2D-DIC) or 3D displacements measurement (3D-DIC) when combined with a stereoscopic camera system.

- The maximum achieved sensitivity is not as good as the one achieved by interferometric techniques like ESPI or Speckle Photography, but the range of application is very high (depending on the speckle size, camera resolution and lens magnification).
- The experimental set-up for 2D-DIC is economical and simple. For 3D-DIC the cost increases due to the use of two cameras and their control.
- In both cases the specimen preparation is low. It consists on merely the application of a white matt coating and a random speckle pattern.
- Both DIC techniques require high computation resources, especially in the case of 3D-DIC.
- Both of them are suitable for dynamic tests.
- 2D-DIC is an easy technique but has the main disadvantage that the specimen surface has to be flat if no telecentric lenses are employed.
- 3D-DIC allows the measurement of non-flat specimens. Since two cameras are employed, it requires a complex calibration procedure before performing the test. This calibration requires up to 6 extrinsic parameters in order to locate the cameras respect to the region of interest. In order to obtain those parameters complex artificial vision algorithms must be employed. That calibration procedure decreases the accuracy of the method and increases the technique complexity.
- For 3D-DIC both cameras need to be triggered at the same time, being more complicated in high speed testing since the synchronization of both cameras is crucial.
- The calibration of 2D-DIC is simple and only requires the use of lateral magnification in case there is no optical aberration.

2.5. Concluding remarks

In this chapter several optical techniques widely employed in experimental mechanics have been presented .

Only two of the reviewed techniques namely Digital Photoelasticity and Thermoelastic Stress Analysis provide direct specific information of interest in mechanical analysis as strain or stress. The remaining techniques require further data post-processing in order to obtain stress or strain maps. However, for photoelasticity the specimen has to be made or covered with a photoelastic material, while in thermoelasticity the specimen has to be cyclically loaded.

Moreover, the techniques encompassed in Electronic speckle photography and interferometry offer, with minimum specimen preparation, a high degree of sensitivity but they are applicable only in the micrometric range of displacements.

Techniques based on the Moiré effect are not as sensitive as the interferometric techniques (although they can get close to it) but their measurements cover a much higher displacement range. The preparation of the specimen and their experimental set-up is tedious. Fringe projection on the contrary, measures out-of-plane displacements with almost no specimen preparation and the experimental set-up is very simple. Furthermore, it allows the measurement of dynamic events and the sensitivity and range of displacement can be adjusted by varying the fringe pitch and the angle of incidence of the projected fringes.

Digital Image Correlation can also adjust the sensitivity and the range of displacements by simply varying the lens magnification and the field of view. The specimen preparation and experimental set-up is relatively simple to perform and it can be applied to the analysis of dynamic events. It is important to notice that from all the techniques presented here, 3D DIC is the only one that makes it possible to measure 3D displacements in dynamic events. To perform 3D-DIC a previous stereo-calibration is necessary and two synchronized cameras are used which makes the technique very expensive if high speed cameras are used. 2D-DIC is limited since out-of-plane displacements cannot be measured.

It can be concluded from this analysis that 2D-DIC and Fringe Projection offer complementary information using a similar set-up. Hence, the combination of both techniques could make it possible to obtain in- and out-of-plane (3D displacements) even in dynamic tests by using a single camera and a projector. This will reduce and simplify the computational resources especially when performing high speed testing. This is the main motivation for this research. In the following chapter a more detailed study of those two techniques will be presented and also previous works where different ways of combining these two techniques are reviewed.

The main aim of this thesis is to develop a technique with the following requirements:

- It has to measure both in- and out-of-plane displacements from which the strain maps could be calculated.
- It should allow for the adjustment of the sensitivity and range of displacements in each specific test.
- It should permit high speed displacements.
- Minimum specimen preparation is required.
- It should be portable, robust and easy to handle. It should also be suitable to be used in a non-controlled environment.
- It should be an economical alternative to 3D-DIC.

Chapter 3. Review of the literature

In the conclusions of chapter 2 a new methodology to achieve in- and out-of- plane displacements by combining Fringe Projection and 2D Digital Image Correlation was suggested. In this third chapter, a review of the literature of Digital Image Correlation, Fringe Projection and methods to join both techniques is presented. The analysis performed in this chapter intends to show the difficulties that must be overcome and the advantages of combining these two techniques simultaneously. Finally, some conclusions will be drawn that will help in the development of the proposed technique.

3.1. Introduction

Over the last thirty years Fringe Projection and Digital Image Correlation (2D and 3D) have experienced a notorious evolution becoming widely applied in experimental mechanics for shape, and both in and out-of- plane displacement measurement. A review of the actual capabilities and applications in experimental mechanics employing Fringe Projection and Digital Image Correlation techniques is performed in this chapter in order to determine their current status. Judging from the wealth of knowledge available concerning FP and DIC techniques, their integration seems to be straightforward. It presents an economical alternative to 3D-DIC when obtaining full-field 3D displacement measurements. However, several aspects of the combined technique have to be solved before it can be considered as versatile and accurate as 3D-DIC.

In this chapter different approaches to combine the two techniques will be discussed. Finally, it will be selected the method that it is considered the most adequate for combining the two techniques to measure a wide range of displacements under static and dynamic conditions.

3.2. Techniques fundamentals: FP and DIC

3.2.1. Fringe Projection

The following epigraph provides an overview of the most important material published on Fringe Projection. Finally, some applications of the technique in the industrial environment have been briefly reviewed.

3.2.1.1. Historical review

Fringe Projection was first employed in 1983. Based on Projection Moiré, it was developed as a first attempt for automatic measurement of shape and deformation by computer processing. Up to that moment Projection and Shadow Moiré techniques were the most commonly employed for shape or out-of-plane displacement measurement.

The first approach was developed by Takeda (Takeda & Mutoh, 1983) who implemented a spatial procedure (Fourier Transform Profilometry) which required only one image per studied stage to measure its shape or out-of-plane displacements. They focused on measuring the differences in the phase of the projected fringes and not on Moiré fringes.

After that approach, Srinivasan, *et al*. (Srinivasan,, et al., 1985) proposed a new method to solve possible problems caused by the divergence of the projected fringes in case they were not collimated. Srinivasan, *et al.* developed the first phase shifting algorithm for phase measurement for Fringe Projection based on previous algorithms consisting on phase retrieval (Bruning, et al., 1974).

The set-up employed in Takeda&Mutoh and Srinivasan *et. al*. approaches consisted of a camera placed perpendicular to the reference plane from which out-of-plane displacements were measured and a slide projector placed oblique to the optical axis of the camera. In the first case (Takeda & Mutoh, 1983) the grating employed had a square wave pattern (Ronchi grating)) while in the second (Srinivasan,, et al., 1985) a senoidal pattern was employed. Nevertheless, in both cases the projected pattern was considered a sinusoidal distribution of light.

During the last three decades, Fringe Projection techniques have evolved and have been refined as a result of the advancements in computing software and hardware (Gorthi & Rastogi, 2010). Thus, different designs have been employed ranging, from a hexagonal projection gratings (Iwata, et al., 2008), to colour encoding methods gratings (C. Wust, 1991) (Pan, et al., 2006).

Those advancements have been focused mainly on the development of better phase measurement procedures from which the out-of-plane distance was measured. As it was explained in the previous chapter, there are two main phase measurement procedures, spatial (single-shot) or temporal (multiple-shot). Although temporal methods give highly accurate measurement, they have to be performed on static objects, and therefore they are sensitive to disturbances, such as vibration (Zhang, 2012). This sensitivity could be minimized by the employing a high speed camera and the required equipment to rapidly obtain three phase-shifted fringe pattern images (Zhang, 2010). However, this procedure substantially increases the cost of the set-up. Therefore, since one of the principal interests of this thesis is on dynamic testing, attention will be focused on single-shot spatial procedures.

Until now, several spatial methods have been developed such a case is Fourier transform Profilometry (Su & Wenjing, 2001), the windowed Fourier transform (Kemao, 2007), or the spatial phase-shift algorithm (Heredia Ortiz, 2004) explained in Chapter 2.

These algorithms computes the phase wrapped between $-\pi$ and π, which needs to be unwrapped in order to obtain the continuous 3D shape data. Initially, phase unwrapping is a straightforward task which identifies phase steps greater than 2π and

adds that value. However, the observed deformed fringe patterns may contain noise, large slopes and/or discontinuities, making it difficult the implementation of phase unwrapping methods (Ghiglia & Pritt, 1998).

3.2.1.2. Fringe Projection applications

Since Fringe projection is a technique that allows simple and cost effective measurements of shape and out-of-plane displacements it is widely used in industry and research. In this epigraph, some applications will be briefly presented to demonstrate its potential and how it can be applied to many different materials, region of interest sizes and tests.

Fringe projection has been employed to study the mechanical proprieties and the failure mechanism of different materials under loading (Leon-Huerta, A., et al., 2008). A dynamic study of the change in thickness of a bone specimen was performed to determine the constriction and the shear bands in the material when under elastic and plastic deformations. For this analysis FTP was employed and the results agreed with those predicted from theory. Genovese, et al. (Genovese, et al., 2006) employed Fringe Projection and Geometric Moiré to perform a hybrid technique for the mechanical characterization of hyperelastic materials. They compared experimental results with those obtained from numerical models. Differences between experimental and numerical results were minimized in using non-linear optimization algorithms to tune up the material properties in the numerical model.

The capability of Fringe Projection to measure 3D shapes has been employed in the location of elements in NDE methods, manufacturing and assembly procedures. Heredia-Ortiz and Patterson (Heredia-Ortiz & Patterson, 2005) proposed an aerospace panel during ultrasonic scan measurements (Figure 3.1.A). During the process, the shape measurement error was lower than 1% of the measured range. The proposed system allowed the location of 2D ultrasound scanned data with in a 3D computer-aided design (CAD) model (Figure 3.1 B)).

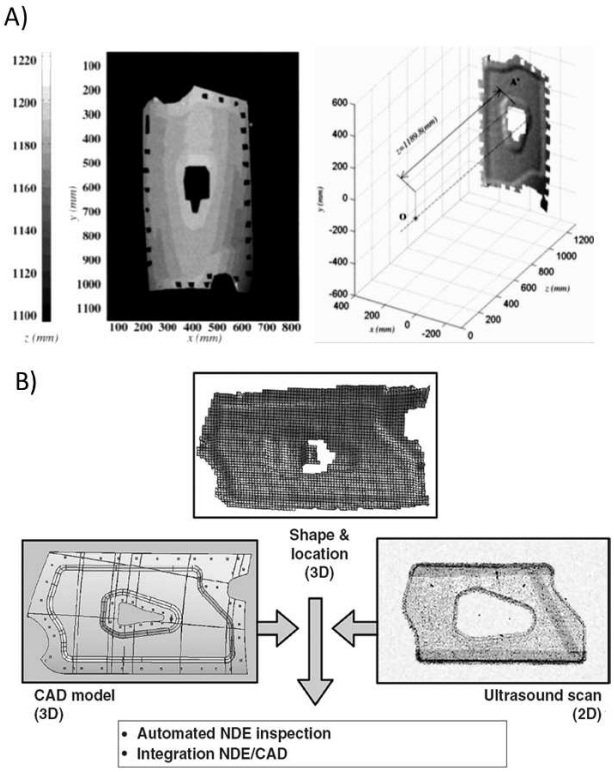

Figure 3.1 A) Surface contour maps for the panel from the aircraft fuselage: Right: combined location and shape data B) The shape and location data can be used to obtain the scan trajectory (Heredia-Ortiz & Patterson, 2003)

A main application of the shape measurement is reverse engineering. Fringe Projection has been used to obtain a 3D CAD model from complex shape elements (Burke, et al., 2002)

Moreover, Heredia–Ortiz and Patterson (Heredia-Ortiz & Patterson, 2003) also employed Fringe Projection for the shape measurement of the turbine blade during a vibration test with an electroboscopic illumination. Figure 3.2.A illustrates the measured turbine blade (450 mm long and 250 mm wide). In this analysis, they were able to achieve a shape sensitivity of 1.1 mm. In addition, the turbine had a 2.5 mm thick photoelastic coating applied onto the lower part of the blade, which was used for stress analysis during vibration tests.

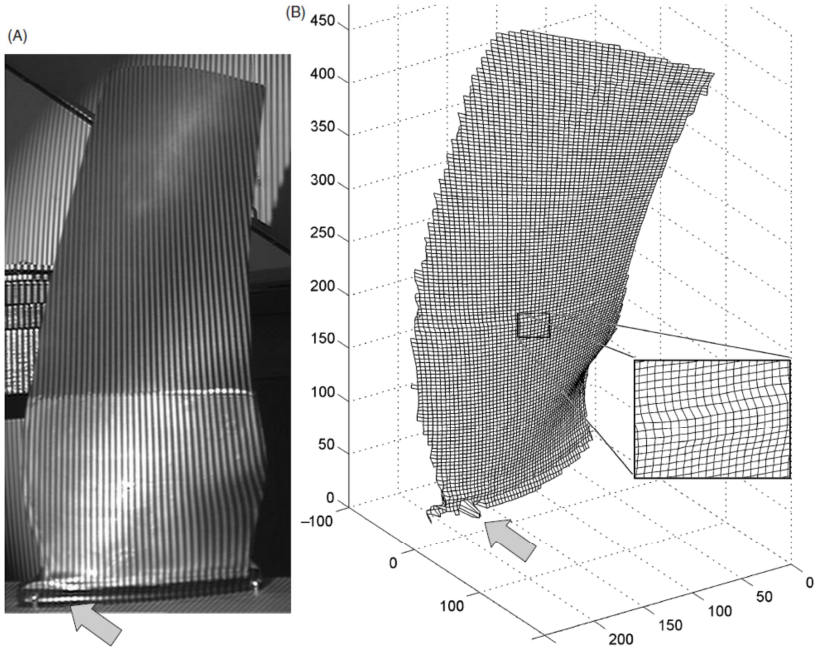

Figure 3.2 Shape determination of a turbine blade using fringe projection. (A) Object image showing the projected fringe pattern over the blade. (B) 3-D mesh of the measured shape. (Heredia-Ortiz & Patterson, 2005)

The possibility of using Fringe Projection in real time applications, employing spatial phase retrieval methods, made it possible to measure out-of-plane displacements measurement during dynamic events. Hence, FP was employed in vibration mechanics without the necessity of electroboscopic illumination. One example is the work conducted in (Rodriguez-Vera, et al., 2009) who implemented FTP methods to measure small displacements due to the vibration of a cantilever beam (3960 μm long, 700 μm wide and 7 μm thick) at an amplitude up to 50 μm with a 1% of accuracy at a resonance frequency of 330 Hz. To capture images at that speed, a frame rate of 1135fps was adopted.

Another dynamic application of Fringe Projection (employing FTP) is the study of the displacement occurring during the vibration of a drumhead (Su, et al., 2006). Thus, the test was performed at 10,000fps over a 250mm diameter drumhead and displacements from -1.79 to 1.84mm where measured with a 0,07 mm uncertainty.

Finally, Fringe Projection has been widely employed to study in Biomechanical problems. An example is the movement of a scapula to determine its cinematic

behaviour avoiding intrusive elements to the skin (Gomes, et al., 2010). This experiment made it possible to study the movement of the muscles and their recovery in case of rehabilitation. Moreover, Fringe projection has been employed to reconstruct the shape of porcine vascular segments subjected to internal pressure (Genovese & Pappalettere, 2006). Since PF only offers shape measurements, the mechanical characterization of those vascular tissues was performed adjusting numerical models using 3D shape information obtained during experiments.

3.2.1.3. Discussion

Since 1983, Fringe projection has been constantly evolving and nowadays it is completely accepted as a standard measurement technique for scientific and industrial applications.

FP has been employed in many different scientific areas for the analysis of shapes and out-of-plane displacements. Nevertheless, since FP is limited to out-of-plane displacements, if mechanical properties are analyses, FP has been always employed together with other technique (numeric (Genovese & Pappalettere, 2006). or experimental (Heredia-Ortiz & Patterson, 2003)l) which complement it.

3.2.2. Digital Image Correlation

In this epigraph a brief historical review of DIC technique will be presented. Finally some general applications of DIC will be discussed.

3.2.2.1. Historical review

Digital Image Correlation (DIC) started its development at the beginning of 1980s (Peters & Ranson, 1981) (Sutton, et al., 1983) based on Electronic speckle photography. At that time it was demonstrated that deformation occurring at small areas over a surface could be measured by capturing images of the surface during the deformation. DIC requires a speckle pattern over the specimen which can be

generated painting it over the specimen. Thus, DIC is more versatile and simpler to use than Electronic Speckle Photography. Moreover, with DIC it is possible to measure displacements from micrometres to meters depending on the size of the speckle. In addition, new algorithms have been developed to extract strains from those measured displacements (Sutton & Chao, 1988).

At the beginning of the technique, a single camera was employed and only in-plane displacements were measured. In addition, the specimen had to be flat and disposed parallel to the camera sensor since to out-of-plane displacements or shape could affect to the lens magnification (Sutton, et al., 2008). Nevertheless, at the beginning of the 1990s, (Luo, et al., 1993) a complex optical calibration was developed through which it was possible to perform 3D Digital Image Correlation by employing two cameras when studding 3D displacements. This event drastically increases the interest in the technique and its applications. 3D-DIC was based on the principles of stereo vision developed in robotics and other shape and motion measurement applications. Thus, with a two-camera stereo vision system it was possible to measure displacements and shape in the three spatial dimensions.

Nowadays there exist several commercial 3D-DIC equipment that make it possible to perform the calibration and displacements measurements in very a short time. Furthermore, the wide adjustable sensitivity and range of displacements that can be measured (by simply selecting the adequate lens magnification and field of view), the possibility to measure dynamic events and the minimal specimen preparation, makes 3D-DIC the most used technique to measure displacement and, indirectly, strain maps (Sutton, et al., 2009). However two major drawbacks are that commercial 3D-DIC systems are expensive and they require complex image processing algorithms.

3.2.2.2. Digital image Correlation Applications

2D and 3D-DIC can be employed for a wide range of displacements (from micrometres to meters) with no special specimen preparation. Both techniques are very versatile and they can be applied for multiple industrial applications.

Although 2D-DIC presents some limitations, multiple applications can be found in the literature. Such an example is the experimental determination of intensity factors and T-stress during fatigue (Vasco Olmo, et al., 2012). Vasco-Olmo *et al*. conducted a series of experiment on polycarbonate Middle Tension specimen. 2D-DIC results were successfully compared with those obtained from photoelasticity.

In addition 2D-DIC has been employed to validate numerical models as presented by Sun and Pang (Sun & Pang, 2008). An experimental investigation was carried out of the near-crack-tip deformation of solder alloy under monotonic tensile loading. 2D-DIC results were compared with those obtained for FE simulations. Differences between the experimental and numerical strain fields were only found at the very near crack tip. They were attributed to some difficulties in modelling the crack tip.

Du, et al. (Du, et al., 2011) applied 2D-DIC to monitor the evolution of a crack in an aircraft panel (4.8m × 1.4m). With this analysis it was possible to investigate the effect of reinforcements within this panel, in the evaluation of the crack path and its speed of propagation. They employed a multi-point over-determinism method to relate the displacement field around the crack to the stress field and they were able to study the mixed mode (I+II) stress intensity factors of the crack successfully. Through this method they were able to obtain full field experimental information with a maximum uncertainty of 5%.

Digital Image Correlation has been also employed in civil engineering applications for the analysis of large scale problems. Yoneyama, *et al*. (Yoneyama, et al., 2007) applied 2D-DIC to measure the deflexion on a bridge when a truck was moving. The main contribution of this work was the application of 2D-DIC to big civil structures with an error of 0.31 mm for a region of interest of 15 meters.

In the automotive industry, Digital Image Correlation is very well established for strain analysis. Such an example is the analysis of principal strains in tires rotating up to 150 miles/hour using 3D-DIC (Schmidt, et al., 2003). For that purpose, an electroboscopic illumination with 500 nanosecond discharge time was employed. Recently, 3D-DIC has been employed in the automotive industry to test six composite inner bonnet liners during high speed tests (Burguete, et al., 2013). The tests consisted on high velocity (70

m/s) low energy (50-300J) impacts. To predict the displacement fields, a Finite Element model was employed and results were compared with those obtained 3D-DIC measurements. The results showed a good level of agreement with the finite element results in the first stage of the impact. In addition, 3D-DIC has been also employed for the measurement of surface strains in many other disciplines such as biomechanics (Sztefek, et al., 2010), in fracture mechanics (Lopez-Pedrosa, et al., 2012) or in theoretical models validation (Xiao, et al., 2013).

Besides the capability of 3D-DIC for measuring displacements and strains, it is also remarkable the potential of 3D-DIC for measuring 3D shapes (López-Alba, et al., 2013). They employed 3D-DIC for damage characterization on composite panels. They were able to characterize the geometry of the damaged area by reconstructing the surface using Bezier polynomial.

3.2.2.3. Discussion

Since 1981, DIC technique has been constantly evolving and nowadays it is completely accepted as a standard measurement technique for scientific and industrial applications.

Different correlation methods have been developed during the last thirty years with accuracies of ±0.015 pixels for 3D-DIC and ±0.01 pixels for 2D-DIC techniques (Sutton, et al., 2009). The accuracy is directly related to the resolution of the cameras employed in the set-up. Thus, as it has been previously explained, DIC techniques are suitable for studying a wide range of measurements problems from terms on millimetres to metres.

2D-DIC has been mostly employed for the analysis of flat surfaces with only in-plane displacements. This has mostly limited the technique to laboratory applications or on applications where out-of-plane displacements can be neglected.

In contrast, 3D-DIC has been more employed for the study of a wide range of problems involving 3D shapes and displacements. Nevertheless, the use of two cameras has increased the cost of the adopted set-up.

3.2.3. Conclusions

Based on the analysis of FP and DIC techniques it can be deducted that the idea of integrating both techniques seems to be an interesting alternative to 3D-DIC for shape and displacements measurements. Both techniques show a similar set-up (one camera arranged perpendicularly to the studied element). In addition both techniques can be applied to different scales problems with high level of accuracy. Therefore, the integration of both techniques to simultaneously measure in- and out-of-plane displacements using a single camera seems to be feasible.

In addition, the integration of Fringe Projection and Digital Image Correlation would contribute to solve some of the drawbacks of each technique independently. Fringe Projection can only provide out-of plane information while 2D-DIC is limited by the fact that it cannot be employed for curved elements or when out-of plane displacements are present.

3.3. Join of Fringe Projection and Digital Image Correlation

3.3.1. Introduction

As previously stated in chapter 2, 2D-DIC and FP have very similar experimental set-up. The optical axis of the camera has to be perpendicular to the specimen surface or, more precisely, to a flat reference surface from which the in-plane displacement will be measured. The major set-up difference is that FP needs from an additional fringe projector. In the case of DIC, only requirement is that the specimen surface requires a random speckle pattern on its surface. When viewing the specimen surface with the camera, fringes and speckle will change their position according to the deformation

experimented by the specimen. Thus, the main problem of combining the two techniques is that the speckle pattern introduces noise in the projected fringe pattern. Moreover, the speckle pattern is superimposed with the fringe pattern when the fringes are projected. If both patterns are not conveniently separated, it will cause the failure of FP and 2D-DIC processing algorithm.

In the next epigraphs it will be reviewed some of the different approaches performed to achieve the integration of both techniques separating both patterns. In addition, special attention will be paid to other drawbacks sources that should be considered in order to accomplish the proposed aims.

3.3.2. Previous approaches for combining Fringe projection and Digital image Correlation

In the literature it can be found a variety of approaches to separate of the information containing the out-of-plane displacement (i.e. fringe pattern) from the information containing the in-plane displacement (i.e. speckle pattern). The most effective and simple method to obtain the fringe pattern and the speckle pattern separately is to acquire them both sequentially by stopping the fringe projector (Barrientos, et al., 2008), (Quan, et al., 2004) and (Nguyen , et al., 2011). Shi, *et al.* (Shi, et al., 2013), were able to acquire several phase-shifted fringe images from a speckled surface eliminating the fringe pattern by evaraging it. However, if dynamic tests are performed, these approach is inadequate due to the fact that the specimen will be at a different stage when speckle images or fringe images are captured.

If dynamic a measurement is performed, the specimen image has to show speckle and fringe patterns for each deformation stage superimposed. One alternative used to separate speckle from fringes is by simple applying a band pass filter to Fourier transform, as performed by Tay, *et al*. (Tay, et al., 2004). An addtioal way proposed by Weber, *et al.* (Weber, et al., 2002) is by using different colours for speckle and fringes. Thus both patterns can be separated using optical colour filters placed at the camera lenses (This imply to use two different cameras). To avoid using more than one

camera, one alternative is to employ the internal Bayer filter of a convetional colour camera (Siegmann, et al., 2011),(Mares, et al., 2011).

Over the following paragraphs, a more detailed discussion of each of the mentioned techniques will be presented.

3.3.2.1. Non Colour Filtering Techniques

Tay *et al.* (Tay, et al., 2004) were the first to measure the 3-D rigid-body displacement of an object by combining fringe projection and digital image correlation using a single camera they employed an optical system as the one shown in Figure 3.3.

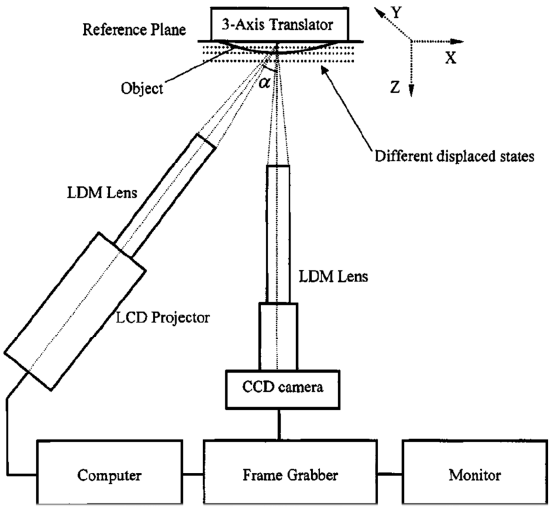

Figure 3.3 Set-up used by Tay, et al., 2004

In this approach, sinusoidal fringes varying from black to white were projected over an object using a (LCD) projector. In this approach the specimen texture was used as speckle pattern to perform 2D-DIC. Hence, surface illumination had to be uniform to ensure that the grey values on the specimen surface did not change during deformation. Speckle pattern images were obtained with the aid of the Fourier transform. Thus fringes frequency was filtered while the background intensity variation was preserved to obtain fringe-free images. This methodology was also employed by other authors (Barrientos, et al., 2008).

Figure 3.4.A shows the Fourier Transform of an image. It has two side lobes that represent the fringes frequencies and the central frequency corresponding to the background intensity variation. In Figure 3.4.B the fringes frequencies are filtered.

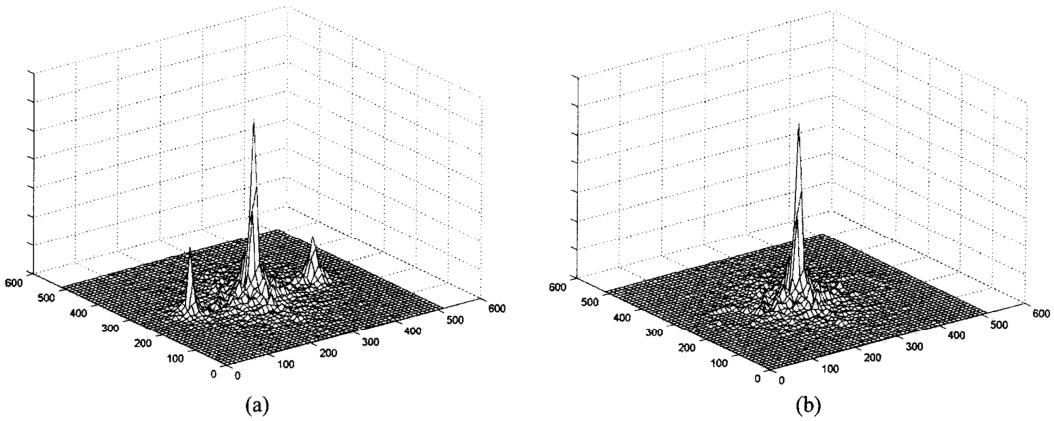

Figure 3.4 Image Fourier spectrum (a) before and (b) after filtering removing fringes frequency (Tay, et al., 2004)

To obtain suitable images for digital image correlation with a complete removal of the frequency fringes, some tasks should be taken into account:

- The carrier fringe frequency should be sufficiently high when compared to the of the background frequency.
- During fringe frequency filtering, the high-frequency speckle that carry information concerning to the texture may be partially removed.

Subsequently FP and DIC are processed separately to obtain out-of-plane and in-plane displacements respectively.

The experiment conducted to test this methodology was a 3-D rigid-body translation of a coin. Tay *et al.* noticed that out-of-plane displacement or shape could affect the optical magnification, hence telecentric lenses were advisable. However, the errors found were within 5% for displacements from 100 mm to 1mm.

Finally, the authors presented several advantages:

- There were no special paintings or coating to prepare the sample.
- The set-up of the experiment and the calibration process was relatively simple.

- The measurement range was wide since by only changing the magnification the field of view could be modified.
- Only one image was required for each displaced state.

However, some disadvantages were also observed. The magnification errors due to the out-of-plane displacements were not determined; the fringe frequency had to be sufficiently high compared to the background frequency, part of the speckle was removed during filtering and also the texture is sensitive to light changes during the test.

Quan *et al.* (Quan, et al., 2004) employed the same basis as previous works to test a steel cantilever beam (length = 153 mm, width = 23 mm, height = 2.96 mm). It was thought that the use of filtered images would also reduce the measurement accuracy due to the low quality of the element texture used as speckle pattern (in terms of size and contrast of the speckle). Hence, Quan *et al.* considered that the method proposed by Tay, *et al*. (Tay, et al., 2004) was thought to be especially suitable for rigid body or large displacement measurement but not in tests where high deformations occurred. It was concluded that if better accuracy was desired, an image of black speckle pattern on white background without fringes should be used for digital image correlation processing. Thus, in this study, two images were, on with projected fringes and another with only speckle for Digital Image Correlation. In addition, the out-of-plane displacements were obtained by calculating the difference of shape between a deformed state and a reference state. The adopted set-up employed by Tay *et al* but, in this occasion, the CCD camera had a telecentric lens to minimize the magnification errors caused by out-of-plane displacements.

Experimental results were compared with theoretical data showing a certain degree of similarity. Maximum discrepancy for out-of-plane displacements was less than 2% and less than 5% for in-plane displacements.

Barrientos *et al.* (Barrientos, et al., 2008) also dared to combine Fringe projection and Digital Image Correlation 2D techniques to measure the evolution of 3D displacements at the surface of a model of the Earth's crust. The main reason why they employed

FP+2D-DIC was to avoid a stereoscopic calibration. The main idea was to use a similar set-up to previous approaches (consisting of a camera placed perpendicular to the specimen and a projector which projects the fringe pattern). To obtain a speckle pattern suitable for 2D-DIC processing, they employed rough texture of the Earth's crust model which was mainly made of sand. To obtain a good speckle contrast, the surface was coherently illuminated. Fringe and speckle images were taken alternately. Results were compared with those obtained using traditional image analysis, however an error quantification was not performed.

More recently, Shi *et al*. (Shi, et al., 2013) presented a new approach to the joining of FP and 2D-DIC with the purpose of establishing an alternative method to ESPI which should provide shape and 3D displacements simultaneously in an order of the magnitude of micrometres. This approach should skip the high stability controlled environment required for ESPI. In the proposed method, sinusoidal black and white fringes and surface texture images were simultaneously obtained instead of being captured by the camera in two temporally discrete steps (Barrientos, et al., 2008) (Quan, et al., 2004). In addition, an alternative method for fringes filtering (Tay, et al., 2005) was employed. In this approach a phase-shifting method was implemented using a grating, a stepper motor, a high-precision thread and limit switches. Thus, four phase-shifted images (Figure 3.5.A) were captured to obtain the out-of-plane measurements. From these four images the texture of the specimen was extracted by measuring the average intensity of the four images captured Figure 3.5.B.

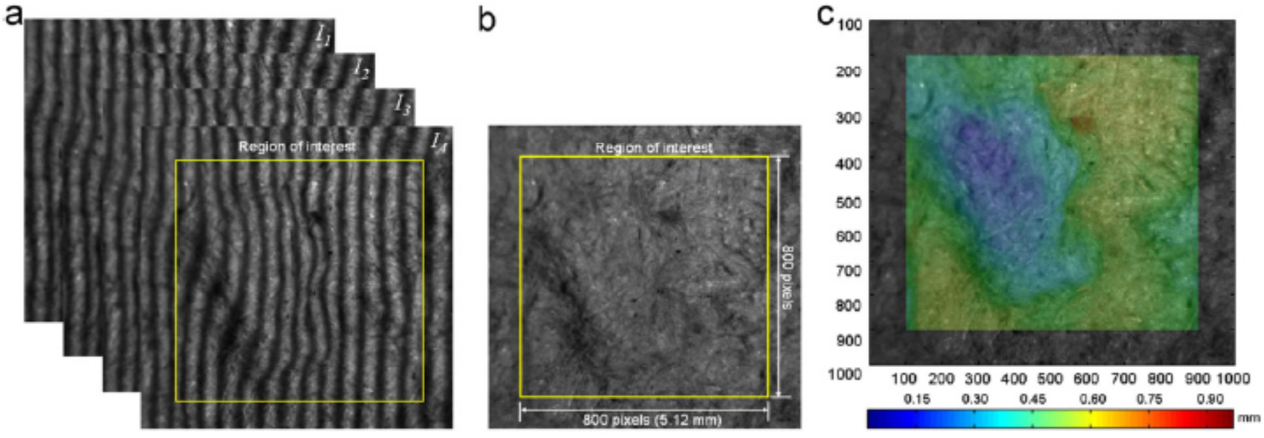

Figure 3.5 (a) Four fringe patterns corresponding to $p = \pi/2$ after phase shifting. (b) image of the specimen texture. (c) Out-of-plane displacement map (Shi, et al., 2013).

This method was proved with a moulded pulp material under tension. It was measured its deformation at different loads to understand its micro-scale mechanical behaviour. With the use of two long-working distance microscopes, the system was also able to measure small objects with a single CCD camera. In addition, it was able to provide an out-of-plane displacement resolution of 0.006 mm and an in-plane displacement resolution of 0.0001 mm. The field of view was approximately 5x5mm^2. The contour data obtained from the phase shifting algorithm is presented in Figure 3.5.C.

The system proposed was an intelligent approach to extract the information required to process fringe and speckle images using a single camera. Nevertheless its point of weakness was that it still suffered problems when measuring dynamic objects due to the temporal phase shifting technique. In addition, there was no information about possible in-plane displacements errors caused by to out-of-plane displacements.

In another recent investigation, Nguyen *et al.* presented a novel approach (Nguyen , et al., 2011), (Nguyen, et al., 2011). The idea was to capture a fringe image and a speckle image for each stage of the test. The out-of-plane displacement at a certain pixel was calculated as the difference of the measured shape between the reference state and the measured shape at the point given by the in-plane displacements.

Moreover, as it was previously explained, the pixels within the facet in which the image was divided were assumed to lie on the same continuous region. However, this assumption may be invalid for a facet that intersects multiple continuous regions, as each region may undergo a different deformation that is, generally, not the same as other regions. Nguyen *et.al.* (Nguyen , et al., 2011) considered that problem and segmented the surface element into different continuous areas before 2D-DIC was performed. This segmentation was based on the 3-D shape measured by Fringe Projection from which it is straightforward to detect discontinuities.

To illustrate this approach, a flat specimen which showed a round hole and a rectangular step on its surface was tested. The camera used for image capturing had a field of view of approximately 700×700 mm^2. The specimen was displaced 10,160 mm out-of-plane. Results are presented in Figure 3.6.

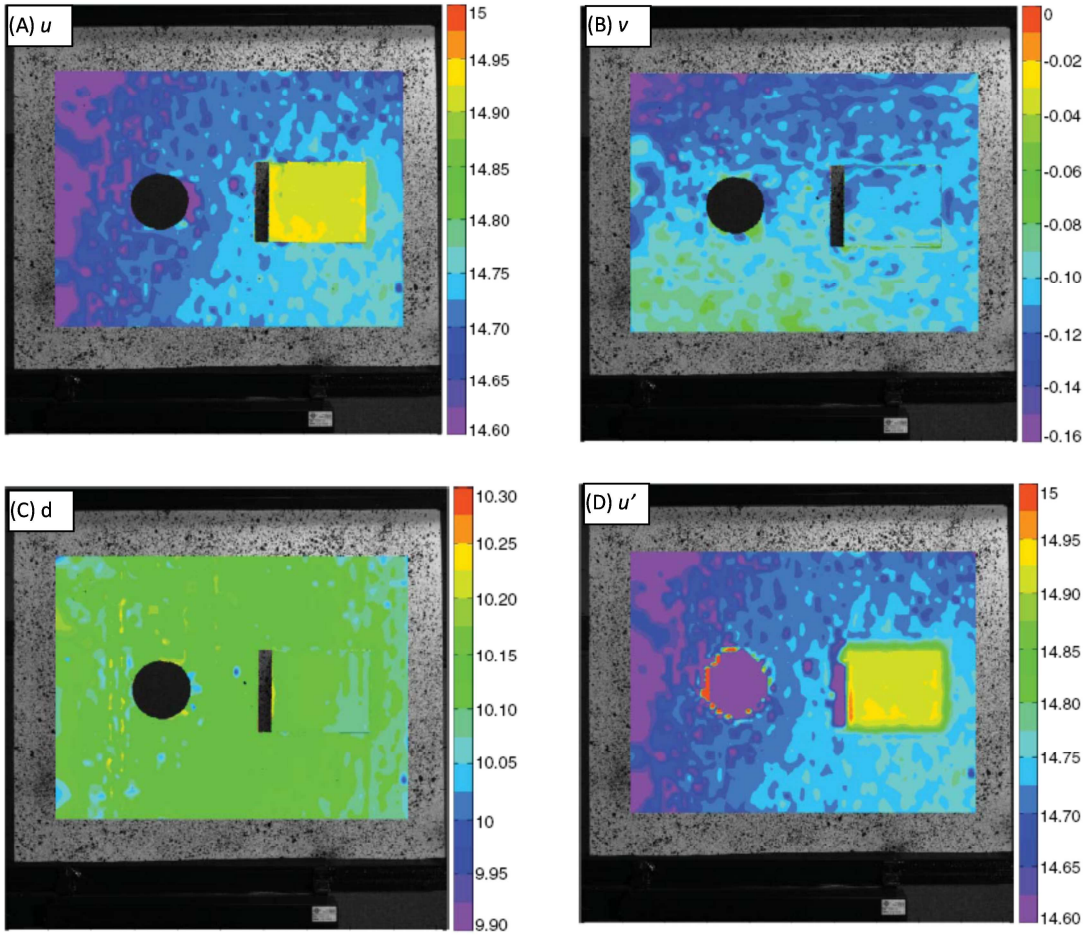

Figure 3.6 Estimated displacement fields corresponding to a true displacement of 10.160 mm. (A,B) Horizontal and vertical image plane displacement components u and v, respectively, expressed in pixels and (C) 3-D displacement magnitude field (d) expressed in millimetres (D) Horizontal image displacement field u' estimated by a standard 2-D-DIC technique without discontinuity detection for the true displacement of 10.160 mm (unit: pixels) (Nguyen , et al., 2011).

The results of the displacement in *X*- direction Figure 3.6.A show that the surface segmentation allows the independent measurement of the step that presents the specimen at its surface. This effect is especially notorious if that displacement map is compared with the results without taking into account the surface segmentation presented in Figure 3.6.D. Nevertheless, it is important to notice the difference in the *X*- displacement at the step region compared with the rest of the surface, when it should be a constant value in the whole image. In addition, *Y*- direction displacements (Figure 3.6.B) shows a gradient of displacements where it should be constant as well.

The same approach was employed by (Nguyen, et al., 2011) but in this case they employed two cameras instead of a single one to cover a wider area of the specimen. They applied their approach by testing an aluminium sheet 1 mm thick bent along four

parallel lines into a 'top hat' profile to introduce geometrical jumps and perspective occlusions. A 6mm displacement was prescribed at the centre point of that specimen to perform an out-of-plane deformation. Results were compared with numerical methods and 3D-DIC. Results highlighted an error of 0.07 mm which was attributed to the propagation of errors due to imperfections in the camera and the projector.

Some disadvantages were found in the approach of Nguyen, *et al*. The first one was that it was not possible to perform dynamic tests since for every step it was required in order to capture fringe and speckle images sequentially. Another mistake was not considering the differences in magnification due to the specimen shape and out-of-plane displacements. This was probably the main source of error during the tests and the reason why the displacement maps in Figure 3.6 do not present constant values.

3.3.2.2. Colour based filtering techniques

An alternative method to all previously presented approaches for fringe and speckle separation is to employ a colour camera for image acquisition. This approach tries to improve the previous ones by making the system suitable for use in dynamic events and by improving problems caused by Fourier filtering, as in the case of Tay, *et al*. The alternative is to encode fringes and speckle patterns required for both FP and 2D-DIC in the RGB signal of a colour image. Thus, the required information for measuring 3D displacements is contained in just one RGB image.

The basis of this approach is that RGB cameras capture colour images and record them as three different images. Each of them is sensitive to one of the RGB colours pattern, i.e. Red, Green and Blue. The idea is to have fringes and speckle in two different colours.

The colour encoding method was first developed by Weber *et al.* (Weber, et al., 2002) who implemented FP and 2D-DIC using two different colours, blue for the projected fringes and red for the speckle pattern. Their purpose was to determine the pressure evolution on an air-bag over time. To perform the experiment two different cameras were used instead of just one single camera. Each one had a different colour filters,

one red and one blue. In this way, one camera could record the speckle and the other fringes. Thus, in-plane and the out-of-plane displacements on the same object surface could be obtained in a separate way.

Siegmann *et al* (Siegmann, et al., 2011) improved this approach by employing a single CCD colour camera to separate fringes and speckle. In this case by a RGB colour encoding technique was employed, i.e. red and blue channels of a single RGB image. In this approach, blue fringes were projected over the surface which presented red speckle over white background. The RGB images were separated into images that were sensitive to red (blue fringes appeared) and to blue (red speckle appeared). After this extraction of both patterns, fringes and speckle images still had some noise and they required some filtering. This was mainly because the image employed a Bayer filter (Bayer, 1976) which causes an interpolation of colours every two pixels. Thus speckle was still observed in fringes images in Figure 3.7. Nevertheless, speckle and fringes images were suitable for 2D-DIC and FP.

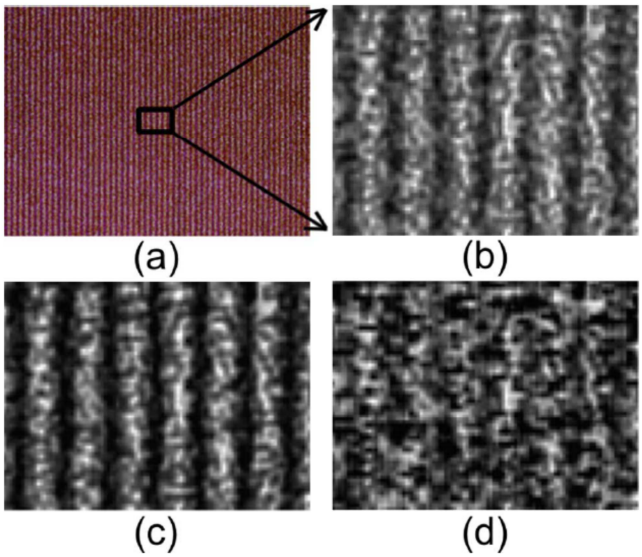

Figure 3.7 Colour encoding approach based on a Bayer Filtered (a) RGB image of the object (b) R, (c) G, and (d) B images. (Siegmann, et al., 2011)

An assessment of the displacements achieved by employing this approach was performed by deforming a sheet of paper which presented both patterns. Results were compared with those obtained by applying fringe projection in the absence of any speckle and 2D-DIC without projecting fringes. The average differences were 1.85%

and 3.35%, for in-plane and out-of-plane displacements respectively. These differences could be minimized with a smaller fringe period, a smaller projector angle and by improving colour balance.

A similar approach was implemented by Mares *et al.* (Mares, et al., 2011). In this case, the object was illuminated with structured light that consisted on a fringe pattern with cyan (blue and green) fringes embedded in a white background. When using an RGB colour camera, fringes appeared in the image that was sensitive to red while the element texture was seen in the image sensitive to blue. Validation experiments consisted on translating an aluminium plate a known distance along the three coordinate axes. The steps were given by a step translation motor with 1.25 micrometres steps. The average error for the present method was from 1% to 5% depending on the period of the projected fringes.

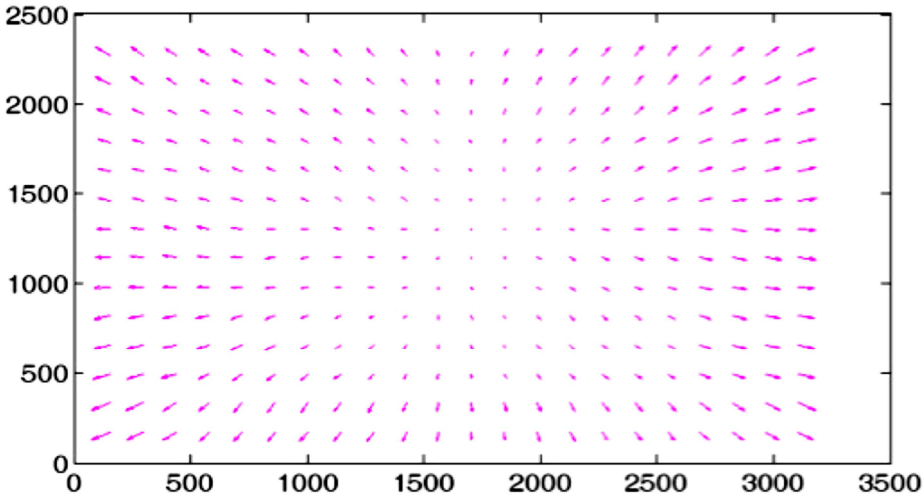

Figure 3.8 In-plane residual error. (a) In obtaining this vector field, the signal on the blue channel (speckle image) is used. The aluminium plate undergoes an out-of-plane displacement of 1.5mm. The maximum residual in-plane displacement is 0.26 mm, and it is located at the corners (Mares, et al., 2011).

In addition, when analysing in-plane displacement when only out-of-plane displacement occur, radial displacements field can be observed, as shown in Figure 3.8. In this figure, a maximum in-plane displacement of 0.26 mm is found. This effect demonstrates that for three-dimensional displacements, the added non uniform in-

plane displacement arising from the out-of-plane displacements will increase the in-plane error.

This effect is due to the variation of the lens magnification as the specimen is out-of-plane deformed or displaced. However, it can be prevented by using a telecentric imaging lens as it was previously stated or it could be numerically compensated. This effect is a highly important issue that no other authors have measured or taken into account when studying in-plane and out-of-plane displacements apart from Quan, *et al.* (Quan, et al., 2004).

This phenomenon of in-plane displacements caused by out-of-plane displacements effect was employed by Tay, *et al*. (Tay, et al., 2005) in the hope of achieving out-of-plane measurements from one single camera. But in this case only out-of-plane displacements could be achieved. An optical study of this phenomenon during the out-of-plane displacements of an object that gets closer to the camera using 2D-DIC was performed (Figure 3.9). As a result of this study an interesting mathematical relation was performed (Eq 3.1) which relates the out-of-plane displacement (d_b in Figure 3.9) of an object placed at a distance *b* from the focal plane and the in-plane displacements measured by 2D Digital image Correlation (*H-h'* in Figure 3.9).

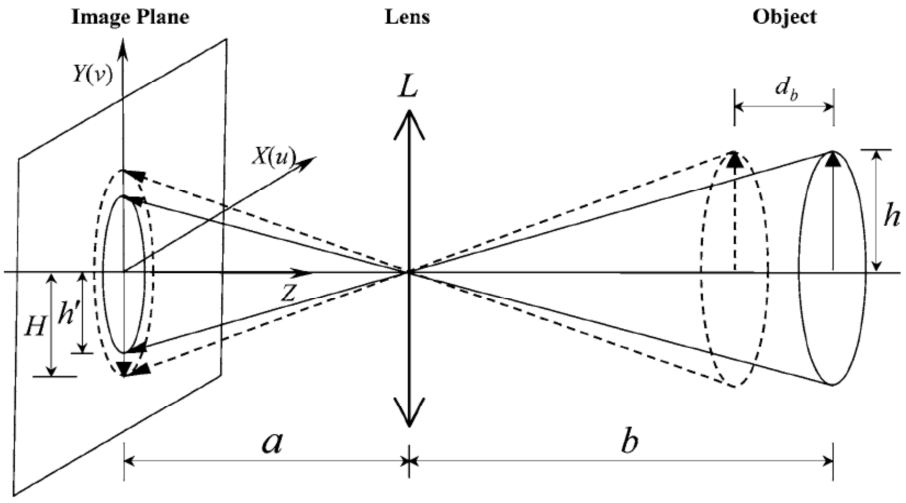

Figure 3.9 Relation between out-of-plane displacement and apparent (Tay., et al., 2005)

$$\frac{H - h'}{h'} = \frac{d_b}{b} \qquad \text{Eq 3.1}$$

3.3.3. Discussion

It has been demonstrated how Fringe Projection and 2D Digital Image Correlation are experimental techniques for full field displacement measurement that are widely used. As a first hypothesis, they seem to be suitable to work in conjunction offering 3D displacement maps. According all the previous work reviewed, it can be concluded that it is possible to develop a system that integrates Fringe Projection and 2D Digital Image Correlation using a single camera to achieve displacements in the three spatial dimensions. This would imply a cost reduction respect to commercial 3D-DIC systems, especially if high speed cameras required.

Different published works combining Fringe Projection and 2D Digital Image Correlation have been reviewed; however none of them explicitly reported the precise measurement of displacements in three dimensions. Nevertheless, some important considerations can be extracted from this review.

Two main approaches for combining Fringe Projection and Digital Image Correlation 2D have been found. One is to acquire fringes and speckle images at the same time. An alternative is to capture speckle images in a sequential way, simplifying the filtering process but the drawback that images cannot be used for dynamic testing. To extract Fringe and Speckle patterns from a single image, three methods have been found, Fourier filtering, RGB encoding and Phase-Shifting extraction. Phase-Shifting extraction needs the specimen to be in the same position for a short period of time, in order to take different images, thus, it cannot be used for dynamic testing. Fourier filtering needs the carrier fringe frequency to be sufficiently high compared to background frequency. In addition, high-frequency speckle can be partially removed due to filtering. Hence, RGB encoding is the best method to integrate FP and 2D-DIC besides of the resultant patterns may show some noise and special attention must be paid to the colour balance.

Aberrations of in-plane displacement due to shape or out-of-plane displacement have been remarked by some authors (Mares, et al., 2011) (Tay, et al., 2004) (Quan, et al., 2004). However, most of them have incorrectly considered it or they have underestimated the effect of errors in the in-plane displacements results. In fact, this aberration is so important that it was employed to achieve accurate out-of-plane displacements (Tay, et al., 2005). Nevertheless, the aberration can be neglected if telecentric lenses are employed (Tay, et al., 2004). However, these kinds of lenses are expensive, heavy and voluminous.

3.3.4. Conclusions

Some concluding remarks could be obtained about previous approaches combining FP and 2D-DIC:

- Some research work has been previously published relating to the integration of Fringe Projection and Digital Image Correlation (2D), however none of them explicitly reported a precise methodology for the measurement of 3D displacement maps.
- Out-of-plane displacement or 3D shape distorts in-plane displacements. Previous approaches correct such a distortion with the aid of a telecentric lens.
- If dynamic tests are required, the best option to separate fringe and speckle patterns from a single image is to employ the RGB decomposing method.

3.4. General Conclusion

From the analysis performed concerning Fringe Projection, it can be observed that it is a technique widely employed in industry that it suitable for dynamic analysis with a low computational cost. Nevertheless it is not possible to measure in-plane displacements and in experimental mechanics is usually combined with other techniques to measure mechanical properties.

Digital Image Correlation is also a widely employed technique in experimental mechanics and industry. 2D-DIC obtains good results for in-plane displacements measurements and it is easy to implement. On the other hand 3D-DIC requires much more computational work to measure 3D displacements.

The main purpose of this thesis is to find a methodology that combines FP and 2D-DIC as a viable low-cost alternative to 3D-DIC. The proposed system should cover the following requirements

- The system must be versatile and be able to study dynamic events. The best option is to employ the RGB colour encoding method using blue fringes and red speckle.

- A very important issue to consider is the error caused in the in-plane displacements due to the out-of-plane deformation. This issue has not been quantified in any other previous works. If this issue is appropriately solved, it will be possible to measure in-plane and out-displacements simultaneously on various non-planar objects under 3D-deformation fields.

- The combination of Fringe Projection and 2D Digital Image Correlation would imply a low-cost alternative for 3D displacements measurements.

Chapter 4. Apparatus and methods

In this chapter the adopted set-up and the required experimental procedures are presented. Aspect such as the image capturing, image pre-processing and processing required to perform Fringe Projection and Digital Image Correlation simultaneously are described. The purpose of this chapter is to present the equipment and methods adopted over the course of this investigation. With this chapter it is intended to establish the experimental methodology for the integration of FP and 2D-DIC that will be applied in the experimentation conducted in this thesis.

4.1. Introduction

The previous chapters presented the basis and state of the art of Fringe Projection and Digital Image Correlation (2D) and the studies that have already been carried out combining both techniques for in-plane and out-of-plane displacement measurements. As previously stated, the principal aim of the researching work presented in this thesis was to implement a methodology suitable for industrial use which allows 2D-DIC and Fringe Projection to be performed simultaneously in order to measure the in-plane and out-of-plane displacements. The requirements of an ideal measurement system for this purpose could be summarised as:

- Adaptable to different applications, specimen of varying sizes in either static or dynamic tests.
- Suitable for use in unfavourable lighting conditions, noise, vibrations or space.

- Cost-effective set-up and processing requirements.

In this chapter the proposed set-up and the necessary hardware and procedures to perform FP+2D-DIC employing a single RGB camera will be presented. The whole set-up and procedures perform a general-purpose system for the measurement of 3D displacements. Hence, this system was generally employed for the majority of the applications considered whilst researching this work. Any possible differences from the presented system will be commented on in the explication of each application.

The calibration, the alignment of the camera-projector system and the in-plane displacement correction due to out-of-plane displacement deserve a separate chapter due to their importance (chapter 5).

4.2. Experimental Set-up

As it was concluded in Chapter 3, colour encoding is required in order to obtain a fringe pattern and a speckle pattern capable of performing FP and 2D-DIC simultaneously. Hence, a blue fringe pattern is projected onto white background and a red speckle pattern surface is employed (Siegmann, et al., 2011). The set-up which achieves those assumptions of simultaneously performing Fringe Projection and Digital Image Correlation basically consist of one RGB camera being placed perpendicular to a reference surface, a colour LCD (or LED) projector being disposed oblique to the optical axis of the camera (as is illustrated in Figure 4.1) and a computer to manage them. In some tests performed throughout thesis, the results of the proposed FP+2D-DIC technique are compared with those obtained with 3D-DIC. Hence, when performing 3D-DIC a second camera must be placed oblique to the optical axis of the first camera.

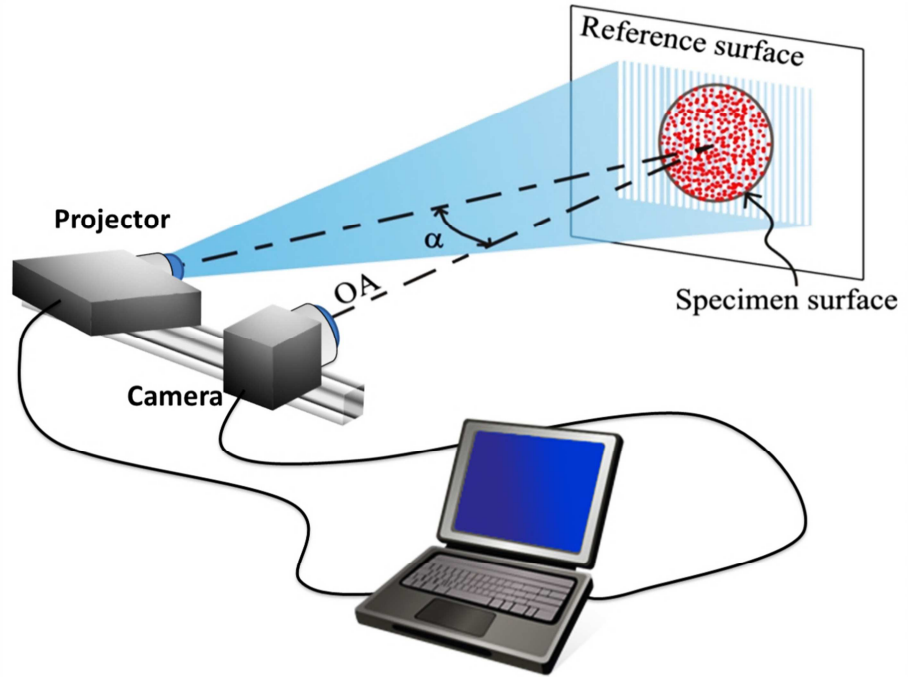

Figure 4.1 Schematic illustration showing set-up for adopted FP+2D-DIC Technique

Thus, different cameras were employed so that digital images could be recorded. The size and type of the sensors was adjusted to the area being studied or the frame rate desired. The fundamental requirement of the camera is the recoding of a single image sensitive to each colour of the RGB pattern. In RGB cameras this is performed by adding a Bayer mask (Bayer, 1976) over the sensor (CCD or CMOS) as illustrated in Figure 4.2. In fact, as it is shown from Figure 4.2, the cameras sensor records the information of each colour in different pixels, resulting in a cloud of one pixel separated points in each colour image representing the intensity of this colour. Hence, the full size image recorded in every channel is the result of interpolating the colour data points.

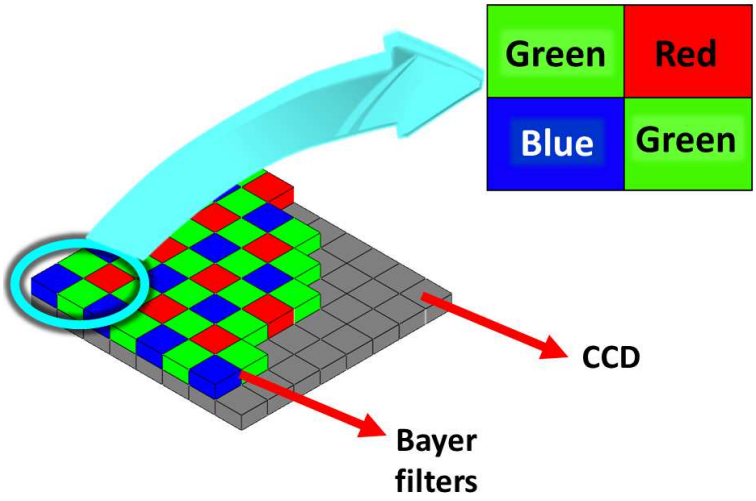

Figure 4.2 Schematic illustration of a Bayer filter

Moreover, diverse projectors have been employed during the course of this investigation. The projector is connected to the computer from which the fringe pattern is executed and commanded to the projector. As in the case of the camera, as much resolution of the LCD display is disposed, better fringe pattern is obtained and a smaller period of fringe can be achieved. In addition, the resolution of the computer transmission affects the resolution of the projected fringe pattern.

Both camera and projector are disposed on a rigid aluminium bar which allows them to be displaced along and to be clamped in the desired position. This aluminium bar is placed upon a tripod head-set which permits the three axis movement controlled by separate handles. This makes the orientation and levelling of the set-up easier. The orientation procedure of the system will be explained in Chapter 5.

The whole system is disposed onto a rigid tripod. This set-up provides a portable, stable and flexible system, suitable for the modification of the complete configuration according to the requirements (size, sensitivity, light...) of the application.

4.3. Methodology of Use

4.3.1. General Considerations

The technique proposed in this thesis allows the measurement of simultaneous in- and out-of-plane displacements over planar or curved object by integrating FP and 2D-DIC using a single RGB camera. Thus, several considerations have to be taken into account:

Fringe Projection combines two images of the fringes projected respectively onto a reference surface (i.e. the reference image) and a studied image (one per determination shape). If the studied element is initially flat, the reference image is the undeformed image of the element. However, if the object is not flat, it is required to measure its shape in the reference state.

Another important consideration is the colour of the fringe and speckle patterns. To obtain good results from the RGB filtering, it is important to project a fringe pattern which varies from totally white (RGB code (255,255,255)) to pure blue (RGB code (0,0,255)). In addition, as presented in previous chapter, a pure red speckle (RGB code (255,0,0)) onto white background (RGB code (255,255,255)) must be employed. It is important to notice that variations of those colours would affect the RGB encoding of the patterns. The speckle pattern has been applied by lightly spraying the surface of the element studied with 3020 RAL code paint. However, the method of application depends on the size of the speckle area. Different methods can be adopted such as applying it manually, painting the speckle using a sponge, printing a random pattern, etc. (Sutton, et al., 2009). The size of the random distributed points which perform the speckle pattern is directly dependent on the magnification of the lenses and the resolution of the camera employed. A recommended size for those points is a variation between 3 and 7 pixels (Sutton, et al., 2009).

The sensitivity of the FP depends on the period of the fringes and the angle of projection which both determines the *fringe constant* as it was presented in Chapter 2. Thus, the period or pitch (p) of the fringes should be as small as possible and consistent with the resolution of the projector and the camera, so that the light

intensity in the image is a senoidal distribution and aliasing effects are not present. In addition, the angle α between the optical axes of the camera and the projector should be as large as possible to obtain as much sensitivity as possible. Nevertheless it is important to ensure that fringes maintain their senoidal light intensity distribution frequency over the studied area. Some authors suggest that the combination of a fine grating and a small angle generally produces betters results than larger angles and coarser gratings for a specific sensitivity (Heredia Ortiz, 2004). This is due to the fact that the large angles of the projector make the system susceptible to the appearance of shadows when out-of–plane deformation and also to the projection of a non-constant pitch fringe pattern due to the projector angle.

This senoidal fringe pattern has been obtained in the test performed during this research by projecting a square fringe pattern and applying a slight defocusing to the lenses of the projector. In this manner, the appearance of any possible noise due to the LCD grid of the projector is avoided.

4.3.2. Set-up of the optical Elements

In this section the general procedure to set-up the different optical devices is described.

Initially, it is necessary to place the tripod with the rest of devices settled on it. If the specific space constrains of the application allow it, it is preferable to place the devices at a greater distance than the size of the studied element, so that aberrations of the lenses are minimized and the projected fringe pattern will easily maintain a constant period.

The camera is manually placed as perpendicular as possible to the reference plane. However, a fine alignment procedure will be presented in the next chapter. It is also a requirement the camera to be aligned with the area of interest so that it is placed on the centre of the image. The projector has to be also aligned with the camera so that the centre of the projected fringe pattern coincides with the centre of the image.

If it is performed 3D-DIC in addition to FP+2D-DIC, it is necessary to place a second camera which is settled oblique to the optical axis of the first one. This camera should be adjusted to view the area of interest at the centre of the image as the previous one. The angle between cameras should be close to 30^{o}. In addition, to avoid fringes in the images captured by this second camera, a special lens (physical colour filter) is added to the camera. Hence, this lens filters out blue wave length (below 450 nm), avoiding the fringe pattern from the acquired images.

Next step consist in focusing the cameras. If zoom lenses are employed, it is necessary to adjust the lens magnification to the area of interest. Then, the focusing and aperture of the lenses are adjusted to create an accurate vision of the patterns and to avoid the appearance of over or sub-exposed areas in the image respectively. A lower aperture produces a darker image (a longer acquisition time or more illumination would be necessary) but creates a larger depth of field which is important if large out-of-plane displacements or shape changes are expected during experiments.

Once the system is settled, the next step is the data (image) collection.

4.3.3. Data collection.

Data collection is based on capturing images at every required deformation stage. As commented previously, the reference image for the Fringe Projection method must be a flat surface placed at a distance z_0 from the optical centre of the lens of the camera and from which the out-of-plane displacement will be are measured. Furthermore, for 2D-DIC the reference image is captured at the reference state of the element specimen.

Images are captured, using the camera own software by acquiring snapshots at a certain frequency. Occasionally, images are captured when a digital signal is commanded to capture images of two cameras at the same time (external trigger).

In the work performed during the thesis, a triggering box which permits the triggering of up to three cameras at once was employed (Figure 4.3).

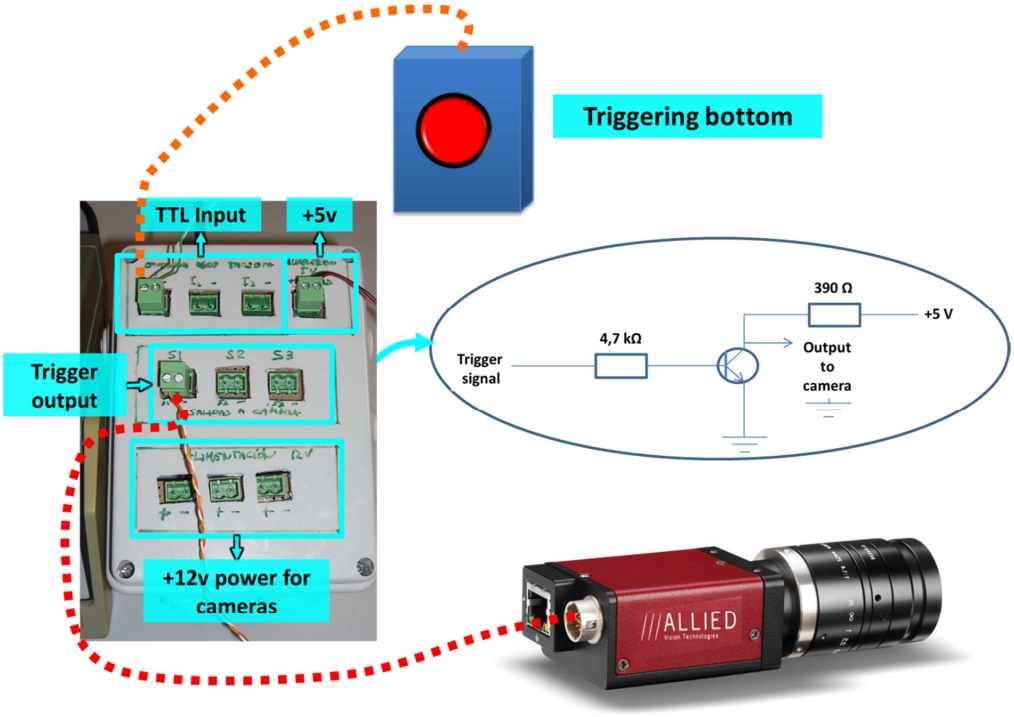

Figure 4.3 Schematic illustration contention of triggering box to camera

4.3.4. RGB image decomposing

One of the fundamentals properties of the proposed system is the capability of obtaining two different patterns (fringes and speckle) from a single RGB image, making it possible to perform dynamic studies. The RGB image decomposition consists of separating the colour image captured by the camera into three images. This separation has been performed by implementing a Matlab routine.

Initially, the colour image is composed in three overlapping matrix. Each matrix cell corresponds to specific pixel information. Subsequently, R matrix (sensitive to the red colour), and B (sensitive to the blue colour), are extracted (Figure 4.4). Hence, R and B matrixes contain the fringe pattern and the speckle pattern respectively.

.

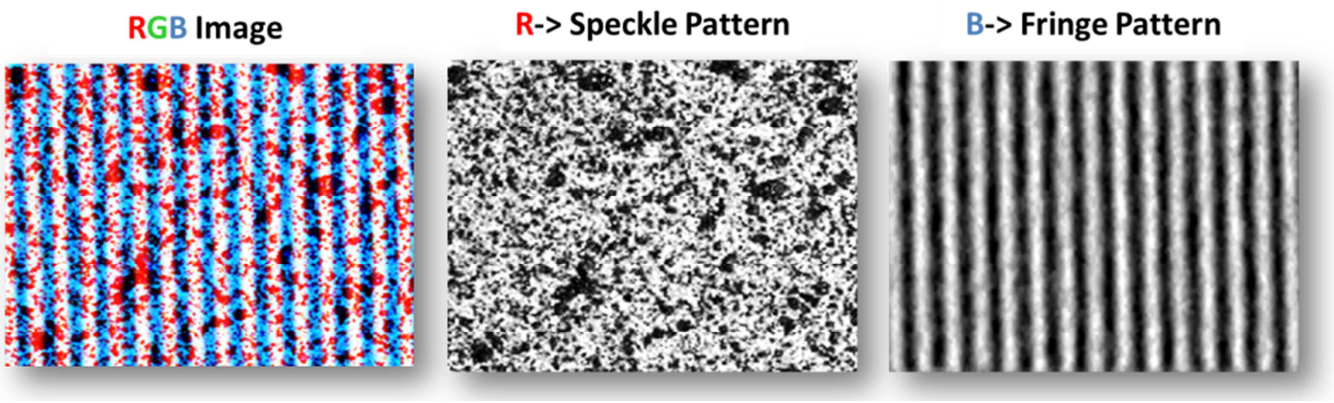

Figure 4.4 RGB image decomposition. Original RGB image left, R matrix centre and B matrix right

4.3.5. Image pre-processing

As discussed in previous chapters, the phase extraction algorithm requires the background illumination and fringe modulation terms (i.e. *r(x,y)* and *b(x,y)* defined in chapter 2) to be uniform. However, sometimes the images captured are not as ideal as desired, due to environmental limitations, electronic or environment noise or because the displacements are so high that during the test some shadows or reflections appears. Hence, some pre-processing is required to improve the fringe pattern is recommended to improve and avoid the appearance of errors during processing.

In a similar way the speckle pattern should vary between a maximum and minimum value of intensity. Thus it can be affected by variations in the background illumination during the test. Noise removal is difficult due to the fact that the speckle pattern is considered as noise, so filtering is inadvisable.

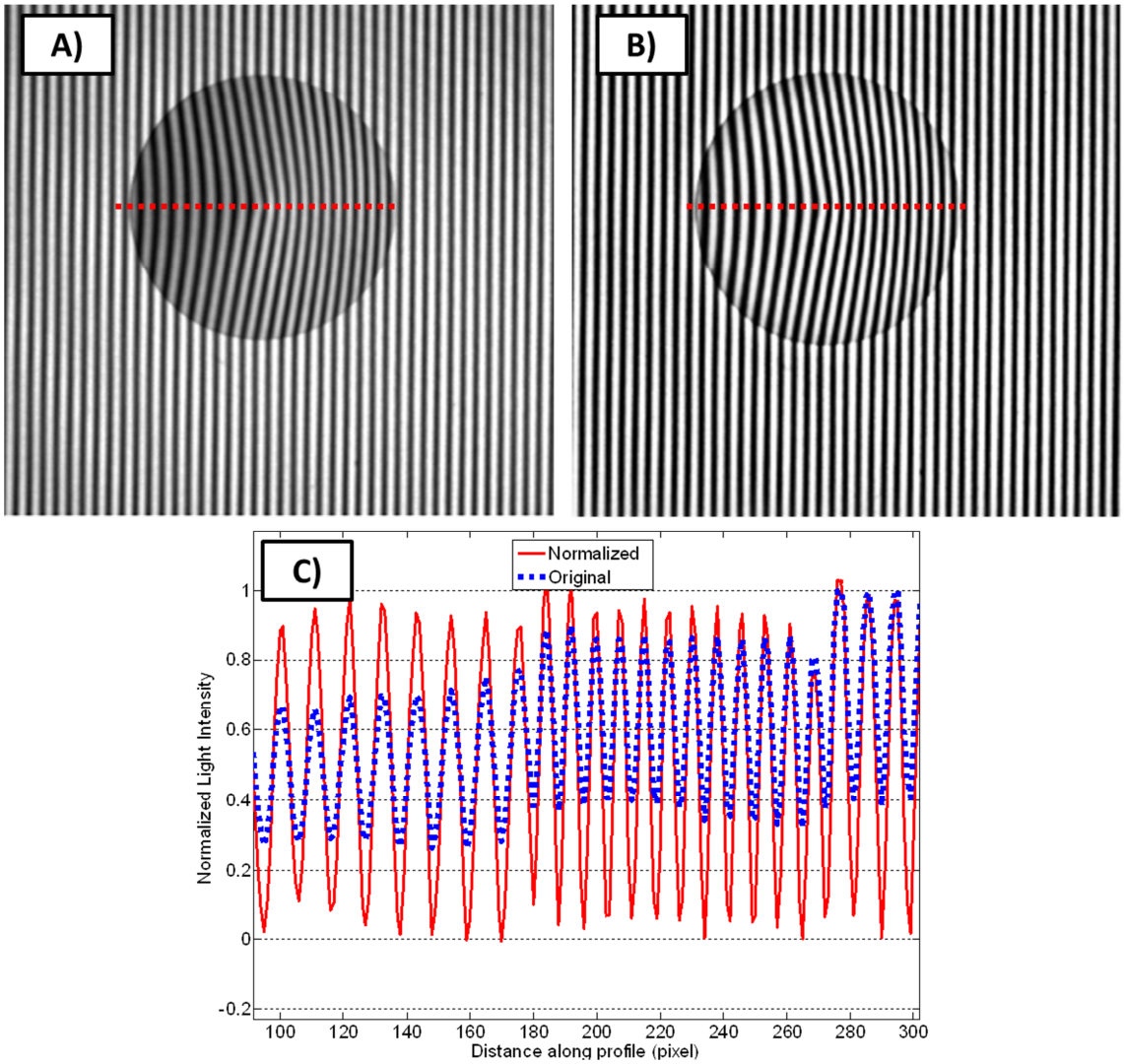

Figure 4.5 A) Original cone image to be pre-processed. B) Cone image normalized conditioned C) Profiles of light intensity comparing original image (blue) and normalized image (red)

In this thesis an adaptable normalization technique was employed to reduce the modulation effect in the background and the amplitude terms in fringe images and to improve the contrast of the speckle images (Heredia Ortiz, 2004) . Figure 4.5.A exhibits the image of a cone that serves to illustrate the effect of this normalization procedure,

The adopted normalization technique consists of dividing the image into facets (square windows). The size of the facets has to be larger than the projected pitch; more than twice this size is recommendable. If the speckle image is the one processed, the facet size has to be more than 3 times larger than the size of the speckle. The reason for the minimum sizes is because the facets upon which the images are divided have to represent the average background illumination of that area where maximum

illumination (no fringes or speckle is present) and minimum illumination (fringes or speckle is present) should be present in each facet. Otherwise, the bigger the facet, the less adaptable it is to local disturbances and the normalization pre-processing tool.

The next step is to calculate the average illumination of each facet and associate the average intensity value to the centre of the facet. Subsequently, a smooth map of average background illumination of the same size is performed by fitting the values of the centre of the facets to a polynomial function. Once the background map is obtained, it is subtracted from the original image obtaining a homogeneous background intensity map.

Finally a normalization procedure is performed to the whole image adjusting the maximum and minimum intensity value to 1 and 0 respectively.

Figure 4.5 shows an image before (Figure 4.5.A) and after (Figure 4.5.B) applying the proposed normalization procedure. Figure 4.5.C show a comparison of both images along the dashed line.

As is illustrated in Figure 4.5.C, the cone image has clearly been improved. It has a homogeneous background in comparison with the original one. Nevertheless, some tests were performed by Heredia (Heredia Ortiz, 2004) and it was discovered that the relation between the maximum projected fringe pitch (p_{max}) and the average pitch is critical. The limit found was that this technique is beneficial for images where $p_{max}<6p$, otherwise the effect could be harmful.

Sometimes, a final filtering step is required when the colours of the fringe and speckle patterns are not right. In this situation, some noise caused by the speckle is present in the fringe pattern. In this case, a smoothing filter is recommended in order to remove this noise from the image. A mean or median filter can be employed but the maximum mask size should be as wide as $p/4$ and at least twice the speckle size to avoid affecting the period of fringes or the shape of the fringe pattern.

For illustration purpose, Figure 4.6 shows an original RGB image which presents blue projected fringes and red speckle onto the specimen. After improving the fringe and

speckle patterns separately, it is possible to recover the RGB image and see that the colour has really improved when compared to the original. The pre-processed image present bright colours, both patterns present more contrast and the fringes are much more defined. The RGB processed image should serve as an example of the brightness of the colours that should be presented by both patterns.

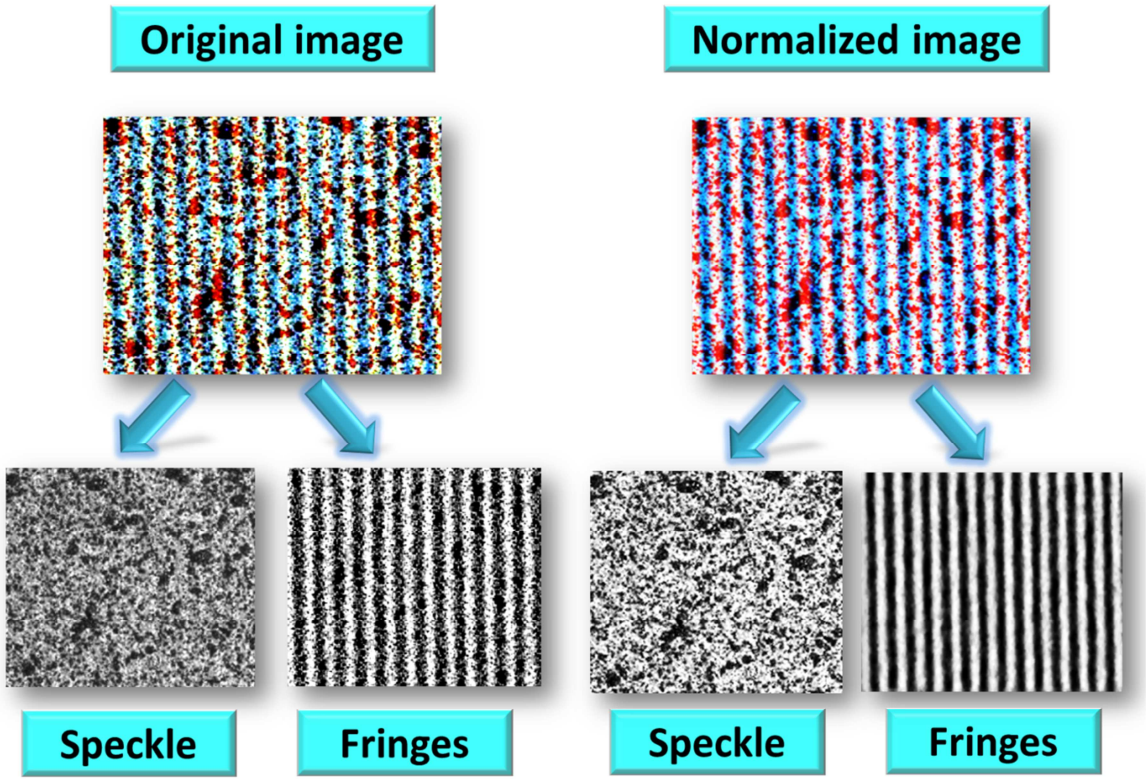

Figure 4.6 Comparison between original and normalized RGB image

4.3.6. Image Processing

Once images have been pre-processed, they are ready to be processed using both Fringe Pattern Analysis and Digital Image Correlation algorithms respectively. In this section the techniques used to obtain out-of-plane and in-plane displacement will be described.

4.3.6.1. Fringe projection technique.

As presented in Chapter 2, Fringe projection technique encompasses three steps: the Phase measurement, the unwrapping process and the phase to height conversion. In this epigraph the algorithms adopted to address each step will be described.

As concluded in chapter 2, the combined technique presented in this Thesis will adopt spatial methods like Fourier Transform Profilometry (Su & Wenjing, 2001) or an "artificial" Phase-Shifting called Phase-Stepping technique in which the phase shifting is digitally performed on the single acquired deformed fringe image (Heredia-Ortiz & Patterson, 2005). These are the most recommendable procedures as they present a good balance between the quality of the results obtained, the required computational time and the simplicity of their implementation.

A wrapped phase map results from the phase measurement step. The adopted algorithm to perform the unwrapping process will be the quality guided unwrapping procedure presented in Chapter 3 following a quality map defined by the statistical variance of the wrapped phase. Starting at a certain pixel, this algorithm removes the phase discontinuities in the wrapped phase map by following a crystal-growing quality-guided path, and by adding or subtracting 2π to the phase values associated with the pixels already processed.

The unwrapping process starts at a certain pixel. This pixel must be selected depending on its quality in order to start at a high quality area and to avoid error propagation. In addition, that starting point is considered as the reference fringe order from which the unwrapped phase is measured. In the case that large out-of-plane displacements are measured and that the complete wrapped phase map presents a different phase order from the reference, it is necessary to capture images of every smaller out-of-plane displacement in order to start the unwrapping process in a pixel placed on the same fringe order as the previous image. Therefore, it is possible to measure the phase difference between one image and the one that immediately precedes it instead of referencing it to the reference image. Hence, the out-of-plane distance measured is the added to that which was measured in the preceding step and the actual step.

Finally, it is necessary to convert the unwrapped phase map into height measurement. Several expressions have been proposed in literature to calculate the surface depth depending on the parameters of the set-up. In this thesis, this conversion is performed by applying a K_f factor which relates the phase and the height measurement inspired in previous approaches (Heredia Ortiz, 2004) (Asundi & Zhou, 1999). In the next chapter the determining of K_f factor will be explained more deeply as part of the alignment and the calibration set-up procedure.

4.3.6.2. Digital Image Correlation

2D-DIC has been performed to measure in plane displacements as part of the FP+2D-DIC system. In addition, in most of the tests addressed throughout this research, the in- and out-of-plane displacements measured with the proposed system have been compared with those obtained by employing 3D-DIC. In this epigraph it will be explained how both DIC analyses have conducted.

2D Digital Image Correlation has been performed by employing the algorithm ZNCC quality guided (Pan, et al., 2010) and employing subpixel resolution measurement (Hung & Voloshin, 2003). However, if large deformation occurs, more complex algorithms must be employed to obtain more accurate results. That is why commercial software (specifically VIC2D developed by Correlated Solutions Inc.) has been employed. Displacement maps provided by 2D-DIC are in pixels units. Conversion to distance units is done by employing the Lateral Magnification factor *L*.

In addition, 3D Digital image Correlation has been performed for comparison purpose. Two different commercial systems have been employed, namely VIC 3D (Correlated Solutions Inc.) and Q-400 (Dantec Dynamics A/S). In both case the first step was the calibration. The calibration procedure is performed by acquiring a series of images of a specific calibration target for each system. The calibration grid was placed in the area of interest of the test performed. In addition, that grid changed its orientation in every image acquired (10 and 20 images were employed).

After acquiring calibration images, the software performed the calculus of the required intrinsic and extrinsic parameters to calibrate the 3D-DIC set-up. Then the systems were ready to capture images during experiments.

4.4. Discussion

In chapter 4 the different algorithms and tools needed to perform Fringe projection and Digital image Correlation 2D simultaneously have shown .

As previously stated, the proposed FP+2D-DIC technique is based on obtaining fringe and speckle pattern from a single RGB image through the employment of a Bayer mask which performs an interpolation between two pixels. It is important to notice that this interpolating reduces the accuracy of the RGB respect of the Greyscale cameras since no real information exists between two pixels. For future work it is advisable to quantitative study what is lost in the accuracy.

During the tests performed, some considerations have arisen relating to image capturing. Some problems were detected in the RGB image-capturing of the cameras. RGB cameras, as previously commented upon, capture a grey scale image (RAW image); nevertheless, every pixel of that image is sensitive to a colour from the RGB pattern and the RGB image is composed. This process is usually performed internally in the camera. However, when employing certain cameras some distortions appear after this process. To avoid these distortions, images were captured in RAW format directly and later converted to RGB image employing Matlab software.

Additionally, it is important to take into consideration that the position and orientation of the projector defines the sensitivity of FP. Special care is required in order to obtain a constant fringe pattern period in the area of interest. This aspect will strongly depend on the specifications of the projector and the distance to the specimen which should be as big as possible, reducing possible optics aberrations of the projector.

Furthermore, it commented some pre-processing methods. It is important to know that those pre-processing tools, especially the filtering, should only be employed when

no better images can be obtained due to some loss of the original data (which could happen during the filtering stage). It is always preferable to spend more time setting the colour balance of the images and the illumination rather than performing filters to the obtained images.

Moreover, the methods employed to perform FP and DIC have been shown. They have been chosen as they present a good balance between an easy implementation and good results (as commented in chapter 3). Nonetheless, novel methods are continuously being developed which could offer better results than those achieved in this thesis, as for instance the Windowed Fourier Transform that was not used due to its computational requirements. It is important to notice that, to reproduce the test performed in this thesis, other alternative methods to 2D-DIC and FP can be employed provided that they offer the same information.

4.5. Concluding remarks

This previous analysis has led to the following conclusions:

- A complete methodology necessary to perform FP+2D-DIC when employing a single RGB camera and a colour projector has been presented.
- The set-up employed makes FP+2D-DIC system suitable for performing static or dynamic tests under different constrictions and sensitivity requirements.
- In-plane displacement maps measured by 2D Digital image Correlation are distorted by out of plane displacements. In the next chapter a procedure to obtain corrected in-plane displacements will be presented.
- Image pre-processing tools have been proposed to improve the processing results when images are captured in unfavourable conditions.
- Three main sources of error in image processing should be taken into account:
    - RGB filtering interpolates between 2 pixels, which decreases the real accuracy of the CCD.

- The model of Fringe Projection and Digital Image Correlation do not take into account any aberrations of lenses.
- Pre-processing tools could lightly affect the shape of the fringe-pattern due to filtering.

Chapter 5. Experimental methodology for in-plane displacements correction using Fringe Projection results

In this chapter the novel experimental methodology for the correction of the distorted in-plane displacement due to out-of-plane displacements is presented. In addition, the calibration procedure for the adopted set-up will be explained. This chapter presents first the adopted mathematical approach to correct in-plane displacement due to out-of-plane deformation. Finally, the experimental implementation of such a model and the methodology used for calibration will be explained and discussed.

5.1. Introduction

As previously stated, one main advantage of combining FP and 2D-DIC techniques is that 3D displacement fields can be quantified with one single camera. Moreover, speckle and fringe patterns can be easily separated if a colour RGB CCD camera is employed. However, as highlighted by (Mares, et al., 2011), in–plane displacements from 2D-DIC are corrupted by out-of-plane deformations.

In this chapter, the distortion of the in-plane displacements will be modelled and studied. The result will be a mathematical expression that makes it possible to correct in-plane displacements measured with 2D-DIC using the out-of-plane information provided by Fringe Projection. In addition, an experimental procedure to calibrate the proposed set-up for the simultaneous implementation of both techniques will be presented and discussed.

5.2. Correction of 2D-DIC displacements

Figure 5.1 schematically illustrates the error induced in the 2D-DIC technique when the measured object experiences out-of-plane displacements during deformation. The scheme is based on a pin-hole camera model. This figure describes in a clear way the relationship between the coordinates of a 3D point at the deformed object surface and its projection onto the image plane (CCD camera sensor) for an ideal pin-hole camera.

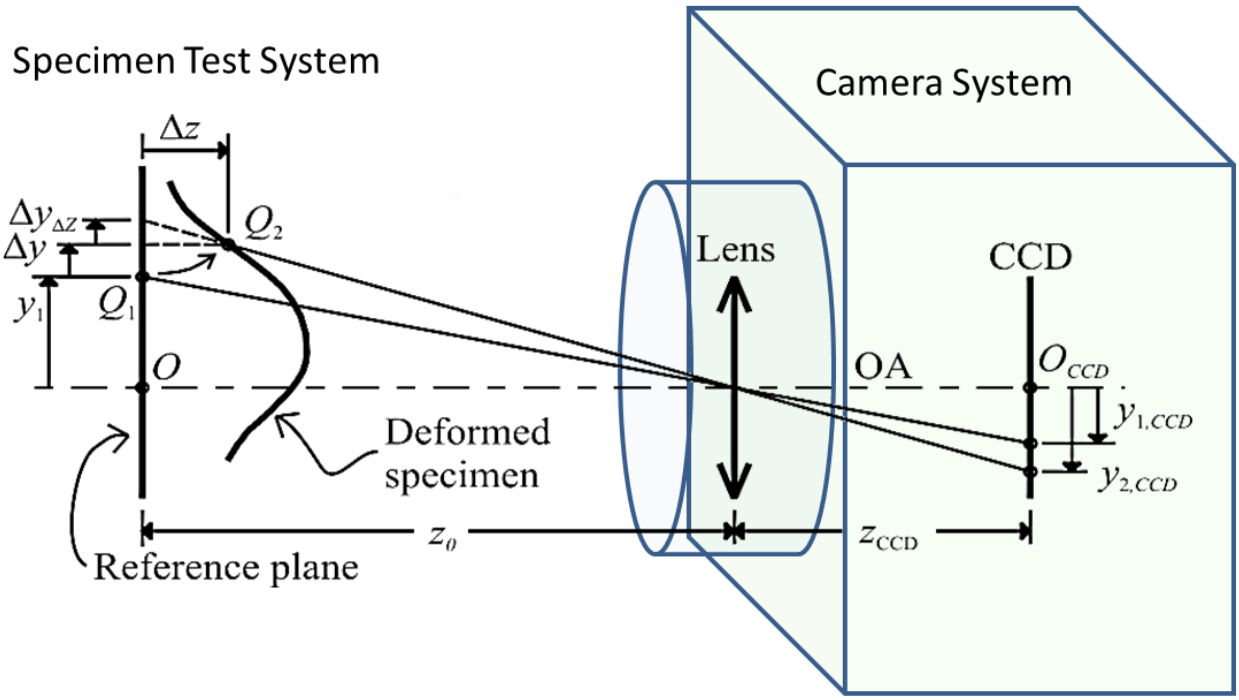

Figure 5.1 Schematic illustration showing the in plane error induced in 2D-DIC when the specimen experiences out-of-plane displacements during a deformation process.

For illustration purposes, it is assumed that the object experiences in and out-of-plane displacements from a flat reference surface (Figure 5.1), denoted as reference plane.

The in-plane displacements observed at the CCD plane have opposite direction to those occurring at the surface of the deformed object. In both cases, the displacements are measured relative to a reference system with its origin at *O,* for the case of the reference plane and O_{CCD} for the CCD plane. Both origins are defined as the intersection of the optical axis (OA) with the reference plane and the CCD plane respectively, as illustrated at Figure 5.1. Nevertheless, the real in-plane displacements $(\Delta x, \Delta y)$ resulting from the movement of a point Q from a position $Q_1 = (x_1, y_1, 0)$ in the reference plane to a position $Q_2 = (x_1 + \Delta x,\ y_1 \Delta y, \Delta z)$ in the deformed specimen (Figure 5.1) does not

correspond to the displacement observed at the CCD camera plane. The observed displacement at the CCD camera plane will be:

$$\Delta \boldsymbol{x_{CCD}} = \boldsymbol{x_{2,CCD}} - \boldsymbol{x_{1,CCD}}$$
$$\Delta \boldsymbol{y_{CCD}} = \boldsymbol{y_{2,CCD}} - \boldsymbol{y_{1,CCD}} \qquad \text{Eq 5.1}$$

Since the in-plane displacements occurring at *Q* are measured using the displacement observed at the CCD plane, the presence of an out-of-plane displacement, Δz, will introduce a virtual in-plane displacement $(\Delta x_{\Delta z}, \Delta y_{\Delta z})$ that has to be subtracted from the measured displacements at the CCD plane to obtain the real in-plane displacements. This is the real in-plane displacements for point *Q* will be:

$$\Delta \boldsymbol{y} = \boldsymbol{L}\Delta \boldsymbol{y_{CCD}} - \Delta \boldsymbol{y_{\Delta z}} \qquad \text{Eq 5.2}$$

Where *L* is the lateral magnification (in mm/pixels) at the distance z_0 between the reference plane and the optical centre of the lens. A similar expression can also be deducted for Δx.

$$\Delta \boldsymbol{x} = \boldsymbol{L}\Delta \boldsymbol{x_{CCD}} - \Delta \boldsymbol{x_{\Delta z}} \qquad \text{Eq 5.3}$$

In addition, the virtual in-plane displacements($\Delta y_{\Delta z}$) due to Δz can be obtained considering that *Q* has only out-of-plane displacement in Figure 5.1 (i.e. maintaining $y_2 = y_1 = y$). Then, by applying the lens transformation equation the following expression is obtained.

$$\frac{\boldsymbol{y}}{\boldsymbol{z_0}} = \frac{\boldsymbol{y_{1,CCD}}}{\boldsymbol{Z_{CCD}}}$$
$$\frac{\boldsymbol{y}}{\boldsymbol{z_0} - \Delta \boldsymbol{z}} = \frac{\boldsymbol{y_{2,CCD}}}{\boldsymbol{Z_{CCD}}} \qquad \text{Eq 5.4}$$

Virtual in-plane displacements measured at the CCD plane (in pixels) can be calculated then as:

$$\Delta \boldsymbol{y}_{\Delta \boldsymbol{z},\boldsymbol{CCD}} = \boldsymbol{y}_{\boldsymbol{2},\boldsymbol{CCD}} - \boldsymbol{y}_{\boldsymbol{1},\boldsymbol{CCD}} = \boldsymbol{y}_{\boldsymbol{2},\boldsymbol{CCD}} \frac{\Delta \boldsymbol{z}}{\boldsymbol{z_0}} = \boldsymbol{y}_{\boldsymbol{1},\boldsymbol{CCD}} \frac{\Delta \boldsymbol{z}}{\boldsymbol{z_0} - \Delta \boldsymbol{z}} \qquad \text{Eq 5.5}$$

To obtain:

$$\Delta \boldsymbol{y}_{\Delta \boldsymbol{z}} = \boldsymbol{L} \Delta \boldsymbol{y}_{\Delta \boldsymbol{z},\boldsymbol{CCD}} = \boldsymbol{L} \boldsymbol{y}_{\boldsymbol{2},\boldsymbol{CCD}} \frac{\Delta \boldsymbol{z}}{\boldsymbol{z_0}} \qquad \text{Eq 5.6}$$

By substituting Eq 5.6 in Eq 5.2 , it is possible to obtain the real in-plane displacements occurring at each point at the object surface during deformation. Eq 5.7 mathematically illustrates the real in-plane displacements occurring at the surface of the deformed object based on displacements measured at the CCD camera plane corrected by the out-of-plane information Δz provided by FP technique.

$$\begin{cases} \Delta \boldsymbol{x} = \boldsymbol{L}[\, \Delta \boldsymbol{x}_{\boldsymbol{CCD}} - \boldsymbol{x}_{\boldsymbol{2},\boldsymbol{CCD}} \frac{\Delta \boldsymbol{z}}{\boldsymbol{z_0}}] \\ \Delta \boldsymbol{y} = \boldsymbol{L}\, [\Delta \boldsymbol{y}_{\boldsymbol{CCD}} - \boldsymbol{y}_{\boldsymbol{2},\boldsymbol{CCD}} \frac{\Delta \boldsymbol{z}}{\boldsymbol{z_0}}] \end{cases} \qquad \text{Eq 5.7}$$

To obtain Eq 5.7, a simplified scenario in which a point *Q* moves from a reference plane to a deformed state has been considered. However a more realistic scenario is when the object moves between two deformed states; one displaced Δz_1 and another displaced Δz_2 from the reference plane. Then, by subtracting Eq 5.7 for these two deformed stages, the following equations are obtained:

$$\begin{cases} \Delta \boldsymbol{x} = \boldsymbol{L}\, \left[\Delta \boldsymbol{x}_{\boldsymbol{CCD}} - \boldsymbol{x}_{\boldsymbol{2},\boldsymbol{CCD}} \frac{\Delta \boldsymbol{z_2}}{\boldsymbol{z_0}} - \boldsymbol{x}_{\boldsymbol{1},\boldsymbol{CCD}} \frac{\Delta \boldsymbol{z_1}}{\boldsymbol{z_0}}\right] \\ \Delta \boldsymbol{y} = \boldsymbol{L}\, \left[\Delta \boldsymbol{y}_{\boldsymbol{CCD}} - \boldsymbol{y}_{\boldsymbol{2},\boldsymbol{CCD}} \frac{\Delta \boldsymbol{z_2}}{\boldsymbol{z_0}} - \boldsymbol{y}_{\boldsymbol{1},\boldsymbol{CCD}} \frac{\Delta \boldsymbol{z_1}}{\boldsymbol{z_0}}\right] \end{cases} \qquad \text{Eq 5.8}$$

Where subscripts 1 and 2 indicate initial and final states during the deformation process.

Thus, according to Eq 5.8 real in-plane displacements can be measured from the displacements observed at the CCD plane using 2D-DIC technique once they are

corrected by the out-of-plane displacements inferred using FP. For the correction process, the following parameters are required according to Figure 5.1:

i) The distance z_0 between the optical centre and the reference surface.

ii) The lateral magnification L at z_0 (in mm/pixels) .

iii) The position of O_{CCD} from where the in-plane displacements are measured at the CCD plane.

The lateral magnification L is easy to obtain by measuring a known in-plane distance between two points at the reference plane. However, z_0 and the position of O_{CCD} cannot be directly measured since the location of the optical centre of the lens and the optical axis are not known. To obtain these two parameters a calibration process is required. It must be noted that to successfully apply Eq 5.7 and Eq 5.8, it is compulsory to have a precise perpendicular alignment between the optical axis (OA) and the reference plane.

5.3. Displacements in Z direction (w-displacements)

Once the in-plane displacements have been corrected with the out-of-plane information, it is possible to calculate *w* displacements (displacements in Z direction). It must be remarked that *w* displacements are not the same as the out-of-plane shape provided by FP technique, since FP cannot quantify if a point in the deformed object has suffered an in-plane deformation. Thus, real displacements in Z direction (*w*-displacements) must be calculated as the height difference referred to the reference plane between two states of deformation, as indicated in Eq 5.9.

$$\boldsymbol{\Delta z(x,y) = z_2(x + \Delta x(x,y), y + \Delta y(x,y)) - z_1(x,y)} \qquad \text{Eq 5.9}$$

5.4. Calibration of FP + 2D-DIC system

As indicated in Eq 5.8, the in-plane displacements correction depends on the distance from the reference plane to the lens plane (z_0). Thus, it is necessary to define a

calibration methodology in order to infer this distance. The proposed calibration method consists on creating in a virtual in-plane displacement in 2D-DIC by translating a plane object a known distance in the direction perpendicular to the camera (Felipe-Sesé, et al., 2014). Thus, z_0 will be the distance that makes the in-plane displacements equal to zero in Eq 5.8.

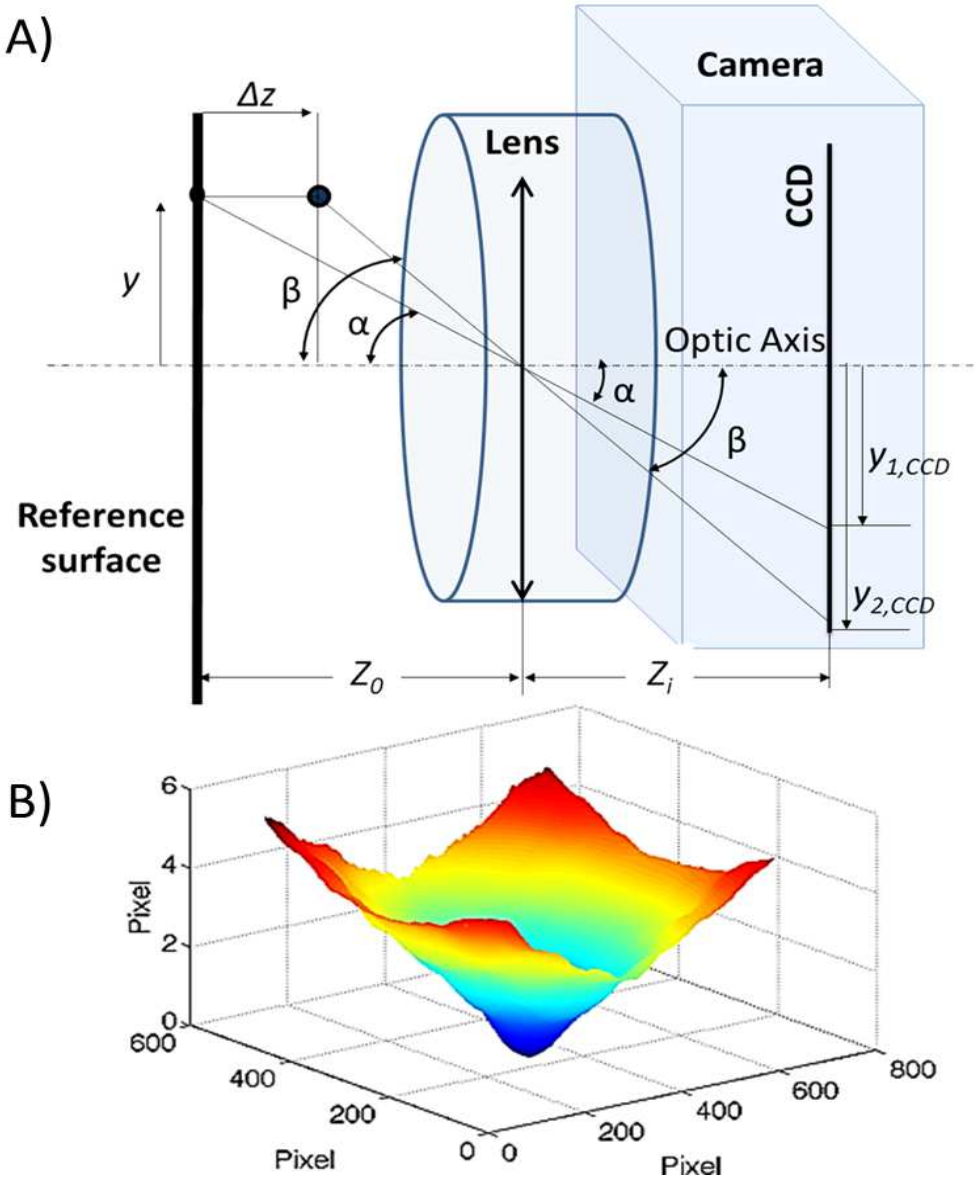

Figure 5.2 A) Illustration showing the schematic set-up for calculating z0 and OCCD, B) Example of cone of radial displacements (CRD).

Thus, as illustrated in Figure 5.2.A two images of the reference surface are captured when it is moved a known distance, Δz, towards the camera plane along the optical axis (OA). Subsequently, these two images are processed using a 2D-DIC cross correlation algorithm. The real in-plane displacements (Δx and Δy) must be zero according to Eq 5.7,

however 2D-DIC provides a value different from zero. However, virtual displacements measured at the CCD camera plane (Δx_{CCD} and Δy_{CCD}) can be related to z_0 and the distance Δz using α and β angles as shown in Figure 5.2.A:

$$\Delta \boldsymbol{x_{CCD}} = \boldsymbol{m}\,(\boldsymbol{x_{2,CCD}} - \boldsymbol{x_{1,CCD}})$$
$$\Delta \boldsymbol{y_{CCD}} = \boldsymbol{m}\,(\boldsymbol{y_{2,CCD}} - \boldsymbol{y_{1,CCD}}) \qquad \text{Eq 5.10}$$
$$\text{With } \boldsymbol{m} = \frac{\Delta z}{\boldsymbol{z_0} - \Delta z}$$

A similar expression was obtained by Tay et al. (Tay, et al., 2005), but in their case a simplified slope $m=\Delta z/z_0$ was considered. Thus, z_0 can be obtained from the slope (m) of the module of the radial displacements Δr_{CCD} which has the shape of a cone with its vertex placed at the optical axis (Figure 5.2.B), as indicated in Eq 5.11:

$$\Delta \boldsymbol{r_{CCD}} = \sqrt{\Delta \boldsymbol{x_{CCD}^2} + \Delta \boldsymbol{y_{CCD}^2}} = \boldsymbol{m}\sqrt{\boldsymbol{x_{1,CCD}^2} + \boldsymbol{y_{1,CCD}^2}} \qquad \text{Eq 5.11}$$

The cone presented in (Figure 5.2.B) is known as cone of radial displacement (CRD).

If experimental data is fitted to Eq 5.11, $\boldsymbol{m}$ can be calculated and z_0 can be inferred according to the equation:

$$\boldsymbol{z_0} = \Delta \boldsymbol{z}\left(\frac{\boldsymbol{1}}{\boldsymbol{m}} + \boldsymbol{1}\right) \qquad \text{Eq 5.12}$$

If the images are acquired first at $z_0+\Delta z$ and subsequently at z_0 the equation would be:

$$\boldsymbol{z_0} = \frac{\Delta \boldsymbol{z}}{\boldsymbol{m}} \qquad \text{Eq 5.13}$$

The vertex of the CRD provides the position O_{CCD} in the CCD camera plane. For a precise displacement of the reference surface along the optical axis (OA), the position of O_{CCD} should not change for different values of Δz. In the majority of the commercial cameras the centre of the sensor is in the intersection of the optical axis (OA) with the CCD plane,

however, the lack of the perpendicular between the reference surface and the optical axis (OA) constitutes itself an important source of error that needs to be experimentally minimized.

Finally, once the system has been calibrated, it is possible to test any specimen with a non-flat surface. The measured displacements will be referred to the reference surface employed in the calibration process.

5.5. Calibration set-up for 3D displacements measurement

Based on the previous calibration procedure, an adjustable set up has been developed that has made it possible to calibrate both techniques simultaneously and to minimize the alignment errors during calibration.

As previously shown, out-of plane displacements are measured along the optical axis (OA) (in *z*-direction). They are referred to a reference surface which has to be perpendicular to the optical axis.

Figure 5.3.A shows the adopted setup used for calibration. It is basically the set-up presented in the previous chapter (camera (1), projector (2) and computer (7)). With some extra elements such as a laser pointer (3), a *z*-displacement platform (4), and a 2-axis tilt platform (5). The system was placed on a tripod headset which has some handles which allows the whole system to be aligned with respect to the reference surface (8). A lateral view of a deformed specimen is shown in Figure 5.3.B.

Over the tripod headset the *z*-displacement platform allows precise *z*-displacement of the camera, the laser and the projector. Over the *z*-displacement platform the 2-axis tilt platform is attached which allows the alignment of the system camera-laser parallel to the *z*-displacement axis (*z*-DA). Finally, the laser has its own alignment mechanism that allows the laser beam (LB) to be aligned parallel to the optical axis (OA) of the camera.

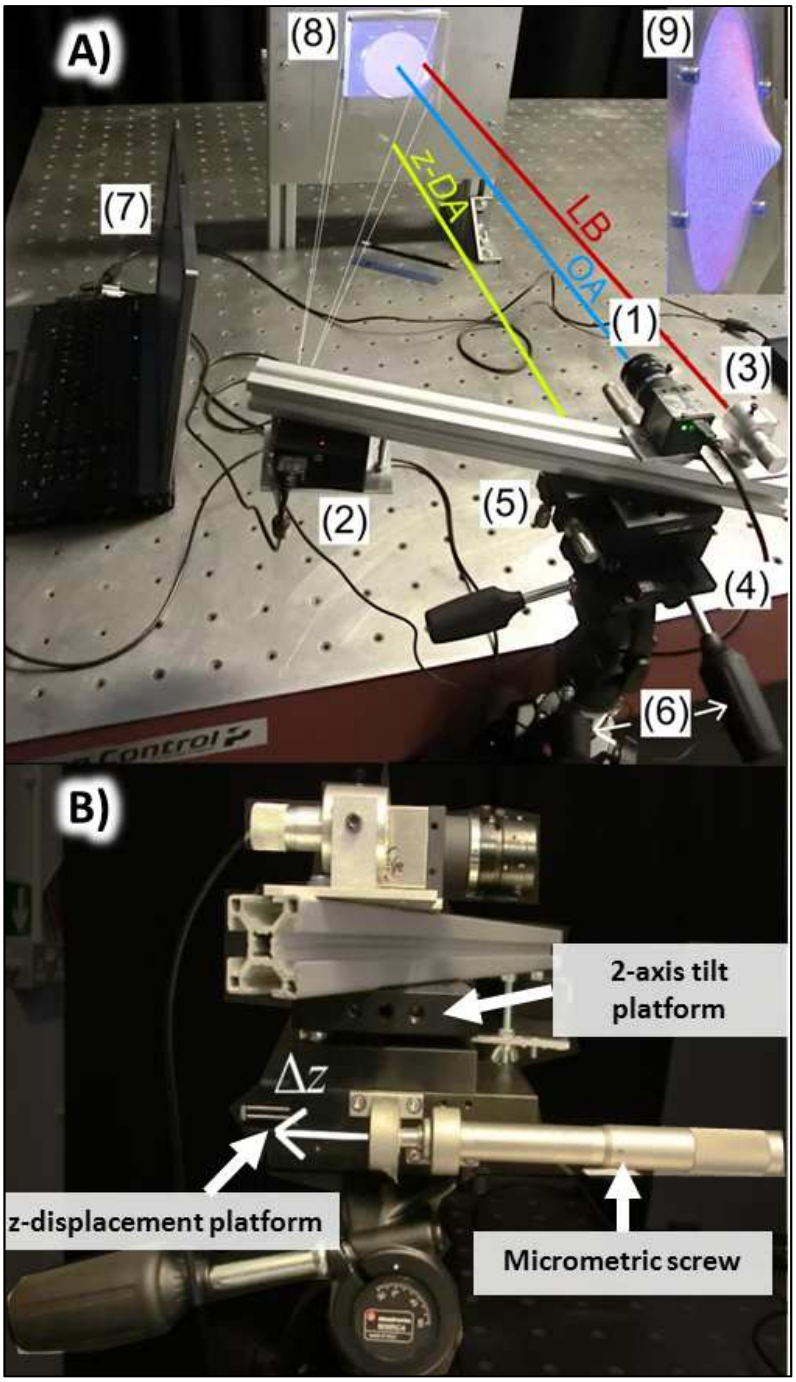

Figure 5.3. Experimental set-up adopted for calibration. B) Lateral view showing a micrometric screw that allows precise displacement along the z- displacement axis (z-DA

For precise parallel alignment of the optical axis with the displacement axis, two images of the reference surface are acquired as the camera is moved a known distance (Δz) along the displacement axis (Z-DA in Figure 5.3.A).

The calibration procedure is computer-aided by a guided-user-interface program written in Matlab (Figure 5.4) which captures, processes and displays the images in real-time in

order to perform both the alignment and calibration. With this program it is possible to acquire two different images (namely at z_0 and $z_0+\Delta z$) in the area of the interface named as A in Figure 5.4. In addition it is possible to define different regions of interest in of those images to set the value of Δz displacement and the number of fringes (N_f), if in Δz displacing the fringes moved more than one unit of the pitch. After acquiring the images, the alignment of *OA* with the z-DA axes is performed (section B in Figure 5.4). Once *OA* and z-DA axes are aligned, it is possible to perform 2D-DIC calculate the distance z_0 and the position of the vertex of the CRD (section C in Figure 5.4). Subsequently, the laser alignment and the calculation of the lateral magnification (L) is conducted (section D in Figure 5.4). Finally, Fringe projection calibration is performed (section E in Figure 5.4).

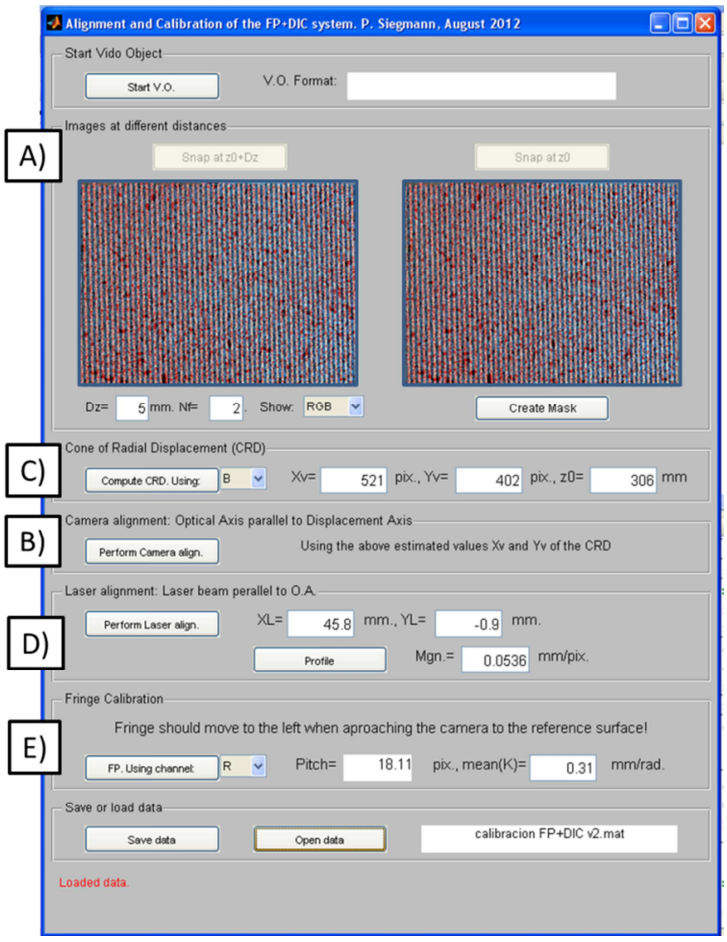

Figure 5.4 Illustration showing the Matlab guided-user-interface program employed for calibration

5.5.1. Alignment procedure and estimation of z_0

The device shown in Figure 5.3 must be placed in front of the reference surface (painted with red speckle pattern on a white background) with the camera CCD plane as parallel as possible to the reference surface. In this case, for the alignment of the calibration device, fringes do not need to be projected on the reference surface.

5.5.1.1. Alignment of the OA with the z-DA

To align the optical axis (OA) parallel to the z-DA axis, two speckle images of the reference surface must be acquired: one at a distance $z_0+\Delta z$ (Figure 5.5.A) and another one at a distance z_0 (Figure 5.5(b)) from the camera to the reference surface. Subsequently, these two images must be processed using a 2D-DIC algorithm to obtain the in-plane displacement modulus $\Delta r = \sqrt{\Delta x_{CCD}^2 + \Delta y_{CCD}^2}$. As a result, the cone of radial displacement (CRD) is obtained (Figure 5.2.B)). The cone of radial displacements indicates that facets move away from the centre of the image. As it was explained in the previous epigraph, these displacement values should be zero, however its values differs from zero since but they are distorted by the Δz out-of plane displacements. Hence, if the slope (***m***) of the cone of radial displacement is calculated and the value of Δz is known, Eq 5.12 can be employed to calculate z_0 considering that $\Delta x=\Delta y=0$.

Figure 5.5.A and B show the acquired images of the reference surface before and after the camera experiences a relative displacement of $\Delta z=30$ *mm*. To reduce computation time, 2D-DIC algorithm is only applied to a cross mask presented in Figure 5.5.C (black dots).

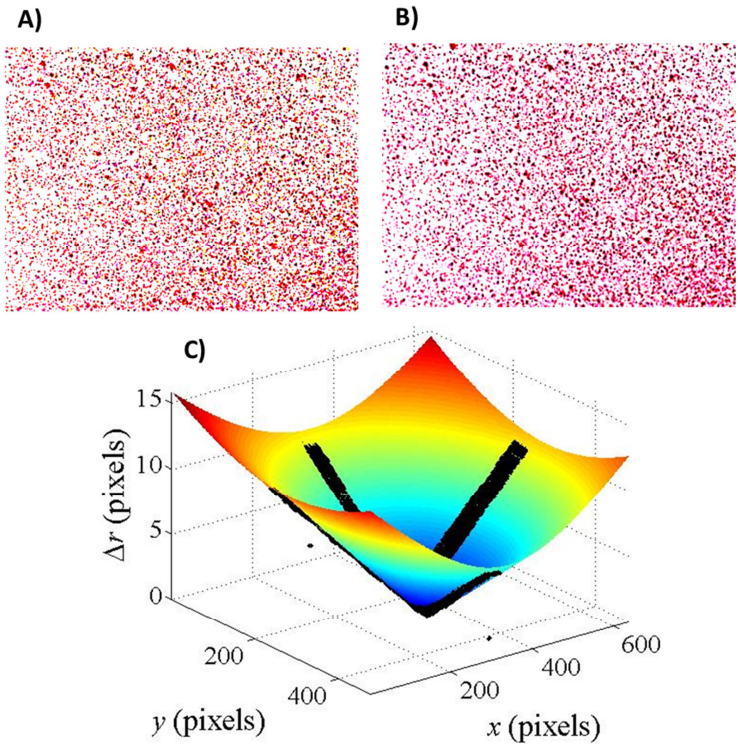

Figure 5.5 Image acquired through the B-channel a) at z0+Δz and b) at z0. c) Computed CRD.

As it can be appreciated in Figure 5.6, if the OA and the z-DA are perfectly aligned, the vertex of the CRD ($P_{V,CCD}$) must be in the centre of the image (C_{CCD}).

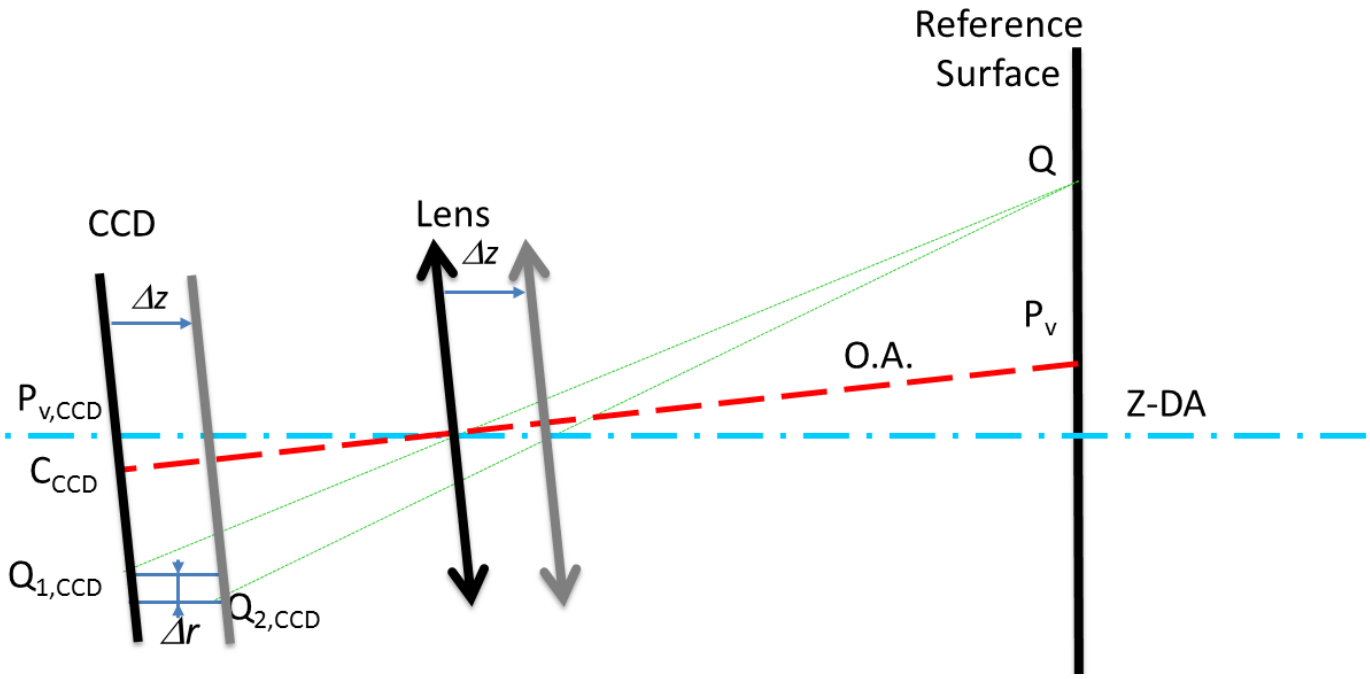

Figure 5.6 Schematic illustration showing of the effect of approaching the reference surface towards the camera a distance *Δz* when the Z-DA is not aligned with the OA

For a perfect alignment of the OA with the z-DA, it is necessary to tilt the 2-axis tilt platform until $P_{V,CCD}$ =(x_v,y_v) coincides with C_{CCD} =(x_c,y_c). This is done by artificially moving the image (I_0) captured at z_0 to the theoretical position where it should be if the OA and Z-DA were perfectly aligned.

Hence, a virtual image is generated. The image I_0 virtually displaced a distance given by and ; resulting: .

Subsequently, using the proposed, guided user interface, a live image I_L (Figure 5.7.A) is superposed over in Figure 5.7.B. Finally, the 2-axis tilt platform is adjusted until the live image I_L coincides with (Figure 5.7.C).

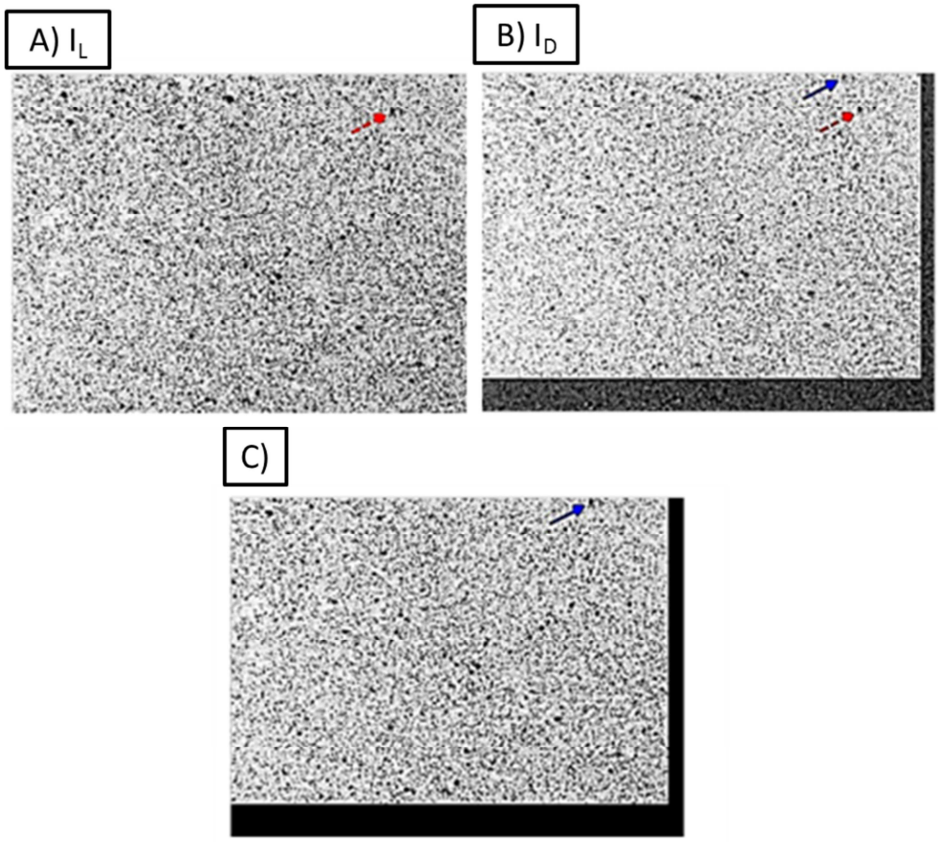

Figure 5.7. Illustration showing the sequence followed for the alignment of the OA with the z-DA. a) Live image I_L, b) superposed image I_D, c) displaced live image until I_D coincides with .

5.5.1.2. Alignment of the OA with the laser beam

Once OA and Z-DA are aligned, both axes must be placed perpendicular to the reference plane. For this purpose, the laser pointer aligned with the OA was employed.

If the relative distance between the centre of the laser beam and the centre of the camera lens was known, a perfect alignment was achieved when the distance between the OA and the centre of the laser beam remains constant as Δz changed. This implied that the laser beam and the optical axis were both parallel.

Using the proposed guided-user-interface, the relative distance between the laser beam and the centre of the camera lens can be visualized (Figure 5.8.A). After that, the alignment screws of the laser were adjusted until the laser spot was within the circle indicating the theoretical position (Figure 5.8 B)). Once the three axes were aligned they had to remain unchanged during experiments.

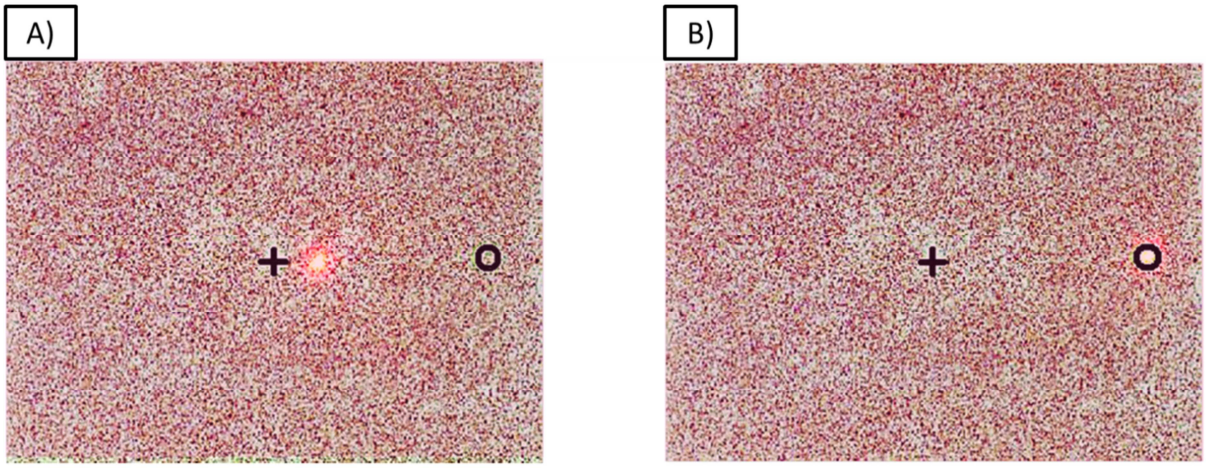

Figure 5.8 Illustration showing the alignment process for the laser beam all and the OA. a) Unaligned, b) aligned.

5.5.1.3. Perpendicular alignment of the OA with the reference surface

Once the OA, Z-DA and the laser beam were aligned, the perpendicular alignment of the OA with the reference surface was achieved when the laser spot reflected from a mirror attached to the reference surface was located at the laser output. This was performed by carefully orientating the whole calibration set-up using the tripod positioning handles.

5.5.1.4. Estimation of z_0

After aligning the OA with the z-DA and the perpendicular alignment of both axes with the reference surface, the estimation of z_0 was be performed. Hence, two speckle with

projected fringes images of the reference surface were acquired: one at a distance $z_0+\Delta z$ (Figure 5.5.A) and another at a distance of z_0 (Figure 5.5.B)) from the camera to the reference surface. Images were processed using 2D-DIC software, the cone of radial displacement (CRD) was obtained and z_0 was calculated from Eq 5.12.

5.5.2. Fringe calibration procedure

The following step to perform the fringe calibration procedure. The displacement Δz produced a fringe shifting, $\Delta\phi$, that was computed by processing the fringe patterns. Fringe images were acquired through R-channel, and processed using a 5-step phase shifting method (Heredia Ortiz, 2004) with a quality guided unwrapping algorithm based on the phase derivative variance (Ghiglia & Pritt, 1998)

The phase extraction algorithm was unable to account for an integer number of fringes (N_f), thus, if fringes moved more than one unit of the pitch, 2π had to be added to the shifted phase. Therefore, it was possible to obtain a fringe constant, K_f, for each of the pixels at position (x,y) instead of an average value for the whole image:

$$\boldsymbol{K_f(x,y) = \frac{\Delta z}{\Delta\phi(x,y) + 2\pi N_f}} \qquad \textbf{Eq 5.14}$$

K_f was employed to compute the out-of-plane displacements of the deformed specimen surface. Figure 5.9 shows an example of the shifted phase (a horizontal profile) for a displacement $\Delta z=10$ *mm* ($N_f=1$). Figure 5.9.B shows the fringe constant for each pixel for a selected region at the reference surface, offering more accuracy than a single value for the whole image. In this example an increase in the fringe constant was observed (0.01 mm/rad) from left to the right. This is due to the divergent fringe projection of the projector that produces an increase of the fringe pitch in the projection direction, as it was pointed out in chapter 4.

The presented calibration procedure was inspired in the methodology proposed by Asundi and Zhou (Asundi & Zhou, 1999), which consisted of obtaining the phase of the reference surface at several different Z positions. As previously shown, the inherent

geometric relationship between the *Z* and the displaced fringe pattern implies that systematic parameters (geometrical parameters and lens-distortion parameters) are not required during calibration. However, in the proposed method only two different positions (at z=0 and *z=10mm*) were employed, and it was assumed that a linear relation between the shifted phase shifting and the z-displacement for each pixel existed (Xiaoling, et al., 2005). This assumption was considered to be accurate enough for a successful comparison between FP and 3D-DIC.

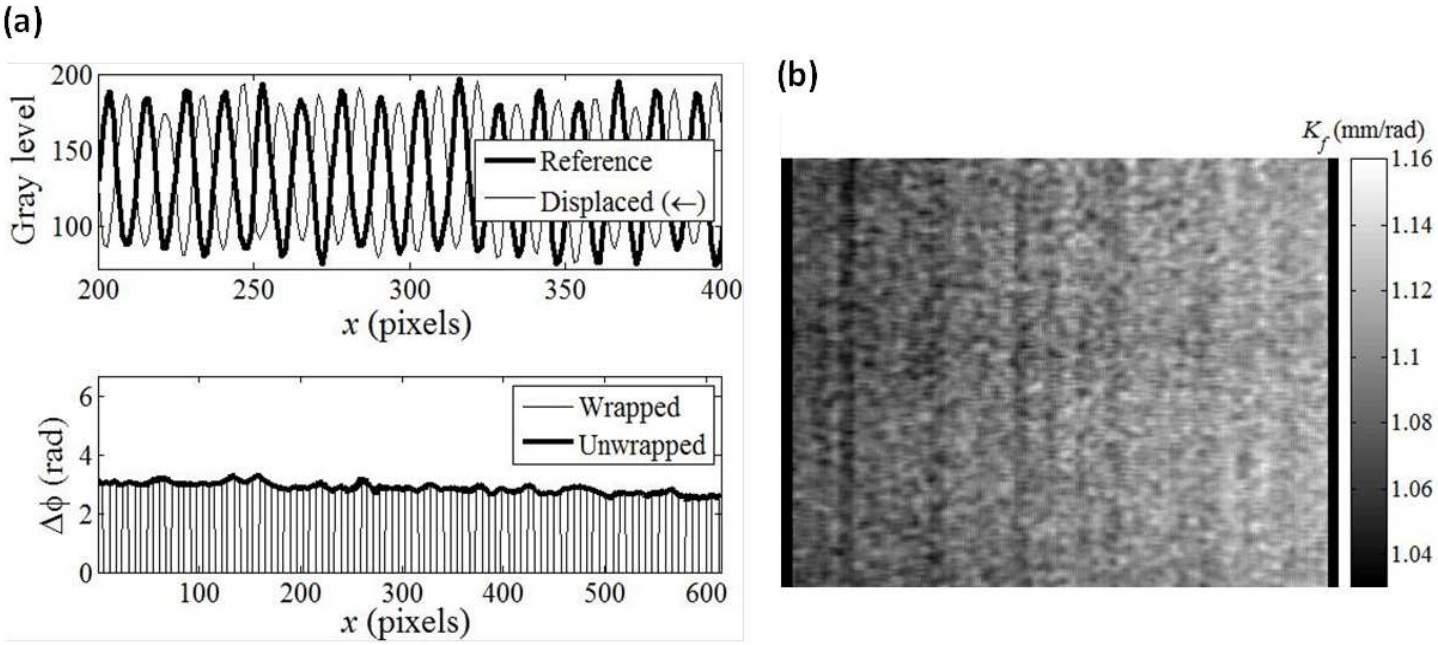

Figure 5.9 Illustration showing the influence of moving the camera Δz =10 mm ($N_f = 1$) towards the reference surface during the calibration of FP technique. a) Horizontal profile showing the shift between fringes (top left) and the measured phase shift. b) Fringe constant for a selected region of the image.

5.5.3. Calibration of 2D-DIC

Since the adopted 2D-DIC algorithm only provides in-plane displacements in pixels a calibration procedure to convert the displacements in pixels into length units is required. The Matlab calibration interface shown in Figure 5.4 implements this possibility by incorporating a calibration routine for 2D-DIC. This routine captures an image of a known distance in length units over the reference surface (distance between two points marked on the reference surface). Subsequently, the number of pixels for the

known distance is related to the length units (for example millimetres) and a relation *L* (px/mm) is obtained.

5.6. Discussion

In this chapter, the objective of developing a mathematical expression for correcting in–plane displacements distorted by out-of-plane displacements has been successfully performed. Hence, FP+2D-DIC can be employed for in-plane and out-of-plane displacements analysis avoiding the use of a telecentric lens. Moreover, the procedure involves a precise calibration and the determination of some factors that require to being looked in more detail to obtain a better understanding of the performance and limitations of this correction methodology.

The in–plane displacement correction procedure is based on the pin-hole model where geometric distortions or blurring of unfocused objects caused by lenses are neglected. Hence, in case those distortions occur, the correction would be affected. This indicates that the proposed procedure is suitable only when the simplifications of the pin-hole model are really negligible.

The adopted correction approach is based on referring the displacements to a reference plane which is settled parallel to the camera sensor (usually CCD). Hence, one major limitation in the correction of 2D-DIC displacements employing PF results is the necessity of a precise perpendicular alignment of the optical axis with a flat reference surface. This implies that if the studied element is curved, it is necessary to perform the calibration employing a flat reference.

In addition, the alignment of the OA and *z-DA is* decisive in order to perform a good correction of the in-plane displacements. Attending to the correction procedure, it is observed that if the axes are not precisely aligned, the correction would be excessive in some areas of the in-plane displacement fields and deficient in others. This is due to the fact that the correction procedure considers the whole surface at a distance z_0, even if there are areas closer to and other farther from the camera sensor.

Moreover, according to Eq 5.7, it is observed that as z_0 gets smaller and as farther away from the centre of the image, the bigger is the required correction of the in-plane displacements for the same out-of-plane displacement. Hence, an error in the estimation of z_0 will affect more on the in-plane correction as smaller is the value of z_0. To study how the estimation of the distance z_0 affects the correction of the in-plane displacement (e.g. Δx) given in Eq 5.7, the error factor (e) of the in-plane correction is defined as follows

$$e := \frac{d}{dz_0}(\Delta x) = Lx_{2,CCD}\frac{\Delta z}{z_0^2} = \tan\gamma\frac{\Delta z}{z_0} \qquad \text{Eq 5.15}$$

where $\gamma = \tan^{-1}\frac{Lx_{2,CCD}}{z_0}$. Hence, $\gamma$is the field of view of the camera lens (larger as larger is the maximum distance from the center of the image). Supposing an out-of-plane displacement of Δz=1mm, the error e is represented in figure X as a function of z_0 for different values of θ(e.g. 5°, 15° and 30°).

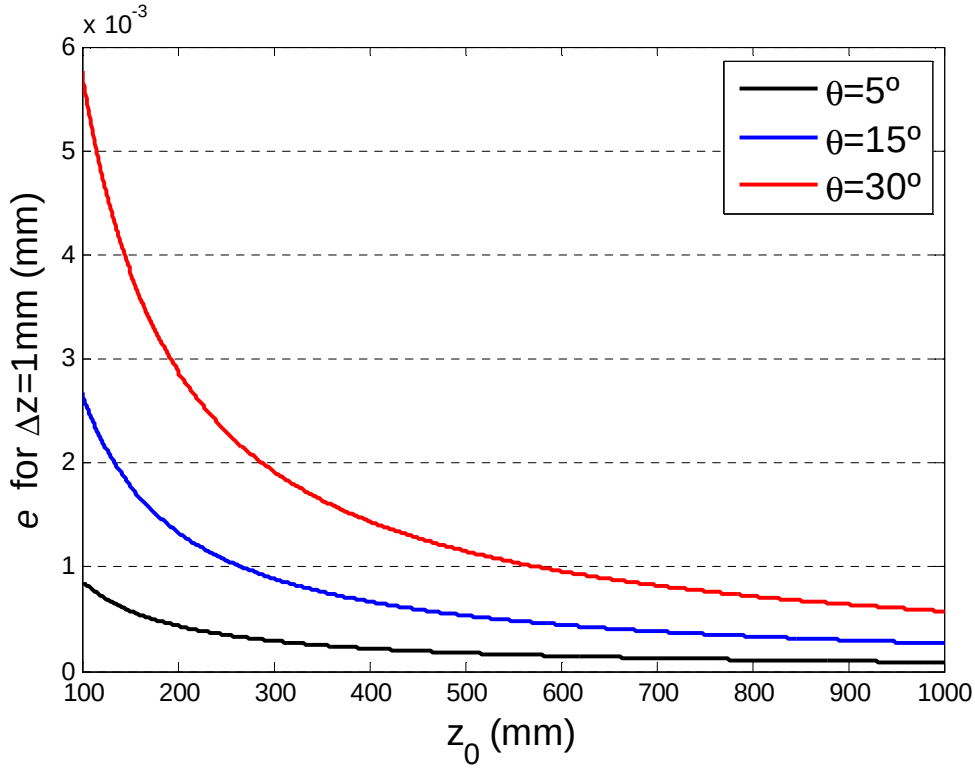

Figure 5.10 Error factor of the in-plane displacement correction when Δz =1 mm

Figure 5.10 shows that, as expected, the error produced in the correction of the in-plane displacement decreases by increasing z_0 and for pixels placed closer to the centre of the image. The actual error for a big mistake of 10% by estimating z_0 is:

$$e \cdot dz_0 = \tan\gamma \frac{\Delta z}{z_0} dz_0 = \tan\gamma \frac{\Delta z}{100} 10 \qquad \text{Eq 5.16}$$

Figure 5.11 illustrate the error of the in-plane displacement correction due to three different out-of-plane displacements (i.e. 1 mm, 10 mm and 20 mm) and for an error in the estimation of z_0 of 10% with respect the field of view. Considering that the employed lenses usually have a field of view around 10° and 30°, the error induced to the in-plane displacement correction would be between 1.8% and 6% of the out-of plane displacement. The accuracy needed in the estimation of z_0 can herewith be calculated depending on the expected amount of out-of-pane displacement and the required resolution for the in-plane displacement.

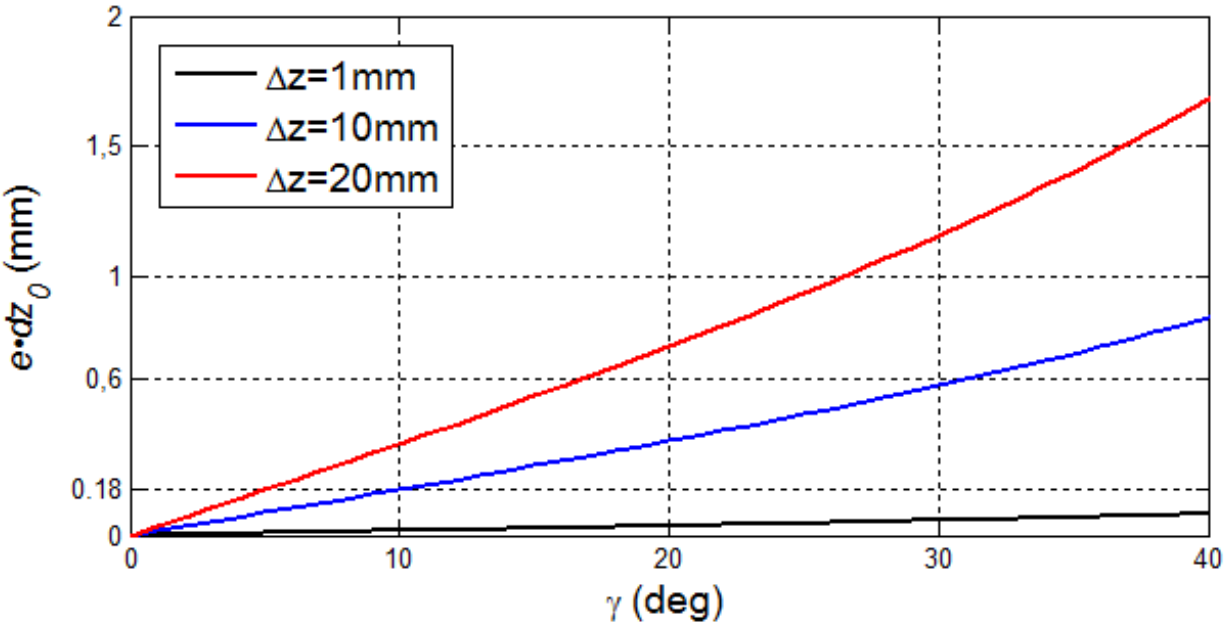

Figure 5.11 Error of the in-plane displacement correction for Δz =1, 10 and 20 mm and an error in the estimation of z0 of 10%.

Moreover, In relation to Fringe Projection calibration procedure, in Figure 5.9 it was noticed a variation in the K_f coefficient due to the divergence of the fringes was noticed.

In this case the assumption of a K_f map instead of a single value for the whole image significantly increases the accuracy of FP

Furthermore, there exists an uncertainty in the determining of the parameters L and K_f. L is selected by clicking two limits of a known distance. Any errors due to the resolution of the camera and the selecting of the pixels could affect the obtained L value. K_f factor is directly affected by the uncertainty of the displacement Δz and by the Fringe projection method employed to measure the difference of phase. Thus, since both parameters could be affected by the procedure to obtain them, it is advisable to repeat each procedure to measure them at least three times and perform the mean value.

5.7. Concluding remarks

The previous analysis had led to the following conclusions

- An optical analysis employing pin-hole model has been performed to study the effect of an element observed by a single camera when it is deformed in three dimensions. Based on this study, a methodology to easily correct the distorted in-plane displacements measured by 2D-DIC employing out-of-plane deformations measured by FP has been developed.

- The correction of the in-plane displacements distortion due to out-of-plane deformation implies the calculation of certain parameters (z_0 and P_v) and the alignment of the camera optical axis perpendicular to a flat reference plane. A calibration procedure has been developed to obtain those parameters and to perform the camera alignment.

- The proposed methodology for Fringe Projection Calibration provides a K_f map instead of a single value for the complete image, which minimizes errors due to divergence of the projected fringe pattern improving the accuracy of the method.

- Nevertheless, the presented correction methodology is sensitive to some error sources which have to be controlled. The first of them is the lack of the perpendicularity of the camera with the reference plane. In addition, the calculation of z_0, the position of the vertex of the CRD (P_v) and factors K_f and L affects directly to the final displacement measurement.

Chapter 6. Technique evaluation: Identification of potential sources of error

In this chapter an evaluation of the proposed technique to measure in-plane and out – of-plane displacement integrating 2D-DIC and PF is performed. The purpose is to find out if the technique operates adequately and to quantify any possible errors. This evaluation allows makes it possible to establish whether or not the technique is suitable to measure 3D displacements. Four different tests have been performed in order to answer this issue. Results have been compared with those obtained with 3D-DIC technique.

6.1. Introduction

In the current chapter the proposed technique has been evaluated in several lab tests. Thus, two sets of experiments have been conducted. The first set of experiments consisted on evaluating the in-plane rigid body motion displacements of a flat object not parallel to CCD plane. This test cannot be performed with accuracy using conventional 2D-DIC, since different specimen surface points at the surface have different magnifications in the CCD of the camera. The second sets of tests consisted on measuring the in-plane deformation in an hyperelastic element with large out-of-plane displacements. The out-of-plane displacements will distort the in-plane displacements measured with 2D-DIC. Thus, the proposed methodology should be able to correct such a distortion.

In all the cases, 3D-DIC technique has been employed in conjunction with FP+2D-DIC to assess the accuracy of the proposed methodology. Figure 6.1 shows a scheme of the adopted experimental set-up.

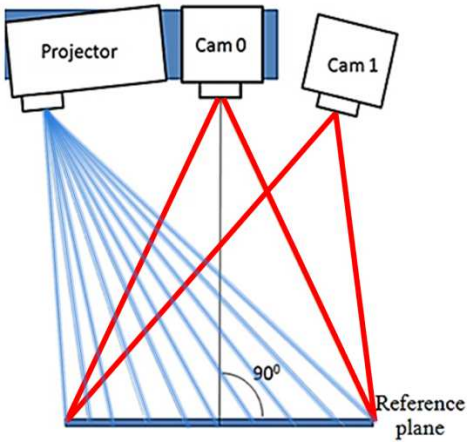

Figure 6.1 Schematic illustration showing the adopted experimental set-up for FP+2D-DIC **and 3D-DIC**

6.2. Quantification of the rigid body motion on an inclined flat moving object

To test the methodology, an initial set of experiments consisting of measuring the rigid body displacement of a flat moving object was performed. During these experiments the specimen was not deformed only displaced. Thus, homogenous displacements maps should be achieved unless some rotation appears. The aim of these basics, experiments was to demonstrate that the in-plane measurements obtained on a non-planar object using 2D-DIC could be corrected successfully using FP measures and the correction procedure proposed in previous chapter.

6.2.1. Experimental set- up

The proposed set of experiments consisted of moving a rotated flat aluminium plate 10 mm thick along a direction parallel to the CCD camera plane. In a first experiment the specimen was rotated around the horizontal axis and it was moved along the same axis (Figure 6.2 A)). In a second test the plate was rotated around the vertical axis and displaced along the same axis in Figure 6.2 B). Initially parameters z_0 and position of the

vertex of CRD were calibrated following the calibration procedure described in chapter 4 and 3D-DIC was calibrated employing a 7mm calibration target (provided by VIC 3D by Correlated Solutions Ltd.). Subsequently, a biaxial test machine with two hydraulic actuators was employed for experiments. As illustrated in Figure 6.5, the aluminum plate painted with red speckle, placed on the machine oblique to the CCD camera plane and displaced in the X and Y directions.

As a reference plane, the same test plate was employed before being rotated. The reference camera (camera 0 Figure 6.1) was placed perpendicular to the reference plane. To ensure that the camera was perpendicular to the reference plane, a mirror was placed over the surface and the camera 0 was focused so that it could see itself at the centre of the image.

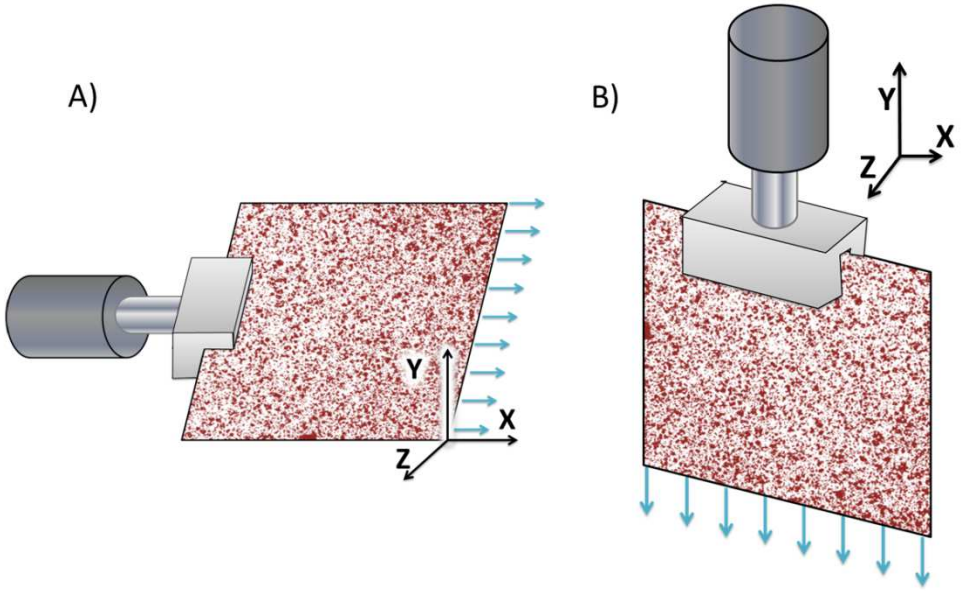

Figure 6.2 Scheme of solid rigid displacement tests A) Displacement in *X*- direction B) displacement in *Y*- direction

While camera 1 was placed with an angle respect to the reference camera to have a stereoscopic view of the object. Camera 0 was a colour CCD camera (Brand Ueye, model UI-2310SE-C-HQ RGB), while Camera 1 was a black and white camera (Brandt Allied Vision Technology, model Guppy Pro) with a blue low pass filter (450 nm) to remove fringes from the captured images. Blue fringes were projected using an LCD projector (Brandt Philips, model PPX2055) placed at an angle to camera 0. Camera 0

and the projector were fixed together to an aluminium bar attached to a tripod, while camera 1 was placed on a separate tripod as illustrated in Figure 6.3.B.

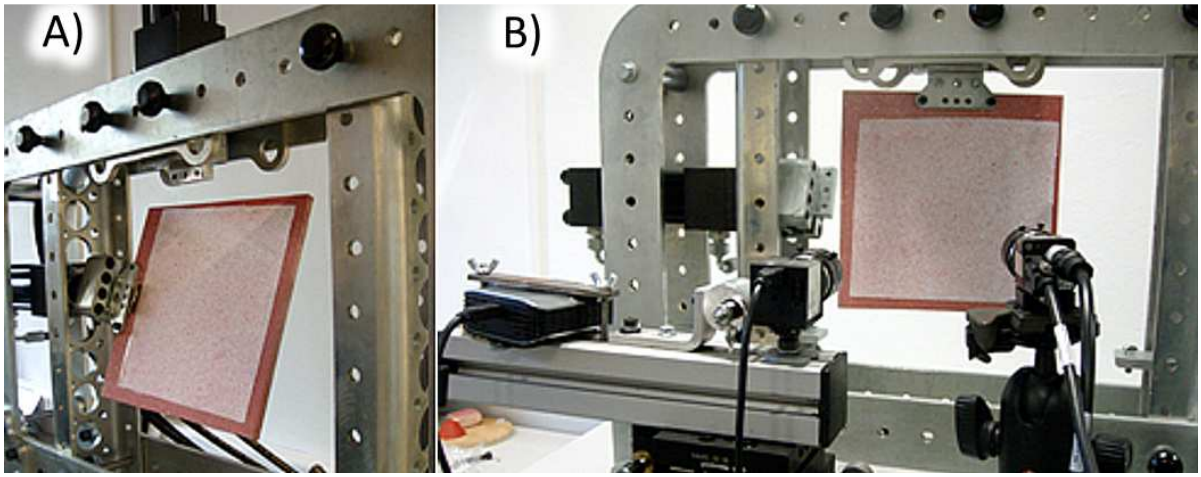

Figure 6.3 Figure showing the experimental set-up adopted A) Displacement in *X*- direction B) displacement in *Y*- direction

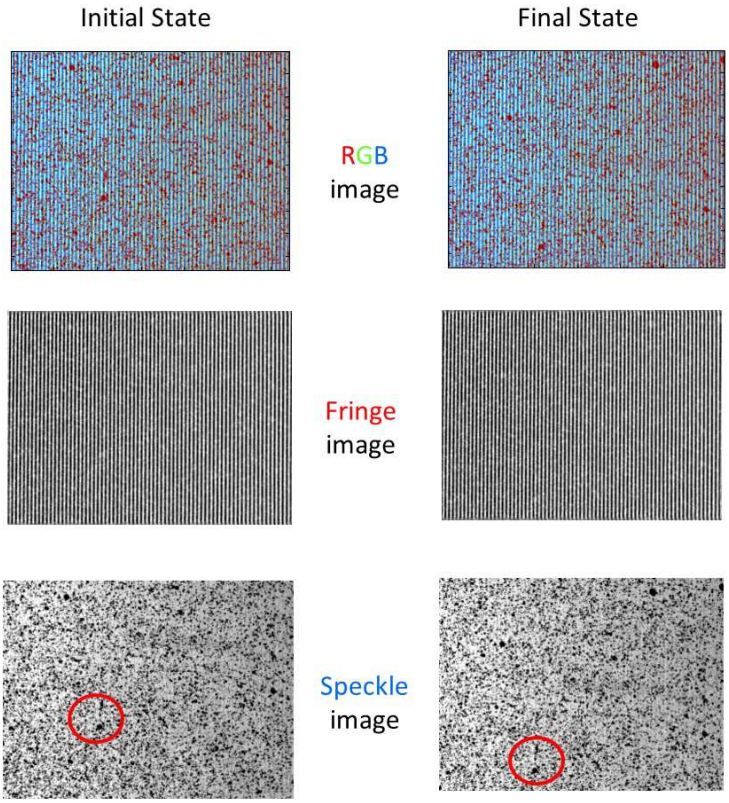

Figure 6.4 Images captured during vertical displacement test. The red circle highlights the speckle displacement. Left column represent the reference state and right column represent the displaced state

To avoid any additional filtering, it was crucial to obtain the right balance in the colour level employed for speckle (red RGB code (255 0 0)) and the projected fringes (light

blue RGB code (0 0 255)). Figure 6.4 and Figure 6.5 shows the captured and extracted fringe and speckle images for both horizontal and vertical displacements tests respectively. However, it can be observed that there still was some remaining high frequency noise in the data after the colour encoding separation. This effect was minimized by using the Fourier phase extraction method (FTP) for Fringe Projection processing. The calibration of Fringe Projection was performed using a 40mm in diameter cone 19 mm high.

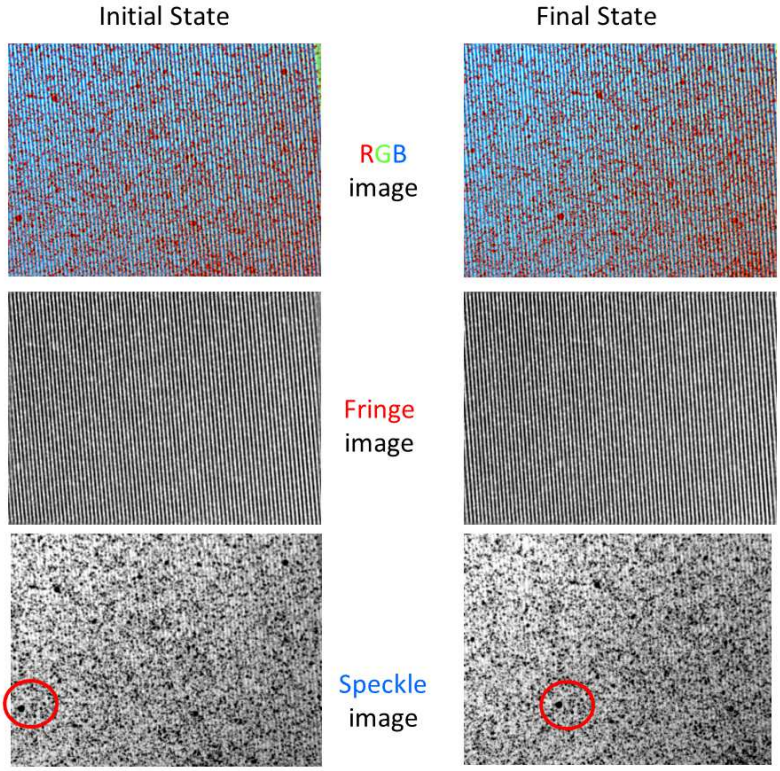

Figure 6.5 Images captured during horizontal displacement test. The red circle highlight the speckle displacement of a speckle Left column represent reference state and right column represent displaced state

To guarantee that images were captured from both cameras, a Matlab routine was developed to trigger both cameras sequentially with a difference less than 0,01 seconds. Images captured using camera 0 were processed to separate fringes and speckle, while images captured with camera 1 were employed, together with speckle images from camera 0, to perform a parallel 3D-DIC analysis using VIC-3D software (produced by Correlation Solutions). In addition, speckle images from camera 0 were also processed using VIC-2D software (produced by Correlation Solutions). Results for

vertical and horizontal displacement are shown in Figure 6.6 and Figure 6.7 respectively.

6.2.2. Results and Discussion

Figure 6.6 shows the measured vertical displacements along a horizontal profile for a plane object rotated around the *Y*- axis as it is moved in the *Y*- direction. During the experiment the object was not deformed, thus the in-plane displacements were constant for whole object, as it is shown by 3D-DIC results. However, the object was not parallel to the CCD camera plane due to its rotation around the *Y*- axis, as it can be observed from the map of out-of-plane displacements obtained using fringe projection. Thus, the in-plane displacements obtained from 2D-DIC were affected by the virtual in-plane displacements due to the difference in the *Z*- coordinates of the object relative to the reference plane, as shown in Figure 6.6. It can be observed that 2D-DIC and 3D-DIC profiles intersect at the location labelled as rotation axis. This location corresponds to the position of the reference plane used for calibration. It is also noteworthy that differences between 2D-DIC and 3D-DIC results increase with the radial distance from the rotation axis. Results obtained using the combination of FP and 2D-DIC show an excellent level of agreement with those obtained using 3D-DIC.

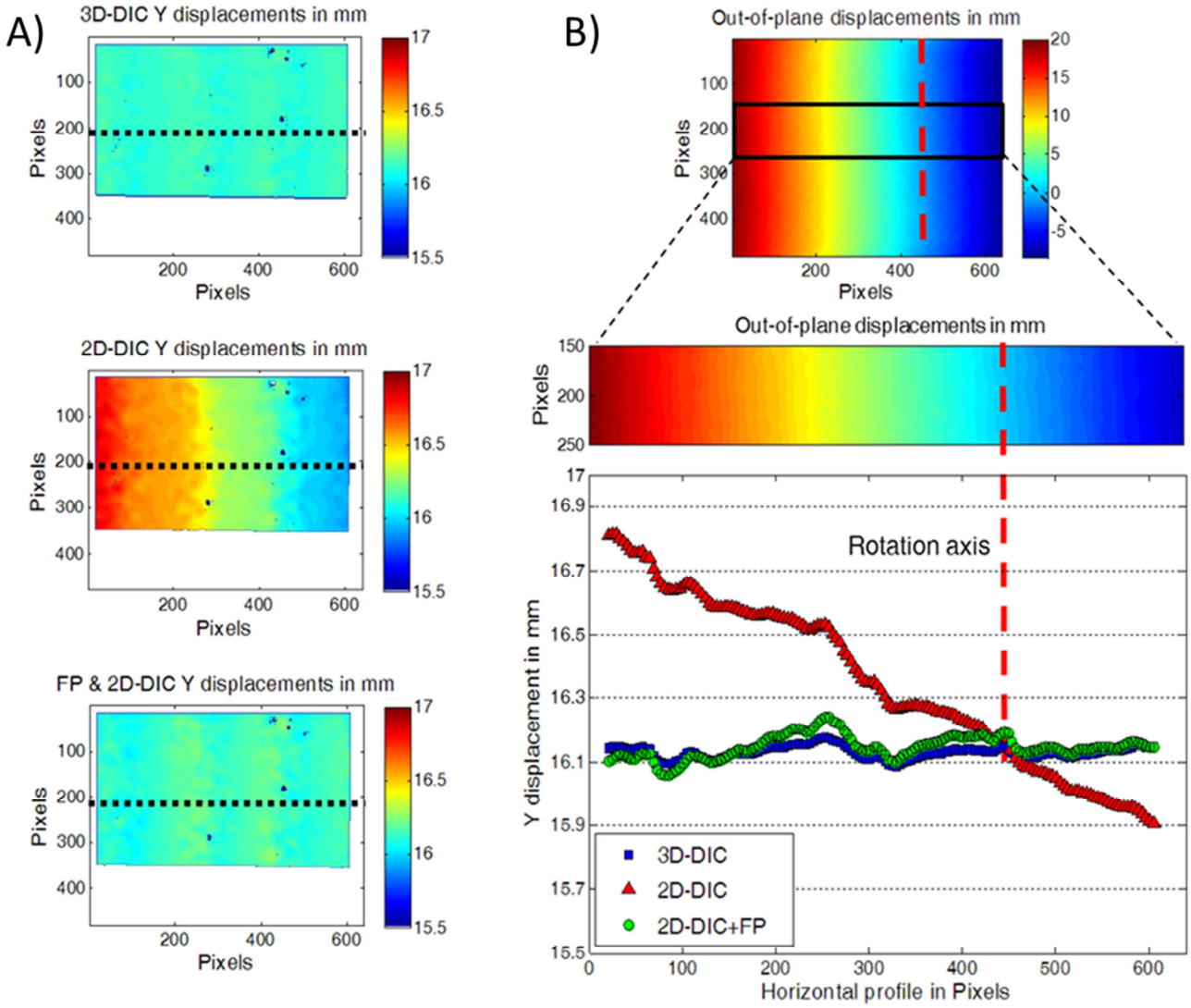

Figure 6.6 A) Results of vertical displacement test. B) Plot representing the measured displacements along the dashed line shown un the displacement maps

Figure 6.7 illustrates the measured horizontal displacements along a vertical profile for the plane object rotated around the *X*- axis as it is moved along the *X*- direction. In this case the level of agreement between 3D-DIC and FP+2D-DIC is again very good, but there are, however, small differences between them. It can be observed from the out-of-plane displacements map that the rotation axis was not completely horizontal which implies that the camera axis and reference plane were not quite perpendicular during calibration.

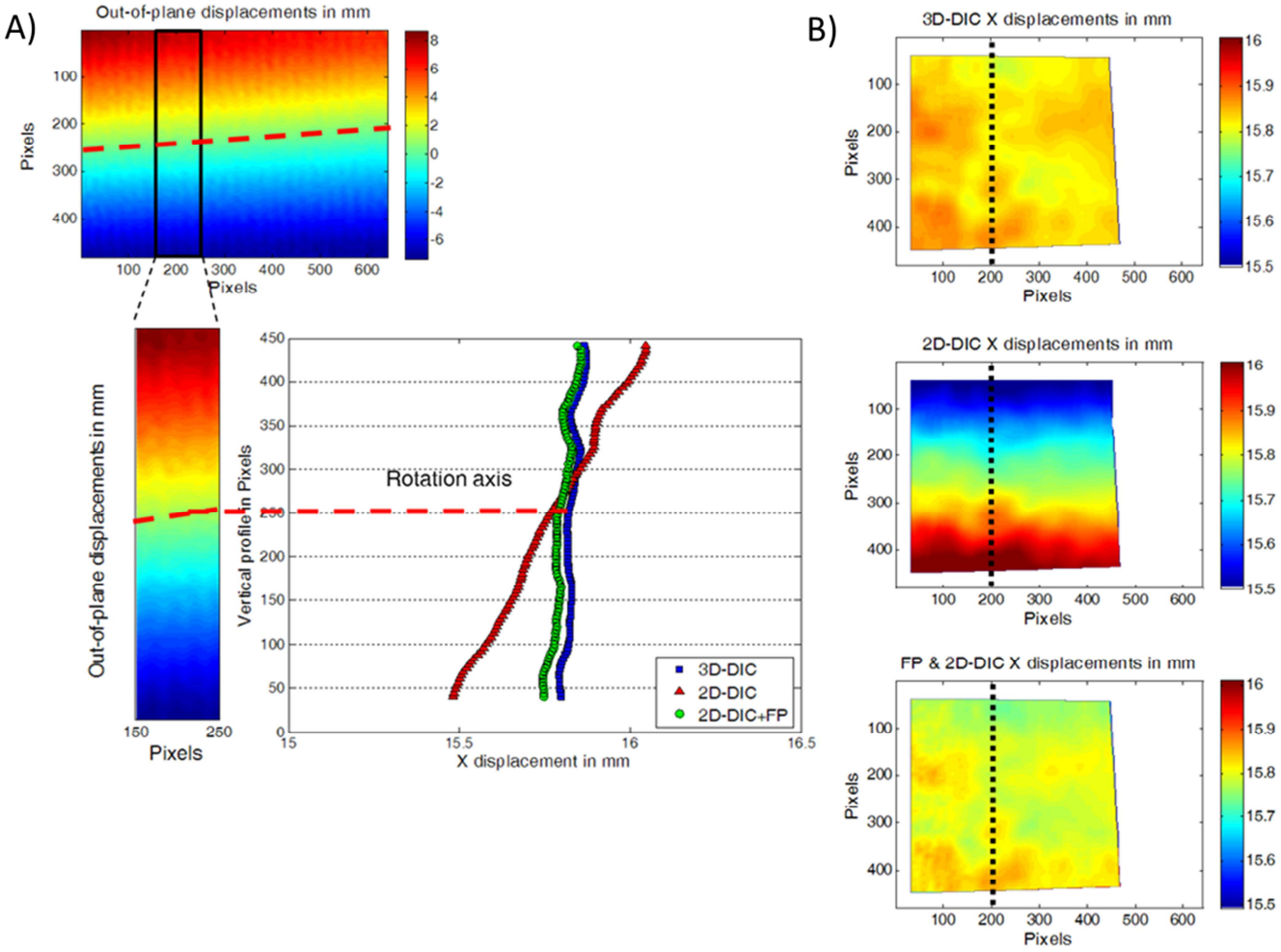

Figure 6.7 Results of horizontal displacement test. Plot representing the measured displacement along the dashed line showing the displacement maps

Thus, two sources of error were detected during the experiments. The first error source was related to the pixel size which leads to an error magnitude the size of one pixel (less than 0.1mm) as can be observed in Figure 6.6 and Figure 6.7. Nevertheless, the spatial precision of the technique can be improved by increasing the camera resolution. The second source of error was related to the perpendicularity between the camera axis and the reference plane. If the camera was placed perpendicular to the reference plane, displacements measured using 3D-DIC and 2D-DIC should be the same at the centre of the image (coordinates in pixels 320, 240) since the optical axis (OA) intersect the CCD plane through its centre. However, it was found that this point (coordinates in pixels 300, 265) was very close to but not at the centre of the image (it was moved -2.4, 3.2 mm from the centre). This suggests that the camera axis was not completely perpendicular to the reference plane, which explains the difference between 3D-DIC and FP+2D-DIC results in Figure 6.7.

6.3. Compression test using a rubber ball

6.3.1. Experimental set-up

The second experiment involved measuring real-time in-plane and out-of-plane displacements on a rubber sphere deformed under a compression load. A 60 mm diameter rubber sphere was pushed against a 41mm hole in a 2mm thick steel plate as illustrated in Figure 6.8. A screw behind the sphere was employed to compress it, creating a 3D deformation field. The set-up of the adopted cameras and the analysis procedures were the same as those described in previous experiments. Figure 6.9 shows a sequence of images captured during the test.

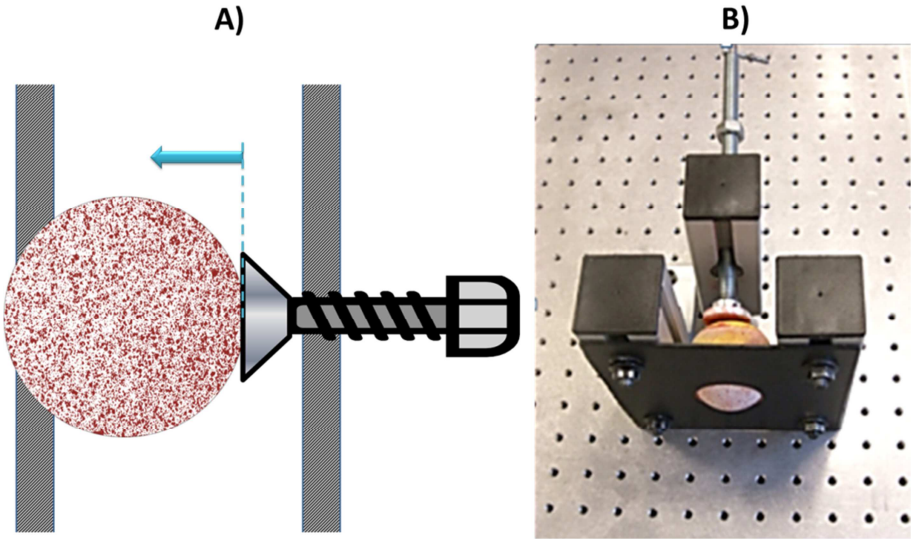

Figure 6.8 Image showing the adopted experimental set-up for the test with an elastic ball A) Lateral scheme B) scheme of the test

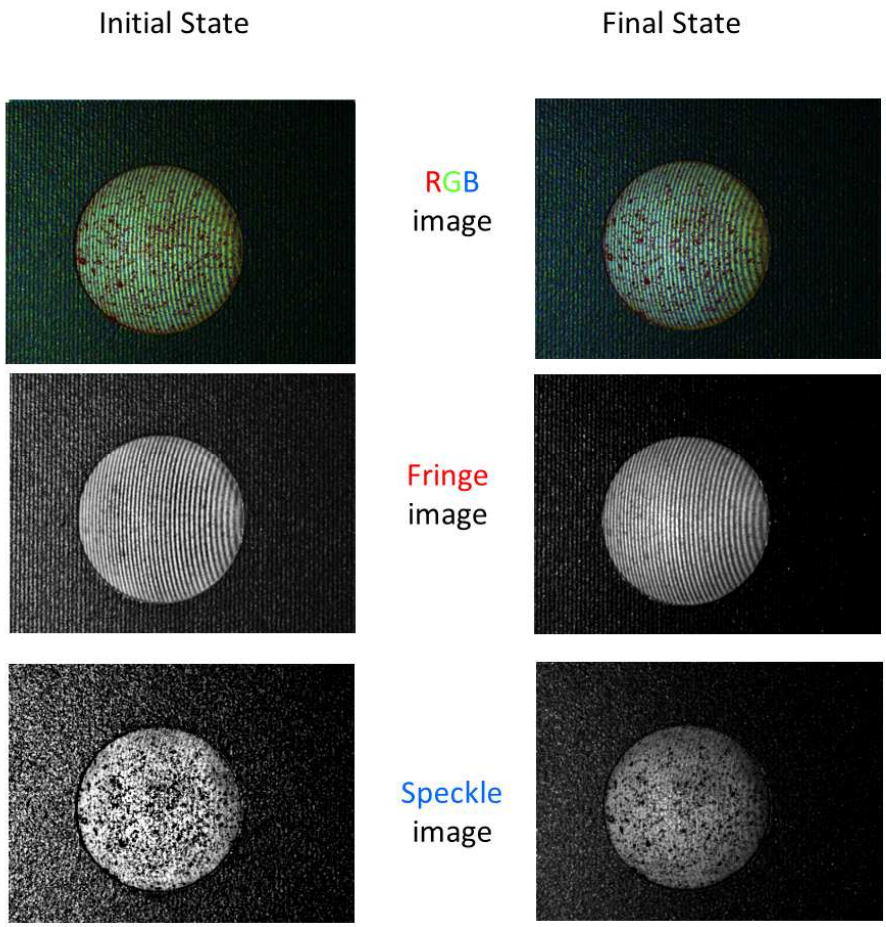

Figure 6.9 Images captured during the ball test. Left column represent the reference state and right column represent the final state

6.3.2. Results and discussion

Figure 6.10 and Figure 6.11 shows *Y*- displacements and *X*- displacements results, respectively. As in previous experiments, 2D-DIC results were clearly affected by virtual in-plane displacements due to the out-of-plane deformations. Again, the combination of FP+2D-DIC made it possible to correct the in-plane displacements using the FP results, resulting in an excellent level of agreement with those results obtained with 3D-DIC.

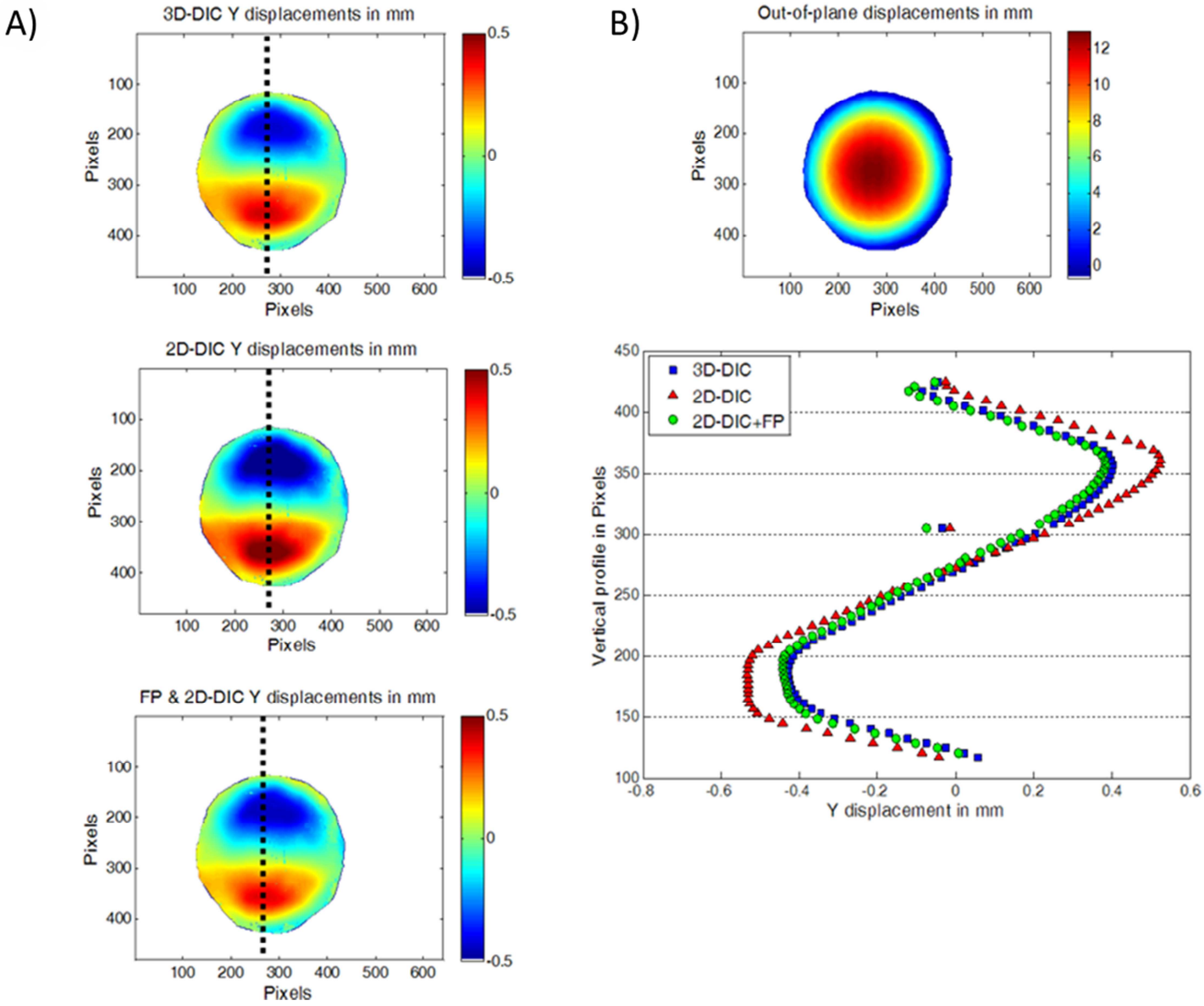

Figure 6.10 A) *Y*- Displacements results obtained from the ball test. B) Plot representing the measured displacements along the dashed line shown in the displacements maps

Figure 6.12 illustrates the average displacement error between 3D-DIC and FP+2D-DIC. It can be observed that this error is no higher than 4 % for *X*- displacements and 6.5 % for *Y*- displacements. As previously discussed, the displacement error was attributed to a small misalignment in the parallelism of the CCD camera plane and the reference plane during calibration.

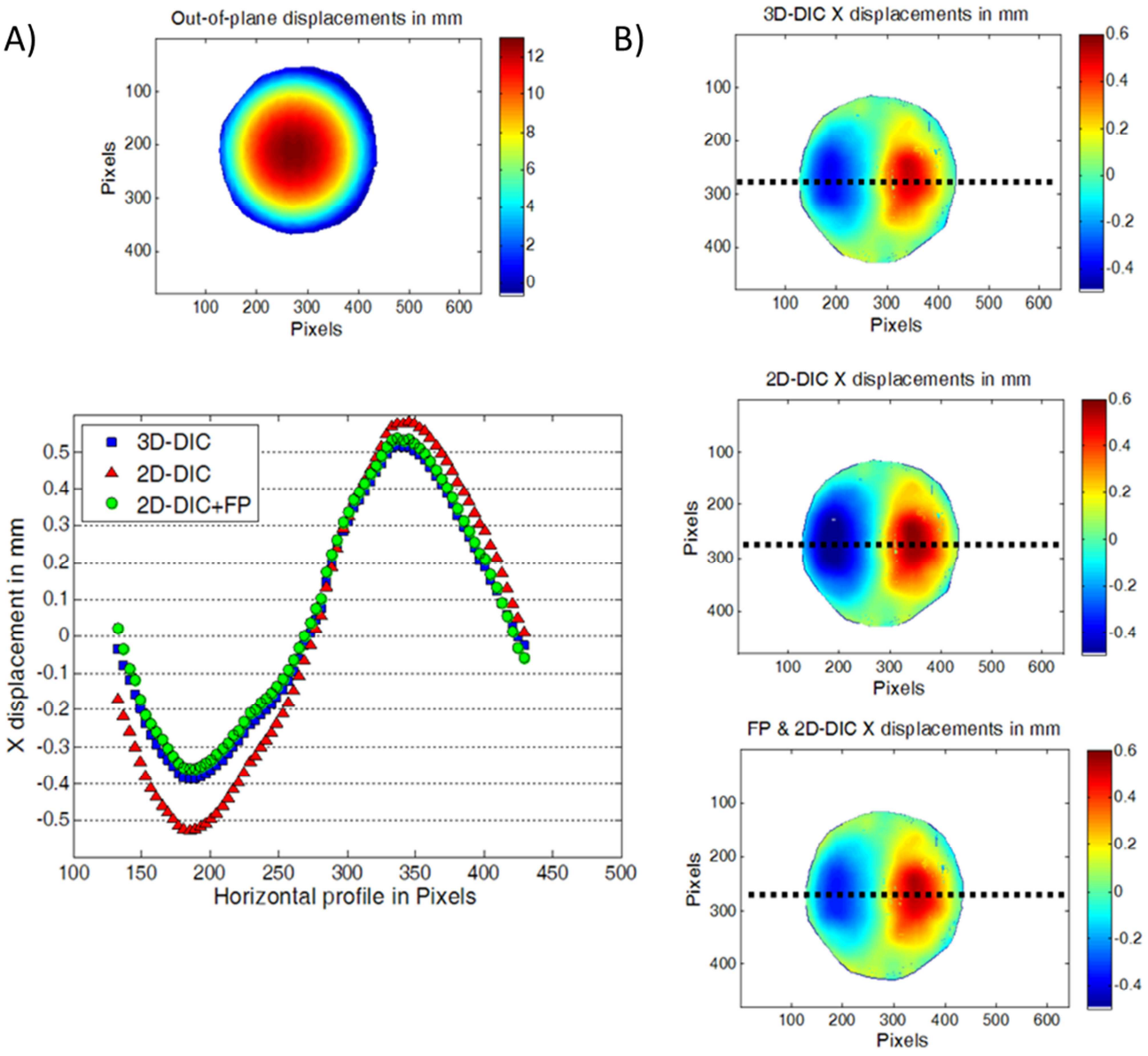

Figure 6.11 A) Plot representing the measured displacements along the dashed line shown in the displacements maps B) *X*- Displacements results obtained from the ball test.

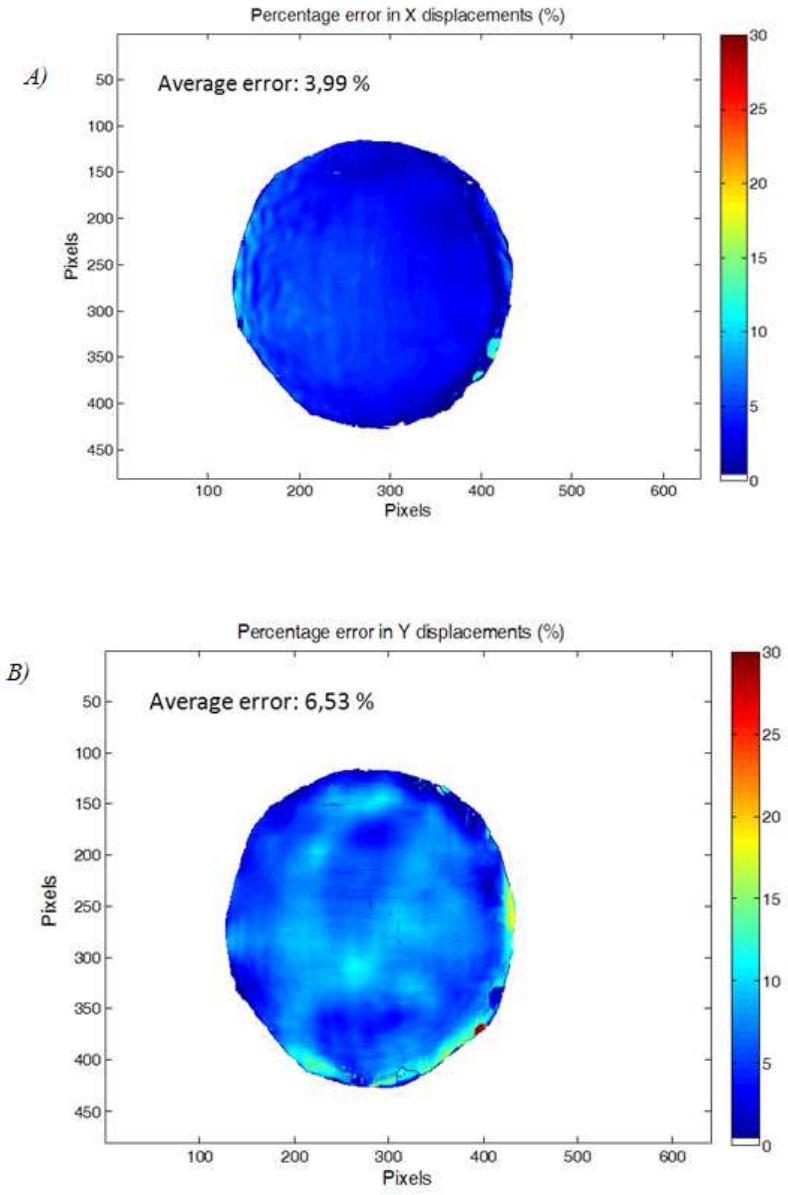

Figure 6.12 Displacement error in % between 3D-DIC and 2D-DIC & FP results for a compression test on rubber sphere a) X displacements, b) Y displacements.

6.4. Test on a silicon membrane

Previous experiments evidenced that the combination of FP+2D-DIC provides accurate 3D displacements measurements using one single camera. However, it has been observed that the misalignment in parallelism between the CCD camera plane and the reference plane during the calibration process constitutes a common source of error. Thus, the proposed method consisting of using a mirror to achieve the perpendicular between the camera axis and the reference plane was not accurate enough. A more robust alignment approach is required in order to achieve accurate results. In the

following experiment the alignment approach described in chapter 4 has been implemented.

6.4.1. Experimental set-up

The specimen employed consisted on an elastic silicone membrane which painted with red speckle and mounted on an aluminium frame as Figure 6.13 illustrates. Behind the frame a screw with a lubricated rounded head pushed the membrane.

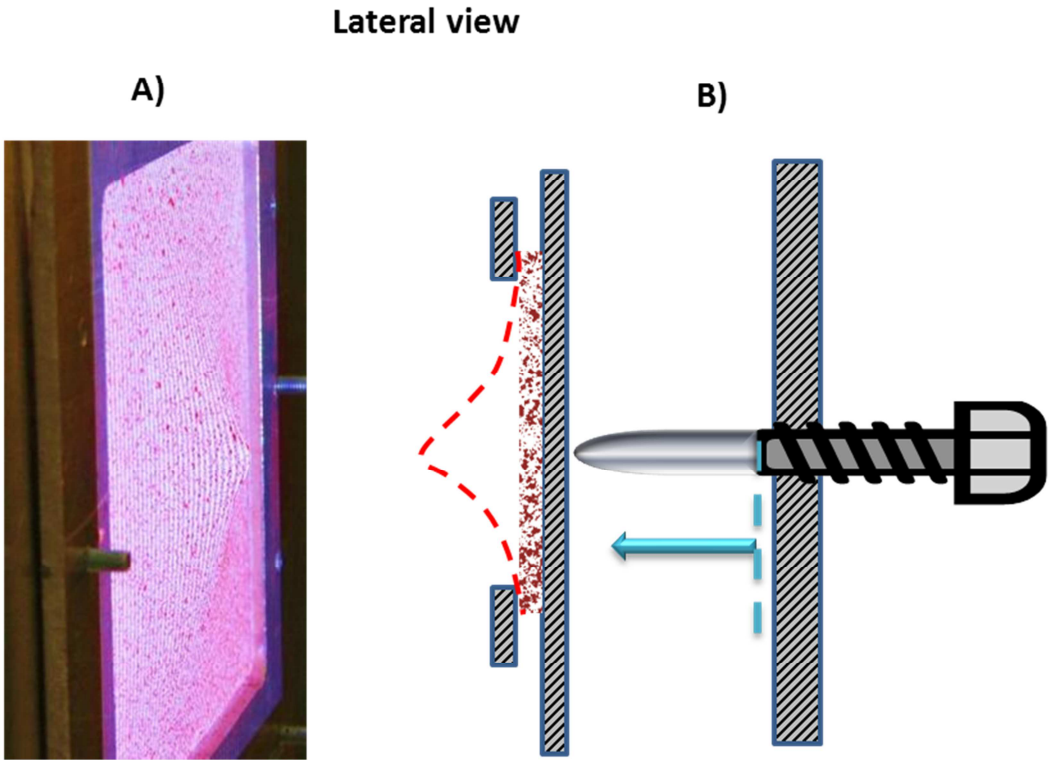

Figure 6.13 A) Lateral view of membrane test B) scheme of the test

As in previous experiments, two cameras (Ueye, model UI-2310SE-C-HQ RGB) and a projector (Samsung SP-H03 pico-projector) were employed. In addition, a laser pointer was included and the whole system was mounted on two moving platforms with micrometric adjustments. Figure 6.14 illustrates the set-up adopted for this test.

Camera 1 in Figure 6.14 was employed as a reference camera for 3D-DIC and to perform FP+2D-DIC. Camera 2 was employed only for 3D-DIC. For 3D-DIC the whole system was calibrated using a 4mm calibration target provided by Correlated Solutions. In addition, to evaluate the resolution of the out-of-plane displacements the

fringe projection system was also calibrated. Thus, both the camera and the projector were moved along the optical axis a using the micrometric screw shown in Figure 6.14. During the process fringes were projected over the reference surface as the wholes system was moved towards the reference plane. As illustrated in Figure 6.15, fringes show a shift value of 0.22 radians for displacement intervals of 0.25 mm. It implies that with the current configuration, the device resolution for out-of-plane displacements was 0.25 mm.

Finally, the membrane deformation was conducted in three different steps, namely 5, 10 and 20 mm. Thus, several images were collected at each deformation step in the following sequence: first camera 1 was triggered with fringes projected over the membrane, after that, fringes were replaced and camera 1 and camera 2 were triggered employing the Matlab routine used in previous tests.

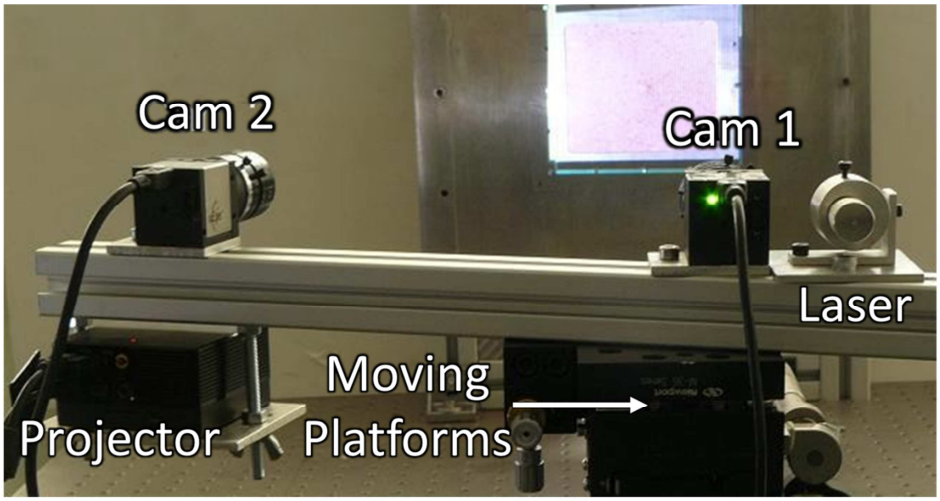

Figure 6.14 Illustration showing the adopted experimental set-up for membrane test.

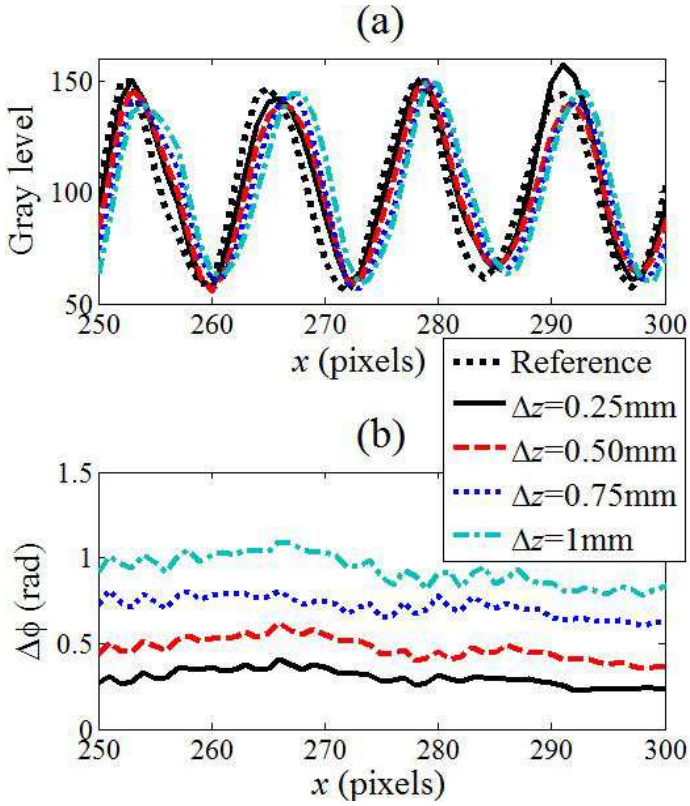

Figure 6.15 Horizontal profiles of: a) the acquired shifted fringes by increasing Δz in steps of 0.25 mm until 1 mm, b) the respective computed fringe shifting

6.4.2. Results and discussion

Figure 6.16 and Figure 6.17 shows the 3D displacement maps of the silicon membrane obtained with FP+2D-DIC device and using 3D-DIC. Each column represents the same degree of deformation and each row the same spatial direction of the measured displacements. In addition, horizontal and vertical profiles are presented through the centre of the displacement maps (along the indicated black dashed line shown in Figure 6.16 and Figure 6.17) for both techniques. Figure 6.18 illustrates *Z*- and *X*-displacements profiles along the horizontal direction in the displacement maps, while the *Y*- displacement profiles were plotted along the vertical direction in the *Y*-displacement maps.

The three different degrees of deformation analysed in the silicon membrane are identified as 1st, 2nd and 3rd in Figure 6.18. If displacements profiles indicated in Figure 6.17 and Figure 6.18 are compared for both techniques it is observed that the level of agreement is extremely high. Nevertheless, FP+2D-DIC results are noisier than those

obtained with 3D-DIC. This is attributed to the presence of some remaining fringes in the speckle image which affects the cross correlation algorithm employed for 2D-DIC analysis. In addition, 3D-DIC software seems to employ a smoothing algorithm to remove noise from the image. However, the differences in the in-plane displacements between both techniques are smaller than 0.1 mm in a range of 1.5 mm of maximum displacement (smaller that 0.7 %). Nevertheless, the resolution for the out-of plane displacements can be adjusted with the fringe pitch and the angle of incidence of the projected fringes, while the in-plane resolution can be improved by increasing the resolution of the camera or by increasing the optical magnification of the lenses.

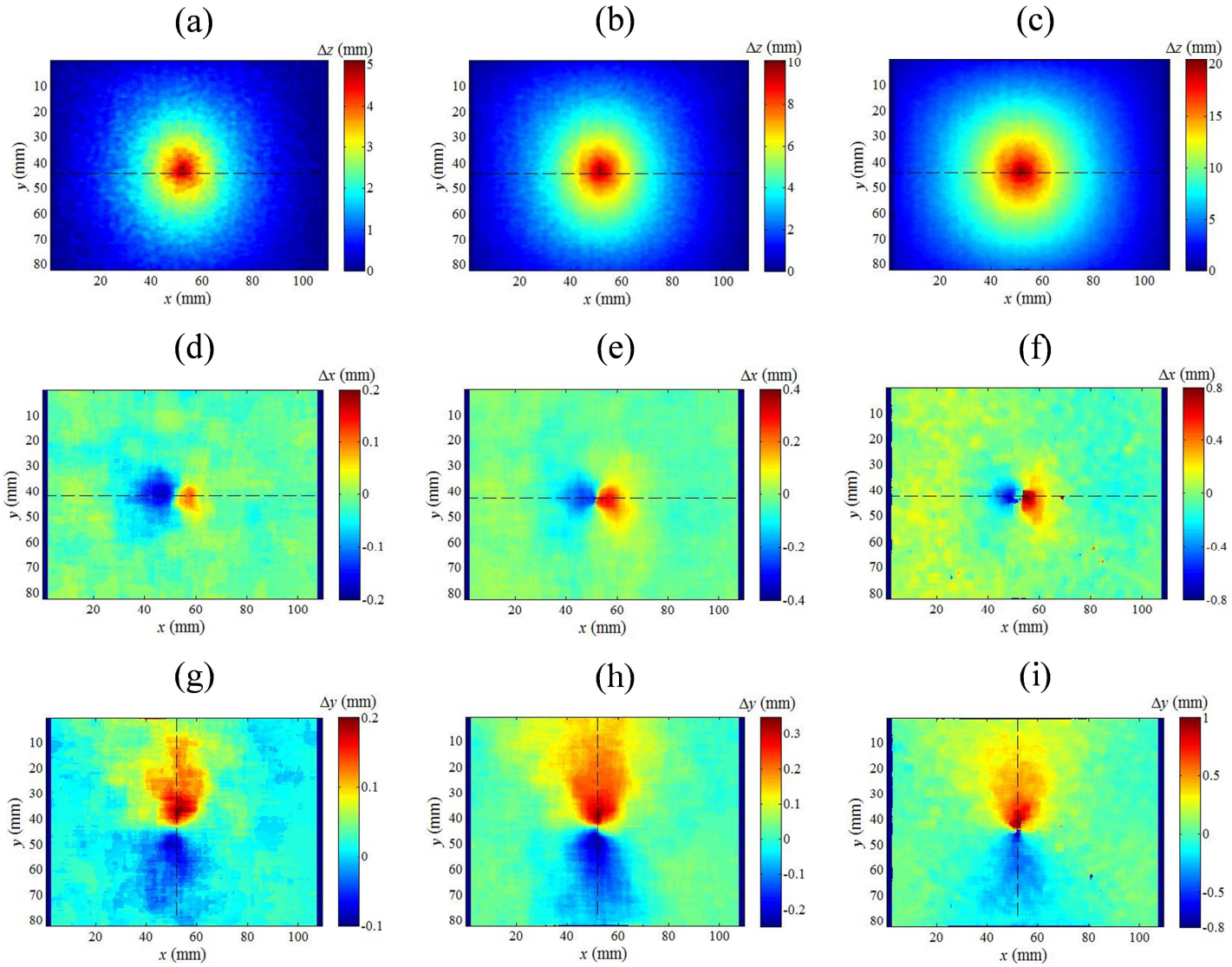

Figure 6.16 Displacements maps obtained using FP + 2D-DIC technique for a silicon membrane at different degrees of deformation. a), b) and c) are the displacements in *Z*- direction, d), e) nd f) in *X*- direction and g), h) and i) in *Y*- direction.

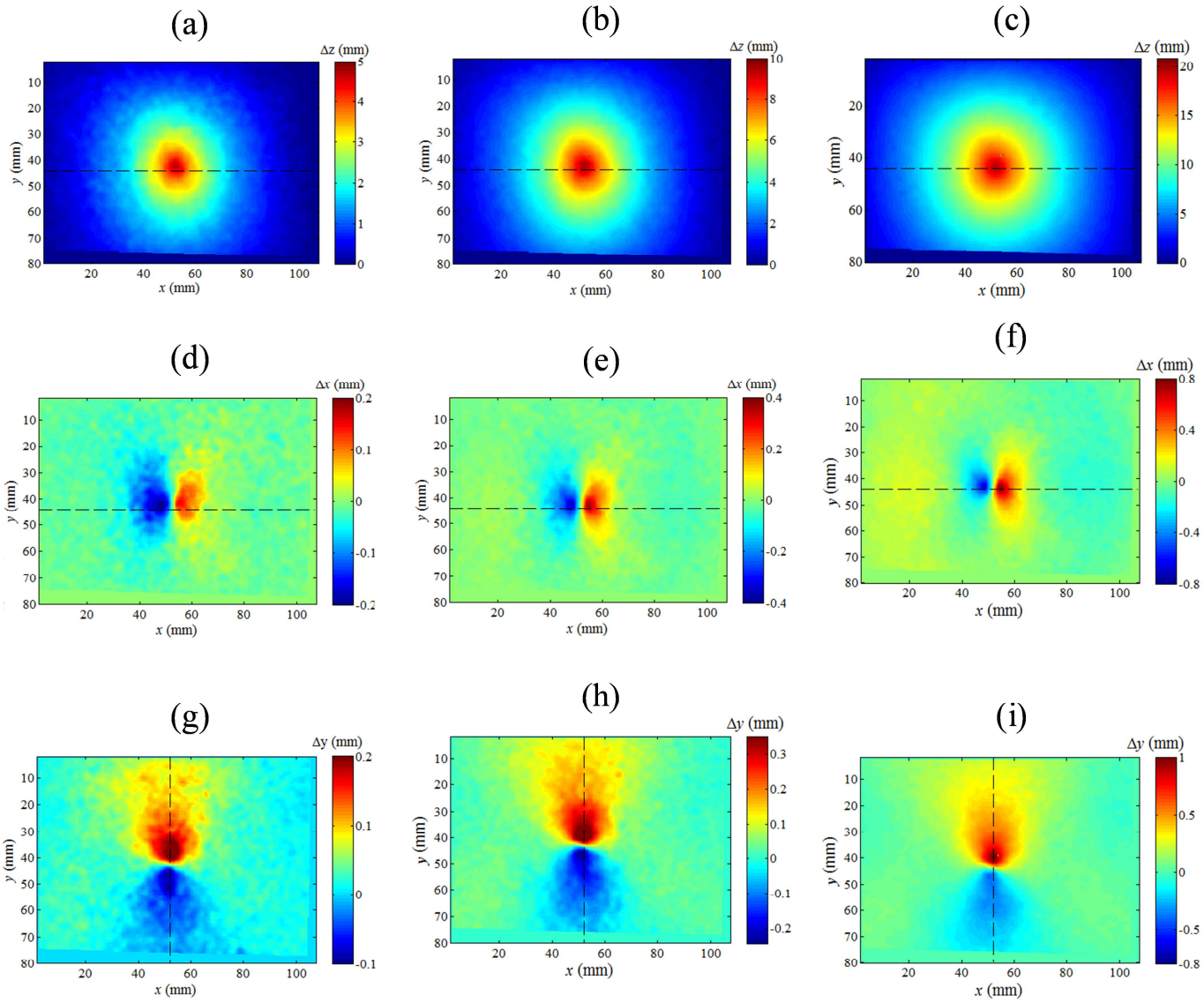

Figure 6.17 Displacements maps using 3D-DIC for a silicon membrane at different degrees of deformation. a), b) and c) are the displacements in *Z*- direction, d), e) and f) in *X*- direction and g), h) and i) in *Y*- direction.

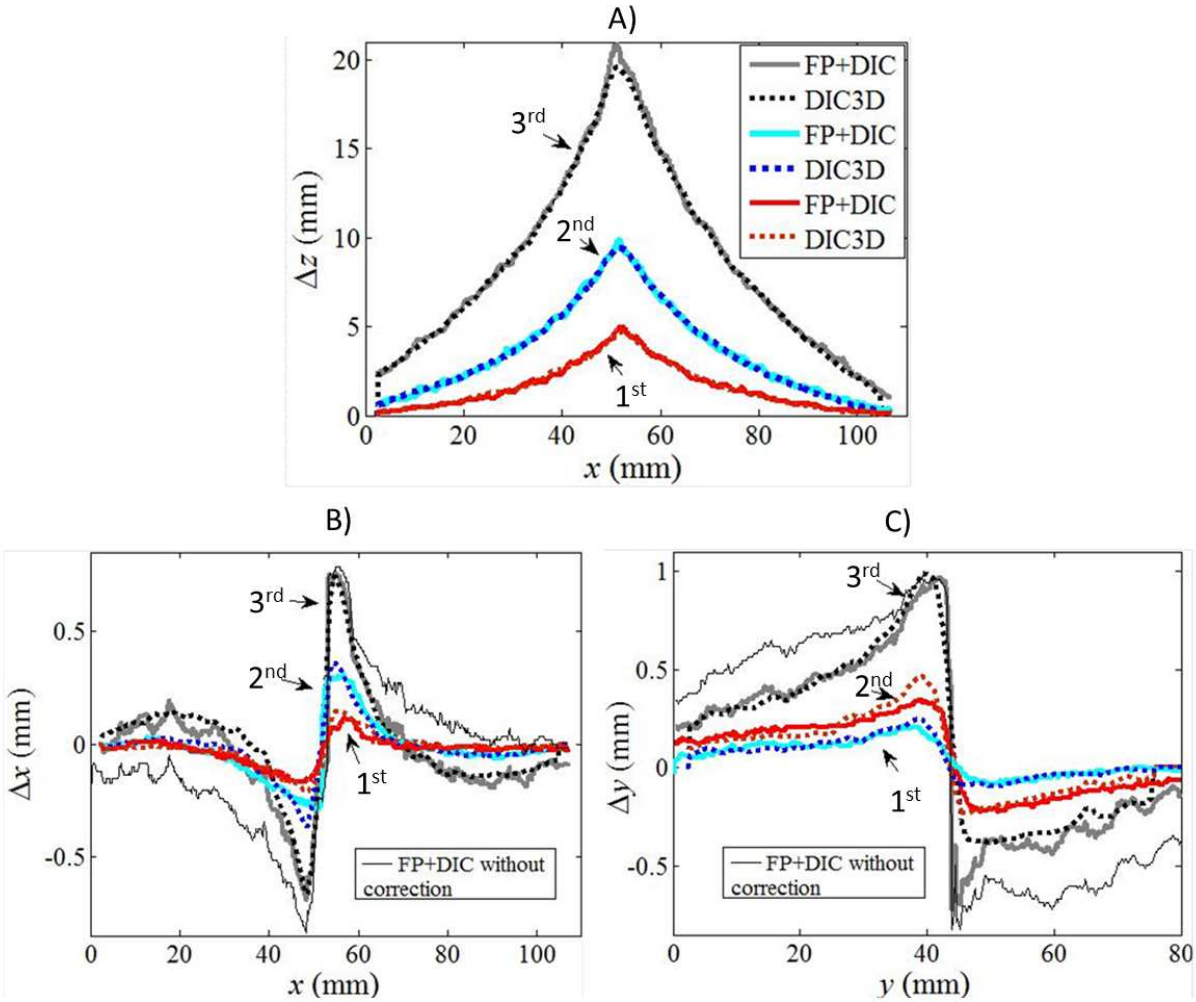

Figure 6.18 Comparison of the displacement profiles for a silicon membrane in a) *Z* , b) *X* and c) *Y* direction, obtained with FP+2D-DIC technique (continuous line) and 3D-DIC (dotted line) for different degrees of deformation: 1st (red), 2nd (blue) and 3rd (black).

6.5. General discussion

The first aspect investigated during the course of this validation procedure was the ability of the FP+2D-DIC to measure in-plane displacements in a flat plane non parallel to the sensor of the camera. Results presented in Figure 6.6 and Figure 6.7 show a good concordance between 3D-DIC and FP+2D-DIC correcting substantially the distorted in-plane displacement measured by 2D-DIC. However, it is noticed that the perpendicular alignment of the optic axis of the camera and the reference plane is an important aspect to consider since it strongly affects the results.

During the test of the ball, it was again detected that the misalignment of the camera affected the results. In Figure 6.10 and Figure 6.11 it is observed that at each side of

the centre of the image FP+2D-DIC results were different from 3D-DIC results. A possible reason for this difference was the misalignment of the optical axis with the perpendicular of the reference plane.

Finally the alignment procedure presented in chapter 5 was applied to the deformation analyses of the silicone membrane. In this case it was noticed that the misalignment effect observed in previous experiments was minimized. In this last validation test, a certain noise was noticed in the out-of-plane displacement results that is due to the effect of the remaining speckle pattern in the fringe pattern. This effect can be corrected by improving the colour balance of the RGB images or by adopting some filtering procedure for the fringe pattern.

Finally, it is interesting to emphasize that the alignment procedure and the colour balance in the RGB images are both critical issues that must be seriously considered as main sources of error in FP+2D-DICs.

6.6. Concluding remarks

The proposed methodology for simultaneous measurement of in-plane and out-of-plane displacement using Fringe Projection and Digital Image Correlation 2D has been experimentally tested and evaluated from which led to the following conclusions:

- It has been experimentally demonstrated that the in-plane displacements measured with 2D-DIC are distorted by the presence of out-of-plane displacements occurring during the deformation of a 3D object. Thus, by accurately measuring the out-of plane displacements, the in-plane displacements can be corrected.

- The methodology has been experimentally validated and a set of experiments has been conducted starting from a very basic experimental set-up consisting of a colour RGB camera and a LCD projector mounted on a tripod. The results have been validated using the 3D-DIC technique and they have shown an excellent level of agreement, highlighting the potential of the proposed method as a low-cost alternative for 3D displacements measurement.

- It has been observed that the lack of the perpendicular between the optical axis and the reference surface constitutes a major source of error.

- A test on a silicon membrane using an enhanced alignment approach has been conducted. And it has been demonstrated that the combination of both FP+2D-DIC techniques can provide displacement measurements with a level of accuracy comparable to other well established techniques such as 3D-DIC.

- It is remarkable that a 640 x 480 pixels CCD camera and a conventional LCD projector provide an out-of-plane resolution of 0.25 mm. In addition, differences smaller than 0.1 mm are observed for in-plane displacements when FP+2D-DIC results are compared with those obtained using 3D-DIC technique.

Chapter 7. Applications of the technique FP+2D-DIC for large displacement events

In this chapter the integration of Fringe Projection and 2D Digital Image Correlation is employed to measure large 3D displacements during static and dynamic loading conditions. A high speed camera has been employed for dynamic testing, resulting in a high economic improvement compare to 3D-DIC. The purpose of this chapter is to apply FP+2D-DIC to real industry and scientific problems to establish this technique as a real low-cost alternative to 3D-DIC.

7.1. Introduction

Nowadays, the investigation of engineering problems that involve the use of large deformation materials such as silicon, rubber or biological materials has been the focus of many researchers (Hamley, 2007). One common field of research for such materials is the analysis of their contact behaviour during indentation experiments. These materials, due to their physical behaviour, exhibit large displacements under contact loading. One major difficulty in the analysis of contact problems in hyperplastic materials is that their mechanical behaviour cannot always be described by theoretical models (Xiao, et al., 2013). Evidence of this can be found in a number of analytical (Hertz, 1881) (Barber & Ciavarella, 2000) (Johnson, 1985) and numerical (Jayadevan & Narasimhan, 1994) (Jaffar, 2002) (Jaffar, 2003) studies that have contributed to a

better understanding of this problem however they often consider different assumptions in their analysis. One example being the assumption that small strains occurs below the elastic limit (Malitis, 2011) (Truman, et al., 1995) (Jaffar, 2002), or the consideration of half-plane elastic behaviour for both the indenter and the soft body material (Dini, et al., 2008) (Ciavarella, et al., 1998), (Jaffar, 2002), (Jaffar, 2003). The assumption that the contact area is much smaller than the radius of the indenter, or that the elements are frictionless (Dini, et al., 2008), (Jayadevan & Narasimhan, 1994), (Jaffar, 2002) or that the external angle of the indenter is very small (Truman, et al., 1995). Some of these assumptions are not always well supported by the lab experiments that were carried out. Although experimental techniques constitute an important alternative when validating analytical models and numerical studies, no substantial work can be found in the literature (Xiao, et al., 2010) (Han, et al., 2012) (Xiao, et al., 2013) for the analysis of large deformation materials.

In this chapter the FP+2D-DIC is applied to the analysis of large displacement problems in rubber materials. Initially the technique is employed during an indentation test on a silicone block. During this test, large 3D displacements are measured using FP+2D-DIC technique and results are compared with those obtained from two different commercial 3D-DIC systems.

After that, a high speed indentation test on the same silicone block is performed. The purpose of this experiment is to illustrate the potential of FP+2D-DIC in study of high speed events. In this case, experimental results are compared with those obtained from Finite Elements modelling.

Finally, the technique is employed to analyse the impact on a rubber sphere. With this experiment it is intended to demonstrate that FP+2D-DIC can be successfully applied for the analysis of large 3D displacements in non-flat specimens.

To conclude the chapter, experimental results are discussed and a series of conclusions are extracted.

7.2. Quasi-static silicone block test

The analysis of contact problems involving soft materials, such as silicon or rubber, will often imply not only large in-plane displacements, but also out-of-plane displacements. Thus, for accurate measurement of specimen deformation during contact loading an experimental technique that accounts for both in-plane and out-of-plane displacements simultaneously are required. At this stage of the thesis FP+2D-DIC is applied to the analysis of a contact problem with a silicone block. The results of tests using the combined FP+2D-DIC technique have been compared with those obtained using two different 3D-DIC commercial systems. For the comparison of the results a novel image decomposition technique has been adopted (Sebastian, et al., 2013).

7.2.1. Estimation of the measurement uncertainty of FP+ 2D-DIC: Static analysis

An initial calibration experiment was conducted to evaluate the minimum measurement uncertainty of FP+2D-DIC technique for static measurements.

The procedure employed to measure the uncertainty was based on the Interlaboratory Study Protocol of the Project Vanessa (Validation of Computational Solid Mechanics Models, Version 26th June 2013) and consisted of a comparison of the results obtained when employing FP+2D-DIC with the theoretical displacement and strain maps. The test consisted on measuring the deformation in a specific Reference Material, with a known theoretical behaviour. Then, the results given by FP+2D-DIC and the theoretical solution were compared. The adopted Reference Material was a 7075-T6 aluminium cantilever beam 40 mm wide, 160 mm long and 2 mm thick. Experimental results obtained with FP+2D-DIC were compared with the theoretical solution for a cantilever beam with a weight of 0,6 kg placed at the tip. In addition, the deflection was also measured during the experiments using a dial indicator as shown in Figure 7.1.

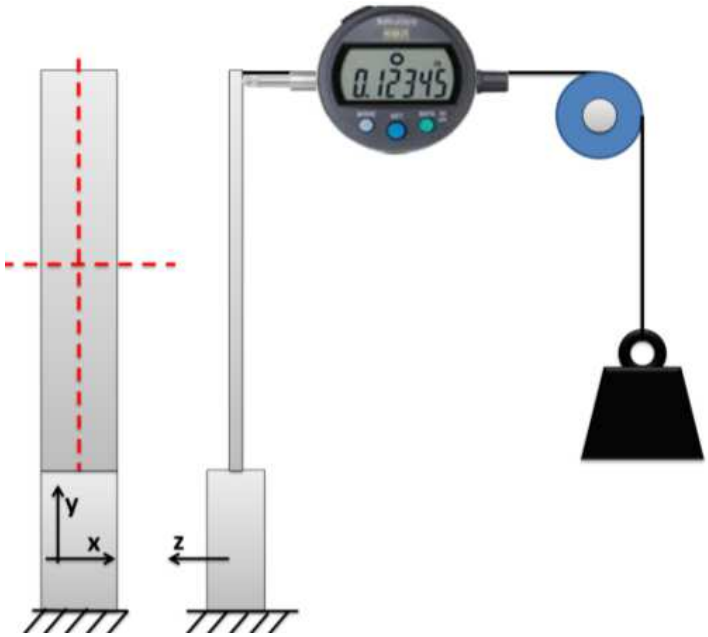

Figure 7.1 Scheme of uncertainty estimation procedure

As the cantilever beam bent, the out-of-plane displacements (Figure 7.2.A) in *Z*-direction and strains ε_{yy} (Figure 7.2. B)) along the vertical red dashed line in Figure 7.1 were measured and compared with those predicted by theory. The selected range for the out-of-plane displacements during the experiments was similar to those expected during contact experiments (from 0 to 1 mm). The experiment was repeated six times to ensure the measurements repetitively.

Figure 7.2.C shows the measured *X*-displacements along a profile parallel to *X*-axis at 80 mm from the base of the cantilever beam. Results predicted by theory indicate that no *X*-displacements must exist, however the 2D-DIC results show a virtual displacement as a result of the out-of-plane displacement (Green line). Thus, 2D-DIC results must be corrected using the out-of-plane information provided by FP. ε_{yy} strain maps were calculated from the displacements maps by employing Green-Lagrange equations which can be found in appendix 1.

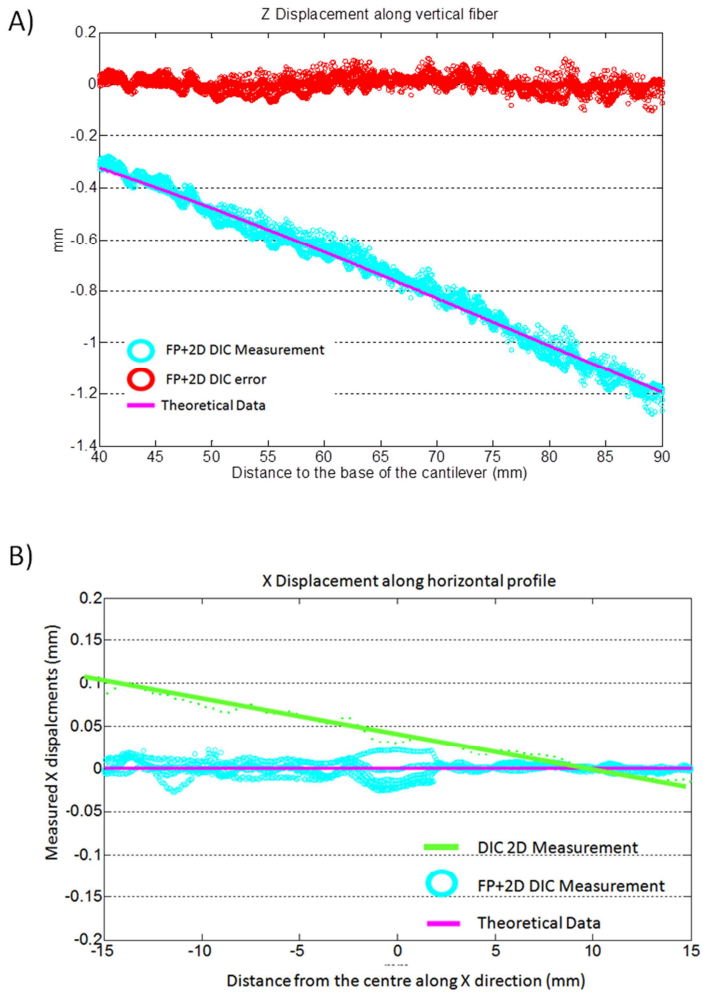

Figure 7.2. A) Vertical profile along the cantilever beam showing the out-of-plane displacements measured during the uncertainty estimation procedure. B) Horizontal profile at 75 mm from the base of the cantilever beam showing the *X*-displacement measured during the uncertainty estimation procedure.

In general terms, the tendency of experimental results presented in Figure 7.2 clearly matches with those predicted by form theory. Nevertheless, there is an uncertainty that was settled to 0.023 mm for out-of-plane displacement, 0.0083 mm for in-plane displacements according to the procedure described in Vanessa project.

7.2.2. Apparatus and experimental set-up for contact experiments

As previously introduced, a set of contact experiments on a 60 x 60 x 20 mm silicone block were conducted. The adopted material was a bi-component silicone QSil 226 (manufactured by ACC Silicones UK). The preparation process consisted of mixing two

components, removing the gas generated during the mixing process with a vacuum pump for 15 minutes, and finally curing the mixture at standard temperature conditions for 24 hours (Figure 7.3).

Figure 7.3 Silicone block manufacturing process

The prepared silicone block was completely transparent. To perform 3D-DIC and FP+2D-DIC the specimen surface was prepared with a very thin matt white paint. The painted specimen surface had a texture appearance similar to fine powder in order to avoid the paint peeling off or cracking during deformation. Subsequently, a speckle pattern was generated with a matt red colour spray (RAL code 3020).

For indentation, a 2024 aluminium wedge was employed with shape and dimensions as illustrated in Figure 7.4 C). To control the displacement of the indenter during the experiments an Instron universal testing machine (model ElectroPuls E3000) was employed. During the tests a sequence of images were captured at different indentation depths, namely 2, 4, 6 and 9mm.

The adopted experimental set-up is schematically shown in Figure 7.4.A, which is based on the basic set-up for FP+2D-DIC described in chapter 4. However, in this case, two 3D-DIC commercial systems were included in the experimental set-up. This set-up consisted of a 1032 by 776 pixels RGB CCD camera (Brandt Allied Vision Technology® model Stingray) with a 16 mm lens and a LCD projector (Brandt Philips® model PPX2055) to project vertical blue fringes (RGB code 0, 0, 255) 5 pixels wide. The camera adopted for FP+2D-DIC set-up was denoted as camera 0 in Figure 7.4. The

results obtained with FP+2D-DIC were compared with those obtained from the two commercial 3D-DIC systems, namely VIC 3D from Correlated Solutions Inc. and Istra Q-400 from Dantec Dynamics. The Correlated Solutions system employed the same camera as FP+ 2D-DIC system (Camera 0) and an additional black and white CCD camera of 1032 by 776 pixels (Brandt Allied Vision Technology®, model Guppy Pro F-125 C) with a 16 mm lens (Camera 1 in Figure 7.4). The Dantec system employed two black and white CCD cameras (model Stingray F-201) with 25 mm lenses (camera 2 and 3 in Figure 7.4 A).

The four cameras and the projector were placed on a tripod located in front of the specimen as shown in Figure 7.4. B.

Before capturing any image, the calibration of all the systems was performed. Dantec system was calibrated using a 30x30 mm target (Dantec code Gl-03-WMB-9x9 30 mm), the Correlated Solutions system was calibrated using a 4mm (10x9 code) target and the FP+2D-DIC system was calibrated using the procedure described in chapter 5.

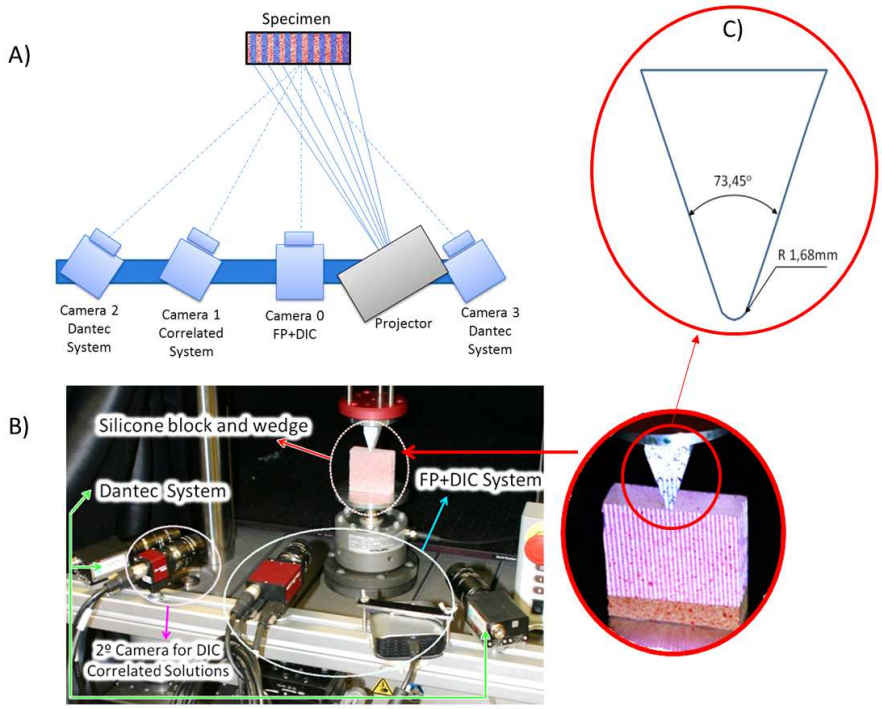

Figure 7.4. A) Schematic illustration showing the implemented experimental set-up. B) Image showing the adopted experimental arrangement employed for both indentation tests. Detail of the silicone block during an indentation A. C) Geometry and dimension of the wedge employed during indentations experiments

To capture the images during the experiments the following sequence was adopted: for each displacement step camera 0 captured one image, subsequently the projector stopped projecting fringes and illuminated the specimen with a green background to improve the contrast in grey scale images. Finally, cameras 1, 2 and 3 captured grey scale images simultaneously for 3D-DIC processing.

The images processed with the Correlated Solutions system employed a 35 pixel facet with 1 pixel of spacing between facets centre to maintain the same image size as FP+2D-DIC results. Nevertheless, for images processed with the Dantec system a 33 pixel facet size with a 5 pixel overlap was employed. To perform FP+2D-DIC, fringe images were processed employing the Phase-Stepping algorithm and speckle images were processed employing VIC 2D software with a 25 pixel facet size and a 1 pixel of spacing between facets centre.

7.2.3. Experimental results

7.2.3.1. Displacement results

In this epigraph displacements maps obtained with FP+2D-DIC and 3D-DIC will be presented and compared. For each indentation step (a total of 4 steps corresponding to 2, 4, 6 and 9 mm indentations were conducted) three displacement maps were obtained, namely *X*-displacements, *Y*-displacements and *Z*-displacements. For illustration purposes, only the last step corresponding to 9 mm indentation is presented in Figure 7.5 A)-I). In addition, a profile plot comparing FP+2D-DIC and 3D-DIC results obtained with VIC 3D software (from Correlated Solutions Inc.) is also included. Results from the 3D-DIC Dantec system are also presented in Figure 7.5 J)-L) but they are not included in the profiles, since the view angle for the reference image in Dantec system was not the same as it was for FP+2D-DIC. In addition, the displacement map size was different, and consequently a direct comparison was not possible.

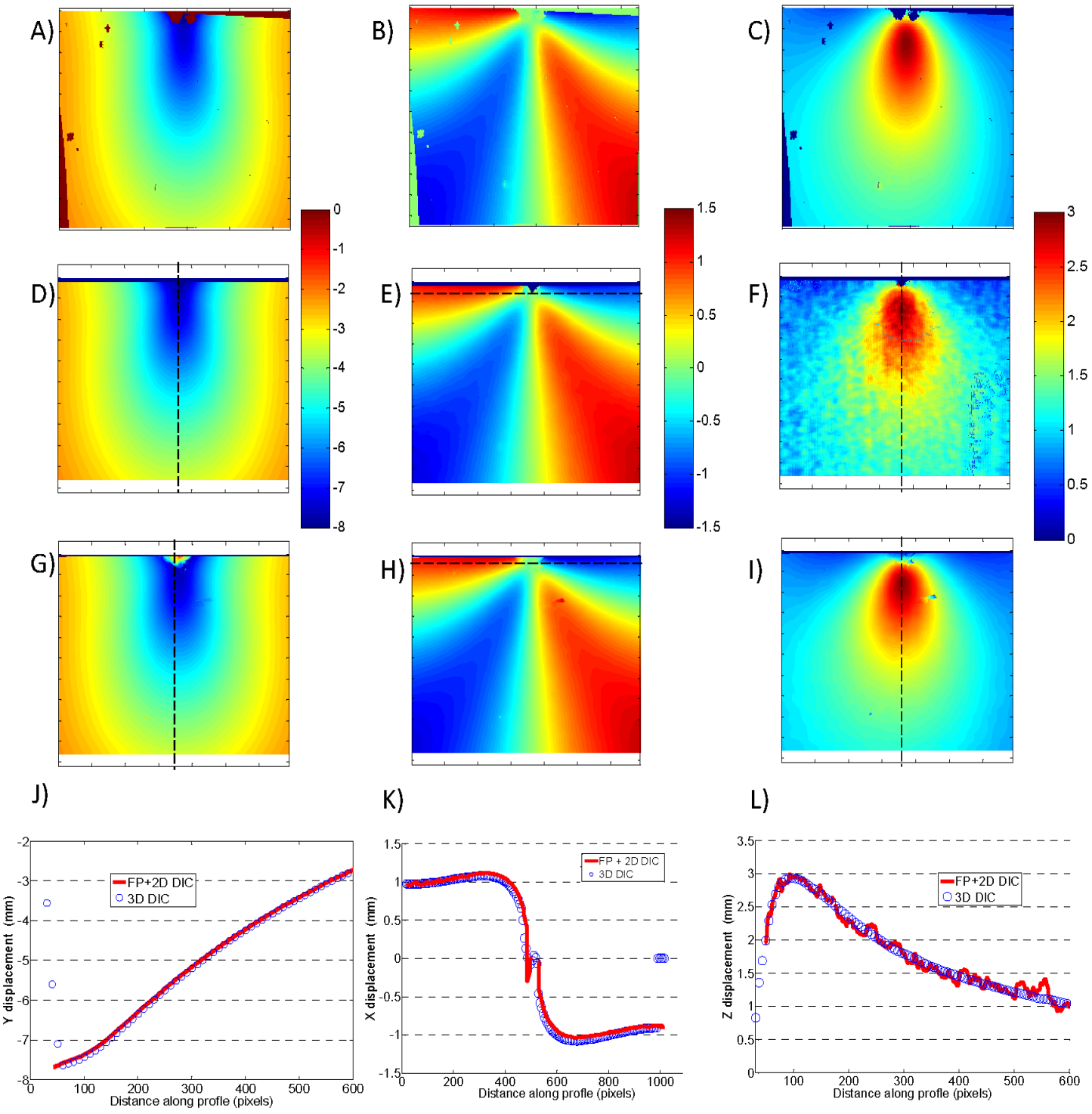

Figure 7.5 Illustration showing results for *Y-,X-,Z-* Displacements provided by 3D-DIC Dantec (A),B),C)); FP+2D-DIC (D),E),F)); 3D-DIC Correlated Solutions (G),H),I)); and profile plots for *Y-,X-* and *Z-* displacements along dashed line (J),K),L));

7.2.3.2. Comparison using Image Decomposition Technique

As previously mentioned, a total of 36 displacements maps for the four indentation steps and the three different systems analysed were obtained. Moreover, Dantec results were not directly comparable with the FP+2D-DIC and 3D-DIC due to the different viewing angle of the cameras. However, a comparison between the three systems was required and an image decomposition method was employed (Sebastian, et al., 2013). The basics of the method consist of converting the information from displacements maps into a vector that can be directly compared for each indentation step. Through this approach it is possible to eliminate the influence of the size of the image and the viewing angles of the cameras, making it possible to perform a direct comparison of the results for all three of the different systems analysed. The required number of shape descriptors is given by a correlation coefficient (cr) between the original (*Or*) and the reconstructed image (*Re*) using *N* shape descriptors or moments:

$$\boldsymbol{cr} = \frac{\sum_X \sum_Y (\boldsymbol{Or_{XY}} - \overline{\boldsymbol{Or}})(\boldsymbol{Re_{XY}} - \overline{\boldsymbol{Re}})}{\sqrt{(\sum_X \sum_Y (\boldsymbol{Or_{XY}} - \overline{\boldsymbol{Or}})^2)(\sum_X \sum_Y (\boldsymbol{Re_{XY}} - \overline{\boldsymbol{Re}})^2)}} \qquad \text{Eq 7.1}$$

Thus, a study of the adequate number of descriptors is required. As shown in Figure 7.6, as the number of shape descriptors (moments) increases, the correlation coefficient increases. It can also be observed that as the number of moments increases the calculated uncertainty (defined as the squared root of the squared difference between the original and the reconstructed images) decreases. Finally, for the comparison of the vectors, 150 descriptors was considered as an appropriate number, which was the quantity that raised the asymptotic maximum of the correlation coefficient in Figure 7.6.

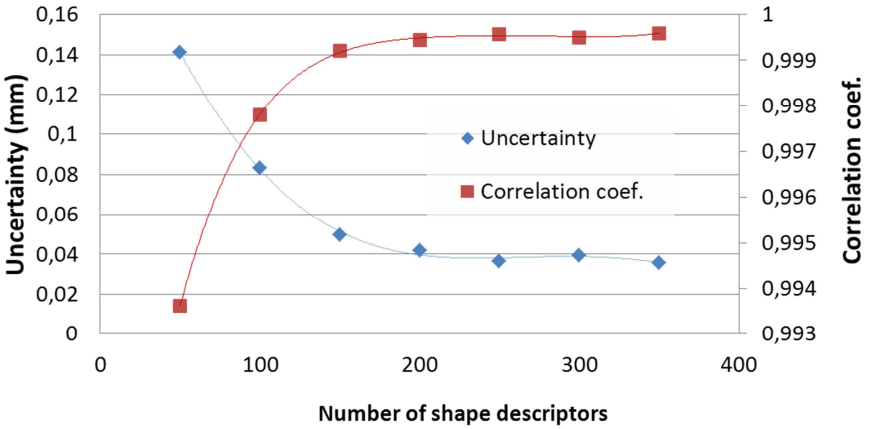

Figure 7.6 Plot showing the influence of the number of moments in the decomposition quality

Figure 7.7 shows a comparison of the calculated uncertainty along the four indentation steps for the three different systems evaluated. It can be observed that the uncertainty increases with indentation for the three different systems. Nevertheless, the calculated uncertainty was very small which indicates that in all the cases the quality of the results was very high.

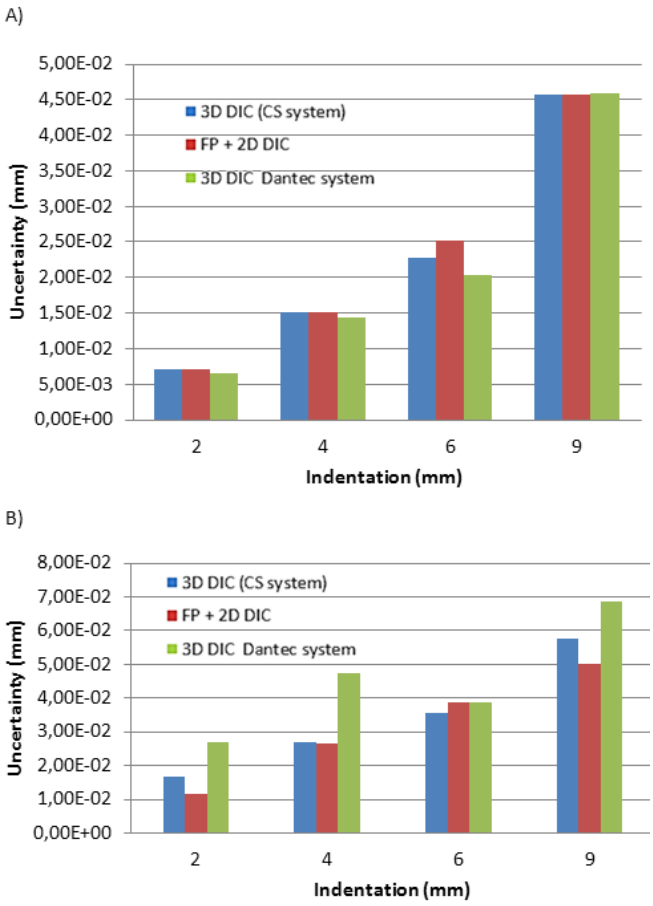

Figure 7.7 Plots showing the variation of the uncertainty for *X*- displacements (A) and for *Y*-displacements (B) for different indentation stages

After determining the proper representative number of shape descriptors or Tchebichef moments, a moment vector for each displacement map was obtained. Figure 7.9 A) and D) shows the scatter plots comparing Tchebichef moments for *Y*-displacement maps at the different indentation steps analysed. Figure 7.9.E shows the scatter plots for a *X*- displacements map corresponding to 9mm indentation. In all the cases 3D-DIC results are plotted on the vertical axis while FP+2D-DIC results are presented on the horizontal axis. Tchebichef moments are fitted by a linear least-square fit (dashed line). A continuous line representing 3D-DIC Tchebichef moments equal to FP+2D-DIC has also been included. Moreover, two bands considering the measurement uncertainty and the uncertainty due to the image decomposition process has also been presented (Sebastian, et al., 2013).

Figure 7.8 shows the distance between Tchebichef moments at different indentation steps for the different methods analysed.

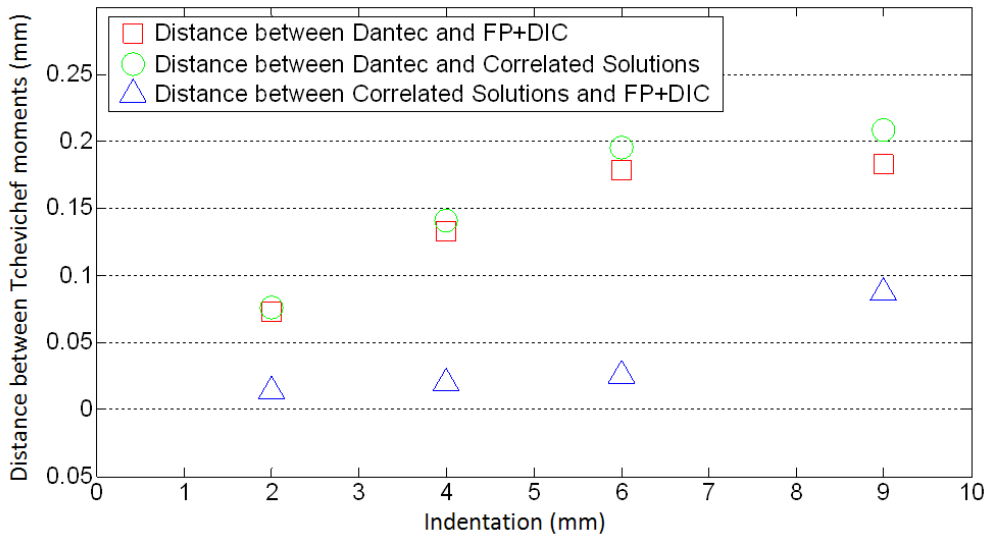

Figure 7.8 Distance between Tchebichef vectors along indentation (mm)

A)

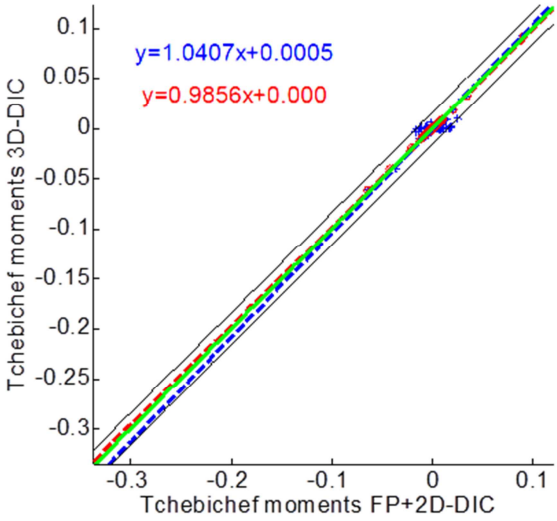

B)

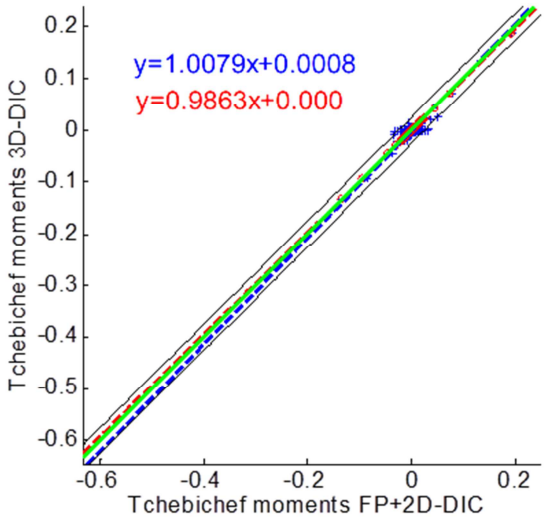

C)

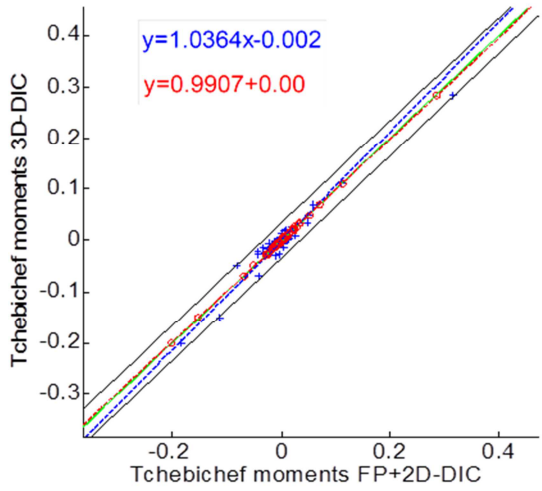

D)

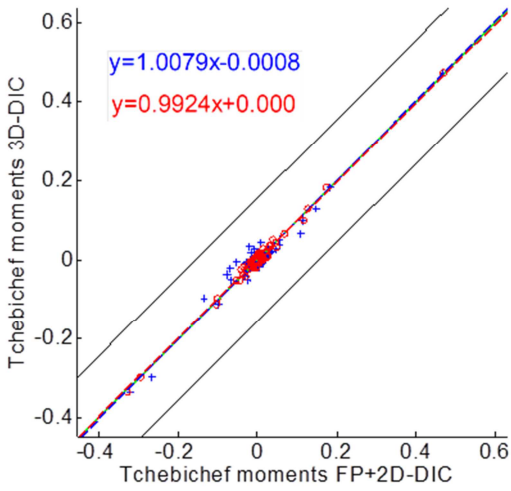

E)

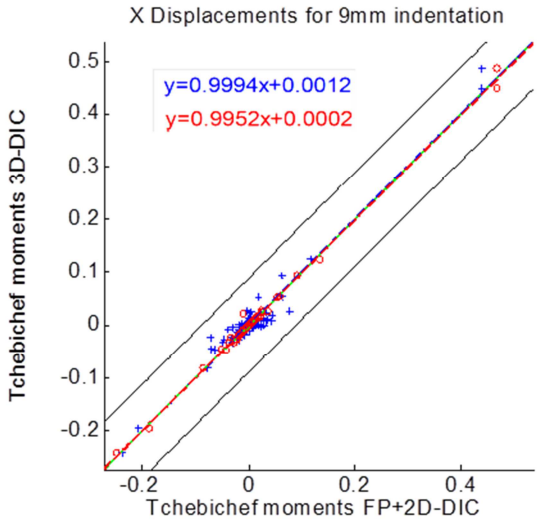

3D DIC Dantec Moments
3D DIC C. S. Moments
Fitting line Moments 3D DIC Dantec/FP+2D DIC
Fitting line Moments 3D DIC C. S. /FP+2D DIC
Line y=x

Figure 7.9 Scatter plots comparing Tchebichef moments for 3D-DIC and FP+2D-DIC. A) *Y*-displacements results for 2 mm indentation B) *Y*-displacements results for 4 mm indentation C) *Y*-displacements results for 6 mm indentation D) *Y*-displacements results for 9 mm E) *X*-displacements results for 9 mm indentation

7.2.3.3. Strain calculation

As presented in previous figures, the silicone block experienced large displacements during the indentation process. Thus, for the analysis of the strains occurring during indentation, Green-Lagrange theory (appendix 1) was adopted for the calculation of strains maps from displacements. Figure 7.10 shows the maps of strains ε_{xx}, ε_{yy}, and ε_{xy} calculated from FP+2D-DIC results for two indentation steps, 2 mm and 9 mm.

7.2.4. Discussion

As has been illustrated in Figure 7.5, the proposed methodology based on FP+2D-DIC provides excellent displacements results when compared with those obtained from 3D-DIC technique. The inferred displacement maps show the same scale of deformation with differences smaller than 0.06 mm respect to 3D-DIC, as it is clearly shown in *X*- and *Y*-profiles in Figure 7.5 J) and K). However, out-of-plane displacements (Figure 7.5.L) are noisier than those measured with 3D-DIC. This is mainly attributed to the phase shifting algorithm employed for fringe projection analysis. It is quite remarkable that the maximum difference between FP+2D-DIC and 3D-DIC in *Y*-displacements occurs at the same location as for *Z*-displacements maps. It implies that *X*- and *Y*- displacements are influenced by the presence of noise in the out-of-plane results. It is also observed that 3D-DIC results present more non-processed areas than 2D-DIC results. This could be due to the fact that 3D-DIC is more sensitive to the presence of speckle irregularities than 2D-DIC.

As previously mentioned, 3D-DIC results from Dantec system cannot be directly compared with those obtained with the FP+2D-DIC system, since the viewing angle of the cameras and the size of the data map are not the same. Thus, an image decomposition technique has been adopted to compare the three different systems analysed. This comparison has been performed through Tchebichef moments obtained for each displacements map with respect to an ideal situation, as Figure 7.9 shows. In all the plots, it can be observed that the gradient of the fitting lines is always within the uncertainty bands, which is indicative of the good correlation between both techniques. It is also

worth noting that there is a better correlation between the FP+ 2D-DIC and 3D-DIC results from Correlation Solutions than from Dantec system. This issue can also be observed in Figure 7.8, where the smallest vector distance always exists between the 3D-DIC results from Correlated Solutions and FP+2D-DIC. Nevertheless, in all the cases the 3D-DIC results from Dantec are still very close to those obtained with the FP+2D-DIC technique. In Figure 7.8 it can also be observed that there is a jump in the vector difference for the 6 mm indentation. This difference can be attributed to the fact that at this indentation step some difficulties occurred during the correlation process for both 3D-DIC systems that resulted in some non-processed points next to the wedge contact region.

Figure 7.10 shows the strains maps calculated from the measured displacements using FP+2D-DIC technique. Strain results have a certain amount of noise, since they were obtained from displacements differentiation, but in all the cases it can be observed that the strain distribution is consistent and similar to the strains maps achieved by other authors (Xiao, et al., 2013).

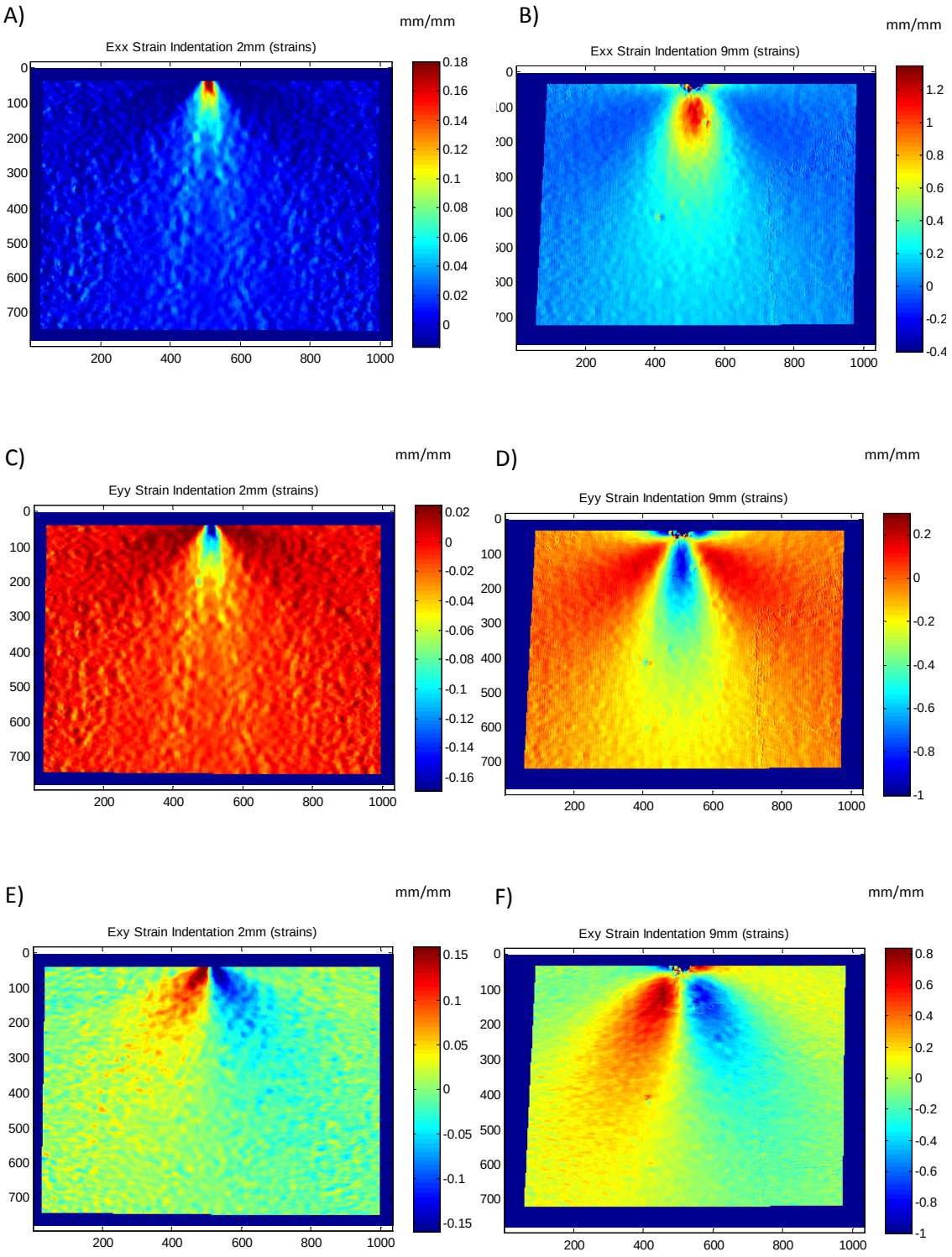

Figure 7.10 Strains maps calculated from FP+2D-DIC displacements maps. Strain map ε_{xx} for 2mm (A) and from 9mm (B) indentation. Strain map ε_{yy} for 2mm (C) and from 9mm (D) indentation. Strain map ε_{xy} for 2mm (E) and from 9mm (F) indentation

7.3. High speed 3D displacement analysis due to the impact on a silicone block

As previously exposed, one major advantage of combining Fringe Projection and Digital image Correlation is the use of one camera instead of two, as in the case of 3D-DIC. This advantage is especially important if the economic cost of the camera is very high, as often happens for high speed cameras.

In this part of the chapter, the potential of the FP+2D-DIC technique during high speed contact experiments is proven. Thus, a set of dynamic experiments consisting of the indentation of a silicone block at high speed conditions were conducted. In a first test (test A) the specimen was indented and subsequently released. In a second experiment (test B) the behaviour of the silicone block was also analysed, but in this case it was started from the block indented, then it was released and subsequently indented again. In both tests the indentation speed rate exceeded 300mm/s.

In this case displacements results were compared with those calculated using Finite Element simulations employing the Image Decomposition approach previously described.

7.3.1. Estimation of the measurement uncertainty for the FP+2D-DIC technique

As in the previous test, an initial experiment was conducted in order to quantify the minimum measurement uncertainty in the results from the FP+2D-DIC technique under dynamic events. The procedure was essentially based on that presented in previous epigraph 7.2.1. The selected reference material was of the same 7075-T6 aluminium cantilever beam 40 mm wide, 160 mm long and 2 mm thick. Experimental results obtained with FP+2D-DIC were compared with the theoretical solution for a cantilever beam excited with a speaker at its first resonance mode (65.5Hz). In addition, out-of-plane displacements were measured at a certain point of the cantilever using a laser vibrometer (Polytec OFV-503 with a 112 μm diameter sampling

point) as shown in Figure 7.11. Seven complete oscillations (Figure 7.12 C)) of the cantilever beam were analysed at a sampling frequency of 800 displacement measurements per second (12,2 measurements for each oscillation).

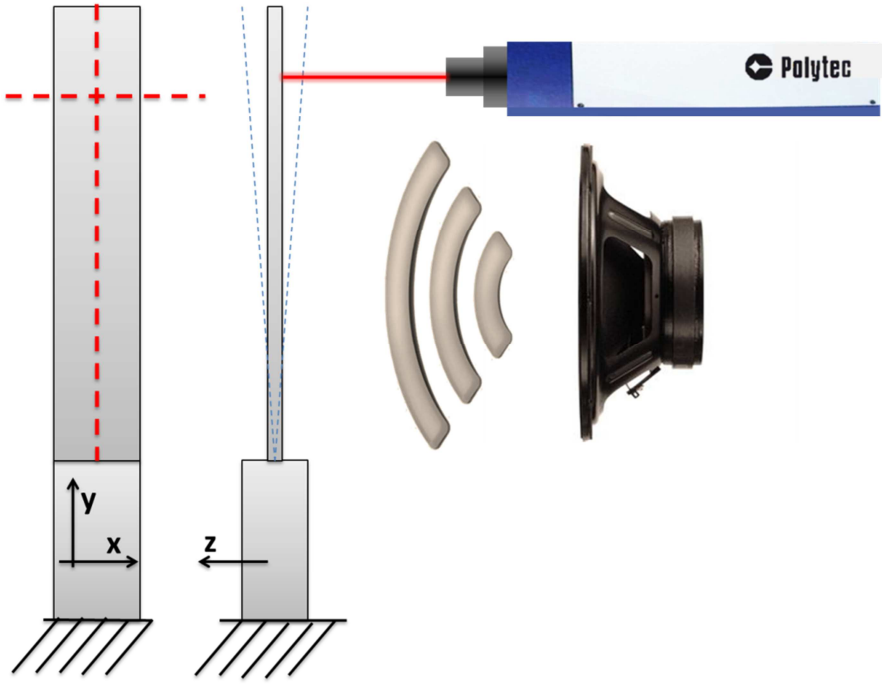

Figure 7.11 Schematic illustration of the methodology adopted for the estimation of the measuring uncertainty of FP+2D-DIC during dynamic analysis.

As the cantilever beam bent, out-of-plane displacements occurred in *Z*- direction (Figure 7.12.A)). Figure 7.12.B shows the measured *X*-displacements along a profile parallel to *X*- axis at 140 mm from the base of the cantilever beam. Results predicted by the theory indicate that no *X*- displacements exist along the profile. However, 2D-DIC results show a virtual displacement as a result of the out-of-plane deformation. Thus, 2D-DIC results must be corrected using the out-of-plane information provided by FP.

In general terms, the tendency of experimental results presented in Figure 7.12 clearly matches with those predicted by the theory. Nevertheless, there is a clear uncertainty established to 0.009 mm for out-of-plane displacement and 0.006 mm for in-plane displacement using the approach described in the Interlaboratory Study Protocol of the Project Vanessa .

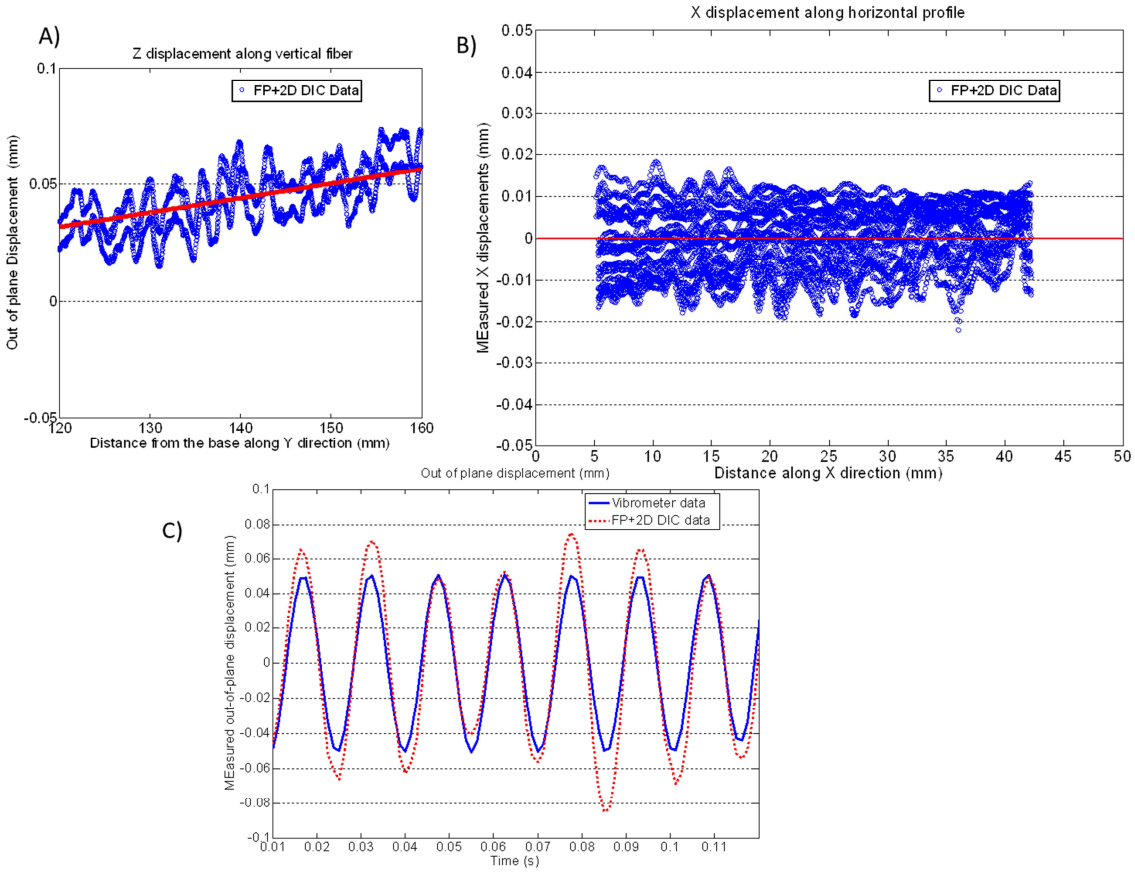

Figure 7.12 A) Vertical profile along the cantilever beam showing the out-of-plane displacements measured during the uncertainty estimation procedure. B) Horizontal profile at 140 mm from the base of the cantilever beam showing the *X*--displacement measured during the uncertainty estimation procedure. C) Out-of-plane displacement measured at the point of laser vibrometer measuring along time of the uncertainty estimation procedure.

7.3.2. Experimental procedure

Two high speed contact experiments on a 60 x 60 x 20 mm silicone block were conducted. Since the silicone block was completely transparent, the specimen had to be carefully sprayed as described in epigraph 7.2. The experimental set-up for FP+2D-DIC is presented in Figure 7.13.

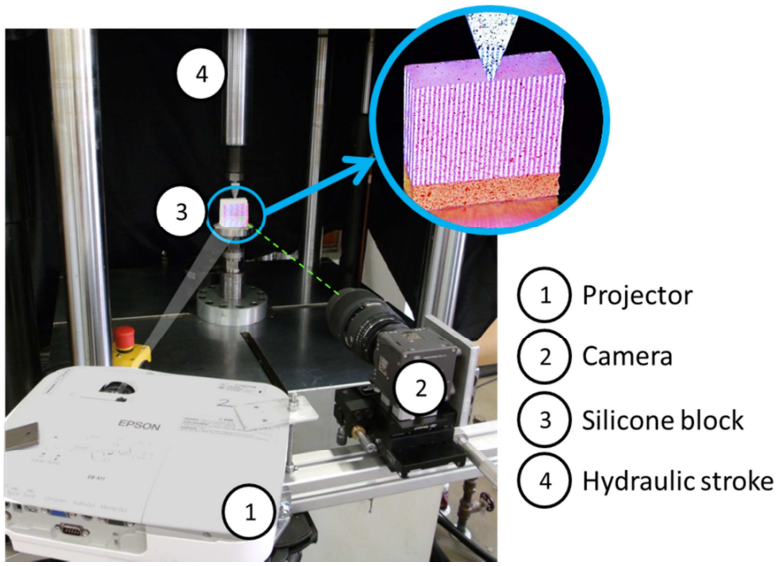

Figure 7.13 Schematic illustration showing the implemented experimental set-up.

A 2024 aluminium alloy wedge was employed to perform the indentation. Moreover, a fine layer of talc powder was applied over the indentation area to avoid the adhesion of the silicone block to the wedge during the experiments. Experiments were conducted using an ESH impact testing machine with a 25kN load capacity managed by a Phoenix Calibration & Services control system to control the displacement of the indenter attached to the hydraulic stroke.

During experiments images were captured at 800 frames per second using an IDT N4-S1 camera (1024 x 1024 pixels resolution) with a 105mm Tamron lens was placed at 715mm from the silicone block. In addition, an Epson EB-x11 LCD projector was employed to project the fringe pattern. No extra light was employed since it affected the contrast of the projected fringes. As in previous test (epigraph 7.2), fringe images were processed employing the phase stepping method while speckle images were processed employing VIC 2D commercial software (facet size 21px and 1px between facets centre).

The FP+2D-DIC system was calibrated following the same calibration procedure developed in chapter 5. However, in this case the micrometric adjust platforms were employed only for the camera due to the fact that the weight of the whole camera-projector set was excessive for them. Hence, FP was calibrated by relating the

difference of phase measured with a calibrated shape i.e. a 50mm diameter cone 10mm high.

Initially a 6mm indentation at 300mm/s followed by a relaxation of the specimen at 1000 mm/s (test A) was performed (Figure 7.14.A). Originally the indentor was placed at 3mm from the silicone edge in order to obtain a constant speed at the moment of contact between the wedge the block. In a second experiment (test B), the specimen started at an indentation of 6mm, which was subsequently relaxed at 1000 mm/s by vertically displacing the wedge 9 mm upwards. After that an indentation of 6 mm was again applied by vertically displacing the wedge 9 mm downwards at 300 mm/s (Figure 7.14.B). The stroke movement speed was conveniently adjusted to investigate if the silicone block exhibited any hysteresis during indentation and relaxation.

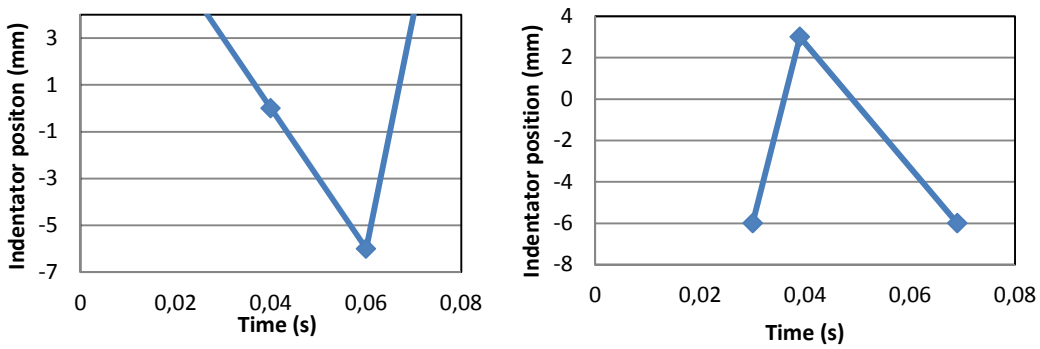

Figure 7.14 Stroke displacement sequence over time for test A (left) and test B (right)

7.3.3. Numerical Modelling

The Experimental results provided by FP+2D-DIC were compared with those obtained from FEM numerical modelling results using explicit dynamic approach. The numerical analysis was conducted with the commercial software Abacus 6.11. For the model of the silicone block and the indenter 13000 four-node reduced integration elements were employed. In addition, Mooney-Rivlin Hyperelastic model defined by Eq 7.2 was adopted and calibrated according to the material properties.

$$\boldsymbol{\sigma} = \frac{\mathbf{2}}{\boldsymbol{J}}(\boldsymbol{C_{10}} + \boldsymbol{C_{01}}\boldsymbol{I_1^*})\boldsymbol{b^*} - \frac{\mathbf{2}\boldsymbol{C_{01}}}{\boldsymbol{J}}(\boldsymbol{b^*})^{\mathbf{2}} + \left[\boldsymbol{k}(\boldsymbol{J}-\mathbf{1}) - \frac{\mathbf{2}\boldsymbol{I_1^*}\boldsymbol{C_{01}}}{\mathbf{3}\boldsymbol{J}} - \frac{\mathbf{4}\boldsymbol{I_2^*}\boldsymbol{C_{01}}}{\mathbf{3}\boldsymbol{J}}\right]\mathbf{I} \qquad \text{Eq 7.2}$$

Where b^* is the distortional left Cauchy–Green vector defined by $\mathrm{b}^* = J^{2/3}\mathrm{F}\mathrm{F}^{\mathrm{T}}$ and σ is he Cauchy stress. Those parameters which determine the behaviour of the silicone were obtained from a similar silicone material that was found in bibliography and then adjusted them to the actual behaviour of the specimen tested. Hence, the material parameters C_{10} and C_{01} were settled to 0.9 and 0.3 respectively and the bulk modulus (J=det(F)) to 20. The tensile strength of the cured silicone material was 4,8 MPa and the material failure was predicted to occur at a maximum elongation of 100%.

A finer mesh (0.15x0.15x0.15 mm elements) was employed to model the contact region and the front and back side of the silicone block, as shown in Figure 7.15, where the strain gradients and the evolution of the displacements rate was expected to be higher. The minimum element size determine the minimum time step in explicit methods, the dimension of the element was set to obtain a good agreement between precision and step time For the rest of the model the size of the elements was set to 1x6x0.3 mm.

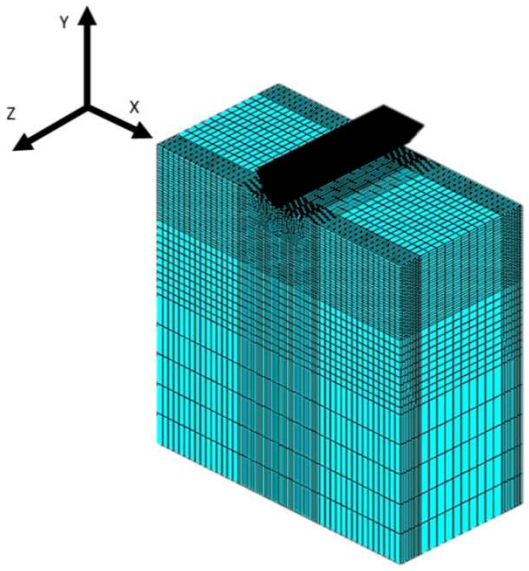

Figure 7.15 Detail of the mesh employed for the block and the wedge for FEM simulations

The indenter was modelled as a non-deformable body using bi-dimensional rigid solid elements, as shown in Figure 7.15. The indentation speed was defined according to the values measured by FP+ 2D-DIC during the experiments**.**

7.3.4. Experimental results

7.3.4.1. Displacements results

In this epigraph experimental and numerical results will be presented, compared and discussed. During each experiment a total number of 99 images were processed. Displacements occurring at a point close to the contact region were monitored. In addition, attention was focused on those images where indentation was at a maximum and minimum in test A and B respectively. Thus, three displacement maps were analysed, namely *X*- displacements, *Y*- displacements and *Z*- displacements.

a) Test A results.

Figure 7.16 shows the displacements over time that occur at a point located at 0,74 mm from the edge of the silicone block. In Figure 7.16.A, the *Y*- displacement (blue line) and *Z*- displacement (green line) measured employing PF+2D-DIC are presented together with the vertical displacement of the wedge (red line) and the *Y*-displacement of a point (green cross) measured with 2D-DIC (pink line).

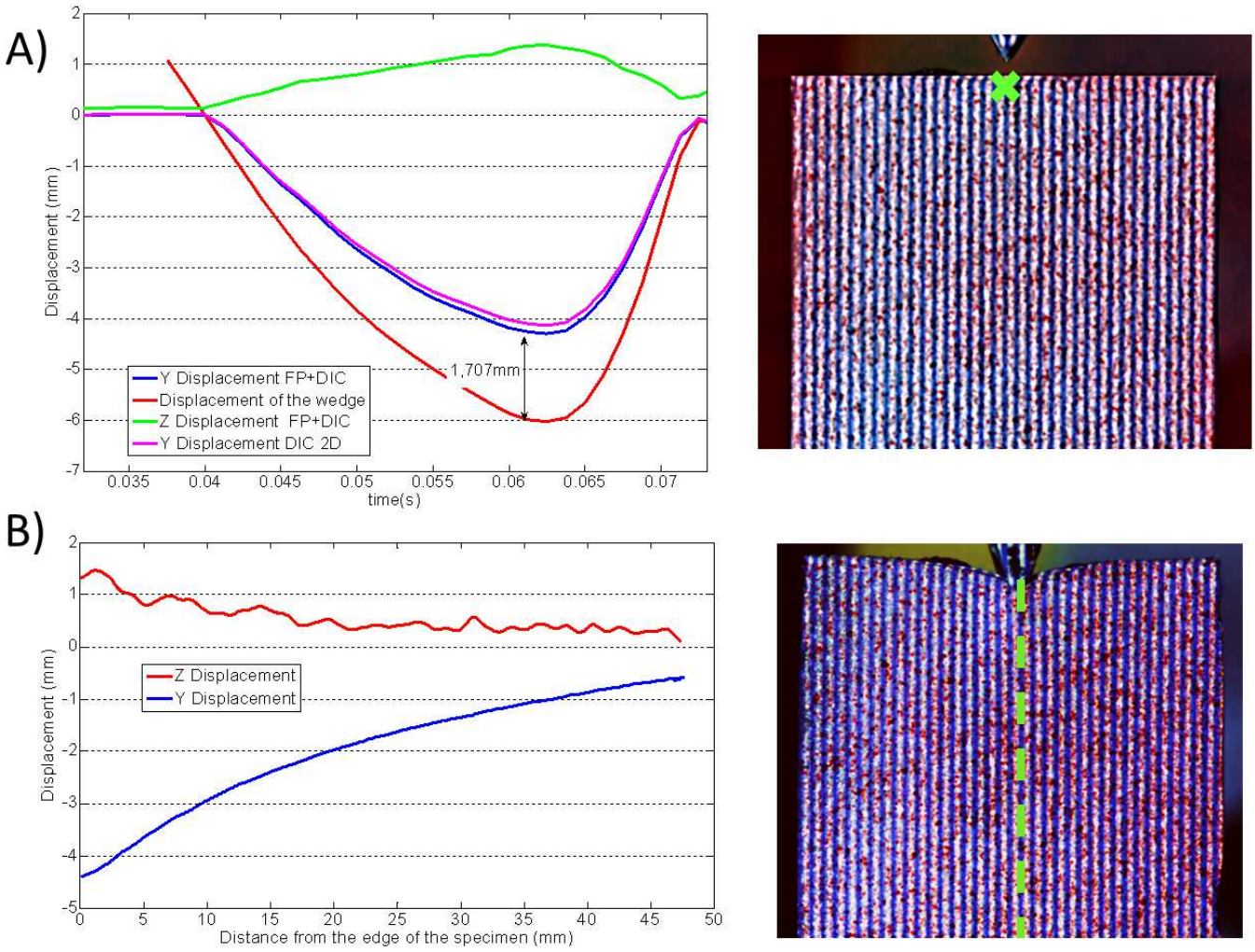

Figure 7.16 A) Temporal evolution of the displacement measured at a point at 0.74mm from the contact area. B) *Z*- and *Y*- displacements measured by FP+2D-DIC along a vertical profile at 0,0625 s

From Figure 7.16 A) it can be observed that the maximum indentation occurs at 0,0625s after starting the test. Figure 7.16 B) illustrates *Y*- and *Z*- displacements along a vertical profile (green dashed line) at 0,0625s.

Figure 7.17 shows the experimental and numerical results corresponding to displacements maps at 0.0625 s during test A.

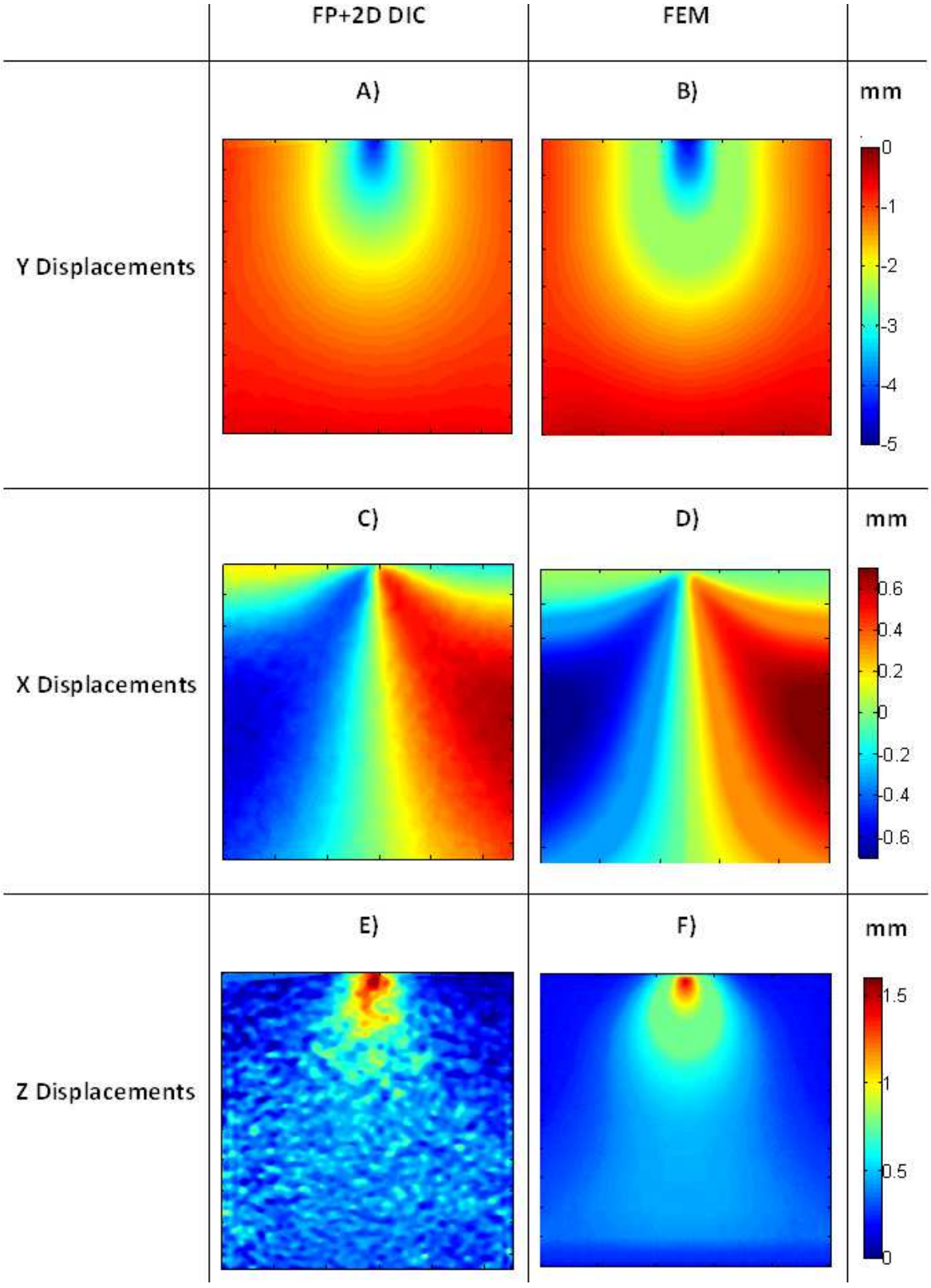

Figure 7.17 Displacements maps from experimental (left column) and numerical (right column) analysis at maximum indentation (0.0625 s) in test A

b) Test B results.

Figure 7.18 shows the measured displacements at a point at 0,37mm from the edge of the silicone block along the time. The maximum wedge displacement during unloading (4,9 mm) occurred at 0,47 seconds after the test started (Figure 7.18. A). It is interesting to show that a rebound of the silicon block occurred when the contact between the wedge and the block was lost.

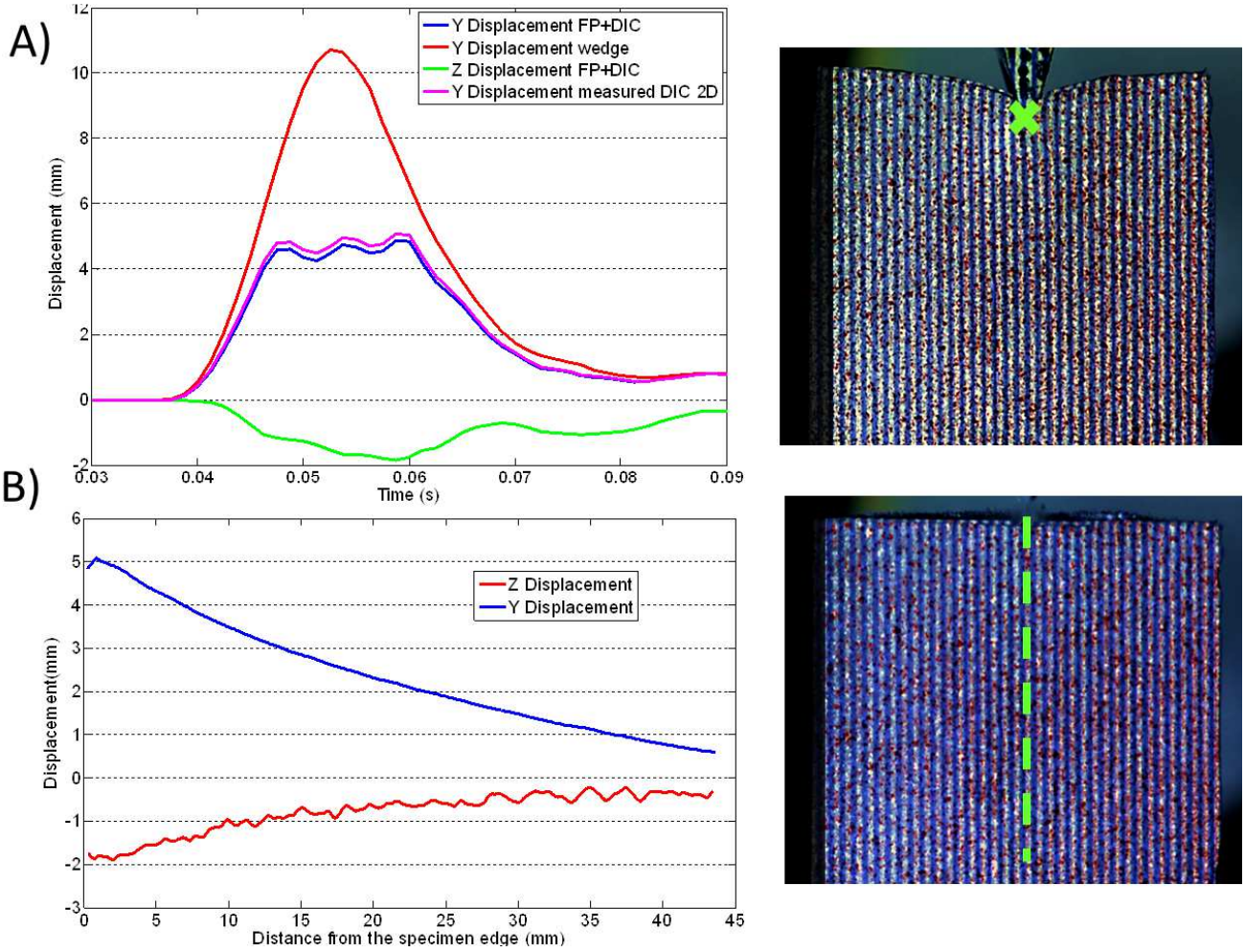

Figure 7.18 A) Temporal evolution of the displacements measured at a point at 0. 37mm from the contact area long time. B) *Z*- and *Y*- displacements measured by FP+2D at 0.047 s along a vertical profile

Figure 7.18 B) illustrates *Y*- and *Z*- displacement along a vertical profile at 0.047 s. Figure 7.19 shows the experimental and numerical displacements maps at 0.047 s.

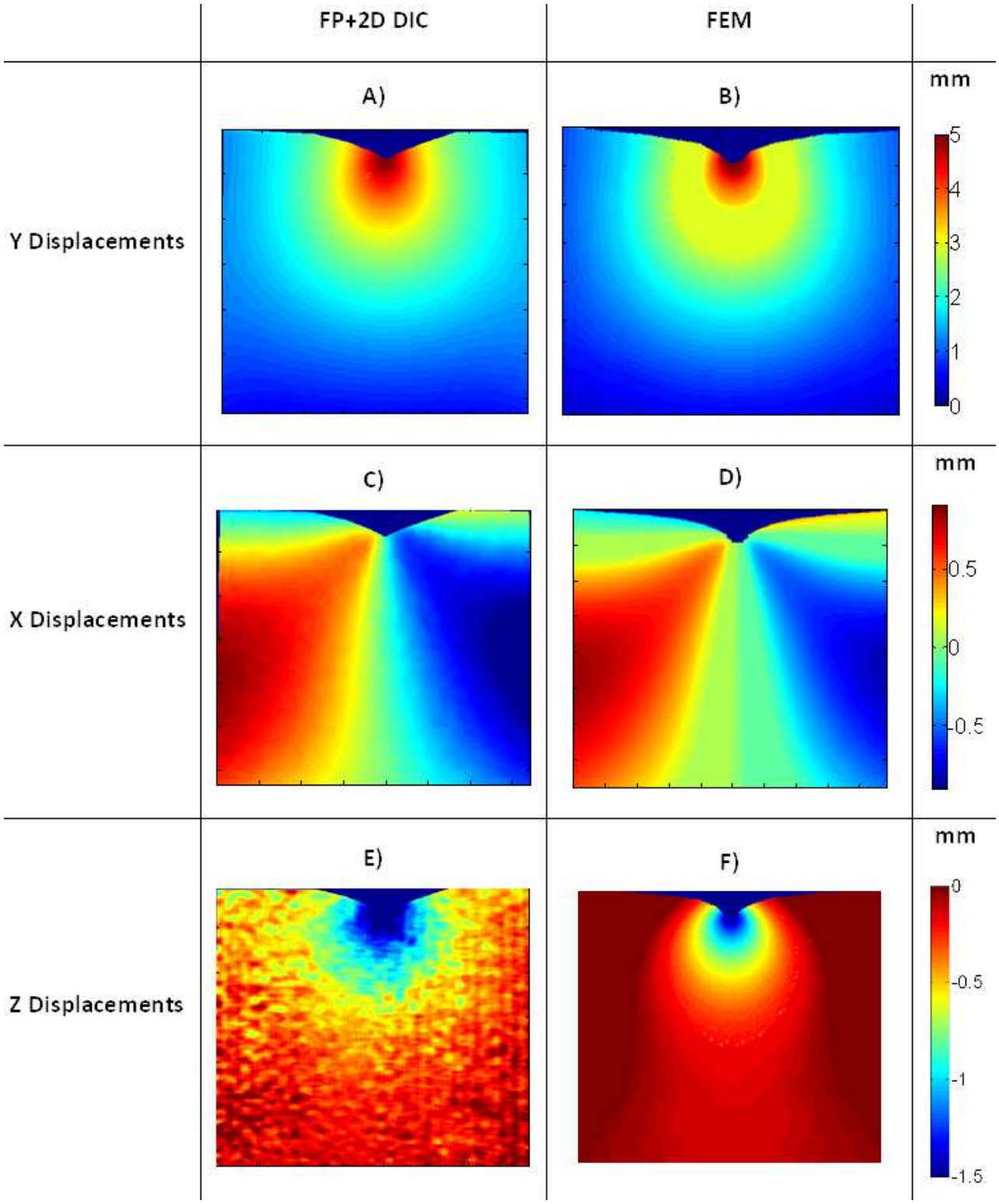

Figure 7.19 Displacements maps for experimental (left column) and numerical (right column) analysis at 0.047 s (maximum displacement of the wedge) in test B

7.3.4.2. Results comparison using image decomposition technique

Direct comparison of the experimental results with those obtained from FE analysis is not easy since the data format of the result and the scale may differ from each other. However, a qualitative comparison between the experimental and numerical results is required and thus, the image decomposition method was employed (Sebastian, et al., 2013). As described in the previous static test (epigraph 7.2), an adequate number of descriptors is achieved when the correlation coefficient is higher than 90%. For the current analysis a number of 100 Tchebichef moments was enough to obtain correlation coefficients between 92% and 99% depending on the displacements map decomposed.

Subsequently, a moments vector was obtained for each displacements map at 0.0625 s in test A and at 0.047 s in test B (Figure 7.17 and Figure 7.19). Figure 7.20 shows scatter moment plots for the different displacements maps analysed, namely in *X*-, *Y*- and *Z*- directions. FEM moments are presented in the vertical axis while FP+2D-DIC moments are shown in the horizontal axis. Tchebichef moments are fitted by a linear least-square fit (dashed line). A continuous line representing FEM Tchebichef moments equal to FP+2D-DIC has also been included (red continuous line). Moreover, two bands considering the measurement uncertainty and the uncertainty due to the image decomposition process have also been presented (pink continuous lines) (Sebastian, et al., 2013).

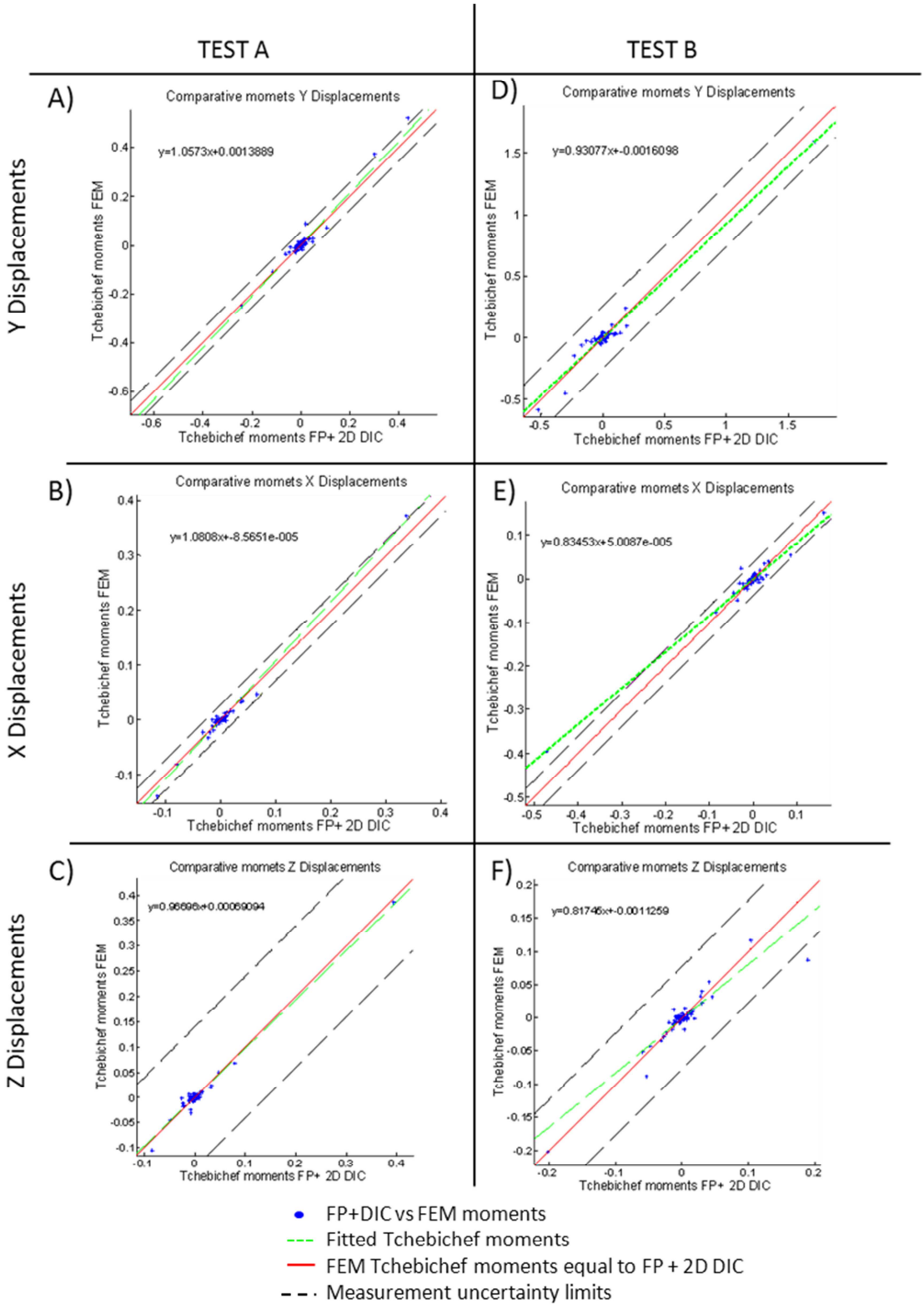

Figure 7.20 Scatter plots comparing Tchebichef moments for 3D-DIC and FEM. In left column *Y*-(A) *X*-(B) and *Z*-(C) displacements maps at 0.0625s are compared. In right columns *Y*-(D) *X*-(E) and *Z*-(F) displacements maps at 0. 047s are compared

7.3.4.3. Strain calculation

Figure 7.21 and Figure 7.22 show the strains maps ε_{xx}, ε_{yy}, and ε_{xy} calculated from FP+2D-DIC employing Green-Lagrange tensor for test A (instant 0,0625s) and test B (instant 0,047s) respectively. In addition, results obtained from numerical simulations at those times are also shown.

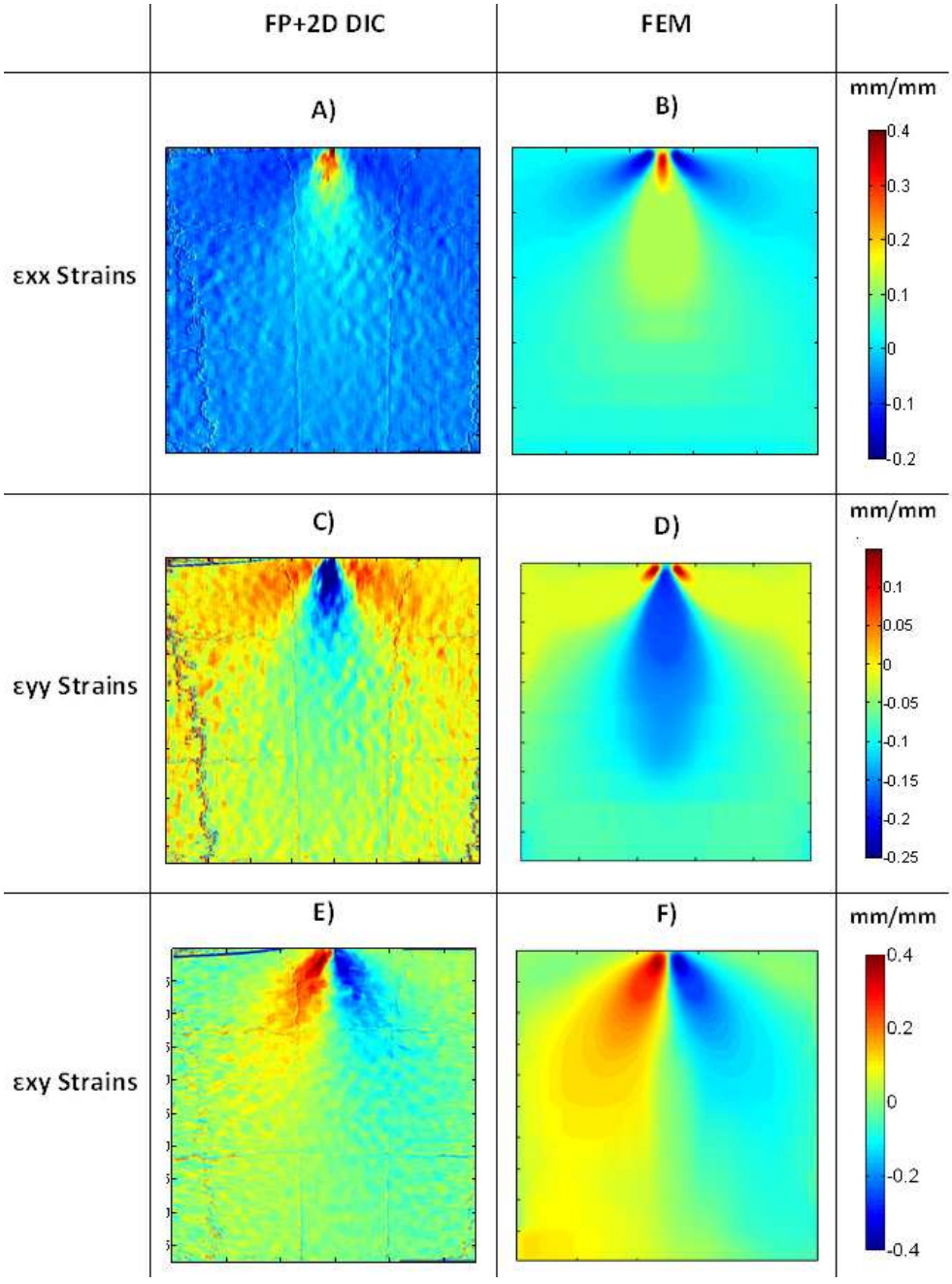

Figure 7.21 ε_{xx}, ε_{yy}, and ε_{xy} strain maps for test A at 0,0625s. Results from FP+2D-DIC (left column) and results from FEM results (right column).

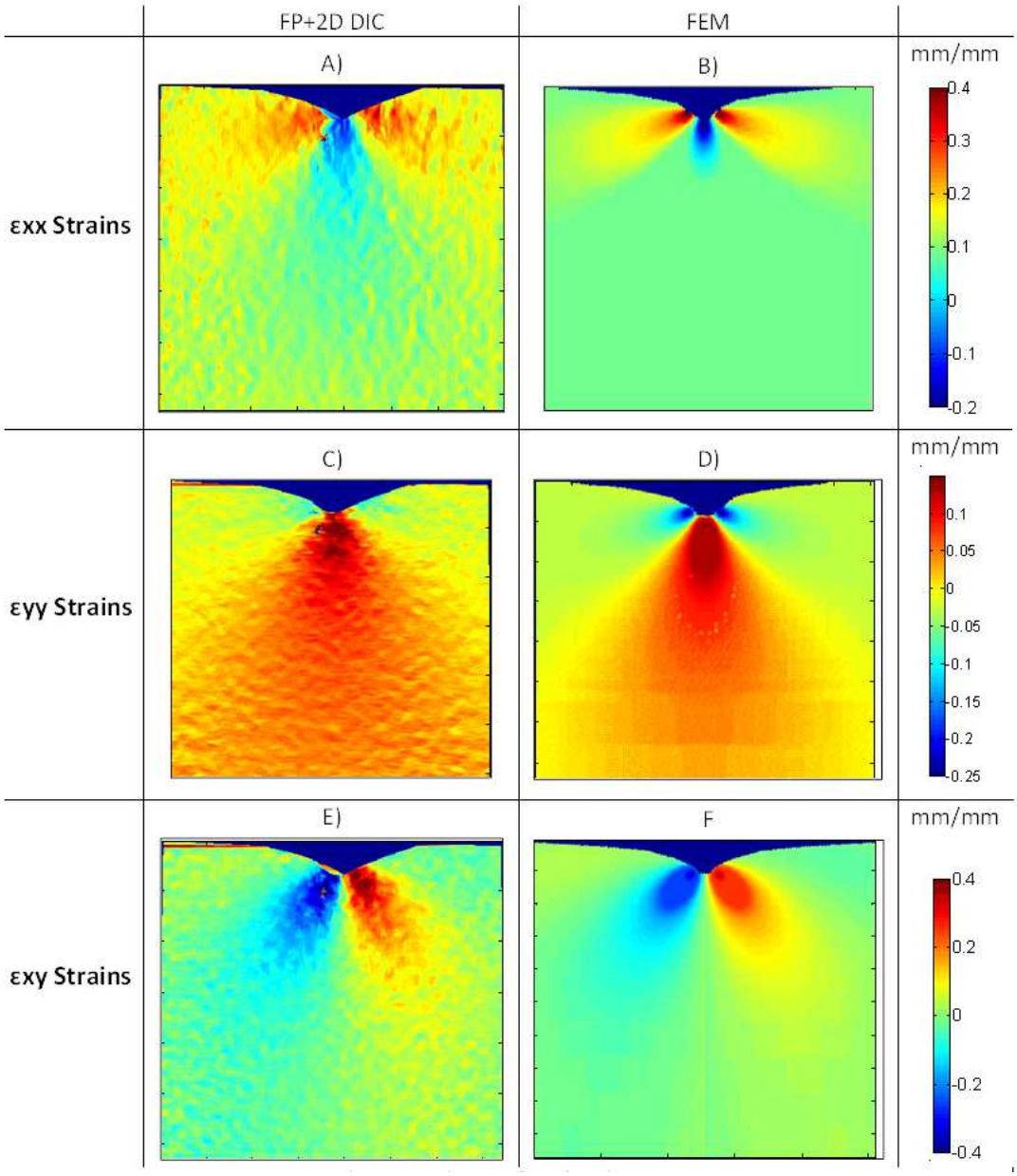

Figure 7.22 ε_{xx}, ε_{yy}, and ε_{xy} strain maps for test B at 0, 047s. Results from FP+2D-DIC (left column) and results from FEM results (right column).

7.3.5. Discussion

This test presented some difficulties in the experimental methodology since high frame rates involves short exposure times during image capture. Thus, more lighting was required. To overcome this problem, images were captured improving the projected contrast of speckle and projected fringe. It was not possible to illuminate the specimen with any light different from the projector since it affected to fringes

contrast. Hence, a projector with higher brightness than that employed in previous experiments was employed. In addition, to obtain bright colour images, a good balance was found between the lens aperture (to adjust the quantity of light that reaches the camera sensor) and the exposure time (which should be reduced to avoid blurred images).

Moreover, the calibration of Fringe Projection was restricted to the use of a single value of K_f instead of a K_f map as it was suggested in chapter 5. This issue could be solved employing more robust micrometric platforms. However, no decrease in the accuracy was detected due to the fact that the distance between the camera-projector and the silicone block was large enough (715mm) to consider a constant period in the field of view of the camera.

In addition, Figure 7.16 shows the temporal evolution of the displacements at a point next to the contact area during test A. Results show that the maximum occurred at the same time as the maximum indentation. It can be observed that there is a substantial difference of 1.707 mm between the displacement of the wedge and the measured *Y*-displacement at the selected point. It is noteworthy that the real displacement of the wedge (red line) is clearly much softer than the commanded ramp in Figure 7.14. The reason for that was that the control was not able to response fast enough. Moreover, it was noticed that the material recovers relatively fast following the wedge. Thus, and no important damping or hysteresis effect seems to appear since the material completely recovers at the instant 0,0725s when the wedge release the block.

Figure 7.18 A shows the temporal evolution of displacements at very close to the contact area in test B. It can be observed that there is no contact between the block and the wedge during the period from 0,045 to the 0,062 s. During this time the block suffers a set of oscillations at a frequency of 13 Hz. Moreover, it is clear that the maximum *Z*-displacement is not occurring at the instant when the contact between the wedge and the silicone block stops, it happens a bit later. This is due to the oscillation experienced by the block when the contact with the wedge is released. In addition, when contact starts again at 0.062 s the out-of-plane displacement is not the same as at 0.045 s since the block is still oscillating. Again, as during test A, the real

displacement of the wedge (red line) is clearly much softer than the commanded ramp.

If displacements maps of test A (Figure 7.17) and test B (Figure 7.19) are analysed, it can be ascertained that both experimental and numerical results match very well. However, in both cases, *Z*- displacements from FP+2D-DIC are nosier due to the presence of remaining speckle in fringe images. Moreover, in *Z*- displacements measured in test B, it was detected that the upper part of the silicone block tilted forward. This effect was not present in results of FEM which suggested that this tilting was due to the oscillation experienced by the silicone block. This hypothesis is consistent with the effect described in the *Z*- displacements of the Figure 7.18 due to a possible movement between the wedge and the block causes by adhesion between them.

Moreover, in the case of test A, *Y*-displacements from FP+ 2D-DIC seem to be more concentrated at the impact area than FEM results. Conversely, in test B displacements maps from FP+2D-DIC seem to be more spread out over the impact area while FEM results are more concentrated along the silicone block. *Y*-displacements seem to be quite sensitive to the way in which the indenter comes into contact with the block. In fact, the wedge is partially driven inside of the silicone block. This behaviour of the silicone affects the results creating the difference between the numerical and experimental results. In addition, this behaviour also explains why the maximum displacements measured at the silicone block do not match with the displacement of the wedge in Figure 7.16.A and Figure 7.18.A.

With reference to the comparison of results employing Image decomposition (Figure 7.20) it is worth nothing that in both cases the moments are placed inside the uncertainty band. In addition, the fitted moments (green dashed line) are also placed inside the uncertainty limits, closely following the 45^{o} line. That means that the differences in the measurement of displacements between FP+2D-DIC and FEM are lower than the proper uncertainty of the decomposing Tchebichef moments. Nevertheless it is clear that bigger differences are found in test B where the fitted shape descriptors (moments) line presents bigger differences with the 45^{o} (especially

for *Z*- displacements) reference line and some moments are found outside of the uncertainty band. The reason for this was that the oscillations of the rubber block during the test, caused some tilting in the specimen.

Respect to the strains maps measured by FP+2D-DIC and predicted by FEM it is observed that maximum and minimum values are similar in both tests A and B. Nevertheless it can be detected that strains maps obtained from FP+2D-DIC displacements measurements are nosier than FEM since the strains maps are calculated from the spatial derivative of displacements. In the case of Test A differences between FEM and FP+2D-DIC of 0,05mm/mm are found in the maximum and minimum values. Moreover, it can be noted that, as occurred in the displacement maps, the strain concentration is higher in strains measured by FP+2D-DIC than those obtained employing FEM. In the case of Test B, differences of 0,1mm/mm are found. In addition, the measured strain concentration is more spread than the strain predicted by FEM. The numeric strain differences between FP+2D-DIC and FEM seem to be excessive however, looking at the strain maps it can be observed that these differences occur due to the fact that FEM results have a higher spatial resolution than FP+2D-DIC, which present more noise.

7.4. High speed compression test on a rubber ball

Previous tests have shown that the proposed technique is able to measure large in-plane and out-of-plane displacements with a good level of accuracy during high speed contact testing. During these experiments, it has been demonstrated that issues such as illumination, exposition time or the contrast between speckle and fringes are critical and they must be carefully analysed. However, the specimens tested so far had flat surfaces. In the present test FP+2D-DIC is employed in order to study the contact behaviour of a non-flat specimen. Thus, a 60 mm diameter fronttennis ball made of rubber, (Figure 7.23), is tested during a compression test at high deformation rate.

Figure 7.23. Illustration showing the fronttennis ball evaluated during a dynamic compression test using FP+ 2D-DIC.

7.4.1. Experimental procedure

A high speed compression experiment on a rubber ball (brand Penn) was conducted at 400mm/s. The adopted experimental set-up (Figure 7.24) was the same as that described in previous high speed experiments (epigraph 7.3). However, in this case, the wedge was replaced by an aluminium compression plate as illustrated in Figure 7.25. Initially, the surface of the ball was prepared by first spraying it with a white matt paint and subsequently spraying it with red speckle.

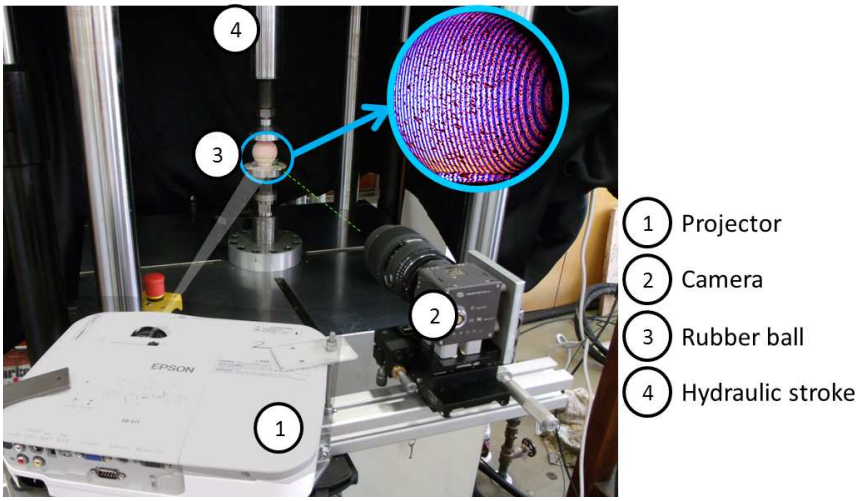

Figure 7.24 Experimental set-up employed for high speed compression test on a frontennis ball

The test machine employed for the experiment was an ESH dynamic impact testing machine with 25 kN load capacity controlled by a Phoenix Calibration & Services system.

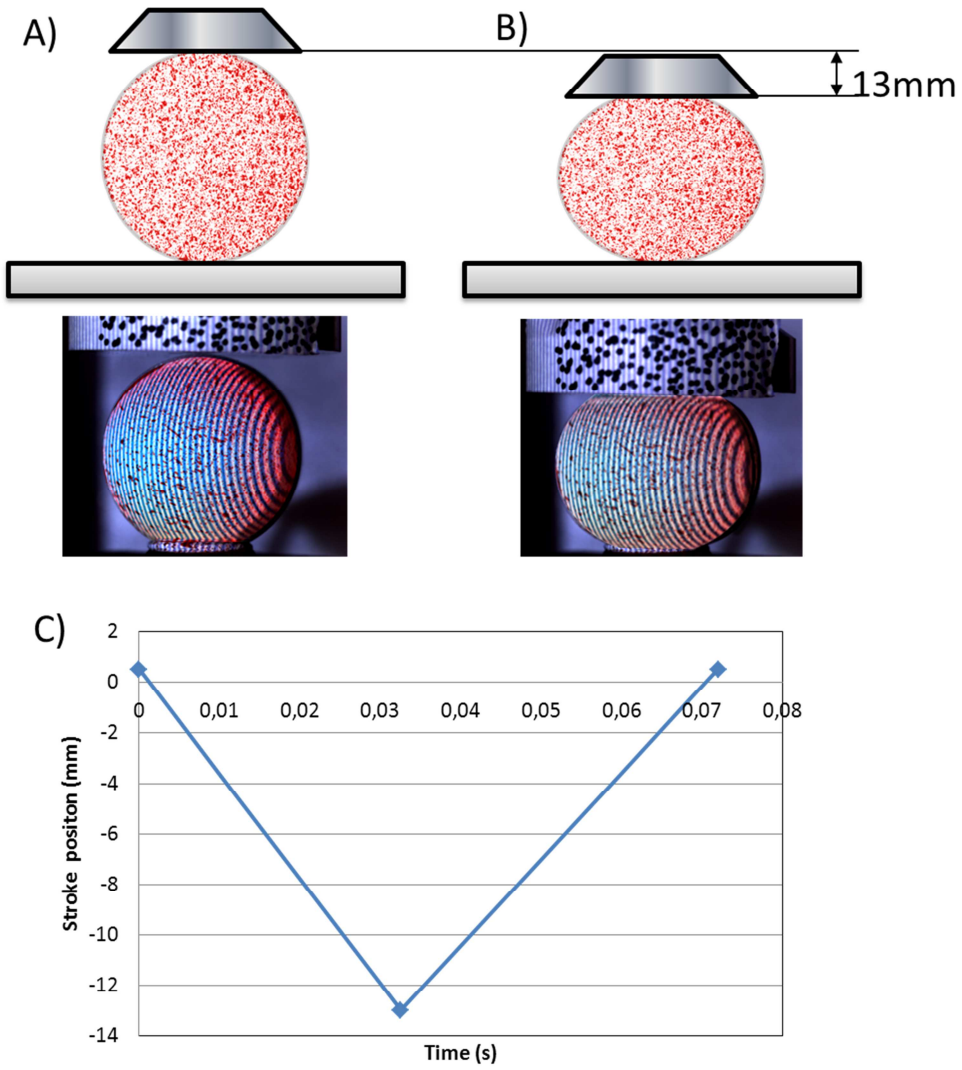

Figure 7.25 Compression ball test A) Schematic illustration and image of the initial state B) Schematic illustration and image of the maximum compression state. C) Stroke displacement sequence

During the experiment the displacement of the hydraulic stroke was set to 13mm at a compression speed of 400mm/s. After the maximum compression displacement was achieved, the stroke was moved back to its initial position at the same displacement speed (Figure 7.25.C).

For this test, images were captured at a frame rate of 500 frames/s at a resolution of 1024 x 1024 pixels using a CMOS colour camera (brand IDT, model N4-Sa) and a 105mm Tamron lens. Fringes and Speckle images were processed employing the Phase Stepping method and VIC 2D software (facet size 19px and 1px between facets centre) respectively.

The FP+2D-DIC system was calibrated following the same calibration procedure employed in the previous test. However, in this case, a flat reference surface was placed just in front of the ball for calibration. Thus, once the distance z_0 was calculated, this surface was removed. Hence, in this case, the measured out-of-plane displacements were referred to the reference surface adopted for calibration.

To capture the images, the camera was first triggered and subsequently the test machine was commanded to perform the test. Thus, images before and during the experiment were captured to study the behaviour of the ball and detect the moment of contact between the compression plate and the ball.

7.4.2. Experimental results

During the test 116 images were captured and processed. Figure 7.26 shows the temporal evolution of the out-of-plane displacements measured at the centre of the ball. From this figure it can be observed that the moment of contact between compression plate and ball at 0,095s. In addition it is clear that the maximum out of plane displacement occurs at 0,13s after the camera started to record images.

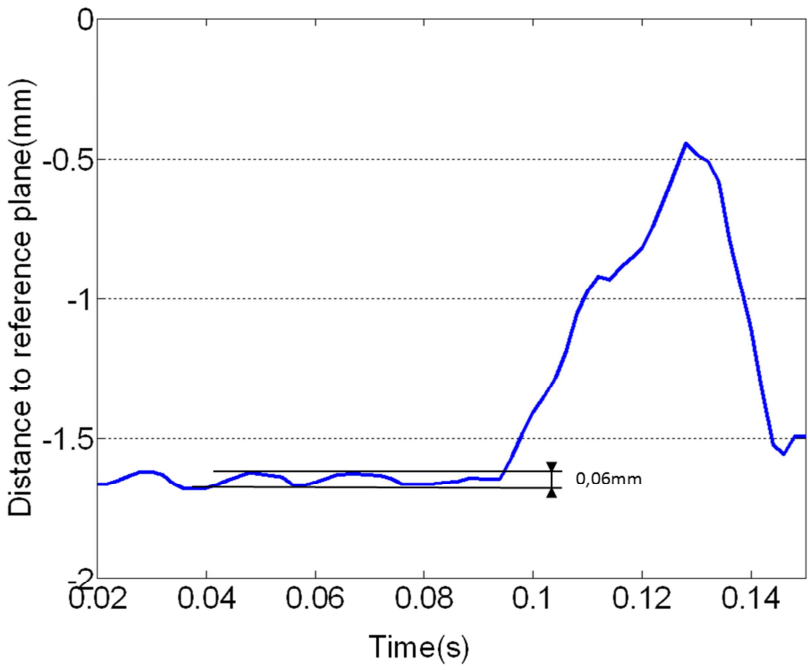

Figure 7.26 Out -of plane displacement measured at the centre of the ball along time

Figure 7.27 illustrates the measured ball displacements at the instant when the maximum displacement of the stroke was reached (0.13 s). Figure 7.27 A) shows the initial shape of the ball. Figure 7.27 B), C) and D) shows *Z*-, *X*- and *Y*- displacements maps when the stroke displacement was maximum (-13 mm). Finally, Figure 7.27 E) and F) show *X*- and *Y*- displacements profiles along red lines drawn in figures 156 C) and D).

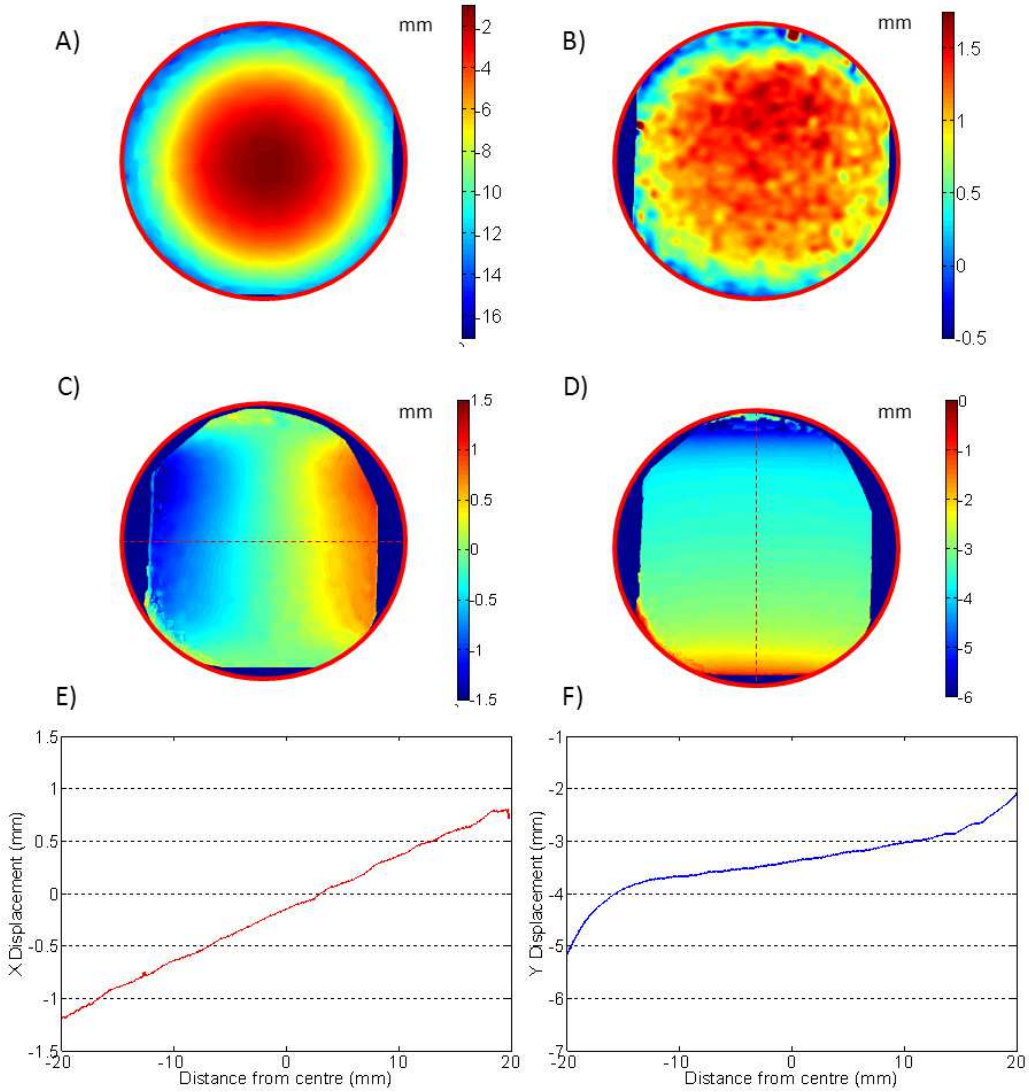

Figure 7.27 A) Shape of the ball before compression B),C),D) *Z*-, *X*- and *Y*- displacements maps at maximum compression in E),F) Displacements profiles along dashed line in C) and D) respectively.

7.4.3. Discussion

Some difficulties were found during this test. First the deformation speed was conditioned by the shape of the ball. Thus, to measure the out-of-plane deformation during the test, a low lens aperture was required to increase the field of view and focus the image when maximum displacement occurred. This means that the amount of light that is reaching the camera sensor was reduced and thus the exposure time had to be increased to obtain bright RGB colours. However, if the exposure time was increased the stroke speed had to be decreased to avoid blurring the images. Hence, a balance between the stroke speed and the exposure time had to be achieved.

In addition, since the studied element was not flat, a flat calibration surface placed just in front of the specimen was employed. After calibrating the FP+2D-DIC system, this surface was carefully removed. Thus, the flat reference plate had a thickness of 1,6mm and, when the plate was removed, Fringe Projection had to measure that the centre of the ball was placed at (-1,6mm) from the front surface of the reference plate.

It should also be taken into account, that the calibration of Fringe projection was performed by employing a cone instead of using the method described in chapter 5.

As illustrated in Figure 7.27, FP+2D-DIC results shows quite well the ball deformation during the test. Nevertheless, part of the lateral area of the ball could not be processed due to the out-of-plane shape of the ball which resulted in a low level of light and focus. Figure 7.26 displays an interesting effect consisting on sinusoidal out-of-plane displacement during the test. The sine had frequency of 50Hz which meant that the vibration of the oil pump was affecting the machine frame. It is worth pointing out that this small displacement of 0.06mm was measured by the proposed technique which highlights the potential of FP+2D-DIC for vibration measurement.

7.5. Conclusions

The previous analysis has led to the following conclusions:

- A set of experiments have been conducted to evaluate the accuracy of the FP+2D-DIC technique. The results have been compared with those obtained by different commercial 3D-DIC systems and numerical simulations using an image decomposition method.

- The technique uncertainty for quasi-static and dynamic analyses has been evaluated using a reference material.

- An initial test was conducted measuring the in-plane and out-of-plane displacements occurring during contact between an aluminium wedge and a silicon block. Results were compared with those obtained using two 3D-DIC commercial systems.

- A similar set of tests was performed involving a dynamic displacement analysis at 300mm/s during a 6mm indentation experiment with an aluminium wedge on a silicon block. Results were compared with those simulated with a Finite Element modelling.

- Finally, FP+ 2D-DIC was successfully employed for the analysis of a non-flat object during a high speed compression test.

- In all the cases results demonstrate a good level of agreement with those obtained with 3D-DIC and FE analyses. However, it has been observed that out-of-plane displacements for FP+2D-DIC are noisier than those obtained by 3D-DIC and FE analysis. This may have consequences in the accuracy of in-plane measurements. Further work is required to study its effect in the measurement accuracy.

Chapter 8. Discusión y conclusiones generales

En este capítulo final de la tesis se realiza de una discusión general para, posteriormente, alcanzar las principales conclusiones de este trabajo de investigación. Por último, también se presentan algunas recomendaciones sobre líneas de trabajo futuro.

8.1. Introducción

El trabajo presentado en esta tesis demuestra que la robustez, versatilidad y sencillez de Proyección de Franjas y Correlación Digital de Imágenes (2D) hacen de ellas una interesante alternativa para la medida de desplazamientos en tres dimensiones simultáneamente.

Sin embargo, el éxito de la integración de ambas técnicas precisa del desarrollo de una metodología experimental específica. En esta tesis, ésta metodología se ha presentado, evaluado y comparado sus resultados con los obtenidos mediante otros métodos convencionales tales como 3D-DIC y FEA.

Por tanto, el resultado de ésta tesis es un sistema de medición de desplazamiento 3D de bajo coste que se caracteriza por ser robusto, fiable, fácil de implementar, de usar y de calibrar, el cual permite obtener unos resultados comparables a otras técnicas ampliamente conocidas tales como 3D-DIC.

En este último capítulo se discutirá y concluirá los principales logros obtenidos durante el curso de esta investigación.

8.2. Discusión General

El principal objetivo de la presente investigación era desarrollar un procedimiento experimental para combinar Proyección de Franjas y Correlación Digital de Imágenes (2D) para medir simultáneamente los desplazamientos ocurridos en el plano y fuera de éste empleando para ello una sola cámara. Esto permitiría la reducción del coste y de los recursos técnicos y computacionales respecto a la utilización de una segunda cámara como es el caso de los sistemas de estereoscópicos. Adicionalmente se pretendía materializar esta idea en un dispositivo de bajo coste adecuado para su uso en entornos industriales capaz de medir desplazamientos en 3D en una amplia gama de aplicaciones y experimentos.

Sin embargo, se observó que no existía una metodología específica para la integración simultánea de FP y 2D-DIC usando una sola cámara. No obstante, se observó que era posible obtener los requeridos patrones de franjas y de speckle a partir de sola imagen RGB. Por lo que estos patrones de speckle y franjas podrían ser procesados separadamente, haciendo posible el estudio de eventos dinámicos (Siegmann, et al., 2011). Asimismo, se observó que la combinación de ambas técnicas no era directa ya que los desplazamientos en el plano estaban distorsionados por el desplazamiento fuera del plano, aunque la mayoría de autores que abordan esta integración de técnicas no consideraban esta distorsión. Por lo tanto, era necesario emplear lentes telecéntricas caracterizadas por ser caras, aparatosas y pesadas(Tay, et al., 2004) (Mares, et al., 2011). Sin embargo, otra opción sería desarrollar una metodología que permitiera corregir la distorsión de los desplazamientos medidos en el plano con los medidos fuera de plano.

En el capítulo 4 se describieron los diferentes aparatos y metodologías necesarias para llevar a cabo Proyección de Franjas y Correlación Digital de Imágenes (2D) mediante una sola cámara RGB. Se estableció el procedimiento para el codificado RGB que

permite la obtención del patrón de franjas y el patrón speckle a partir de una imagen en color, la cual contiene ambos patrones superpuestos en dos colores diferentes (Bayer, 1976). No obstante, se observa que existe una reducción de la resolución de una imagen en color respecto a una imagen monocromática de las mismas características.

Para llevar a cabo el procesado de Proyección de Franjas y de Correlación Digital de Imágenes 2D se escogieron las metodologías más robustas y las que ofrecen el mejor equilibrio entre resultados y tiempo de cálculo. Además, el montaje experimental adoptado fue diseñado para cubrir una amplia gama de aplicaciones con especial atención a los diferentes requisitos de sensibilidad y de tamaño del área de interés estudiada.

En el capítulo 5 se llevó a cabo un estudio de los efectos ópticos producidos cuando un elemento mecánico experimenta desplazamientos dentro y fuera de plano al mismo tiempo con el propósito de estudiar la distorsión de los desplazamientos medidos por 2D-DIC debido a la deformación fuera del plano. Basado en este estudio, se pretende desarrollar una metodología para corregir tal distorsión. Para realizar dicho estudio, se adoptó un modelo de lente pin-hole, del que se obtuvo una relación matemática para corregir los desplazamientos medidos en el plano. Esta expresión matemática depende de la distancia desde el centro óptico de la lente a un plano de referencia (z_0). Por lo tanto, esta metodología requiere de una calibración para obtener ese parámetro además de los necesarios para procesar PF y 2D-DIC. Además, se demostró que era imprescindible alinear perpendicularmente de la cámara con el plano de referencia. Para satisfacer estos requisitos, se ha propuesto un completo y sencillo procedimiento de calibración y alineación.

En el Capítulo 6 se realizó la validación de la metodología propuesta para integrar FP y 2D-DIC. En éste capítulo se llevaron a cabo cuatro experimentos en los que ocurren grandes desplazamientos. Dos de ellos consistían en medir los desplazamientos del solido rígido en un objeto plano inclinado, mientras que los otros dos consistieron en el análisis de la deformación 3D de materiales hiperelásticos. En ambos casos, los resultados de FP+2D-DIC se compararon satisfactoriamente con los obtenidos con 3D-

DIC encontrando diferencias inferiores a 5%. Además, se demostró que la falta de perpendicularidad con el plano de referencia es una de las principales fuentes de error. No obstante, el procedimiento de alineación propuesto minimiza esta fuente de error.

Como resultado del análisis realizado en los capítulos 5 y 6, se concluyó que la metodología propuesta cumple satisfactoriamente con el objetivo de medir simultáneamente los desplazamientos fuera y dentro de plano empleando una sola cámara. Sin embargo, se ha demostrado que el procedimiento de alineación y la calibración es crucial para obtener unos resultados precisos.

Por último, en el capítulo 7 se presenta tres experimentos en los que ocurren grandes desplazamientos en 3D. La primera prueba consistió en una identación cuasi-estática de un bloque de silicona; la segunda fue la identación a alta velocidad del mismo bloque de silicona y la prueba final fue someter una esfera de caucho a una compresión a alta velocidad. Además, se realizó una estimación de la incertidumbre de la técnica de la que se obtuvo un valor de $\pm$0.0083 mm para los desplazamientos en el plano, y $\pm$0,023 mm para los desplazamientos fuera del plano en condiciones estáticas. En los ensayos dinámicos la incertidumbre disminuye a $\pm$0,009 mm fuera del plano y a 0,006 mm en el plano. En todos los casos, los resultados se compararon con éxito con los obtenidos a partir de 3D-DIC o del Análisis de Elementos Finitos mediante un método de descomposición de imágenes. En todos los casos los porcentajes de error fue inferior al 3% del desplazamiento máximo. No obstante, los resultados de desplazamiento fuera de plano medidos mediante FP presentan más ruido que los obtenidos con 3D-DIC. Esto se atribuye a la presencia de restos de speckle en el patrón de la franjas.

Los resultados presentados en los capítulo 6 y 7 demuestran el potencial de FP+2D-DIC como una alternativa real para la medición de desplazamientos en 3D con un nivel de precisión comparables con los obtenidos con otras técnicas. Sin embargo se ha observado que, debido a la presencia de ruido, podría ser interesante el empleo de alguna técnica de filtrado para los desplazamientos fuera del plano para disminuir su incertidumbre. Además, si el elemento analizado no es plano, es necesaria la incorporación de una superficie plana para el proceso calibración. Esto podría

considerarse una fuente adicional de error, por lo que se debe prestar una atención especial durante el proceso de calibración.

Por otra parte, durante los ensayos de alta velocidad, la iluminación se demuestra ser un parámetro crucial. Sin embargo, se observó que no era posible emplear más iluminación que la proporcionada por el proyector a fin de obtener un buen contraste patrón de franjas.

Por último, la exactitud y repetitividad de los resultados obtenidos durante los ensayos realizados en esta tesis llevan a considerar a FP+2D-DIC como una alternativa de bajo coste para 3D-DIC. Además, ésta técnica alternativa, requiere algoritmos que son mucho más fáciles de implementar y son ampliamente conocidos, por lo que es mucho más fácil de implementar en contraste con 3D-DIC debido a que sus algoritmos son bastante más complicados y requieren mayores recursos computacionales, dando lugar a la adquisición de costosos sistemas comerciales.

8.3. Conclusiones Generales

Partiendo de que la investigación llevada a cabo en esta tesis tiene como objetivo llevar a cabo la integración de Proyección de Franjas y Correlación Digital de Imágenes (2D) para la medida de desplazamientos en el plano y fuera de éste, a continuación se presenta un resumen de las principales conclusiones alcanzadas:

- Un novedoso sistema óptico para la medición de desplazamientos 3D basado en la combinación de FP y 2D-DIC ha sido desarrollado. Este sistema tiene las siguientes características:
    - Permite la corrección de los desplazamientos medidos en el plano (distorsionados debido a la deformación fuera del plano) empleando para ello 2D-DIC evitando así el uso de lentes telecéntricas.
    - Precisa de un simple proceso de alineación y calibración respecto a una superficie de referencia plana.

- El sistema es compacto, portátil y muy adaptable a las necesidades específicas de diferentes experimentos o ensayos.
- El sistema permite la realización de ensayos dinámicos sin interrupciones.
- El sistema representa una reducción de costes significativa en comparación con 3D-DIC ya que evita el uso de una segunda cámara. Además, el coste computacional también se reduce ya que no se precisan de los algoritmos complejos requeridos para la correlación 3D por lo que es posible implementar fácilmente los algoritmos necesarios.

- Se han estudiado y evaluado los algoritmos necesarios para el procesamiento de imágenes con el objetivo de medir desplazamientos y deformaciones empleando FP+2D-DIC. Estos algoritmos ofrecen un comportamiento robusto y un buen equilibrio entre el tiempo de procesamiento y precisión las mediciones.

- Se ha desarrollado un original y novedoso procedimiento para la necesaria alineación y calibración del sistema, el cual permite obtener resultados exactos y de alta resolución de una manera simple y robusta.

- El sistema ha sido empleado con éxito para medir desplazamientos en 3D en diferentes experimentos (estáticos y dinámicos). Los resultados se han comparado con los obtenidos con otras técnicas ópticas y numéricas. En todos los casos, las diferencias estuvieron por debajo del 5%. Estas pruebas realizadas muestran el potencial de FP+2D-DIC y su capacidad para realizar ensayos a alta velocidad sobre objetos curvos ofreciendo un alto nivel de precisión.

8.4. Recomendaciones para futuras líneas de investigación.

En este apartado se presentan algunas ideas para llevar a cabo en trabajos futuros que no han podido ser consideradas debido a restricciones de tiempo o de recursos.

- La corrección numérica propuesta para los desplazamientos 2D distorsionados requiere de un procedimiento de calibración respecto a un plano de referencia paralelo al sensor de la cámara. Esta restricción ha implicado un método de calibración que simplifica enormemente el procedimiento. Sin embargo, se piensa que este proceso de calibración se puede mejorar, evitando el uso de cualquier superficie de referencia. En lugar de ello, se propone un objeto o tableta de calibración para reducir al mínimo la incertidumbre en la medición de la alineación objetos no planos.

- Otro aspecto que podría ser introducido en el procedimiento de calibración es el ajuste de color. Podría emplearse una tableta de calibración del color para llevar a cabo un ajuste automático de color. Esto mejoraría la calidad de las imágenes capturadas y, por lo tanto, los resultados del filtrado de patrones por RGB. Ésto repercutiría positivamente sobre la incertidumbre de los resultados de desplazamiento.

- También sería interesante realizar un análisis para evaluar la pérdida de precisión de FP+ 2D-DIC cuando se emplea una cámara de color en lugar de una cámara monocromática ya que, como se comentó en el capítulo 4, las cámaras de color realizan una interpolación cada dos píxeles para obtener una imagen continua de color. Este estudio podría mejorar la metodología de adquisición de imágenes y podría mejorar la precisión de la técnica propuesta.

- En el capítulo 7 se validó la técnica de FP+2D-DIC con métodos numéricos durante el ensayo dinámico realizado. Sin embargo, los resultados sólo han sido comparados empleando Descomposición de Imágenes en el instante de máximo desplazamiento. Esta comparación se mejoraría mediante la comparativa de los resultados de la técnica a lo largo de toda la duración del ensayo. Esto podría llevarse a cabo mediante la comparación de los momentos más importantes o descriptores de forma a lo largo del tiempo.

- Los resultados de la prueba dinámica en el capítulo 7 demuestran que FP 2D-DIC es una buena alternativa para analizar experimentos dinámicos y vibración. Por lo tanto, una futura línea de trabajo interesante podría ser la aplicación de FP+2D-DIC para el análisis de vibraciones.

- Un trabajo interesante sería emplear FP+2D-DIC para ensayar grandes componentes industriales, tales como estructuras aeroespaciales o componentes de automoción.

Chapter 8. General discussion and Conclusions

In this final chapter a general discussion is presented to subsequently reach major conclusions of this research. Finally, some recommendation for future work are also presented

8.1. Introduction

The work presented in this thesis demonstrates that the robustness, versatility and simplicity of Fringe Projection and Digital Image Correlation (2D) make them both an interesting alternative to simultaneous measuring 3D deformation fields.

However, the successful integration of both techniques requires the development of an experimental methodology. In this thesis this methodology has been presented, evaluated and the obtained results compared with those achieved with other standard methods such as 3D-DIC and FEA.

The result is a low-cost 3D displacement measurement system that is robust, reliable, simple to implement, to use and to calibrate, and with measuring capacities comparable to other well-known techniques such as 3D-DIC.

In this final chapter it will be discussed and concluded the major achievements obtained during the course of this investigation.

8.2. General Discussion

The main objective of the current investigation was to develop an experimental procedure to combine Fringe Projection and 2D Digital Image Correlation to simultaneously measure in-plane and out-of-plane displacements using one single camera. This could reduce the technical and economic cost of using a second camera as in the case of stereoscopic systems. I was also intended to convert this idea into low-cost system suitable for industrial environments and able to measure 3D displacements in a wide range of applications and experiments.

However, it was observed that it did not exist a specific methodology for the simultaneously integrating of FP and 2D-DIC sing a single camera. Nevertheless, it was observed that it was possible to obtain fringe patterns and speckle pattern in one RGB image. Thus speckle and fringe patterns could be processed in a separate way making it possible to study dynamic events (Siegmann, et al., 2011). In addition, it was observed that the combination of both techniques was not straightforward since in-plane displacements were distorted by out-of-plane displacement. Moreover, most of authors who addressed the integration of both techniques wrongly neglected that distortion. Hence, it was necessary to employ expensive, big and heavy telecentric lenses (Tay, et al., 2004) (Mares, et al., 2011). However, another option was to develop a methodology to correct the in-plane distortion using out-of-plane information. Hence, the objective of the thesis was to develop a novel and original low-cost technique to integrate FP and 2D-DIC for the in- and out-of-plane displacement analysis suitable to static or dynamic experimentation in industrial environments.

In chapter 4 it was described the different apparatus and methodologies required to perform Fringe Projection and 2D Digital Image Correlation employing a single RGB camera. It was explained the basis of RGB filtering which made it possible to obtain the fringe pattern and speckle pattern from a single colour image containing both patterns superimposed in two different colours (Bayer, 1976). Nevertheless, it was noticed that a resolution reduction occurred when compared a monochromatic camera with a same characteristics. To perform Fringe Projection and 2D Digital Image Correlation the most robust procedures and those with the best balance between good results and

computation time have been employed. In addition, for the adopted set–up was designed to cover a wide range of applications paying special attention to sensitivity requirements and size of the area of interest.

In chapter 5 it was performed a study of the optical effects occurring when a mechanical element experiences in-plane and out-of plane displacements at the same time. The purpose was to study the in-plane distortion measured by 2D-DIC due to out-of-plane deformation. In addition, it was intended to develop a methodology to correct such a distortion. For this study, a pin-hole lens model was adopted, from which it was obtained a mathematical relation to correct in-plane deformation. This mathematical expression depends on the distance from the optical centre of the lenses to a reference plane (z_0). This methodology needs from a process to obtain all the required parameters for Fringe Projection and Digital Image Correlation. In addition, the perpendicular alignment of the camera with the reference plane was found to be crucial. To satisfy those requirements, an easy calibration and alignment procedure has been proposed.

Chapter 6 was dedicated to the validation of the proposed methodology to integrate FP and 2D-DIC. In this chapter four large displacements experiments were conducted. Two of them consisted on measuring the rigid body motion at an inclined flat object, while the other two consisted on the evaluation of the 3D deformation in hyperelastic materials. In both cases, FP+3D-DIC was successfully compared with 3D-DIC with differences lower than 5%. In addition, it was proved that a lack of perpendicularity with the reference plane is one of the main sources of error. A proposed alignment procedure minimizes this source of error.

As a result of the analysis performed in chapter 5 and 6, it was concluded that the proposed methodology makes it possible to successfully study simultaneous in- and out-of-plane displacement using single camera. Nevertheless, the proposed procedure to perform both alignment and calibration has been demonstrated to be essential to obtain accurate.

Finally, in Chapter 7 it was presented three tests with large 3D displacements. The first test consisted in a quasi-static indentation of a silicone block; the second test was the high speed indentation of the same silicone block and the final test was a rapid compression of a rubber ball. In addition, an estimation of the uncertainty of the technique was performed obtaining a value of 0.0083 mm for in-plane displacements and 0.023 mm for out-of-plane displacements under static conditions. Out-of-plane and in-plane uncertainty decreases to 0,009 mm and 0,006 mm respectively in dynamic tests. In all the cases results were successfully compared with those obtained from 3D-DIC or Finite Elements Analysis together with a decomposition method. In all the cases the error percentages was lower than 3% of maximum displacement. Out-of-plane displacement results from FP presented more noise than those obtained with 3D-DIC. This was attributed to the presence of speckle in the fringe pattern.

The results presented in chapter 6 and 7 demonstrate the potential of FP+2D-DIC as a real alternative for 3D displacements measurement with a level of accuracy comparable with those obtained with other techniques. Nevertheless it was observed that some filtering for the out-of-plane displacements may be interesting to apply to decrease the uncertainty of those displacements due to the presence of noise. In addition, if the tested element is not flat, a flat surface surface must be used for calibration. This could introduce an extra source of error; thus, especial care must be taken during the calibration process.

Moreover, during high speed tests, illumination was a crucial parameter. However, it was observed that it was not possible to employ more illumination than that provided by the projector in order to obtain a good fringe pattern contrast.

Finally, the accuracy and repetitively of the results obtained during the test performed in this thesis have led to FP+2D DIC to be considered as a low-cost alternative to 3D-DIC. In addition, the alternative technique proposed, requires algorithms that are much easier to implement and are well known in the literature, making the technique much easier to be implemented in contrast to 3D-DIC technique due to the quite complicate algorithms and high computational resources which led to expensive commercial systems.

8.3. General Conclusions

Regarding to the investigation presented in this thesis which aimed to perform the integration of Fringe Projection and Digital Image Correlation (2D) for the in- and out-of-plane displacement analysis, a summary of the main conclusions achieved is presented:

- A completely novel optical system for 3D displacements measurement based on the combination of FP and 2D-DIC has been developed. This system has the following characteristics:
    - It allows the correction of the measured in-plane displacements (distorted due to out-of-plane displacement) employing 2D-DIC and avoiding to use telecentric lenses.
    - It requires a simple alignment and calibration process based on a flat reference surface.
    - The entire system is compact, portable and widely adaptable to the specific needs of different tests.
    - The system allows performing dynamic tests without interruption.
    - The whole system represents a significant cost reduction compared to 3D-DIC since it avoids the use of a second camera. In addition the computational cost is also reduced since no complex algorithms for 3D correlation are required making it possible to implement easily the required algorithms.
- The required image processing algorithms to extract the displacement and strain information from FP+2D-DIC have been presented and evaluated. Those algorithms offer a robust behaviour and a good balance between processing time and measurements accuracy.

- An original procedure to perform the required alignment and calibration has been developed. The system allows for accurate and high resolution results in a simple and robust manner.

- The system has been successfully evaluated to measure in- and out-of-plane displacements in different experiments (static and dynamic). R have been compared with those obtained with other optical and numerical techniques. In all the cases, the reported differences were smaller than 5%. The performed tests show the potential of FP+2D-DIC and its capability to perform high speed tests in non-flat objects with high level of accuracy.

8.4. Recommendations for future research.

In this epigraph some additional ideas and future work that have not been considered due to time constrains or limited resources are presented.

- The proposed numerical correction of distorted in-plane displacements requires a calibration procedure always referred to a flat plane parallel to the camera sensor. This approach implies a calibration method that greatly simplifies that procedure. However, it is thought that the calibration could be improved by avoiding the use of any reference surface. Instead, a calibration target is proposed to minimize the alignment uncertainty when measuring non-flat objects.

- Another aspect that should be introduced in the calibration procedure is the colour balance. A colour calibration target could be employed to perform a colour adjustment. This would improve the quality of the images captured and, hence, the RGB pattern encoding results. This would have a positive impact on the accuracy of the displacement results.

- An analysis to evaluate the loss of accuracy in FP+2D-DIC when a colour camera instead of a monochrome camera is employed would be also interesting since,

as it was commented in chapter 4, colour cameras perform an interpolation every two pixels to obtain a continuous colour image. This study could improve the image acquisition methodology which could improve the accuracy of the proposed FP+2D-DIC technique.

- The proposed FP+2D DIC technique has been validated using numerical methods during dynamic events. However, results have been compared employing Image Decomposition only for the maximum displacement instant. This comparison could be improved by comparing the results of the technique over time. This could be performed by comparing the most important moments or shape descriptors over time.

- Results from dynamic test in chapter 7 demonstrate that FP+2D-DIC is a good alternative for dynamic and vibration experiments. Hence, an interesting future work line could be the application of FP+2D-DIC to vibration analysis.

- A final interesting work would be to employ FP+2D-DIC to test big real industrial components such as aerospace structures or automotive components.

Bibliography

- Asundi, A. K., 2002. *MATLAB for Photomechanics. A primer.* First Edition ed. Oxford: Elsevier Science Ltd.
- Asundi, A. & Zhou, W., 1999. Unified calibration technique and its applications in optical triangular profilometry. *Applied Optics,* Volumen 38, pp. 3556-3561.
- Barber, J. & Ciavarella, M., 2000. Contact mechanics.. *International Journal of Solids and Strucctures,* 37(1-2), pp. 29-43.
- Barrientos, B., Cerca, M., García-Marquez, C. & Hernández-Bernal, C., 2008. Three-dimensional displacement fields measured in a deforming granular-media surface by combined fringe projection ad speckle photography. *Applied Optics,* 10(10), p. 104027
- Bayer, B., 1976. *Color Imaging Array.* US, Patente nº Patent US 3971065 A..
- Belgen, M., 1967. Structural stress measurements with an infrared radiometer. *ISA Trans,* Volumen 6, pp. 49-53.
- Bruning, J. y otros, 1974. Digital Wavefront Measuring Interferometer for Testing Optical Surfaces and Lenses,. *Applied Optics,* Volumen 13.
- Burguete, R. y otros, 2013. Analysis of Displacement Fields from a High Speed Impact using Shape Descriptors. *The Journal of Strain Analysis for Engineering Design,* Volumen In press.
- Burguete, R. & Patterson, E., 1997. A photoelastic study of contact between a cylinder and a half-space.. *Experimental Mechanics ,* 37(3), pp. 314-323.
- Burke, J., Bothe, T., Osten, W. & Hess, C., 2002. Reverse engineering by fringe projection.. *Proceedings of SPIE ,* Volumen 4778, pp. 312-324.
- C. Wust, D. C., 1991. Surface profile measurement using color fringe projection. *Mach Vision Appl,* 1991(4), pp. 193-203.
- Chen, W., Yang, H., Su, X. & Tan, S., 1999. Error caused by sampling in Fourier transform profilometry. *Optic Engeneering,* 36(6), p. 1029–1034.
- Ciavarella, M., Hills, D. & Monno, G., 1998. Contact problems for a wedge with rounded apex.. *International Journal of Mechanical Sciences,* 40(10), pp. 977-988.
- Cloud, G., 1998. *Optical Methods of Engineering Analysis.* Cambridge: Cambridge University Press.
- Cloud, G., 2002-2010. Back to Basics. Optical Methods in Experimental. *Experimental Techniques.*
- Dally, J. & Riley, W., 1991. *Experimental Stress Analysis.* New York: McGraw-Hill.
- Diaz-Garrido, F., 2004. *Developement of a Methodology for Thermielastic Investigation of the Effective Stress Intensity Factor.* s.l.:University of Sheffield.
- Dini, D., Barber, J., Churchman, C. & Sackfield, A. D., 2008. The application of asymptotic solutions to contect problems chacarterised by logarithmic singularities. *European Joirnal of MEchanics A-Solids,* 25(5), pp. 847-858.

- Du, Y., Díaz, F., Burguete, R. & Patterson, E., 2011. Evaluation Using Digital Image Correlation of Stress Intensity Factors in an Aerospace Panel. *Experimental Mechanics,* Volumen 51, pp. 45-57.
- Faugeras, O., 1993). *Three-Dimensional Computer Vision: A Geometric Viewpoint.* Cambridge: MIT Press,.
- Faugeras, O. & Devernay, F., 1994. Computing Differential Properties of 3-D Shapes from Stereoscopic Images without 3-D models. *INRIA Report,* pp. 208-213.
- Faugeras, O., Luong, Q. & Papadopoullos, T., 2001. *The Geometry of Multiple Images.* Cambridge: MIT Press.
- Felipe-Sesé, L., Diaz-Garrido, F., Dorado-Vicente, R. & Siegmann, P., 2012. *Calibración del montaje óptico para determinación de desplazamientos en el espacio mediante Correlación Digital de Imágenes 2D y Proyección de Franjas.* Castellón, ISSN: 0212-5072.
- Felipe-Sesé, L., Siegmann, P., Díaz, F. & Patterson, E., 2014. Simultaneous in-and-out-of-plane displacement measurements using fringe projection and digital image correlation. *Optics and Lasers in Engineering,* Volumen 52, p. 66–74.
- Felipe-Sesé, L., Siegmann, P., Díaz-Garrido, F. & Patterson, E., 2014. Integrating fringe projection and digital image correlation for high quality measurements of shape changes. *Optical Engineering,* Issue In press.
- Ferreiraa, N., Abramof, E., Corat, E. & Trava-Airoldi, V., 2003. Residual stresses and crystalline quality of heavily boron-doped diamond films analysed by micro-Raman spectroscopy and X-ray diffraction. *Carbon,* 41(6), p. 1301–1308.
- Genovese, K., Lamberti, L. & Pappaletter, C., 2006. Mechanical characterization of hyperelastic materials with fringe projection and optimization techniques. *Optics and Lasers in Engineering,* Volumen 44, pp. 423-442.
- Genovese, K. & Pappalettere, C., 2006. Whole 3D shape reconstruction of vascular segments under pressure via fringe projection techniques. *Optics and Lasers in Engineering,* Volumen 44, p. 1311–1323.
- Ghiglia, D. & Pritt, M., 1998. *Two-Dimensional Phase Unwrapping: Theory, Algorithms, and Software.* New York: Wiley&Blackwell.
- Gomes, P. y otros, 2010. MEasurement of scapular kinematics with Moiré Fringe Proyection technique. *Journal of Biomechanics,* Volumen 43, pp. 1215-1219.
- Gorthi, S. & Rastogi, P., 2010. Fringe Projection Techniques:Whither we are?. *Optics and Laser in Engineering,* 48(2), pp. 133-140.
- Greene, R. J., Patterson, E. & Rowlands, R., 2008. Themoelastic Stress Analysis. En: W. Sharpe, ed. *Springer Handbook of Experimental Mechanics.* New York: Springer, pp. 743-767.
- Greene, R., Patterson, E. & Rowlands, R., 2008. Thermoelastic Stress Analysis. En: W. Sharpe, ed. *Springer Handbook of Experimental Solid Mechanics.* New York: Springer Science+Business Media.
- Hamley, I., 2007. *Intriduction to Soft Matter-Revised Edition..* West Sussex: John Wiley & Sons Ltd.

- Han, Y., Rogalsky, A., Zhao, B. & Kwon, H., 2012. The application of digital image techniques to determine the large stress–strain behaviors of soft materials. *Polymer Engineering & Science,* 52(4), p. 826–834.
- Heredia Ortiz, M. E., 2004. *Novel developments of moire techniques for industrial applications.* Sheffield: University of Sheffield.
- Heredia-Ortiz, M. & Patterson, E., 2003. Deformation Data from Thermal Marking. *Strain,* Volumen 39, p. 149–152.
- Heredia-Ortiz, M. & Patterson, E., 2003. On the Industrial Applications of Moiré and Fringe Projection Techniques. *Strain,* Volumen 39, p. 95–100.
- Heredia-Ortiz, M. & Patterson, E., 2005. Location and Shape Measurement Using a Portable. *Experimental Mechanics,* June, 45(3), pp. 197-204.
- Hertz, H., 1881. Uber die Berührung fester elastischer Körper. *Journal für die reine und agewandte Mathematik,* Volumen 92, pp. 156-171.
- Huang, L., Kemao, Q., Pan, B. & Asundi, A. K., 2010. Comparison of Fourier transform, windowed Fourier transform, and wavelet transform methods for phase extraction from a single fringe pattern in fringe projection profilometry. *Optics and Lasers in Engineering,* Volumen 48, p. 141–148.
- Huang, L., Kemao, Q., Pan, B. & Asundi, A. K., 2010. Comparison of Fourier transform, windowed Fourier transform, and wavelet transform methods for phase extraction from a single fringe pattern in fringe projection profilometry. *Optics and Lasers in Engineering,* Volumen 48, p. 141–148.
- Huang, P., Hu, Q., Jin, F. & Chiang, F., 1999. Color-encoded digital fringe projection technique for high-speed three-dimensional surface contouring. *Optic Engeneering ,* Volumen 38, pp. 1065-1071.
- Hung, P.-C. & Voloshin, A. S., 2003. In-plane strain measurement by digital image correlation. *J. Braz. Soc. Mech. Sci. & Eng,* 25(3), pp. 215-221.
- Huntley, J., Nguyen, T., Burguete, R. & Coggrave, C., 2012. Multiple-view Shape and Deformation Measurement by Combining Fringe Projection and Digital Image Correlation. *Strain,* 48(3), pp. 256–266,.
- Huygens, C., 1690. *Traité de la Lumiere,* Leyden : s.n.
- Idesawa, M., Yatagai, T. & Soma, T., 1977. Scanning moiré method and automatic measurement of 3-D shapes. *Applied Optics,* 16(8), pp. 2152-2162 .
- Iwata, K. y otros, 2008. Three-dimensional profiling using the fourier transform method with a hexagonal grating projection. *Applied Optics,* 37(4), pp. 827-849.
- Jaffar, M., 2002. Frictionless contact between an elastic layer on a rigid base and a circular flat-ended punch with rounded edge or a conical punch with rounded tip.. *Interneational Journal of Mcehanical Sciences,* 44(3), pp. 545-560.
- Jaffar, M., 2003. Computation of stresses and deformations for a two-dimensional sliding contact betwee an elastic layer and a rigid indenter with a rounded profile.. *Journal of Strain Analysis for Engineering Design,* 38(2), pp. 161-168.
- Jayadevan, K. & Narasimhan, 1994. Finite.Element simulation of wedge indentation.. *Computers & Structures,* 57(5), pp. 915-927.
- Johnson, K., 1985. *Contact Mechanics.* Cambridge : Cambridge University Press.

- Kemao, Q., 2004. Windowed Fourier transform for fringe pattern analysis. *Applied Optics,* 43(13), pp. 2695-2702.
- Kemao, Q., 2007. Two-dimensional windowed Fourier transform for fringe pattern analysis: Principles, applications and implementations. *Optics and Lasers in Engineering,* Volumen 45, p. 304–317.
- Korsunsky, A., 2001. The influence of punch blunting on the elastic indentation response. *Journal of Strain Anñalysis for Engineering Design,* 36(4), pp. 391-400.
- Leon-Huerta, A., Martinez, A., Rayas, J. & Cordero, R., 2008. Dynamic measurement of strain in test specimen by fringe projection.. *Proceedings of SPIE International Society for Optical Engineering,* Volumen 7063.
- López-Alba, E., López-García, R., Dorado-Vicente, R. & Díaz-Garrido, F., 2013. Caracterización geométrica de daños superficieales empleando ópticas de campo completo. *Revista Iberoamericana de Ingeniería Mecánica,* 17(1), pp. 111-120.
- Lopez-Pedrosa, M., Zanganeh, M., Tai, Y. & Pinna, C., 2012. Digital Image Correlation (DIC) analysis in relation to damage development in third generation AA2050-T851 aluminium alloy. *Journal of Physics: Conference Series,* Volumen 382.
- Luo, P., Chao, Y. & Sutton, M., 1993. Accurate measurement of three-dimensional deformations in deformable and rigid bodies using computer vision. *Experimental Mechanics,* 33(3), pp. 123-133.
- Malitis, P., 2011. Contact with stick zone between an indenter ad a thin incompressible layer.. *Europea Joural of Mechanics A-Solids,* 30(6), pp. 884-892.
- Mares, C., Barrientos, B. & Blanco, A., 2011. Measurement of transient deformation by color encoding. *Optics Express,* 19(25), pp. 25712-25722.
- McEnteggart, I., 2008. Ch. 13 Extesometers. En: W. Sharpe, ed. *Springer HAndbook of Experimental Mechanics.* New York: Springer Science+Business Media.
- Nguyen , T., Huntley, J., Burguete, R. & Coggrave, C., 2011. Shape and displacement measurement of discontinuous surfaces by combining fringe projection and digital image correlation. *Optical Engineering,* 50(10).
- Nguyen, T., Huntley, J., Burguete, R. & Coggrave, C., 2011. Multile-view Shape and Deformation Measurement by Combinig Fringe Projection and Digital Image Correlation. *Strain,* 48(3), pp. 256-266.
- Pan, B., Kemao, Q., Xie, H. & Asundi, A., 2009. Two-dimensional digital image correlation for in-plane displacement and strain measurement: a review. *Measurement Science and Technology,* Volumen 20, p. 17.
- Pan, B., Wang, Z. & Lu, Z., 2010. Genuine full-field deformation measurement of an object with complex shape using reliability-guided digital image correlation. *Optics Express,* 18(2), pp. 1011-1023.
- Pan, B., Xie, H., Guo,, Z. & Hua, T., 2007. Full-field strain measurement using a two-dimensional Savitzky-Golay digital differentiator in digital image correlation. *Optical Engineering,* 46(3), p. 033601.
- Pan, J., Huang, P. & Chiang, F., 2006. Color phase-shifting technique for three-dimensional shape measurement. *Optical Engeneering,* Volumen 45.
- Patterson, E., 2008. *XIth International Congress and Exposition.* Orlando,, Society for Experimental Mechanics Inc., p. 5.

- Patterson, E. & Wang, Z., 1991. Towards full field automated photoelastic analysis of complex components. *Strain,* Volumen 27, pp. 49-56.
- Patterson, E. & Wang, Z., 1998. Simultaneous observation of phase stepping images for automated photoelasticity.. *Journal of Strain Analysis,* Volumen 22, pp. 1-15.
- Peters, W. & Ranson, W., 1981. Digital imaging techniques in experimental stress analysis,. *Optical Engeneering,* 21(3), pp. 427-432.
- Peters, W. & Ranson, W., 1982. Digital imaging techniques in experimental stress analysis,. *Optical Engineering,* Volumen 21, pp. 427-431.
- Quan, C., Tay, C. & Huang, Y., 2004. 3-D deformation measurement using fringe projection and digital image correlation. *Optik,* 115(4), p. 164–168.
- Ramesh, K., 2000. *Digital Photoelasticity: Advanced Techniques and Applications.* New York: Springer.
- Rodriguez-Vera, R., Genovese, K., Rayas, J. & Mendoza-Santoyo, F., 2009. Vibration analysis at microscale by Talbot fringe projection method. *Strain,* Volumen 45, pp. 249-258.
- Schadler, L. & Galiotis, C., 1995. Fundamentals and applications of micro Raman spectroscopy to strain measurements in fibre reinforced composites. *International Materials Reviews,* 40(3), pp. 116-134(.
- Schmidt, T., Tyson, J. & Galanulis, K., 2003. Full-Field dynamic displacement and strain measurement-Specific Examples using advanced 3D Image correlation.. *Experimental Techniques,* Volumen 27, pp. 22-26.
- Sebastian, C., Hack, E. & Patterson, E., 2013. A approach to the validation of computational solid mechanics models for strain analysis. *J. Strain Analysis,* Volumen 48, pp. 36-47.
- Sharpe,, W., Gan, Y. & Steinchen, W., 2008. *Springer Handbook of Experimental Solid Mechanics. Ch 23. Speckle Methods.* Sharpe (Ed.) ed. New York: Springer Science+Business Media,.
- Sharpe, W. & al, e., 2008. *Springer Handbook of Experimental Solid Mechanics.* New York: Springer.
- Sharpe, W., Almer, J. & Winholtz, R., 2008. X-Ray Stress Analysis. En: Sharpe, ed. *Springer Handbook of Experimental Mechanics.* New York: Sprnger, pp. 801-820.
- Sharpe, W. & Andonian, A. A., 2008. Optical Methods. En: *Springer Handbook on Experimental Stress Analysis.* New York: Springer Science+Business Media.
- Sharpe, W., Daniel , P. & Bongtae, H., 2008. *Springer Handbook of Experimental Solid Mechanics Ch. 22 Moiré Interferometry.* Sharpe Ed. ed. New York: Springer Science+Business Media.
- Sharpe, W. & Krishnaswamy, S., 2008. Photoacoustic Characterization of Materials. En: Sharpe, ed. *Springer Handbook of Experimental Mechanics.* New York: Springer, pp. 769-800.
- Sharpe, W. N., 2008. *Springer Handbook of Experimental Solid Mechanics.* New York: Springer.

- Sharpe, W. N. & Sutton, M., 2008. *Springer Handbook of Experimental Solid Mechanics Ch.20 Digital Image correlation for Shape and Deformation Measurements.* Sharpe Ed. ed. New York: 2008.
- Sharpe, W. & Pryputniewicz, R., 2008. *Springer Handbook of Experimental Solid Mechanics. Ch 24 Holography.* Sharpe Ed. ed. New York: Springer Science+Business Media.
- Shi, H., Ji, H., Yang, G. & He, X., 2013. Shape and deformation measurement system by combiing fringe projection and digital image correlation.. *Optics and Lasers in engieering,* Volumen 51, pp. 47-53.
- Shough, D., Kwon, O. Y. & Leary, D. F., 1990. High-speed interferometric measurement of aerodynamic phenomena. *SPIE Propagation of High Energy Laser Beams through the Earth´s Atmosphere,* Volumen 1221, pp. 394-403.
- Siegmann, P., Álvarez-Fernández, V., Díaz-Garrido, F. & Patterson, E., 2011. A simultaneous in- and out-of-plane displacement measurement method. *Optics Letters,* 36(1), pp. 10-12.
- Siegmann, P., Backman, D. & Patterson, E., 2005. A robust approach to demodilating and unwrapping phase stepped photoelastic data. *Experimental Mechanics,* Volumen 45(3), pp. 278-289.
- Sjödahl, M., 1994. Electronic speckle photography: increased accuracy by non-integral pixel shifting. *Applied Optics,* 33(28), pp. 6667-6673.
- Srinivasan,, V., Liu, L. & Halioua, M., 1985. Automated phase-measuring profilometry: a phase mapping approach. *Applied optics,* 24(2), pp. 185-188.
- Sun, B. y otros, 2013. 3D Computational Imaging with Single-Pixel Detectors. *Science ,* 340 (6134), pp. 844-847 .
- Sun, Y. & Pang, J., 2008. Experimental and numerical investigations of near-crack-tip deformation in a solder alloy. *Acta Materialia,* Volumen 56, pp. 537-548.
- Sutton, M. A., McNeil, S. R., Helm, J. D. & Chao, Y. J., 2000. Advances in Two-Dimensional and Three-Dimensional Computer Vision. *Photomechanics,* Volumen 77, pp. 323-372.
- Sutton, M. A. y otros, 1983. Determination of displacements using an improved digital correlation method. *Image and vision computing,* 1(3).
- Sutton, M. & Chao, Y., 1988. Measurement of strains in a paper tensile specimen using computer vision and digital image correlation. *Tappi J.,* 71(3), pp. 173-175.
- Sutton, M., Orteu, J. & Schreier, H. W., 2009. *Image Correlation for Shape, Motion and Deformation Measurements.* New York: Springer Science+Business Media.
- Sutton, M. y otros, 2008. The effect of out-of-plane motion on 2D and 3D digital image correlation measurements. *Optics and Lasers in Engineering,* Volumen 46, p. 746– 757.
- Su, X. & Wenjing, C., 2001. Fourier transform profilometry: a review. *Optics and Lasers in Engineering,* Volumen 35, p. 263–284.
- Su, X., Zhang, Q., Li, J. & Li, Z., 2006. Optical 3D shape measurement for vibrating drumhead. *Proceedings International Society for Optics and Photonics,* Volumen 6027, pp. 449-455.

- Sztefek, P. y otros, 2010. Using digital image correlation to determine bone surface strains during loading and after adaption of the mouse tibia. *Journal of Biomechanics,* Volumen 43, pp. 599-605.
- Takeda, M., 1995. Current trends and future directions of fringe analysis. *Proc. SPIE 2544, Interferometry VII: Techniques and Analysis,* Volumen 2544, p. 9.
- Takeda, M., 2013. Fourier fringe analysis and its application to metrology of extreme physical phenomena: a review. *Applied Optics,* 52(1), pp. 20-29.
- Takeda, M. & Mutoh, K., 1983. Fourier transform profilometry for the automatic measurement of 3-D object shapes. *Applied Optics,* December, 22(24), pp. 3977-3982.
- Tan, X. H., Kang, Y. & Patterson, E., 2012. Calibration of a 3-D Digital Image Correlation system for large deformation contact problems. *Journal of Physics: Conference Series,* 328(1).
- Tavares, P. & Vaz, M. A., 2006. Orthogonal projection technique for resolution enhancement of the Fourier transform fringe analysis method. *Optics Communications,* 266(465–468).
- Tay., C., Quan, C., Huang, Y. & Fu, Y., 2005. Digital image correlation for whole field out-of-plane displacement measurement using a single camera. *Optics Communications,* Volumen 251, pp. 23-36.
- Tay, C., Quan, C., Huang, Y. & Fu, Y., 2005. Digital image correlation for whole field out-of-plane displacement measurement using a single camera. *Optics Communications,* Volumen 251, pp. 23-36.
- Tay, C., Quan, C., Wu, T. & Huang, Y., 2004. Integrated method for 3-D rigid-body displacement measurement using fringe projection. *Optical Engineering,* 43(5), pp. 1152-1159.
- Truman, C., Sackfield, A. & Hills, D., 1995. Contact mechanics of wedge and cone indenters.. *International Journal of Mechanical Sciences,* 37(3), pp. 261-275.
- *VANEESA, 2013. ILS Protocol for the Calibration of Optical Systems for Dynamic and Static Deformation Measurement, VANESSA, 2013.* [En línea] Available at: http://www.engineeringvalidation.org/
- Vasco Olmo, J., Diaz-Garrido, F., Dorado-Vicente, R. & Lopez-García, R., 2012. Cálcio de factores de intesificación de tensiones mediante técnicas opticas de campo completo. *Revista Iberoamericana de Ingeniería Mecánica,* 16(2), pp. 93-106.
- W.N., S. & Sutton, M., 2008. *Springer Handbook of Experimental Solid Mechanics. Ch.20 Digital Image Correlation for Shape and Deformation Measurements.* Sharpe Ed. ed. New York: Springer Science+Business Media.
- Watson, R., 2008. Bonded Electrical Resistance Strain Gages. En: W. Sharpe, ed. *Springer Handbook of Experimental Solid Mechanics.* New York: Springer Science+Business Media.
- Weber, H., Lichtenberger, R. & Wolf, T., 2002. The Combination of Speckle Correlation and Fringe Projection for the Measurement of Dynamic 3-D Deformations of Airbag Caps. *IUTAM Symposium on Advanced Optical Methods and Applications in Solid Mechanics,* Volumen 82, pp. 613-626.

- Weber, W., 1830. Über die spezifische Wärme fester Körper insbesondere der Metalle. *Annalen der Physik und Chemie ,* Volumen 20, p. 177–213.
- Xiaoling, Z. y otros, 2005. Calibration of a fringe projection profilometry system using virtual phase calibrating model planes. *Journal of Optics A Pure and Applied Optics,* Volumen 7, p. 192–197 .
- Xiao, T., Kang, Y. & Patterson, E., 2013. An experimental study of the contact of a rounded rigid indenter with a soft material block. *Journal of Strain Analysis,* Volumen In press.
- Xiao, X. y otros, 2010. Displacement and Strain Measurement by Circular and Radial Gratings Moiré Method. *Experimental Mechanics,* 50(2), pp. 239-244.
- Yoneyama, S., Kitagwa, A., Kitamura, K. & Kikuta, H., 2005. *Deflection distribution measurement of steel structure using digital image correlation.* s.l., s.n.
- Yoneyama, S., Kitagwa, A., Kitamura, K. & Kikuta, H., 2007. Bridge deflection measuement using digital image correlation. *Experimental Techniques,* 31(1), pp. 34-40.
- Zappa, E. & Busca, G., 2008. Comparison of eight unwrapping algorithms applied to Fourier-transform profilometry. *Optics and Lasers in Engineering,* Volumen 46, p. 106–116.
- Zhang, S., 2010. Recent progresses on real-time 3D shape measurement using digital fringe projection techniques. *Optics and Lasers in Engineering,* Volumen 48, p. 149–158.
- Zhang, Z., 2012. Review of single-shot 3D shape measurement by phase calculation-based fringe projection techniques. *Optics and Lasers in Engineering,* 50(8), p. 1097–1106.

Appendix 1. Strain calculation

In most of mechanical applications it is desired to find strain maps during testing. Optical techniques studied in this thesis only achieve surface displacements occurring at the specimen surface. Nevertheless, the study of the strain (**$\boldsymbol{\varepsilon}$**) occurring at the specimen surface is as well an important issue. Strain is the fundamental magnitude that measures the deformation of a solid. It is a dimensionless property of a specimen being tested that relates the extension experimented per original length $\left(\boldsymbol{\varepsilon} = \frac{\Delta Longitude}{Initial\ longitude}\right)$.

From this strain it could be extrapolated some approximations about the stress (**σ**) in the material close to the surface using Hooke law. The stress if defined as force per unit area$\left(\boldsymbol{\sigma} = \frac{Force}{Area}\right)$. The stress vector change it direction depending the sign of the stress.

$$\sigma = E \cdot \varepsilon \qquad \text{Eq A1.1}$$

Where *E* is the Young modulus of the material.

This relation between strain and stress is possible as long as the material shows linear behaviour (Figure A1.1). If the material shows a non. Linear behaviour such as rubber, Eq A1.1 is not applicable.

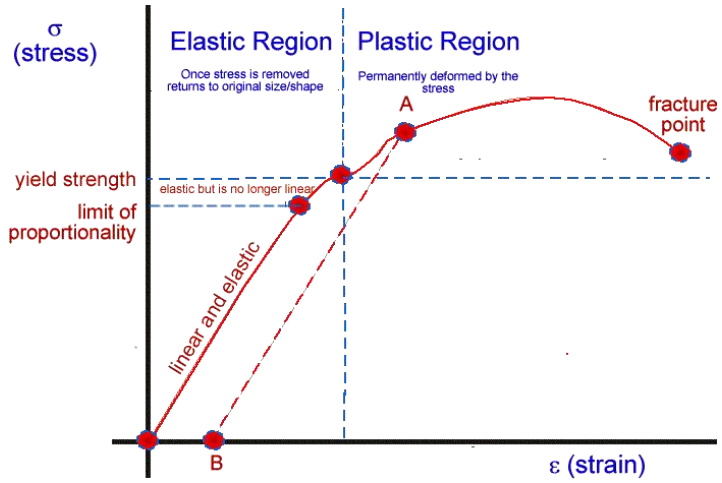

Figure A1.1 Diagram stress vs. strain diagram

The relation between strain and displacement is determined by the basic theory of elasticity as:

$$\varepsilon_x = \frac{\partial u}{\partial x}, \quad \varepsilon_y = \frac{\partial v}{\partial y} \quad \gamma = 2\varepsilon_{xy} = \frac{\partial v}{\partial x} + \frac{\partial u}{\partial y} \qquad \text{Eq A1.2}$$

Where *u,v* are the components of displacement in the x and y directions respectively. These equations can be applied only when the deformation is small enough so that the displacement gradients are small compared to unity. In this thesis a new technique to achieve large 3D displacements developed. In this case, the deformed and undeformed configurations of the material are significantly different and the non-linear or second-order terms of the finite strain tensor cannot be neglected. Thus the strain-displacement relation performed in this thesis is based in the Green-Lagrange tensor of deformations.

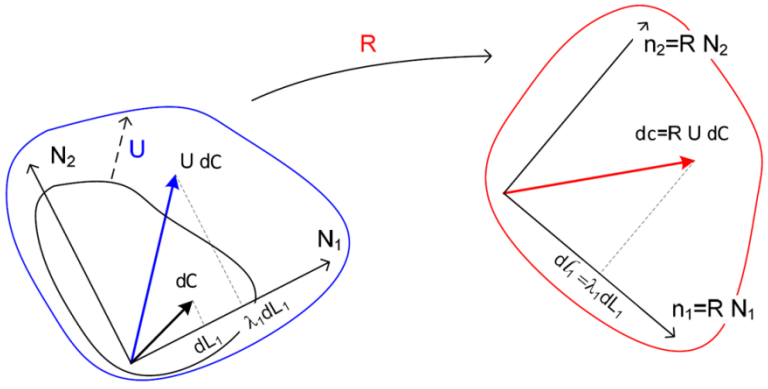

Figure A1.2 Polar decomposition of strain gradient tensor

The squared distance (***ds***) of two points infinitely close on the surface of the solid in the initial state and the deformed state, defined by their coordinates ***C*** and ***c*** respectively, is expressed as:

$$(ds^o)^2 = dC^T dC$$
$$(ds)^2 = dc^T dc \qquad \text{Eq A1.3}$$

The difference in the distance could be expressed as function of the tensor ***F***:

$$(ds)^2 - (ds^o)^2 = dc^T dc - dC^T dC$$
$$= dC^T F^T F dC - dC^T (F^T F - I) dC \qquad \text{Eq A1.4}$$

Being $dc = \boldsymbol{F} d\boldsymbol{C}$;

This squared difference of the distance referred to the initial state defines the value of the strain tensor of Green-Lagrange between initial (o) and final state (*t*) in the solid deformation:

$$(ds)^2 - (ds^o)^2) 2dC^T \, E \, dC$$
$$E = \frac{1}{2}(F^T F - 1) \qquad \text{Eq A1.5}$$

This tensor should be expressed as a function of the displacements replacing the value of the gradient tensor of deformations F:

$$E = \frac{1}{2}[(I + H)^T (I + H) - I]$$
$$E = \frac{1}{2}[H + H^T + H^T H] \qquad \text{Eq A1.6}$$

Replacing the displacement gradient, Eq A1.7 is obtained:

$$E = \frac{1}{2}\left[\frac{\partial u}{\partial C} + \left(\frac{\partial u}{\partial C}\right)^T + \left(\frac{\partial u}{\partial C}\right)^T \frac{\partial u}{\partial C}\right]$$
$$E_{x,y} = \frac{1}{2}\left[\frac{\partial u}{\partial y} + \left(\frac{\partial v}{\partial x}\right)^T + \sum_k \left(\frac{\partial u_k}{\partial X_x}\frac{\partial u_k}{\partial X_y}\right)\right] \qquad \text{Eq A1.7}$$

It must be noted that the tensor of Green-Lagrange is not sensitive to solid rigid rotations. A vector expression for Eq A1.7 is performed:

$$\vec{E} = \begin{Bmatrix} \frac{\partial u}{\partial x} \\ \frac{\partial v}{\partial y} \\ \frac{\partial u}{\partial y} + \frac{\partial v}{\partial x} \end{Bmatrix} + \frac{1}{2} \begin{bmatrix} \frac{\partial u}{\partial x} & 0 & \frac{\partial v}{\partial x} & 0 \\ 0 & \frac{\partial u}{\partial y} & 0 & \frac{\partial v}{\partial y} \\ \frac{\partial u}{\partial y} & \frac{\partial u}{\partial x} & \frac{\partial v}{\partial y} & \frac{\partial v}{\partial x} \end{bmatrix} \begin{bmatrix} \frac{\partial u}{\partial x} \\ \frac{\partial u}{\partial y} \\ \frac{\partial v}{\partial x} \\ \frac{\partial v}{\partial y} \end{bmatrix} \quad \text{Eq A1.8}$$

It cab be written as:

$$\varepsilon_x = \frac{\partial u}{\partial x} + \frac{1}{2}\left[\left(\frac{\partial u}{\partial x}\right)^2 + \left(\frac{\partial v}{\partial x}\right)^2\right]$$

$$\varepsilon_y = \frac{\partial \boldsymbol{v}}{\partial y} + \frac{1}{2}\left[\left(\frac{\partial u}{\partial y}\right)^2 + \left(\frac{\partial v}{\partial y}\right)^2\right] \quad \text{Eq A1.9}$$

$$\gamma = 2\varepsilon_{xy} = \frac{\partial v}{\partial x} + \frac{\partial u}{\partial y} + \frac{\partial u}{\partial x} \cdot \frac{\partial u}{\partial y} + \frac{\partial v}{\partial x} \cdot \frac{\partial v}{\partial y}$$

A comparison between the short and long expressions was made by Tan Xiao *et Al* (Xiao, et al., 2013) and it was demonstrated that the difference between expression s increases with the magnitude of displacements. It is more convenient to employ Eq A1.9 instead of Eq A1.2.

Appendix 2. Data comparison image decomposition technique.

In experimental Mechanics it is always important to compare results from one technique employed with those obtained using other techniques or methods. Sometimes the results of those different techniques are difficult to compare since each technique offers their data in a different way, matrix, image, size, point of view, etc. An ideal method to compare data should be independent of these factors. Image decomposition is a technique that is useful for this issue. It decomposes an image in a vector with variable elements which depends on the shape and value of results and not on the point view or size of the image. In this way it is possible to compare images (or data matrix) from different techniques in an easy way.

Comparison using image decomposition technique consists in reducing the information provided by displacements maps by containing them in a vector. Then vectors of every are compared for every stage desired. The more similar are the vectors, the more similar is the data..

In this Thesis, the adopted Image Decomposition technique is based on Tchebichef polynomials **T***(x,y)* to decompose displacement images **Or***(x,y)*.

$$\boldsymbol{Or}(\boldsymbol{x},\boldsymbol{y}) = \sum_{\boldsymbol{k=0}}^{\boldsymbol{N}} \boldsymbol{S_k T_k}(\boldsymbol{x},\boldsymbol{y}) \qquad \text{Eq A2.1}$$

Where the coefficients $\boldsymbol{S_k}$ are called as feature or shape vector of the displacement map $I(x,y)$. They are determined by:

$$\boldsymbol{S_k} = \sum_{\boldsymbol{k=0}}^{\boldsymbol{N}} \boldsymbol{I}(\boldsymbol{x},\boldsymbol{y})\boldsymbol{T_k}(\boldsymbol{x},\boldsymbol{y}) \qquad \text{Eq A2.2}$$

Polynomials are dimensionless and *N* is the number of shape descriptors.

A study of the adequate number of descriptors must be made. The number of shape descriptors needed is given by the one that obtain a good correlation coefficient (*r*>90%) between the original image (***Or***) and the reconstructed (***Re***). Where the correlation coefficient ***cr*** is given by:

$$\boldsymbol{cr} = \frac{\sum_X \sum_Y (\boldsymbol{Or_{XY}} - \overline{\boldsymbol{Or}})(\boldsymbol{Re_{XY}} - \overline{\boldsymbol{Re}})}{\sqrt{(\sum_X \sum_Y (\boldsymbol{Or_{XY}} - \overline{\boldsymbol{Or}})^2)(\sum_X \sum_Y (\boldsymbol{Re_{XY}} - \overline{\boldsymbol{Re}})^2)}} \qquad \text{Eq A2.3}$$

Another descriptor to measure the quality of the reconstruction is the average squared residual or uncertainty (***u***):

$$\boldsymbol{u^2} = \frac{\boldsymbol{1}}{\boldsymbol{n}} \sum_{\boldsymbol{x,y}}^{\boldsymbol{n}} (\boldsymbol{Re}(\boldsymbol{x},\boldsymbol{y}) - \boldsymbol{Or}(\boldsymbol{x},\boldsymbol{y}))^2 \qquad \text{Eq A2.4}$$

The lower is its value, the better is the reconstruction. Normally, both variables find their maximum and minimum respectively, at the same number of moments.

In addition, an uncertainty band must be plotted. This band is the result of the uncertainties of the technique and the uncertainty of the proper decomposition process (Sebastian, et al., 2013) according to the following equation:.

$$s_1 = s_2 \pm u(s_2) \qquad \text{Eq A2.5}$$

Where s_1 and s_2 are the shape descriptors representing the data fields from the first and second technique respectively and $u(s_2)$ is the uncertainty in the feature vector describing the data from the experiment (Eq A2.5):

$$\boldsymbol{u(s_2)} = \sqrt{\boldsymbol{u_{calibration}}^2 + \boldsymbol{u_{reconstruction}}^2} \qquad \text{Eq A2.6}$$

Figure A2.1 shows an example of the representation of the moments when comparing two techniques. In addition it is represented the hypothetic case when moments of both techniques are equal (45^o solid green line). Tchebichef moments are defined by red crosses and must be placed as close as possible to that green line. Both results are considered similar enough when the moments are placed inside the uncertainty band (blue band).

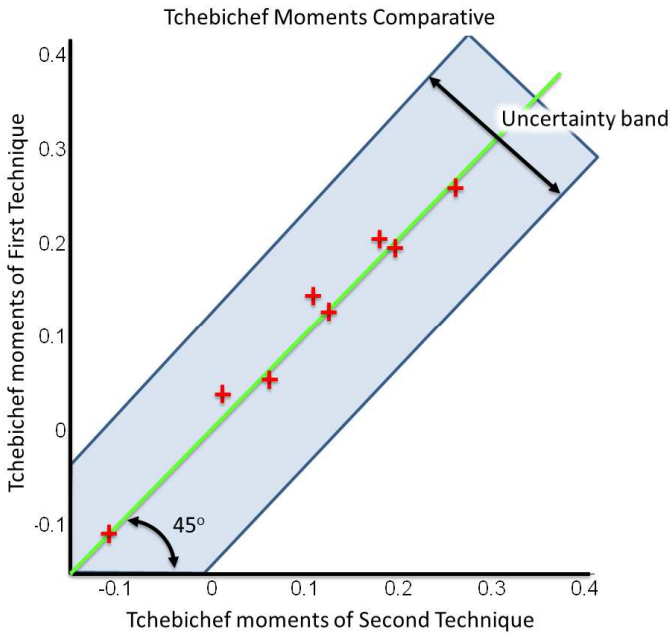

Figure A2.1 Illustration of Shape Descriptors comparison.

Published work

- **Papers in international journals**:
    - *Aplicaciones industriales de técnicas ópticas de campo completo para la medida de tensiones y deformaciones en elementos de máquinas*. Lopez-Alba, E., Felipe-Sesé, L., Vasco-Olmo, J. & Diaz-Garrido, F., 2013.. *Dyna Colombia,* Volumen 181, pp. 98-108.
    - *Simultaneous in-and-out-of-plane displacement measurements using fringe projection and digital image correlation*. Felipe-Sesé, L., Siegmann, P., Díaz, F. & Patterson, E., 2014. *Optics and Lasers in Engineering,* Volumen 52, p. 66–74.
    - *Integrating fringe projection and digital image correlation for high quality measurements of shape changes.* Felipe-Sesé, L., Siegmann, P., Diaz-Garrido, F. & Patterson, E., 2014.. *Optic Engineering,* p. In press.
- **Papers in international conferences**:
    - *Tratamiento de imágenes para sistemas ópticos de medida 3D*. L. Felipe-Sesé , F. A. Díaz, R. Dorado-Vicente, R. Lopez-García. 10º Congreso Iberoamericano de Ingeniería Mecánica, Oporto, Portugal, 2011
    - *A novel low-cost approach for 3D displacement measurement using Fringe Projection and Digital Image Correlation*. L. Felipe-Sesé. The British Society for Strain Measurement's 9th International Conference on Advances in Experimental Mechanics. Cardiff University.2013.

- **Papers in national conferences**:

  - *Calibración de sistemas fotomecánicos mediante transformaciones perspectivas*. L. Felipe-Sesé, E. López-Alba, F.A. Díaz, R. Dorado. XVIII Congreso Nacional de Ingeníería Mecánica. Ciudad Real. 2010.

  - *Sistema de bajo coste para la medida de formas en tres dimensiones*. L. Felipe-Sesé, E. López-Alba, F.A. Díaz, R. Dorado. XVIII Congreso Nacional de Ingeníería Mecánica. Ciudad Real. 2010.

  - *Calibración del montaje óptico para determinación de desplazamientos en el espacio mediante Correlación Digital de Imágenes 2D y Proyección de Franjas* Felipe-Sesé, L., Diaz-Garrido, F., Dorado-Vicente, R. & Siegmann, P XIX Congreso Nacional de Ingeníería Mecánica. Castellon. 2012.

  - *Comparativa de técnicas de filtrado de imágenes para el procesado conjunto de las técnicas de Correlación Digital de Imágenes 2D y Proyección de Franjas.* Felipe-Sesé, L., Diaz-Garrido, F., Dorado-Vicente, R., Siegmann, P. XIX Congreso Nacional de Ingeníería Mecánica. Castellon. 2012.

- **International Awards**

  - Second prize at the Young Stress Analyst Competition 2013 at The British Society for Strain Measurement's 9th International Conference on Advances in Experimental Mechanics 2013 at Cardiff University.

- **Patents**

  - Dispositivo Portátil para la medida de mapas de desplazamientos de superficies en las tres direcciones espaciales (Portable device for three espatial dimesions displacement map measuremet). España. Nº P201330411 March 2013.